Network pharmacology of the MPP^+ cellular model of Parkinson's disease

Harriet Anne Keane

St. Anne's College

University of Oxford

A thesis submitted for the degree of

Doctor of Philosophy

September 2014

This thesis is to dedicated to the memory of
Paul Andrew Robertson
27th April 1988 - 18th May 2014

Abstract

Parkinson's disease (PD) is an incurable neurodegenerative motor disorder caused by the inexorable loss of dopamine neurones from the substantia nigra pars compacta. Cell loss is characterised by the perturbation of multiple physiological processes (including mitochondrial function, autophagy and dopamine homeostasis) and much of this pathophysiology can be reproduced *in vitro* using the mitochondrial toxin MPP^+ (1-methyl-4-phenylpyridinium). It was hypothesised that MPP^+ toxicity could be modelled using protein-protein interaction networks (PPIN) in order to better understand the interplay of systems-level processes that result in eventual cell death in MPP^+ models and PD.

Initially, MPP^+ toxicity was characterised in the human, dopamine-producing cell line BE(2)-M17 and it was confirmed that the neurotoxin resulted in time and dose dependent apoptosis. A radio-label pulse-chase assay was developed and demonstrated that MPP^+-induced decreased autophagic flux preceded cell death. Autophagic dysfunction was consistent with lysosome deacidification due to cellular ATP depletion.

Pertinent PPINs were sampled from publically available data using a seedlist of proteins with validated roles in MPP^+ toxicity. These PPINs were subjected to a series of analyses to identify potential therapeutic targets. Two topological methods based on betweenness centrality were used to identify target proteins predicted to be critical for the crosstalk between mitochondrial dysfunction and autophagy in the context of MPP^+ toxicity.

Combined knockdown of a subset of target proteins potentiated MPP^+ toxicity and the combined resulted in cellular rescue. Neither of these effects was observed following single knockdown/overexpression confirming the need for multiple interventions. Cellular rescue occurred via an autophagic mechanism; prominent autophagosomes were formed and it was hypothesised that these structures allowed for the sequestration of damaged proteins. This thesis demonstrates the value of PPINs as a model for Parkinson's disease, from network creation through target identification to phenotypic benefit.

Acknowledgements

First, I must thank my supervisor Prof. Richard Wade-Martins for giving me the opportunity to work in his laboratory. I would also like to thank e-Therapeutics for their continued support of this project and in particular my industrial supervisors Dr. Steven Zimmer, Dr. Alan Whitmore, Dr. Jack Scannell and Dr. Brendan Jackson who each brought a different dimension to this work. This DPhil was conducted through the Systems-Approach to Biomedical Sciences Industrial Doctorate Centre and I am grateful for all the staff at the Doctoral Training Centre, and particularly Lisa Bligh, for ensuring that this programme ran so smoothly. I would also like to thank Prof. Charlotte Deane and Prof. Elspeth Garmen for their advice and support over the last four years.

The Wade-Martin's laboratory has been a fantastic place to work and I owe a huge debt of gratitude to all those who have created such an enjoyable working environment. There is not space here to thank everyone in the group who assisted me during this project, but I would like to thank Dr. Brent Ryan for his patience in teaching me molecular biology techniques. His help enormously eased the, somewhat daunting, transition from Chemistry undergraduate to Neuroscience DPhil. I am also enormously grateful to all of those who spent their evenings and weekends proofreading my thesis and in particular Dr. Natalie Connor-Robson, Dr. Ruth Faram, Dr. Benjamin Hunn, Dr. Hugo Ribeiro Fernandes and Dr. Amy Smith who each ploughed through an entire chapter.

Paul Roberston was a huge part of my experience in the Wade-Martins group. I will always be grateful for his laughter, his companionship on many late nights in the laboratory and his assistance in my perpetual battles with R. It fills me with enormous sadness that his thesis will never be submitted.

Beyond the Wade-Martins group, several individuals have provided valuable assistance on the networks aspect of this project. I would like to thank Prof. Charlotte Deane for taking the time to review *Chapter 4* and her helpful suggestions relating to this work. I am also grateful for the advice of Prof. Caleb Webber following my transfer of status. I have greatly enjoyed working with Andrew Elliott who always found the time to try and explain the more mathematical aspects of networks and whose valuable insights contributed hugely to this project.

Without doubt the best thing about my time at Oxford has been the people I have met. I owe a huge debt to the fellow DPhil students from across the university who have always been there to pick me up when I felt utterly defeated by Science. There are too many such individuals to name, but I would like to thank Dr. Paul Crewe, Dr. James Hillis, Melissa Jansen van Rensburg, Joanna Lee, Dr. Justine Schluntz, Dr. Joe Staines and Amy Varney for being there when I needed them most.

The Oxford University Women's Boat Club has been a massive part of my life over the past eight years and I am indebted to the remarkable women with whom I have had the honour of sharing this journey. In particular I would like to thank the Blue Boats of 2011 and 2013 and Christine Wilson for teaching me how much I am capable of and reminding me that there was a world beyond my DPhil.

My final thanks are for my parents and my sisters without whose unfaltering support I would never have been able to complete this project.

Contents

List of abbreviations

3T3	Cell line NIH 3T3
5HIAA	5'hydroxyindole-3-acetic acid
6-OHDA	6-hydroxydopamine
7-AAD	7-aminoactinomycin D
AADC	Amino acid decarboxylase
ABL1	Tyrosine-protein kinase ABL1
AD	Alzheimer's disease
AIF	Apoptosis inducing factor
AMBRA1	Activating molecule in BECN1-regulated autophagy protein 1
AMPT	Alpha-methyl-*p*-tyrosine
ANOVA	Analysis of variance
ATG	Autophagy related
ADP	Adenosine diphosphate
ATP	Adenosine triphosphate
ATP13A2	Probable cation-transporting ATPase 13A2
BAX	Apoptosis regulator BAX
BC	Betweenness centrality
BCL2	Apoptosis regulator BCL-2
CCCP	Carbonyl cyanide *m*-chlorophenyl hydrazone
CMA	Chaperone mediated autophagy
CNS	Central nervous system
DA	Dopamine
DAPI	4',6-diamidino-2-phenylindole
DAPPLE	Disease Association Protein-Protein Link Evaluator
DAT	Dopamine transporter
DAVID	Database for Annotation, Visualization and Integrated Discovery
DJ1	Protein DJ1
DMEM	Dulbecco's modified Eagle medium
DMV	Dorsal motor nucleus of the vagus nerve
DOPAC	3,4-dihydroxyphenylacetic acid
DRP1	Dystrophin-related protein 1
EGFP	Enhanced GFP
ER	Endoplasmic reticulum
ERK2	Extracellular signal-regulated kinase 2
ETC	Electron transport chain
FBS	Foetal bovine serum
FDA	Federal Drug Authority
GABARAP	Gamma-aminobutyric acid receptor-associated protein
GBA	Glucosidase β acid
GBRL1	Gamma-aminobutyric acid receptor-associated protein like 1
GBRL2	Gamma-aminobutyric acid receptor-associated protein like 2
Gcase	Glucocerebrosidase
GFP	Green fluorescent protein
GO	Gene ontology
GSK3β	Glycogen synthase kinase 3β

GWAS	Genome wide association studies
HPLC	High-performance liquid chromatography
HSC70	Heat shock cognate 70
HVA	Homovanilic acid
ICC	Immunocytochemistry
IKKE	Inhibitor of nuclear factor κB kinase subunitϵ
iPSC	Induced pluripotent stem cell
KD	Knockdown
KEGG	Kyoto Encyclopaedia of Genes and Genomes
KO	Knockout
LAMP	Lysosome-associated membrane glycoprotein
LB	Lewy body
LC3	Microtubule-associated proteins 1A/1B light chain 3
***L*-DOPA**	*L*-3,4-dihydroxyphenylalanine
LPR	Lowest pubmed re-use
LRRK2	Leucine-rich repeat kinase 2
M17	Cell line BE(2)-M17
MAPK	Mitogen-activated protein kinase
MAPT	Microtubule associated protein tau
miRNA	Micro RNA
MAO	Monoamine oxidase
MPP^+	1-Methyl-4-phenylpyridinium
MPTP	1-Methyl-4-phenyl-1,2,3,6-tetrahydropyridine
mRNA	Messenger RNA
mTOR	Mammalian target of rapamycin
MTS	((3-(4,5-Dimethylthiazol-2-yl)-5-(3-carboxymethoxyphenyl)-2-(4-sulfophenyl)-2H-tetrazolium
MTT	3-(4,5-Dimethylthiazol-2-yl)-2,5-diphenyltetrazolium
NEDD4	E3 ubiquitin-protein ligase NEDD4
Nemo	NF-κB essential modifier
nNOS	Neuronal nitric oxide synthase
OE	Overexpression
OM	Opti-MEM
OMIM	Online Mendelian Inheritance in Man
P53	Cellular tumour antigen P53
P62	Ubiquitin-binding protein p62
Parkin	E3 ubiquitin-protein ligase parkin
PBS	Phosphate buffered saline
PCA	Perchloric acid
PD	Parkinson's disease
PI	Propidium iodide
PINK1	PTEN induced putative kinase 1
PPI	Protein-protein interaction
PPIN	Protein-protein interaction networks
PPP2R2B	Serine/threonine-protein phosphatase 2A 55 kDa regulatory subunit B β isoform
ROGID	Redundant object group identifier
ROS	Reactive oxygen species
RT	Room temperature
SEM	Standard error of the mean
shRNA	Small hairpin RNA
siRNA	Small interfering RNA
SNAP	Soluble NSF attachment protein
SNCA	α-Synuclein
SNARE	SNAP receptor
SNP	Single nucleotide polymorphism

SNpc	Substantia nigra pars compacta
TAP	Tandem affinity purification
TCA	Trichloroacetic acid
TFAM	Mitochondrial transcription factor A
TFEB	Transcription factor EB
TH	Tyrosine hydroxylase
TMRM	Tetramethylrhodamine
TRAF6	TNF receptor associated factor 6
UCHL1	Ubiquitin carboxyl-terminal esterase L1
VDAC1	Voltage-dependent anion-selective channel protein 1
VMAT2	Vesicular monoamine transporter 2
VTA	Ventral tegmental area
WB	Western blot
WT	Wild type
Y2H	Yeast two hybrid
ZFN	Zinc finger nuclease

List of Figures

List of Tables

Chapter 1

Introduction

1.1 Parkinson's disease

Parkinson's disease (PD) is the second most common neurodegenerative disease. The risk of PD increases with age and a prevalence of approximately 1% is seen globally at age 60 [1], with one study suggesting a prevalence as high as 4.3% over 85 [2]. The incidence of PD is higher in men than women for reasons that are not fully understood, but may relate to hormonal differences [1–3]. As of 2005, there were 4.1 million PD patients globally, a figure expected to rise to 8.7 million by 2030 [4].

The cardinal symptoms of PD are bradykinesia (slowness of movement), postural instability, resting tremor and rigidity [5]. Non-motor symptoms (olfactory dysfunction, cognitive deficits, constipation, depression and sleep disorders) may also be present and often precede motor symptoms [5].

1.1.1 Pathological features

Motor symptoms are caused by the depletion of the neurotransmitter dopamine (DA) from the striatum. DA has opposing effects on the direct and indirect pathways of the basal ganglia resulting in the activation of the former and the inhibition of the latter, in PD this balance is altered leading to the cardinal motor symptoms [6]. DA depletion is a result of the selective death of DA neurones in the substantia nigra pars compacta (SNpc) [7]. Surviving neurones are characterised by eosinophilic inclusions known as Lewy bodies (LB) and Lewy neurites [8]. Lewy inclusions are predominantly made up of the protein α-synuclein [9] and are a key diagnostic marker of PD. Clinical symptoms are observed when approximately 50% of nigral DA

A9 neurones and 80% striatal DA are lost [10]. However, the GABAergic neurones of the SNpc and the DA neurones of the nearby ventral tegmental area (VTA) (A10 neurones) are relatively spared in PD [11].

Thorough studies of PD neuropathology conducted by Braak *et al.* resulted in the 'Braak hypothesis' which states that, 'the neuronal damage does not develop randomly but, rather, follows a predetermined sequence' [8, 12]. Braak disease staging divides Lewy pathology into six stages [8] with the dorsal motor nucleus of the vagus nerve (DMV), olfactory bulb and nucleus the first affected regions and the disease spreading up the brainstem. Lewy pathology is not seen in the SNpc until stage 3 and SNpc cell loss/depigmentation are key markers of stage 4. As PD progresses, Lewy pathology spreads and degeneration in initially affected regions becomes more severe so that in stage 5 and 6 Lewy pathology is observed in the neocortex, the SNpc is almost entirely denuded and the olfactory system is characterised by extended Lewy neurites. It is thought that the early, non-motor symptoms of PD result from extranigral degeneration, for example the loss of smell as a result of changes to the olfactory system [8, 12] and that clinical PD is only observed when the disease reaches Braak stage 3 [12]. Although it has been reported the neurodegeneration precedes LB pathology [13], there is a close correlation between the regions affected by LB pathology and those where cell loss occurs, suggesting that these processes are intimately linked [14].

1.2 Causes of Parkinson's disease

1.2.1 Monogenic mutations causing Parkinson's disease

A minority (5-10%) of PD cases are familial, caused by inherited monogenic mutations [3, 15, 16]. There are 20 known PARK loci [17], the most common of which are listed in *Table 1.1* [3, 15, 16, 18]. These mutations can be divided into those causing dominant and recessive PD. Broadly speaking, the mutations resulting in dominant familial PD can be linked to autophagy or vesicle dysfunction and those causing recessive forms of the disease connected to mitochondrial dysfunction. A more detailed explanation of the roles of the proteins linked to familial PD will be given throughout the introduction to this thesis. Although there are differences between sporadic and familial PD, the study of genetic causes has provided insights into the disease mechanism and models for the investigation of idiopathic PD.

Gene	Protein	Inheritance	Mutation	Average age of onset (years)	Disease characteristics
PARK1, α-Synuclein (*SNCA*) [19–21]	α-Synuclein	Dominant	A30P, E46K, A35T, H50Q, G51D, A53T, duplications, triplications.	mutations: 60, duplications: 36-65, triplications: 24-48	Progressive parkinsonism, autonomic dysfunction, cognitive decline, dementia, disease progression is more rapid with triplications, wide-spread LB pathology, nigral and hippocampal neurone loss.
PARK2, Leucine-rich repeat kinase 2 (*LRRK2*) [22, 23]	LRRK2	Dominant	R1441C/G/H, Y1699C, I2012T, G2019S, I2020T.	60	Symptoms similar to sporadic PD although some studies suggest slower progression, penetrance is incomplete and age dependent [24]. LB pathology is pleomorphic with non-specific SN degeneration, brainstem LB disease, neurofibrillary tangles and TDP43 inclusions seen in some cases.
PARK6, PTEN induced putative kinase 1 (*PINK1*) [25]	PINK1	Recessive	Q129X, P196L, G309D, W437X, G440E, Q456X, deletions are rare.	<45	Slowly progressing parkinsonism, postural instability, sleep disorders, LB pathology unknown.
PARK2 [26]	E3 ubiquitin-protein ligase parkin (Parkin)	Recessive	Missense, exonic deletion/duplication/triplication	<45	Slowly progressing parkinsonism, dystonia, some cases show LB pathology, predominantly nigral neurone loss.
PARK7 [27]	Protein DJ1 (DJ1)	Recessive	E163K, L166P, exonic deletions.	<40	Parkinsonism, behavioural and psychiatric abnormalities, amyotrophy, cognitive impairment, LB pathology is unknown.
PARK5, ubiquitin carboxyl-terminal esterase L1 (*UCHL1*) [28]	UCHL1	Recessive	I93M, S18Y.	56	Similar to sporadic PD, LB pathology unknown.
PARK9 Probable cation-transporting ATPase 13A2 (*ATP13A2*) [29]	ATP13A2	Recessive	F182L, G504R, G877R, exonic deletions.	<20	Atypical parkinsonism (Kufor-Rakeb syndrome), supranuclear gaze palsy, spasticity, dementia, neuroradiological atrophy and iron accumulation in basal ganglia.

Table 1.1: **Parkinson's disease (PD) may be caused by monogenic mutations.** Monogenic mutations known to cause either dominant or recessive familial PD. For each gene common mutations, average age of onset and disease characteristics are given.

1.2.2 Genetic variants conferring increased susceptibility to Parkinson's disease

Beyond monogenetic mutations, large scale genome wide association studies (GWAS) have identified an increasing number of polymorphisms which infer increased risk of PD and these data are collected on the PDgene webpage [30, 31].

Initial studies suffered from low power due to small sample size. However the parallel 2009 studies of Simon-Sanchez *et al.* (individuals of European descent) and Satake *et al.* (individuals of Japanese descent) had sufficient power to detect a number of variations conferring increased risk [32, 33]. Both studies identified variants in *SNCA* as conferring increased risk and the European study was able to replicate results from the Japanese study indicating that variations at the PARK16 locus and within *LRRK2* conferred increased risk (although these results were not significant following corrections for multiple testing in the European cohort). However, differences were also identified between the populations with variations at the microtubule associated protein tau (*MAPT*) locus conferring increased risk in only the European cohort and polymorphisms in bone marrow stromal cell antigen 1 (*BST1*) associated with PD in just the Japanese group.

Numerous subsequent GWAS have been conducted and identified additional genetic variants associated with increased risk of PD, although variations are seen between different ethnic populations [34]. The largest single cohort is the 23andMe group and a 2011 study of 3426 patients and 29,624 controls was able to replicate 20 previously published genetic associations and identify two new susceptibility loci [35]. The 23andMe study estimated the heritability of PD as at least 27%, yet found that only 6-7% of the total genetic risk of developing PD was accounted for by the identified susceptibility loci. The missing heritability may be due to single nucleotide polymorphisms (SNPs) with low frequency, SNPs not represented on arrays or SNPs with low effect sizes which do not reach the stringent significance thresholds required following corrections for multiple testing [34].

Within recent months, Nalls *et al.* published a large scale meta-analysis of previous GWAS including 13,708 cases and 95,282 controls of European descent and nearly eight million SNPs [31]. Nalls *et al.*'s study identified 26 SNPs as significantly associated with PD and 24 of the SNPs were replicated in an independent set, including six new loci (*Table 1.2*). The authors generated risk profiles and calculated that the fifth risk quintile has 3.31 times the risk of the first quintile of developing PD.

Recent studies have looked to explain the heritability of PD beyond SNPs that are individu-

Nearest gene(s)	Odds ratio	P value
SNCA	0.76	$4.16\text{x}10^{-73}$
MAPT	0.769	$2.37\text{x}10^{-48}$
TMEM175-GAK-DGKG	0.786	$1.02\text{x}10^{-43}$
GBA-SYT11	1.824	$1.37\text{x}10^{-29}$
MCCC1	0.842	$2.14\text{x}10^{-21}$
STK39	1.214	$1.15\text{x}10^{-20}$
ACMSD-TMEM163	0.875	$9.13\text{x}10^{-20}$
BST1	1.126	$9.44\text{x}10^{-18}$
RAB7L1-NUCKS1	1.122	$1.66\text{x}10^{-16}$
LRRK2	1.155	$5.24\text{x}10^{-14}$
INPP5F	1.624	$4.34\text{x}10^{-13}$
GPNMB	1.110	$1.18\text{x}10^{-12}$
HLA-DQB1	0.826	$1.19\text{x}10^{-12}$
BCKDK-STX1B	1.103	$2.43\text{x}10^{-12}$
CCDC62	1.105	$6.02\text{x}10^{-12}$
RIT2	0.904	$7.74\text{x}10^{-12}$
MIR4697	1.105	$9.83\text{x}10^{-12}$
VPS13C	1.113	$1.23\text{x}10^{-11}$
FAM47E-SCARB2	0.907	$2.95\text{x}10^{-11}$
DDRGK1	1.111	$3.04\text{x}10^{-11}$
GCH1	0.904	$5.85\text{x}10^{-11}$
SIPA1L2	1.131	$4.87\text{x}10^{-10}$

Table 1.2: **Nalls *et al.* study identifies 24 SNPs as significantly associated with PD.** For each SNP the nearest gene, odds ratio and P value for association are given - values are for the combined (discovery and replication) phase with 19,081 cases and 100,833 controls [31]

ally significant at a GWAS level. Using genome-wide complex trait analysis, Holmans *et al.* investigated SNPs which were associated with PD, but were not individually significant, as a group and thereby explained a larger portion of PD heritability [36]. A pathway based analysis was used to identify biological functions that were enriched in the genes in which these SNPs occurred and provided evidence of immune-related genetic susceptibility (beyond SNPs in the HLA locus) to PD.

In an alternative approach, Hill-Burns *et al.* performed GWAS on stratified groups of PD patients (sporadic and familial - defined as patients who have a first or second degree relative with PD, but without Mendelian inheritance) and illustrated that, although stratification decreased the power of the study, generating a more homogenous sample group allowed additional loci to be identified [37]. Such an approach may be fruitful in determining the aetiology of heterogeneous diseases, such as PD.

GBA mutations and PD

The glucosidase β acid (*GBA*) gene codes for the lysosomal enzyme glucocerebrosidase (GCase) and homozygous mutations in *GBA* result in the lysosomal storage disorder Gaucher's disease

[38]. Physicians noticed an increased incidence of parkinsonism in Gaucher's patients, and their families, and it has since been shown that heterozygous *GBA* mutations confer an increased risk of PD, with a particular prevalence in Ashkenazi Jews [39].

1.2.3 Environmental factors contributing to development of idiopathic Parkinson's disease

The majority of PD cases are idiopathic and environmental factors are thought to be a key determinant of their development [40].

Prevalence studies have demonstrated that age is a causal factor in the development of PD and that there is an increased incidence of disease in men [41]. However, smoking and coffee drinking are protective [42, 43]. Although the mechanism is not clear, it has been suggested that the decreased complex I activity observed in smokers may contribute to their decreased vulnerability to PD [44] and caffeine is an inhibitor of adenosine A_{2A} receptors.

Key environmental risk factors for PD include exposure to pesticides which act through complex I inhibition [45] and traumatic brain injury [46, 47]. There are multiple hypotheses as to how the latter may lead to PD including: acceleration of disease progression in individuals with high α-synuclein levels [46], causing temporary disruption to the blood brain barrier allowing increased exposure to neurotoxins [47], or triggering an acute reaction which initiates a cascade of neurodegeneration [47].

1.3 Models of Parkinson's disease

Various experimental models have been developed to explore the aetiology of PD and investigate potential therapeutics. Broadly speaking, experimental models may be divided into genetic and neurotoxin models with both *in vivo* and *in vitro* systems employed in each category. The different approaches mirror the known genetic and environmental factors that lead to PD. This thesis focuses on the screening of molecular targets and *in vitro* model were considered the most effective system in which to conduct this work. Below follows a discussion of induced pluripotent stem cell (iPSC) and neurotoxin models.

1.3.1 Induced pluripotent stem cell (iPSC) derived neurones

In 2006 Yamanaka and colleagues developed a ground breaking protocol to reprogramme fibroblasts to iPSC, which can differentiate into cells from all three germ layers [48, 49]. In 2008 this work was extended to generate iPSC from patients with familial diseases, including PD and Gaucher's disease [50]. Protocols have subsequently been developed to allow the differentiation of iPSC to DA neurones, offering unique access to a population of GIRK2 positive A9 neurones known to be vulnerable in PD [51].

Following the establishment of such protocols, iPSC-derived neurones have been used to investigate the phenotypes in neuronal cells carrying PD causing mutations with mitochondrial dysfunction, α-synuclein accumulation, oxidative stress and changes to autophagy observed [52–59].

Questions have been raised about the utility of iPSC-derived lines in the investigation of idiopathic PD, particularly given initial reports of no phenotypic differences between lines derived from controls and idiopathic PD patients [60]. However the 2012 study of Sanchez-Danes *et al.* differentiated iPSC derived from both familial (*LRRK2* G2019S) and idiopathic PD patients [59]. In both sets of cells, decreased neuronal arborisation and accumulation of autophagosomes were observed following extended culture times; the authors suggested that these changes were the result of autophagic defects. These results have yet to be reproduced by other groups and therefore the utility of iPSC-derived lines for modelling sporadic PD is still an issue of contention [61].

A key advance in the use of iPSC-derived lines has been the correction of genetic mutations to generate isogenic lines. Such a correction was first reported by Soldner *et al.* who used zinc finger nuclease (ZFN) technology to both correct and generate mutations in *SNCA* [58]. Such an approach was recently put to elegant use in an exploration of lines containing *GBA* mutations [57]. Schondorf *et al.* demonstrated that lines carrying the *GBA* mutation displayed α-synuclein accumulation, autophagic and lysosomal defects and that these phenotypes were reversed following correction of the mutation [57].

Despite the clear utility of iPSC-derived lines, such approaches do have a number of limitations [62]. The reprogramming protocol can introduce karyotypic abnormalities, point mutations and copy number variations [63] and therefore careful screening of genetic and phenotypic stability must be conducted, further increasing the time requirements and costs of the protocol. Further, there is evidence of clonal variation (for example in protein expression levels) even when lines are derived from a single individuals [62] which complicates comparisons between lines from different

individuals. Although reprogramming returns cells to a pluripotent state, there is evidence that cells have an 'epigenetic memory' with cells retaining methylation patterns characteristic of their somatic tissue of origin undermining their ability to truly model DA neurones [64]. Beyond the generation of iPSC, current differentiation protocols yield variable and heterogeneous cell populations [65] which can make it difficult to expose phenotypes only evident in DA neurones particularly as many differentiation protocols result in yields of DA neurones as low as 10% [62].

Given the limitations of iPSC, as well as the high costs and long time scales required for generation of DA neurones, it is suggested that iPSC-technology should be used in concert with other experimental models of PD.

1.3.2 Neurotoxin models of Parkinson's disease

The three neurotoxins most commonly used in the modelling of PD are 1-methyl-4-phenylpyridinium (MPP^+)/1-methyl-4-phenyl-1,2,3,6-tetrahydropyridine (MPTP), rotenone and 6-hydroxydopamine (6-OHDA) all of which have been employed in both *in vivo* and *in vitro* systems [66] (*Figure 1.1*).

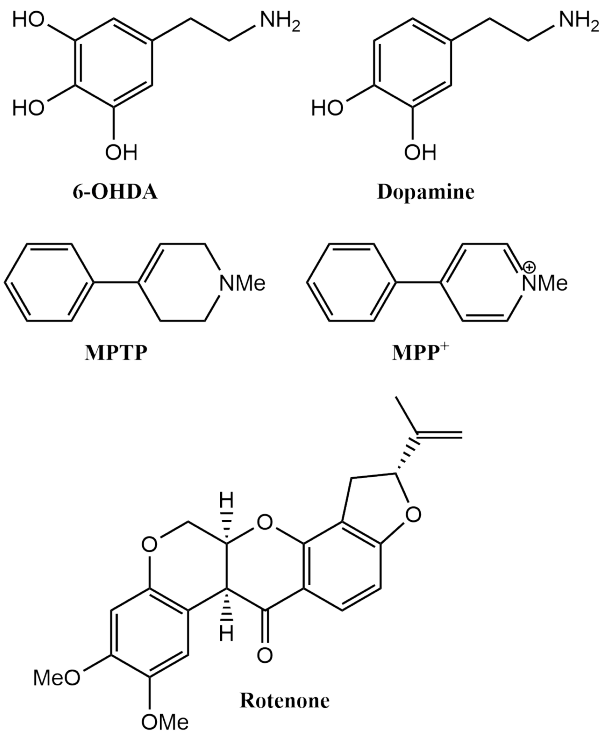

Figure 1.1: **Neurotoxins commonly used to model Parkinson's disease.** The structure of dopamine is provided for comparison.

In 1979, MPTP was discovered to cause parkinsonism following accidental exposure in drug users [67] and MPTP was subsequently shown to induce parkinsonism in mice and non-human primates [67, 68]. The compound is oxidised by monoamine oxidase B (MAO-B) to form the

active metabolite MPP^+ [69], which is taken up into DA neurones via the dopamine transporter (DAT) [70] where MPP^+ acts as a complex I inhibitor [71–73] (For further details of the mechanism of action of MPP^+ see *Subsection 3.1.1*). MPTP treated non-human primates and mice exhibit all the cardinal symptoms of PD (tremor, rigidity, bradykinesia and postural instability) and are responsive to the major drugs used to treat PD including *L*-DOPA (*L*-3,4-dihydroxyphenylalanine) [66, 68]. The remarkable phenocopy is explained by the pattern of nigrostriatal cell death; non-human primates treated systemically with low doses of MPTP mimic the pattern of neurone loss observed in PD with profound DA depletion in the SNpc, caudate nucleus and putamen [74]. Along with the relatively rapid neurone loss, the key distinction between sporadic PD and MPTP-induced parkinsonism is the lack of LB pathology [75]. However, some reports indicate that MPTP treated primates and rodents show increased α-synuclein expression in the SNpc, which precedes cell loss and at later time points increased α-synuclein immunoreactivity is also observed [76–78]. The active metabolite MPP^+ is also used *in vitro*, causing mitochondrial dysfunction and subsequent death of DA neurones allowing the cellular pathways implicated in PD to be investigated. It should be noted that *in vitro* studies of MPP^+ treatment only inconsistently demonstrate increased α-synuclein expression with some experiments resulting in unaltered protein levels [79, 80].

Exposure to rotenone, another complex I inhibitor, has been linked to increased risk of PD [45]. Unlike MPP^+, rotenone is not specific for DA neurones and is not a DAT substrate, it is a systemic toxin which enters cell throughout the body. However, rats do display the preferential loss of DA neurones and a DA related motor phenotype when chronically treated with rotenone, perhaps due to the vulnerability of DA neurones to mitochondrial stress [81]. A key advantage of the rotenone rat model is the formation of proteinaceous inclusions that are positive for ubiquitin and α-synuclein [82]; although this has not been repeated in other animal species [83].

6-OHDA is a DA derivative found in the urine of patients treated with *L*-DOPA [84]. When injected directly into the brains of rodents, selective loss of DA neurones is observed and has been shown to be dependent on the presence of α-synuclein [85]. Like MPP^+, 6-OHDA is a DAT substrate [66]; however, rather than acting as a complex I inhibitor, the deleterious effects of 6-OHDA are a direct result of reactive oxygen species (ROS) generation [86] and can be ameliorated by the overexpression (OE) of cellular anti-oxidants [87]. 6-OHDA treated rodents exhibit a series of motor defects including characteristic circling behaviour [66].

The neurotoxin models each have key advantages and disadvantages: presence or absence of proteinaceous inclusions, ease and safety of administration, extent of previous characterisation and effects on bioenergetic function [88]. However, all are unified in being acute rather than

chronic models of neurodegeneration. MPP^+ is viewed as the most appropriate cellular model due to its extensively investigated mechanism, excellent PD phenocopy in non-human primates, α-synuclein accumulation and safety of use [66].

1.3.3 *Saccharomyces cerevisiae* as a model of Parkinson's disease

An intriguing alternative approach to modelling PD utilising *Saccharomyces cerevisiae* has been pioneered by Lindquist and colleagues [89–94]. Initially, it was shown that human α-synuclein OE led to inclusion formation and dose dependent toxicity in *S.cerevisiae* [89] and that toxicity was due to vesicular trafficking defects [90]. Genome-wide expression screens identified genes whose OE was capable of rescuing α-synuclein toxicity in *S.cerevisiae* and the OE of the mammalian orthologs was shown to be protective in other model organisms [91]. Highlighting the utility of the *S.cerevisiae* model, OE of the ortholog of ATP13A2 was shown to be protective against α-synuclein toxicity - mutations in *ATP13A2* lead to recessive juvenile parkinsonism [91].

The generation of *S.cerevisiae* lines expressing higher levels of α-synuclein revealed mitochondrial dysfunction and the generation of ROS as key pathways in α-synuclein toxicity [92]. A chemical screen identified several small molecules that were able to ameliorate α-synuclein toxicity and these findings were replicated in a *Caenorhabditis elegans* disease model and primary rat neuronal cultures OE mutant α-synuclein or treated with rotenone [92].

In 2013, Tardiff *et al.* reported that N-aryl benzimidazole (NAB) could reverse α-synuclein toxicity in *S.cerevisiae*, *C.elegans*, primary rat neuronal cultures and human cortical neurones derived from iPSC [93]. The authors demonstrated that at higher concentrations NAB inhibited cell growth through the same mechanism of action as α-synuclein toxicity rescue. To identify the target of the more potent analogue NAB2, the authors screened a large genetic library to identify genes whose mutation or OE allowed for cell growth following NAB2 treatment. The resulting hits formed a network of related genes centred on the yeast ortholog of E3 ubiquitin-protein ligase NEDD4 (NEDD4) and the authors suggest that NAB2 acts via the E3 ligase NEDD4 to promote vesicle trafficking [93]. NAB2 also decreased nitrosative stress and improved endoplasmic reticulum (ER) trafficking in iPSC-derived cortical neurones harbouring an A53T α-synuclein mutation [94].

However, it should be acknowledged that α-synuclein is not endogenously expressed in the experimental species *S.cerevisiae*, *C.elegans* or *Drosophila melanogaster* which may explain the toxicity observed and limit the relevance of non-mammalian animal models.

1.4 Systems-level processes implicated in Parkinson's disease

Although the causes of PD are unknown, a number of processes have been implicated as linking genetic and sporadic forms of the disease. This thesis aims to view PD from a systems biology perspective considering the interplay of multiple factors and biological process in a 'top down' approach, which can be contrasted with reductionist paradigms that study problems from the bottom up - often at the level of a single gene or protein [95, 96].

1.4.1 α-Synuclein

The protein α-synuclein lies at the centre of PD: mutations [19] and multiplications [20] in *SNCA* lead to familial PD (*Subsection 1.2.1*), SNPs within the locus increase an individual's risk of PD [31] (*Subsection 1.2.2*) and α-synuclein is a key component of LB [9] (*Subsection 1.1.1*). α-Synuclein has also been linked to neurotoxin-induced parkinsonism as α-synuclein knockout (KO) mice are resistant to MPTP [97] and exposure to the neurotoxin increases α-synuclein levels in *in vitro* systems [98–100].

The synuclein family (α-, β- and γ-synuclein) are conserved across vertebrate species and expressed at high levels in the brain [101], but the normal function of α-synuclein is not well understood. α-Synuclein has three domains: an amino terminal lipid binding α-helix, a β-amyloid binding domain and a carboxy-terminal acidic tail. α-Synuclein may also misfold to a β-sheet rich form which is prone to assembly of fibrils, aggregates and amyloid plaques. It has been suggested that aggregation and fibril formation are mediated by ubiquitination [102], phosphorylation [103], truncation [104] and HDAC6 [100]. α-Synuclein fibrils are able to catalyse the formation of aggregates by recruiting otherwise soluble molecules of the protein [105] and mutant forms of the protein undergo more rapid oligomerisation [106].

It is generally accepted that α-synuclein is natively unfolded [107] and forms an α-helix only upon binding to lipid membranes [108]. However, the 2011 work of Bartels *et al.* suggested that α-synuclein may exist as a native tetramer which resists aggregation and the authors proposed that the monomer form of α-synuclein was potentially harmful [109]. Evidence for the α-synuclein tetramer came from protein isolation under non-denaturing conditions, native gel electrophoresis, *in vitro* linking, circular dichroism spectroscopy, scanning transmission electron microscopy and analytical ultra-centrifugation. However, these results have not been reproduced by other groups and Bartels *et. al*'s conclusions have been contested [110]. Burre *et al.* explored the structure of purified α-synuclein in solution and unpurified α-synuclein as a component of brain cytosol and

suggest that the divergent results achieved by Bartels *et al.* may be due to erthrocyte specific post translational modifications or multimerisations. Although Burre *et al.* reproduce Bartels *et al.*'s gel filtration results indicating that α-synuclein elutes in a peak with apparent mass of 63 kDa, they suggest that this is more likely to be due to an increased hydrodynamic radius as a result of the dynamic nature of α-synuclein. Further, although Burre *et al.* recapitulate the band of approximately 65 kDa on native gels, this band is retained following boiling, which would disrupt any tetrameric protein. In contrast to the work of Bartels *et al.*, the circular dichroism spectroscopy data reported by Burre *et al.* indicates a protein with no secondary structure except upon membrane binding. Finally, Burre *et al.* offer size-exclusion chromatography with multi-angle laser-light scattering data as evidence that α-synuclein is monomeric. In conclusion, until the results of Bartels *et al.* are reproduced by independent groups the concept of α-synuclein as a physiological tetramer is unlikely to gain traction within the scientific community.

The synuclein family proteins are known to associate with synaptic vesicles and have been linked to synaptic DA release [111] and this may be due to the synuclein family's role as chaperones of the SNAP (Soluble NSF Attachment Protein) Receptor (SNARE) complex [112]. The SNARE complex mediates synaptic membrane vesicle fusion and synaptobrevin, syntaxin and SNAP-25 are all key complex members [113]. There is some evidence that α-synuclein may affect the transport of DAT to the synapse and in *in vitro* α-synuclein knockdown (KD) studies DAT transport, cell surface DAT levels and the rate of DA uptake are all decreased [114–116]. However, only subtle changes in neurotransmission are seen in α-synuclein KO mice [101].

Some reports indicate that nigral α-synuclein levels increase with age leading to decreases in TH (tyrosine hydroxylase) activity and DA levels priming neurones for degeneration [117]. There is also some evidence of increased α-synuclein messenger RNA (mRNA) and protein levels in the affected regions of the brains of sporadic PD patients [118]. There are some reports of OE of α-synuclein leading to neuronal death in *in vitro* [119] and *in vivo* [120, 121] models. However, these results are not consistent with some *in vivo* α-synuclein OE models displaying non-specific [122, 123] or non-existent [124, 125] neurodegeneration. Further, many of the modules with the strongest evidence of 'PD-like' pathology require modifications or truncations of native α-synuclein, limiting their relevance to modelling sporadic PD [126]. Although α-synuclein OE models based on the TH promoter are widely used, they inevitably fail to reproduce extra-nigral α-synuclein pathology [126].

The mechanisms of α-synuclein cytotoxicity are not fully understood, but it has been suggested that it is α-synuclein oligomers rather than LB which are harmful and that LB are formed as a protective mechanism [119, 127], a hypothesis which is supported by the fact the neurode-

generation precedes LB formation [13] and cytotoxicity following the application of exogenous α-synuclein oligomers to SH-SY5Y cells [128]. However, the data are not conclusive and Ko *et al.* reported the inducible formation of α-synuclein in a differentiated neuronal cell line with no loss to cellular viability [129]. Further, the formal possibility remains that it is infact the monomeric species that is cytotoxic [101]. Hypotheses for α-synuclein toxicity include: disruption of autophagy (*Subsection 1.4.2*), tau mediated microtubule instability [130, 131] (*Subsection 1.4.7*), disruption of ER-Golgi trafficking [90] (*Subsection 1.4.7*), damage to ER membranes leading to chronic ER stress [132] (*Subsection 1.4.4*), mitochondrial fragmentation [133], mitochondrial accumulation [134] and complex I inhibition [134] (*Subsection 1.4.3*).

α-Synuclein lies at the centre of the prion hypothesis of PD [14]. *In vivo* studies demonstrate that α-synuclein can be transferred from host to grafted cells in mice OE the human form of the protein [135]. Further, injection of pre-formed α-synuclein fibrils into the brains of wild type (WT) mice seeds aggregate formation and leads neurodegeneration [136]. The work of Freundt *et al.* demonstrated that α-synuclein fibrils can be transported along axons [137] and in recent months it has been reported that hind-limb intra-muscular injection of α-synuclein fibrils led to CNS α-synuclein inclusions and a progressive motor phenotype [138]. Further, aggregate formation was attenuated where the sciatic nerve was severed [138]. α-Synuclein is released from neuronal cells in exosomes which allow for the spread of the protein between cells [139] and levels of exosomal α-synuclein in blood plasma are significantly raised in PD patients [140]. Such a theory would also explain the presence of LB pathology in grafted neurones in the brains of PD patients [141], but is still an area of active research.

1.4.2 Autophagy

Autophagy is the process of cellular self-digestion by which damaged or unwanted organelles and long lived proteins are recycled. Autophagy may be subdivided into three key classes: macroautophagy (commonly referred to as autophagy), chaperone mediated autophagy (CMA) and microautophagy (*Figure 1.2*). These processes are particularly important in long lived, post-mitotic, cells such as neurones and autophagy dysfunction has been implicated in neurodegeneration [142].

Regulation of autophagy

Autophagy is controlled by approximately 35 autophagy related (ATG) proteins which are highly conserved between species. The genes are under the control of the master regulator transcription

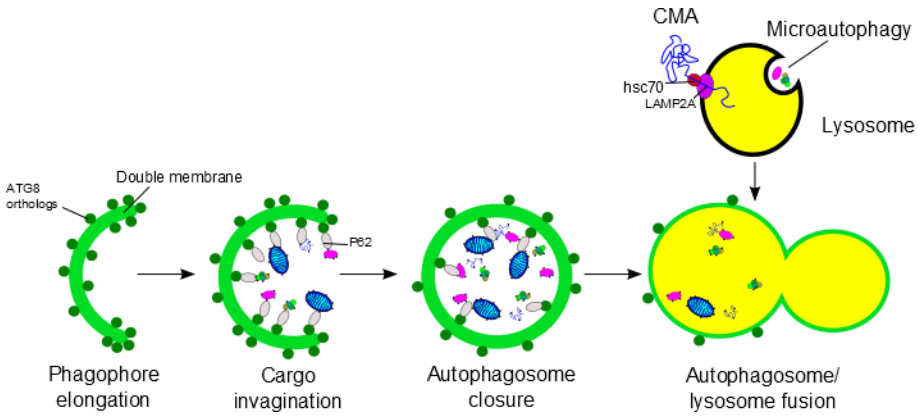

Figure 1.2: **Schematic showing the main stages of autophagy.** In macroautophagy, a double-phospholipid-bilayer cup (the phagophore) is formed and engulfs the cargo targeted for degradation. Once the membrane has closed around the cargo, to form a spherical vesicle, it is termed an autophagosome. Autophagosomes are formed throughout the cell then transported, in a dynein dependent fashion, to the microtubule organising centre where they fuse with lysosomes to form autophagolyosomes [143]. Autophagosome trafficking is essential for degradation and where trafficking is impeded aggregates are formed [99, 144]. The lysosome contains the proteases required for protein degradation and maintains the low pH needed for their function. Once proteins and organelles have been degraded their constituent amino acids are transported back into the cytoplasm and reused [145]. CMA facilitates the breakdown of long lived soluble proteins with a specific pentapeptide motif (KFERQ) and is estimated to be responsible for the degradation of approximately 30% of cytosolic proteins [146]. The pentapeptide motif is recognised by the chaperone heat shock cognate 70 (HSC70), the protein unfolded and translocated across the lysosomal membrane via lysosome-associated membrane glycoprotein 2A (LAMP2A). The final form of autophagy is microautophagy during which the lysosome directly engulfs a portion of the cytoplasm [145].

factor EB (TFEB) which also controls lysosome biogenesis allowing a coordinated response to external stimuli [147]. Basal autophagy occurs at all times however, the process is upregulated under starvation conditions (either a shortage of glucose or amino acids) or in response to growth factors such as insulin [148].

Under nutrient rich conditions the mTOR (mammalian target of rapamycin) complex 1 (mTORC1) complex phosphorylates and inactivates the serine/threonine-protein kinase ULK1 (ULK1)-ATG13- FAK family kinase-interacting protein of 200 kDa (FIP200) complex (ULK1-ATG13-FIP200 complex), ortholog of the ATG1 complex in yeast. However, several pathways sensing starvation conditions converge on the mTORC1 complex and mTORC1 inhibition leads to the activation of the ULK1 complex [149]. ULK1 activation results in the activation of the phosphatidylinositol 3-kinase catalytic subunit type 3 (VPS34)-Beclin1 (mammalian ortholog of ATG6) complex [149]. VPS34 is a class III PI3 kinase and its activation leads to the synthesis of phosphatidylinositol 3-phosphate, a key component in the autophagosome membrane [149]. Beclin1 is widely considered to be central to both the regulation of autophagy and the crosstalk between autophagy and apoptosis [150]. However, Beclin1 independent routes for the upregulation of autophagy have been investigated [151] of particular relevance, extracellular

signal-regulated kinase 2 (ERK2) mediated autophagy in response to neurotoxin exposure has been demonstrated under some experimental conditions [152–154].

In most situations, the formation of the phagophore is mediated by two, highly conserved, conjugation systems: the conjugation of ATG12 to ATG5 and the conjugation of ATG8 orthologs (following their cleavage by ATG4) to the lipid phosphatidylethanolamine [149]. The former reaction is mediated by ATG7 and ATG10 and the ATG5-ATG12 complex interacts with ATG16L in a non-covalent manner to form a complex which is essential for phagophore formation; the latter reaction is mediated by ATG3 and ATG10 [149]. The ATG8 orthologs (LC3 (microtubule-associated proteins 1A/1B light chain 3) and GABARAP (gamma-aminobutyric acid receptor-associated protein) subfamilies) act as scaffolds recruiting proteins to the phagophore, allowing the selective degradation of ubiquitinated proteins and stabilising complexes including the ULK1 complex [155]. It should be noted that the presence of an ATG5/ATG7 independent pathway for macroautophagy has also been discovered, in which ATG8 ortholog lipidation is also absent [156]. However, although ATG5/ATG7 independent autophagy has been demonstrated in KO mice, it is not clear to what extent the pathway is active under physiological conditions.

Autophagy in PD

The Cre recombinase enzyme catalyses recombination between two LoxP sites; a gene sandwiched between two LoxP sites is said to be flanked by LoxP (floxed). Mice expressing Cre recombinase under the control of both general and tissue specific promoters are available, the nestin promoter allows for specific neuronal expression of Cre recombinase. The cross of a $Atg7^{flox/flox}$ and a nestin-*Cre* results in the neuronal expression of Cre-recombinase in mice with floxed *Atg7* and the genes deletion, achieving a neuronal specific *Atg7* KO. The neuronal KO of *Atg5* or *Atg7* leads to the ablation of autophagy and consequent neurodegeneration in mice, even in the absence of disease related proteins [157, 158]. Inducible Cre strains are also available such that Cre recombinase is only expressed (and KO only achieved) upon exposure to an inducing agent (typically doxycycline, tetracyclin or tamoxifen) this allows the ablation of autophagy to be achieved after embryonic development.

Further evidence for the role of autophagy in neurodegeneration comes from PD post mortem brain samples which have increased autophagosomes [7]. There was some debate as to whether autophagosome accumulation indicated increased autophagy or a blockage in the autophagic pathway [145]. However, additional data indicate lysosomal dysfunction in the brains of PD patients [159, 160].

Further evidence of lysosomal dysfunction in PD comes from the increased risk of PD in individuals either homo- or heterozygous for *GBA* mutations [161]. Fibroblasts from individuals with *GBA* mutations, cells treated with GCase inhibitors, GBA KD or expressing of mutant forms of the GCase protein exhibit mitochondrial dysfunction, oxidative stress and the accumulation of α-synuclein offering potential mechanisms for increased PD risk [38, 161, 162]. Gegg *et al.* conducted a study of post mortem tissue from sporadic PD patients and those carrying *GBA* mutations [163]. The authors reported decreased GCase levels and activity in both groups with no change in lysosomal number or *GBA* mRNA. The two groups showed similar α-synuclein accumulation and LB pathology suggesting that PD pathology follows a similar pathway in sporadic and heterozygous *GBA* mutation cases [163]. The authors extended their work to an *in vitro* study and demonstrated that α-synuclein OE or PINK1 KD result in decreased GCase activity and propose that, 'PD pathology is exacerbated and accelerated, but not necessarily initiated, by *GBA* mutations' [163]. In an alternative approach, a recent study of iPSC-derived neurones from individuals with *GBA* mutations highlighted impaired autophagosome/lysosome fusion and increased α-synuclein levels suggesting that autophagic defects may lead to the increased prevalence of PD among individuals with heterozygous *GBA* mutations [57].

Providing a further link between autophagy and PD, severe lysosomal defects are seen in patients with the homozygous *ATP13A2* mutation which leads to hereditary parkinsonism [164]. The protein is also found at decreased levels in the brains of sporadic PD patients [29, 164].

Autophagic degradation of α-synuclein

The central PD protein α-synuclein is degraded via CMA [165] and macroautophagy [166]. Intriguingly neither mutant α-synuclein nor post-translationally modified forms of the protein can be broken down by CMA and both mutant and DA-modified α-synuclein block CMA for other proteins [165, 167]. Inhibition of CMA leads to a subsequent increase in macroautophagy, which may explain the increased number of autophagosomes observed in the brains of PD patients [168]. α-Synucelin may also be degraded via the proteasomal pathway; however, there are conflicting results as to the effect of proteasomal inhibitors on cellular levels of α-synuclein *in vitro* [171].

Decreased levels of the CMA proteins LAMP2A (lysosome-associated membrane glycoprotein) and HSC70 (chaperone heat shock cognate 70) have been reported in the brains of PD patients and is thought to be due to an upregulation of the miRNA (micro RNA) supressing their expression [168, 169]. Decreased CMA may partially explain the increased levels of α-synuclein

seen in PD. Further, differential levels of CMA have been suggested to underlie the selective protein aggregation and cell death seen throughout the brain [170]. OE of LAMP2A decreases α-synuclein levels in both *in vitro* and *in vivo* disease models [171].

α-Synuclein monomers and aggregates can also be degraded by macroautophagy [166, 172]. LB in PD patients colocalise with several key autophagy proteins including ubiquitin-binding protein p62 (P62), ubiquitin and LC3 and it has been suggested that LB may form as the result of failed autophagic degradation of toxic α-synuclein oligomers [159, 164, 172, 173]. The neuronal transcription factor myocyte enhancer factor 2D (MEF2D) provides a potential link between the autophagic degradation of α-synuclein and neuronal cell death. MEF2D is essential for neuronal survival and is also a CMA substrate [174]. OE of both mutant (A53T) and wild type α-synuclein resulted in the accumulation of a non-functional form of MEF2D, a decline in overall MEF2D function and cytotoxicity [174]. An alternative link between the autophagic degradation of α-synuclein and cell death came from the observation that increased α-synuclein levels inhibited the earliest stages of autophagosome formation thereby preventing the degradation of other proteins and organelles [175].

Links between other genes mutated in familial PD and autophagy

There are links between other genes mutated in familial PD and autophagy. Parkin and PINK1 are essential for mitophagy, the breakdown of damaged mitochondria via the autophagic pathway [176, 177] in response to mitochondrial depolarisation [176–178]. PINK1, in concert with Beclin1 [179], recruits parkin to damaged mitochondria where the ligase ubiquitinates the mitochondria allowing the organelles to be aggregated and degraded in a P62 dependent fashion [180, 181]. Recent mechanistic investigations into mitophagy indicated that PINK1 phosphorylated both ubiquitin and parkin, but that the reaction between parkin and ubiquitin was dependent on ubiquitin and not parkin's phosphorylation state [182]. It has been hypothesised that inhibition of the PINK1 and parkin pathway may lead to the build-up of damaged and dysfunctional mitochondria thereby increasing cellular oxidative stress [176, 178].

LRRK2 also plays a role in regulating autophagy. The protein is found in autophagosomes and expression of the mutant R1441C form of the protein leads to the inhibition of autophagy and accumulation of partially degraded autophagic bodies in *in vitro* PD models [183]. Further, normal, but not G2019S mutated, LRRK2 is a CMA substrate [56] and iPSC-derived neurones with G2019S-*LRRK2* mutations displayed defects in autophagosome clearance and increased autophagosome numbers [59]. The work of Plowey *et al.* demonstrated that the neurite short-

ening caused by *LRRK2* mutations occurred via an autophagic mechanism as neurite retraction seen upon OE of the G2019S form of LRRK2 was exacerbated by co-treatment with rapamycin and ameliorated following ATG7 KD [184]. This work illustrated how excessive autophagy, as well as the blockage of the process, can be harmful [184].

Finally, OE of the neuroprotective protein DJ1 promotes autophagy in both *in vivo* and *in vitro* models of PD via a Beclin1 dependent mechanism [185]. The evidence of links between autophagy and many of the proteins mutated in familial PD have led to the suggestion that the autophagy/lysosome pathway unifies familial forms of PD [142, 160].

Neurotoxins and autophagy

Neurotoxins used to model PD also lead to the dysregulation of autophagy with evidence that MPTP/MPP^+ [186, 187], rotenone, paraquat and 6-OHDA treatment all result in the accumulation of autophagosomes [188, 189]. There is debate as to whether autophagosome accumulation reflects increased autophagy or a blockage in the process [188]. However, these toxins have been shown to result in lysosomal [159] and trafficking dysfunctions [190] which inhibit autophagic flux.

1.4.3 Mitochondrial dysfunction

Multiple sources of evidence place mitochondria at the centre of PD aetiology. The mitochondria are the key site of cellular adenosine diphosphate phosphorylation (ADP) via the tricarboxylic acid cycle, which occurs in the mitochondrial matrix, and oxidative phosphorylation, which occurs on the inner mitochondrial membrane [191]. Parkinsonism causing neurotoxins MPP^+ and rotenone are complex I inhibitors and lead to cell death downstream of mitochondrial dysfunction (*Subsection 1.3.2*). Monogenic mutations in the mitochondrial proteins PINK1 and parkin disrupt mitophagy and lead to an accumulation of dysfunctional mitochondria (*Subsection 1.4.2*) [176, 178]. Further, iPSC-derived neurones carrying *PINK1* mutations have decreased complex I activity and a decreased mitochondrial membrane potential [52]. The parkinsonism inducing *ATP13A2* mutation also results in decreased ADP phosphorylation despite increased oxygen consumption rate - indicating mitochondrial dysfunction [192]. The inability of *ATP13A2* mutant fibroblasts to maintain a pool of functional mitochondria is though to be as a result of lysomal dysfunction and the consequent inhibtion of mitophagy.

Mitochondrial dysfunction is also linked to sporadic PD, with lower complex I activity in the SNpc [193], skeletal muscles [194] and platelets [195] of patients. Complex I deficiency may

arise from mutations in mitochondrial DNA and decreased complex I activity is seen in cybrid lines carrying mitochondria from PD patients [196]. Abundant mitochondrial mutations and deletions are observed in the SNpc of both aged control and PD patients, however, there is no significant difference between the two groups [197]. Tissues with a high dependence on oxidative phosphorylation (such as the brain) have a low tolerance for mitochondrial mutations and this could partially explain the selective degeneration seen in PD [191]. Mitochondrial mutations may also lead to decreased expression of mitochondrial genes and mice with a conditional KO of mitochondrial transcription factor A (*TFAM*) in DA neurones showed decreased expression of mtDNA and exhibited progressive motor defects and loss of DA neurones [198]. MPP^+ also decreases TFAM mediated mitochondrial gene expression [199].

The balance of mitochondrial fission and fusion is essential for mitochondrial health and where this is disrupted, dystrophin-related protein 1 (DRP1) dependent mitochondrial fragmentation may occur. Such fragmentation is observed in several genetic models of PD including: G2019S *LRRK2* mutations [200], *DJ-1* mutations [201], *ATP13A2* mutations [192], α-synuclein OE [133] and loss of parkin or PINK1 function [202]. MPP^+ treatment also results DRP1 dependent in mitochondrial fragmentation [203, 204]. The observation of mitochondrial fragmentation across a wide range of PD models implies that fragmentation may be a downstream effect of other pathogenic processes.

Within neurones, mitochondria are transported away from the cell body to the axonal and dendritic processes to provide adenosine triphosphate (ATP) required for synaptic activity [191]. The neurones of the SNpc are characterised by their long, unmyelinated axons and DA mouse neurones exhibit unusually slow mitochondrial transport which is further decreased following MPP^+ treatment [190]. Such slow transport may explain the increased vulnerability of the terminals of DA neurones to degeneration.

1.4.4 Oxidative stress

Mitochondrial dysfunction leads to the increased generation of ROS (high energy oxygen species including radicals, peroxides and superoxides) and cellular oxidative stress - the state where ROS overwhelm antioxidant mechanisms. There is also evidence of increased protein/lipid/DNA oxidation and nitration in the brains of idiopathic PD patients [205]. There is debate as to whether oxidative stress is causal or an effect of cell death; however, cybrid lines carrying mitochondria from PD patients with decreased complex I activity exhibit increased ROS levels and subsequent α-synuclein oligomerisation [206]. Decreased antioxidant levels are also seen in

the SNpc of PD patients with diminished glutathione observed early in disease progression [207].

DJ1 provides a link to familial PD, the protein is oxidised under conditions of oxidative stress and relocalises to the mitochondria, protecting cells [208]. Further support for the role of oxidative stress in PD comes from neurotoxin models. Complex I inhibition results in ROS production [209] and glutathione oxidation [210]. Additionally, co-treatment with antioxidants or [98, 204, 211] OE of cellular antioxidants [212] is protective, demonstrating that ROS production (downstream of mitochondrial dysfunction) is required for cell death. 6-OHDA is able to cause selective neurodegeneration through the generation of ROS in DA neurones, despite not interacting with complex I [66].

ROS lead to cell death by a number of mechanisms. Perier *et al.* demonstrated that ROS oxidise cardiolipin and result in an increased readily releasable pool of cytochrome C - priming cells for of apoptosis regulator BAX (BAX) mediated cell death [213]. Additionally, ROS lead to oxidation of lysosomal membranes impeding autophagy [159](*Subsection 1.4.2*) and damage to DNA [205].

Cellular iron is a further source of oxidative stress. Iron is accumulated in the SNpc of PD patients [193] and increased transferrin transcription occurs following MPP^+ treatment [98]. Cellular iron leads to the production of hydroxyl radicals via Fenton chemistry [214]; iron influx is required for cell death [98] and upregulation of α-synuclein expression [215] in MPP^+ models.

Oxidative stress is a major cause of ER stress. The ER is the site of protein and lipid synthesis (in addition to Ca^{2+} storage) and during ER stress proteins cannot be properly folded and therefore accumulate [216]. In response to ER stress cells initiate the unfolded protein response (UPR) a series of processes including: inhibiting protein translation, accelerating protein degradation and increasing levels of molecular chaperones. Some DA neurones of PD patients (although not controls) are immunoreactive for UPR markers and these neurones also exhibit α-synuclein accumulation [217]. In mice OE WT and mutant human α-synuclein, the protein accumulated in the ER and accumulation was decreased by treatment with the anti-ER stress compound salubrinal [132].

Beyond environmental toxins and mitochondrial dysfunction, DA and calcium influxes are major sources of oxidative stress (*Subsections 1.4.5* and *1.4.6*).

1.4.5 Dopamine

DA depletion and reduced DA release are hallmarks of PD [10]. DA is synthesised from tyrosine which is converted to *L*-DOPA by TH in a rate limiting reaction; *L*-DOPA is then converted to DA by amino acid decarboxylase (AADC) (*Figure 1.3*). DA is degraded to 3,4-dihydroxyphenylacetic acid (DOPAC) by MOA in a process generating H_2O_2 and DA may also be auto-oxidised to DA quinones [218] which are a key source of oxidative stress. The formation of quinones and ROS may contribute to the selective vulnerability of DA neurones. Further, vulnerable A9 neurones are unique in their neuromelanin pigmentation. Neuromelanin is an auto-oxidation product of DA and may be neuro-protective due to its ability to sequester iron [219]. However, the release of neuromelanin, upon cell death, activates the surrounding microglia and can initiate an aggravating inflammatory response [219].

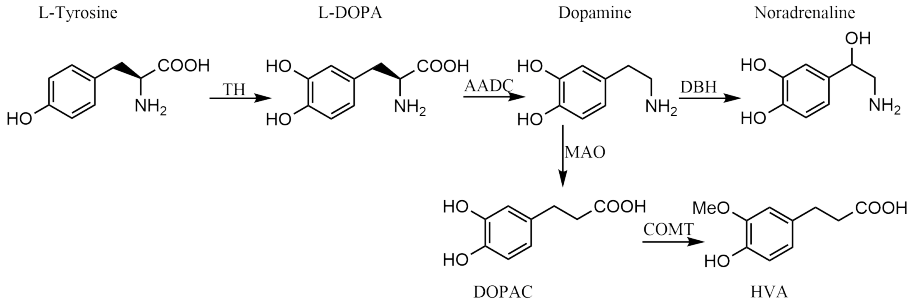

Figure 1.3: **Dopamine biosynthesis.** Key intermediates and enzymes in dopamine biosynthesis and degradation.

DA exposure alone is neurotoxic *in vitro* [220] and some reports indicate that DA is required for α-synuclein toxicity and that α-synuclein potentiates the generation of ROS from DA [119]. It also seems probable that ROS generated following MPP^+ treatment partially originate from the oxidation of DA [221]. DA toxicity is ameliorated by co-treatment with anti-oxidants [222].

To prevent cytotoxicity, DA is sequestered to cytoplasmic vesicles, sequestration is controlled by vesicular monoamine transporter 2 (VMAT2). Mice expressing decreased levels of VMAT2 display a progressive loss of DA neurones and motor defects [223]. Whereas, mice OE VMAT2 show increased vesicular DA content and synaptic DA release [224]. Further, vesicles extracted from the brains of PD patients show decreased VMAT2 mediated DA uptake [225].

DA may also potentiate rotenone toxicity [226, 227]. Although depletion of DA using the TH inhibitor alpha-methyl-*p*-tyrosine (AMPT) did not affect rotenone vulnerability of PC12 cells. Dukes *et al.* found that methamphetamine co-treatment did increase rotenone vulnerability, indicating a role for DA in rotenone toxicity. In a contrasting approach, Kweon *et al.*'s study into the effect of DA on rotenone neurotoxicity utilised two immortalised neuronal cell lines (DA

MN9D and non-DA MN9X) in a post-mitotic state [227]. The DA cells were shown to be more vulnerable to rotenone although their vulnerability was not altered by DA depletion. However, cytotoxicity in the two populations occurred via different mechanisms with the non-DA cells more affected by oxidative stress and the DA cells displaying decreased ATP and mitochondrial membrane potential [227].

A key link between α-synuclein and DA comes from α-synuclein's role in synaptic DA release (*1.4.1*). Further, α-synuclein affects DA synthesis through supressing transcription and preventing the activation of TH and decreasing AADC activity, although not levels [111, 116].

Other proteins mutated in familial PD have been linked to DA release and in a BAC transgenic *LRRK2* mouse model displaying few other phenotypes, increased DA release (compared to WT mice) was observed following electrical stimulation. The increased DA release was abolished when mutant (G2019S) LRRK2 was expressed [228].

1.4.6 Calcium influx

Large, poorly buffered influxes of calcium ions may contribute to the selective vulnerability of the DA neurones of the SNpc [229–231]. All neurones maintain a negative resting potential by pumping sodium ions out of cells. Typically, when depolarisation reaches a threshold level an action potential is triggered (sodium channels are opened resulting in a reversal of membrane potential) and travels down the neurone. This process allows communication between neurones. An influx of calcium ions is also observed following depolarisation, but calcium channels are slow to close such that the extent of calcium influx depends on the length of the spike. Cells with slow autonomous pace-making function (including those of the SNpc) exhibit broad spikes and therefore large oscillations in calcium concentration [229, 230]. Calcium influx is exacerbated by the high levels of L type voltage dependent calcium channels (LTCC) (in particular $Ca_V1.3$) in the DA neurones of the SNpc [229]. Evidence of the importance of calcium influx in PD comes from a recent study of post mortem brains which demonstrated changes in the subtypes of calcium channels in a manner that would be predicted to increase calcium flux [232] and epidemiological studies which demonstrate that individuals treated with LTCC inhibitors have a decreased risk of PD [233]. Further, iPSC-derived neurones from PD patients with heterozygous *GBA* mutations exhibited increased intracellular calcium levels [57].

To maintain a concentration gradient both calcium and sodium ions must be pumped out of neurones or sequestered in organelles including mitochondria, lysosomes and the ER. Sequestration is an ATP dependent process and the energy demands for maintaining a calcium gradient

are particularly high as there is 20,000 fold concentration difference between the cytoplasm and extra-cellular space [229]. Cells of the SNpc also exhibit low levels of calcium binding proteins (such as calbindin or parvalbumin) increasing the effective concentration gradient to be maintained [229]. In contrast, the VTA, which contains DA neurones relatively spared in PD, has high levels of calbindin and does not display significant calcium oscillations [229, 231]. Further other areas of the brain severely affected in PD (including the DMV, locus coeruleus, raphe nuclei and olfactory bub) are unified by their slow pace-making activity and calcium oscillations [229, 230]. Maintaining a steep calcium concentration gradient, in the face of repeated ion influxes, leads to a high metabolic demand [234]. High metabolic demands result in a small respiratory reserve in affected cells leaving them vulnerable to sudden demands for energy [229, 234]. Further, high metabolic demands lead to higher levels of oxidative stress and increased mutations in mitochondrial DNA that pre-dispose the cells to death [230, 231].

Beyond its role in creating high metabolic demands, calcium plays an important role in other cellular processes implicated in PD. It has been suggested that calcium may regulate autophagic flux [187], contribute to α-synuclein aggregation [235], upregulate AADC activity [231] and that PINK1 can prevent calcium dysregulation [178, 214].

Calcium has also been linked to neurotoxin models of PD with increased intracellular calcium levels observed following MPP^+ or 6-OHDA treatment in PC12 cells [236]. Calcium influx is blocked using calcium channel blockers or chelators and, in the case of MPP^+ treatment, neurotoxicity is rescued by the prevention of the calcium influx which is thought to be required for mitochondrial membrane permeabilisation [236].

1.4.7 Intracellular transport

Intracellular trafficking has been suggested as a unifying systems-level process in PD aetiology with the proteins α-synuclein and tau particularly implicated [237]. Although PD is not a tauopathy, *MAPT* is consistently identified as a susceptibility locus following GWAS (*Subsection 1.2.2*) with the H1 haplotype conferring increased risk (the H2 haplotype results from a 970 kb inversion [238]). Tau is highly expressed in neurones and stabilises microtubules. The protein exists as six splice isoforms and the two haplotypes lead to differing ratios of the splice products [239] with the H1 haplotype favouring isoforms more prone to aggregation [240]. A key link between tau and α-synuclein comes from reports of tau immunoreactive LB in the brains of PD patients [241] and the observation of synergistic fibrillisation [242]. Further, α-synuclein is required for MPP^+ induced, GSK-3β (glycogen synthase kinase 3β) mediated tau

hyperphosphorylation which encourages tau fibrillisation [130, 131].

α-Synuclein is synthesised in the cell body and then axonally transported to the synapses, disturbances to α-synuclein transportation have been suggested as a link between α-synuclein and tau and as a pathological mechanism in PD [243]. Tau plays a key role in regulating the motor proteins dynein and kinesin which transport cargo towards the cell centre and periphery, respectively, and the interactions between tau and motor proteins are splice-isoform dependent with shorter isoforms having a greater effect on both motor proteins [244]. Additionally, decreases in kinesin levels occur in the early stages of sporadic PD and has been suggested that inhibition of intracellular transport may lead to the accumulation of α-synuclein in the cell body and axons where it overwhelms autophagic machinery, eventually leading to LB and Lewy neurites respectively [243].

Roy *et al.* have recently reported a *D.melanogaster* line in which tau and α-synuclein are co-expressed [245]. The abnormal phenotypes (including neurone loss and motor defects) observed were more severe when the proteins were co-expressed suggesting that the proteins partake in a common pathway [245]. The animals exhibited abnormal microtubule organisation and axonal aggregates (indicating impeded axonal transport) confirming the roles of tau and α-synuclein in cellular transport and the importance of such transport for cellular viability.

1.4.8 Selective vulnerability of the dopamine neurones of SNpc - a multi-hit hypothesis for Parkinson's disease

Many of the processes implicated in PD are systemic, yet the DA neurones of the SNpc are preferentially lost with the DA neurones of the VTA relatively spared [11] (*Section 1.1.1*). The particular vulnerability of the DA neurones of the SNpc is thought to stem from a number of factors including their highly branched architecture leading to a large surface area, the oxidative stress induced by the presence of DA (*1.4.5*) and poorly buffered Ca^{2+} influxes (*1.4.6*) [229, 230].

In 2004, Braak *et al.* noted that neurones affected in PD were characterised by long, thin axons and lack of myelin sheath leading to high energy demands [12]. More recent quantitative analysis of the DA neurones of the rat brain suggested that a single DA SNpc neurone had between 100,000 and 200,000 synapses, markedly more than any other type of neurone, and estimated to be an order of magnitude greater than the DA neurones of the VTA [246]. One estimate placed the number of synapses of a human DA neurone of the SNpc as high as 1 - 2.4 million with a total axon length of 4.5 m [246]. Such an enormous, unmyelinated arbor would place cells under huge bioenergetic demands to maintain cellular transport, protein synthesis and degradation,

membrane potential and synaptic transmission and Bolam and Pissadaki hypothesised that high energy demands place the cells in a position of unique vulnerability to any systemic mitochondrial dysfunction [246].

Driven by the observations that multiple monogenic mutations cause familial PD, Sulzer suggested that PD is the result of 'multiple hits' such that the combination of several processes leads to the death of DA neurones [247]. Sulzer further proposed that such hits could include changes to protein breakdown or sequestration (including those induced by α-synuclein), the accumulation of neuromelanin, mitochondrial dysfunction and neuroinflammation [247].

It is suggested that PD is caused by the interplay of multiple systems-level processes, as outlined above. There are clear interplays between the different processes and the balance of factors may vary between individuals, perhaps contributing to the heterogeneous nature of PD. Given such a multifactorial disease a systems biology approach allows for the interactions between dysfunctions in multiple systems to be modelled and it is suggested that such approaches will allow a better understanding of PD.

1.5 Current pharmacological Parkinson's disease treatments

There are currently no treatments capable of curing PD or slowing disease progression and after over 40 years of clinical use the DA precursor *L*-DOPA remains the 'gold-standard' treatment [248]. *L*-DOPA treatment increases DA levels in the brain, relieves motor symptoms and increases life expectancy [249]. However, many patients begin to experience 'wearing-off' effects and prolonged *L*-DOPA treatment almost inevitably results in dyskinesia which may be a source of significant disability [248].

L-DOPA is frequently administered in adjunct to MAO-B or catechol-*O*-methyltransferase (COMT)-inhibitors such as rasagiline and entacapone [250, 251]. These drugs prevent the degradation of DA and *L*-DOPA respectively and therefore increasing levels of the neurotransmitter. Combined treatment regimens lead to improved patient outcomes when compared to *L*-DOPA monotherapy [252]. An alternative adjunct to *L*-DOPA therapy is carbidopa (a systemic AADC inhibitor) which prevents the conversion of *L*-DOPA to DA outside of the brain. DA agonists (such as apomorphine, bromocriptine or cabergoline) are also used in the treatment of PD [253], these drugs activate the DA receptor in the absence of DA [254].

Other approaches that have been considered include the use of iron chelators and adenosine A_{2A} receptor antagonists. Iron levels are increased in the SNpc of PD patients and iron chelators

(such as desferrioxamine and deferiprone) are effective in PD models [255]; further drugs combining MAO inhibition and iron chelation have been developed, although these are not currently approved [256]. Adenosine A_{2A} receptor antagonists, such as caffeine [257], increase the effect of DA on the DA receptors [258]. Within the last year, the first A_{2A} receptor antagonist istradefylline was granted approval in Japan and a recent meta-analysis indicated that istradefylline leads to significant improvements in motor function when used in conjunction with *L*-DOPA [259].

Given the multifactorial nature of PD there has been significant interest in developing drugs that are capable of acting at multiple targets [260]. Although such drugs are not currently in use, molecules combining MAO inhibition and iron chelation [256] or MAO and adenosine A_{2A} receptor antagonism [261] appear promising in experimental models of PD. More generally, beyond PD, it has been demonstrated that the proteomic effects of drug combinations can be predicted from the linear superimposition of single drug treatments supporting the idea that combinatorial pharmacological treatments may be effective across a range of diseases [262].

1.6 Drug discovery

Traditionally drug discovery has focussed on Ehrlich's concept of a 'magic bullet' whereby a small molecule could be designed to make a single intervention and cure a disease [263–265]. Recent years have seen major advances in many areas relating to drug discovery: considerably larger chemical libraries and more rapid synthesis, rapid DNA sequencing, extensive libraries of 3D protein structures, high-throughput screening, transgenic mice and enhanced knowledge of disease mechanisms [263, 265, 266].

However, there has been a steady fall in the number of drugs approved per (inflation adjusted) billion dollars spent on research such that, on average, each new drug costs approximately $1.8 billion to develop [267]. Despite an estimated combined annual pharmaceutical R&D expenditure of $50 billion only 25 new molecular entities were approved by the US Federal Drug Authority (FDA) in 2013 [268]. Compounding low approval rates, many new approvals are drugs for targets which are already targeted by currently marketed drugs, so called 'me toos' [263, 268]. Additionally, increased regulatory burden and the larger, multi-centre trials required have contributed to an average development time of 13.5 years - a substantial period with patents limited to 20 years [267].

Despite considerable investment only 7% of small molecule drugs progress from candidate selec-

tion to market, with considerably less success for drugs targeting the CNS [263]. Of particular concern is the high attrition rate during clinical development (only one in nine molecules entering clinical trials results in approval), particularly as clinical stages are estimated to represent 63% of the total drug development cost [263]. Considerable savings would be made if inevitably unsuccessful drugs could be identified earlier [265, 267]. The primary reasons for late stage failures are poor efficacy and poor safety profiles. Improving the quality of target selection is one of the most important challenges facing the pharmaceutical industry [263, 265].

Combined, all currently marketed drugs have only a few hundred molecular targets, suggesting that there is still considerable space for new pharmaceuticals [265] and a number of hypotheses for the low success rates of pharmaceutical R&D have been proposed [263]. For a new drug to garner FDA approval it must be demonstrated that the drug is superior to currently available treatments; therefore, the required standard (in terms of efficacy or side effect profile) for drug approval in any therapeutic area will always increase. Further, in an effort to improve patient safety, the risk tolerance of regulatory agencies has consistently decreased such that drugs historically improved would no longer be considered to have an acceptable risk profile [263].

However, the ideology behind single target drug discovery may be flawed, explaining the poor efficacy of drugs which have high potency for desired target and the stubbornly low number of new drug approvals [263, 264, 269, 270]. Further, a focus on the end stage symptoms (e.g. inflammation) may not fully account for the different molecular pathways leading to similar outcomes [270]. This thesis aims to convince the reader that networks allow the complex interplay of factors to be considered and provide a superior system for modelling biology.

1.7 Modelling biological systems as networks

Networks are increasingly used to model complex systems across a diverse range of disciplines [96] and offer a compromise between extreme reductionism and an overly complicated knowledge of everything [265]. In a biological context, a species is represented by a node and nodes are connected by edges which represent some relationship between two species [95]. There are a number of different types of biological networks with nodes and edges representing different biological species and their interactions [95, 96]. In a gene network each node represents a gene and an edge may represent correlated expression (for example two genes are simultaneously up or down regulated following a given external stimulus) or similar or synergistic phenotypes in KO models [96]. Alternatively, in a metabolic network a node represents a metabolic species (for example a sugar molecule) and an edge represents that two such species can be intercon-

verted, normally by an enzymatic process [96]. This thesis focuses on protein-protein interaction networks (PPIN); in such networks a node represents a protein and an edge signifies that two proteins can physically interact.

This thesis considers PPIN the most appropriate network model as proteins are the most druggable biological species and the vast majority of currently approved drugs target proteins [271]; this work aims to validate targets that could potentially be used as drug targets. Gene networks have a powerful role to play in identifying the underlying causes of diseases [96, 272]. However, this thesis aims to identify points where an intervention might have a positive result, whether or not the protein was the underlying cause of the disease. This distinction has been described as that been between etiological and palliative drugs [273], where this thesis, in common with the majority of currently successful drugs [271], focuses on the latter.

In PPIN, proteins which undergo an interaction have been demonstrated to be involved in similar cellular functions [274] and a protein's characteristics may be predicted from those of its neighbours [275], termed, 'guilt by association' [274]. Through the extension of 'guilt by association', networks can be constructed to model biological systems and predictions made about the underlying organism. Although the human interactome is far from complete and reported protein protein interactions (PPI) have a high error rate, a considerable amount of human PPI data has been collected [276].

1.8 Concepts of network pharmacology

Biological networks are robust to single interventions (for a more detailed explanation see *Subsection 4.1.2*) and therefore, any 'magic bullet' would be unlikely to be effective. There is increased acceptance of the idea that multiple interventions will be required to treat complex diseases and overcome the problems of resistance [263, 270]; either through the combination of multiple drugs [277] or, despite the inherent challenges, by the design of drugs able to intervene at multiple targets [260].

Current drugs are known to exhibit a degree of promiscuity (interaction with proteins other than its target) [264, 265, 269, 273]. Even imatinib mesylate, the prototype specific small molecule inhibitor, exhibits multiple binding modes [278]. As multi-target approaches have become more accepted, drugs have been designed to interact at two established sites and it has been suggested that this property should be screened for during drug development [264]. The most effective drugs may have relatively weak binding affinity at a number of strategic positions, as opposed

to the nanomolar potency at a single target that is often a key selection criteria in the screening of potential drugs [265, 269]. Weaker, multi-target binding has also been proposed as a method to decrease the problems of drug resistance and toxicity [265]

Network pharmacology states that such strategic targets can be identified through network analysis and that therapeutics should be designed to have maximum impact on the system as a whole, rather than at a single site [264, 265]. Network pharmacology could be used to predict potential side effects, repurpose currently approved drugs for new application or prioritise leads identified from screening. However, it must be acknowledged that data regarding the molecular footprint of small molecules is far from complete and only 10-14% of proteins are currently considered 'druggable' [271].

Therefore, this work limits itself to using a network approach to identify proteins whose modulation can alter a disease state, whether or not they would be druggable; *in vitro* KD can be used to specifically delete a node and thereby validate a target. A number of others have used networks, including PPIN, to suggest potential drug targets [279–283] although there has so far been little experimental validation of network predictions.

1.9 Aims of thesis

There is an enormous unmet need for treatments for PD, a multifactorial disease with unknown aetiology. Network pharmacology in general, and PPIN in particular will be investigated as an avenue for identifying critical proteins in an MPP^+ model of the disease. Should such targets be successfully identified and results replicated in other PD models these proteins could be used as a starting point for designing multi-target PD drugs. This task will be approached in three main stages (corresponding to the results chapters of this thesis):

1. Exploration of the MPP^+ model in a human, dopaminergic, neuronal cell line to determine the effect of the neurotoxin on key systems-level processes and optimisation of sensitive assays.

2. The construction of PPIN to model MPP^+ toxicity and the identification of proteins predicted to be pivotal to neurotoxicity.

3. Testing of *in silico* predictions in the *in vitro* disease model.

Chapter 2

Materials and methods

2.1 Experimental methods

Except where otherwise stated, all reagents were purchased from Sigma.

2.1.1 Cell culture

The human DA neuroblastoma cell line BE(2)-M17 (M17) [284] (ECACC 95011816) and the mouse fibroblast cell line NIH 3T3 (3T3) [285] (ECACC 93061524) were obtained from the European collection of cell cultures. M17 cells were cultured in Opti-MEM (OM) (Gibco) supplemented with 10% v/v foetal bovine serum (FBS), 100 U/ml penicillin and 0.1 mg/ml streptomycin at 37 °C and in 5% CO_2. 3T3 cells were cultured in Dulbecco's modified Eagle medium (DMEM) (Sigma) supplemented with 10% v/v foetal bovine serum, 4 mM glutamine, 100 U/ml penicillin and 0.1 mg/ml streptomycin at 37 °C and in 5% CO_2. Cells were not grown beyond 25 passages and aliquots were stored at -80 °C.

Plates were pre-treated with poly-*L*-lysine (Sigma) and cells were seeded in 6, 12, 24 or 96-well plates at a seeding density of 1 x 10^5 cells/mL and grown overnight prior to treatment. Cells were treated with MPP^+ (Sigma), bafilomycin A1 (Abcam), rapamycin (Calbiochem), antimycin A, AMPT (Sigma) and CCCP (carbonyl cyanide *m*-chlorophenyl hydrazone) at the concentrations described for periods from 15 min to 96 h. All solutions were filtered (0.22 μm) prior to use.

2.1.2 Western blot

Cells were washed once with unsupplemented OM and then incubated in western blot (WB) lysis buffer [50 mM Tris, pH 8.0, 150 mM NaCl, 1 % v/v NP-40, 0.5 % w/v sodium deoxycholate,

0.1 % w/v sodium dodecyl sulfate (SDS), 1 X protein inhibitor cocktail (Roche)] for 30 min on ice. The lysate was cleared by centrifugation for 5 min at 1000 g and the supernatant retained. Protein content was quantified via bicinchoninic acid (BCA) assay (Sigma) in accordance with the manufacturer's instructions. Protein samples (20 μg) were boiled in 1 X Laemelli buffer [60 mM Tris pH 6.8, 2% SDS, 10% glycerol, 5% β-mercaptoethanol, 0.01% bromophenol blue] for 5 min. Protein was separated by SDS-polyacrylamide gel electrophoresis (10, 12 or 15% v/v resolving gel or 4-15% pre-cast gradient gel (Biorad)) and blotted on to a 0.45 μm polyvinylidene difluoride (PVDF) membrane (Immobolin) using a wet blotting protocol, or via the Trans-Blot-Turbo system (BioRad), according to manufacturers' instructions. Blots were blocked in WB blocking buffer [Tris-Buffered Saline (TBS), 1% v/v Tween-20 , 5% w/v milk] for 2 h at room temperature (RT) and then probed with primary antibodies diluted in WB blocking buffer overnight at 4 °C (*Table 2.1*). Following primary antibody incubations, membranes were washed three times with TBS, (1% v/v Tween-20) and the appropriate goat anti-rabbit or goat anti-mouse horseradish peroxidase-conjugated secondary antibodies (Bio-Rad) were applied for 1 h at RT, diluted in WB blocking buffer (1 in 5000 dilution). After washing, chemiluminesence was produced using Immobilon western chemiluminescent HRP (HorseRadish Peroxidase) substrate (Millipore). Images were photographed using Chemidoc XRS with images collected every 10 sec for 15 min and the most appropriate images selected for analysis. The intensity of each band was measured using gel analysis tool in ImageJ. Expression was normalised to actin levels in the same blot and expressed relative to untreated cells.

Antibodies were initially validated by comparing the apparent molecular mass of the band detected (estimated using Spectra Multicolor Broad Range Protein Ladder (Thermoscientific)) and the expected molecular mass of the protein. For proteins modulated, diminished intensity of band following siRNA mediated KD was used to further validate antibodies.

2.1.3 Assessment of cell viability

Several assays were employed to estimate cellular viability following transfection, MPP^+, bafilomycin A1, antimycin A, AMPT and CCCP treatment. The BioTek synergy HT plate reader was used to measure absorbance and fluorescence and the Dynex Technologies MLX 96 Well Plate Luminometer was used to measure luminescence. In all cases, each treatment condition was conducted in triplicate and values averaged; values for blank well were subtracted. Viability assays were conducted in 24- or 96-well plates with the exception of cell counts, which were conducted in 12-well plates.

Protein	Antibody type	Manufacturer and product number	WB concentration	ICC concentration
α-Synuclein	Mouse polyclonal	BD Biosciences, 610786	1:500	n/a
β-Actin	Rabbit polyclonal	Abcam, ab8227	1:2000	n/a
14-3-3ζ	Rabbit polyclonal	Santa Cruz, sc-1019	1:100	n/a
Calmodulin	Rabbit monoclonal	Abcam, ab45689	1:500	n/a
Cleaved caspase-3	Rabbit polyclonal	Alexa Fluor 488 conjugate	n/a	1:500
GABARAP	Rabbit polyclonal	Source Bioscience Lifesciences, 18723-1-AP	1:1000	1:500
GBRL1	Rabbit polyclonal	Source Bioscience Lifesciences, 11010-1-AP	1:1000	1:500
GBRL2	Rabbit polyclonal	Source Bioscience Lifesciences, 18724-1-AP	1:1000	1:500
LAMP1	Mouse polyclonal	Santa Cruz, sc-20011	1:200	1:200
LAMP2A	Rabbit polyclonal	Abcam, ab18528	1:1000	1:500
LC3B	Rabbit polyclonal	Sigma, L7543	1:500	n/a
LC3B	Rabbit polyclonal	Cell Signaling, #2775	n/a	1:100
mTOR	Mouse monoclonal	Cell Signaling, #4517	1:1000	n/a
Nemo	Rabbit polyclonal	Abcam, ab137363	1:500	n/a
P53	Rabbit monoclonal	Cell Signaling, #2527	1:500	n/a
P62	Mouse monoclonal	Abcam, ab56416	1:2000	1:500
P62	Rabbit monoclonal	Abcam, ab109012	n/a	1:500
PPP2R2B	Rabbit monoclonal	Abcam, ab157461	1:500	n/a
Tom20	Rabbit polyclonal	Santa Cruz, sc11415	n/a	1:1000

Table 2.1: **Antibodies used for western blot and immunocytochemistry**

Normalisation of data

Neutral red absorbance, TMRM fluorescence, MTT/MTS absorbance, luminescence from the ATP assay, cell counts and fluorescence from the live cell protease assay are reported as normalised values where 100% is the value achieved in untransfected, non-MPP^+ treated cells. This process ensured consistency between experiments where different aliquots of viability reagents, different cell densities and different treatment times with viability reagents were used. The normalisation process allowed treatment times with viability reagents (e.g. neutral red solution) to

be varied to ensure sensitivity at each time point, as cell proliferation resulted in increasing cell density. Normalisation was performed for each biological repeat and normalised values were then averaged to give the results and SEM displayed. For experiments conducted over a time course, normalisation was repeated at each time point. Average, unnormalised control values are given for each normalised figure as an indication of the raw data values obtained. Image quantification was normalised such that untreated samples had an intensity of one, no unnormalised values are reported as these are arbitrary, depending on the exposure selected for quantification. Protein degradation is reported as an absolute value without normalisation.

MTS

Cell proliferation was measured using Promega Cell Titer 96 AQueous Non-Radioactive Cell Proliferation Assay (MTS ((3-(4,5-dimethylthiazol-2-yl)-5-(3-carboxymethoxyphenyl)-2-(4-sulfophenyl)-2H-tetrazolium) and electron coupling reagent phenazine methosulfate (PMS)). Following treatment, cells were washed once with OM and then MTS solution was applied according to the manufacturer's instructions, using Phenol Red-free OM media (Gibco). Plates were incubated for a further 2 h and absorbance was measured at 490 nm to assess the extent of MTS to formazen conversion.

MTT

Alternatively, cell proliferation was measured using Sigma Cell Growth Determination Kit (MTT (3-(4,5-dimethylthiazol-2-yl)-2,5-diphenyltetrazolium)). Following treatment, cells were washed once with OM and then MTT solution was applied (stock solution was diluted 10 fold in FBS and antibiotic supplemented OM), 500 μL was applied to each well of a 24 - well plate or 100 μL to each well of a 96-well plate. Plates were incubated for a further 2 h, the MTT solution removed, cells washed once with OM and then lysed with MTT lysis solution (0.1 N HCl in *iso*propanol (Sigma), 500 μL in 24-well plate or 100 μL in 96-well plate). Absorbance was measured at 490 nm to assess the extent of MTS to formazen conversion.

Cell counts

Cell counts were used to measure the number of live cells. Cells were viewed under bright-field microscopy (20 x magnification) using Nikon Eclipse TC2000-U; three representative fields of view were photographed for each well and images were randomly labelled to ensure blind counting. A 400x400 pixel region was randomly selected within each image and all live cells

were manually counted using ImageJ. Only morphologically normal cells (those with intact processes) were counted as live.

Tetramethylrhodamine (TMRM)

Tetramethylrhodamine (TMRM) fluorescence was used as a marker of membrane potential. Following treatment, cells were incubated with 150 nM TMRM (Invitrogen) for 5 min and then washed four times with PBS (phosphate buffered saline). Fluorescence was measured at 544 nm excitation and 590 nm emission.

Neutral red

Neutral red accumulation was used a marker of acidic lysosomes. Lysosome acidification is ATP dependent; therefore where cell and lysosome number are content, ATP depletion results in decreased neutral red accumulation [286]. Cells were treated with 40 μg/L neutral red (Sigma) for 2 h and then washed with PBS. Destain solution [50% (v/v) ethanol, 1% (v/v) glacial acetic acid] (500 μL in 24-well plates or 100 μL in 96-well plates) was added to each well and plates were shaken for 5 min to ensure even mixing. Absorbance was measured at 540 nm.

Cellular ATP

Cell-Titer-Glo Luminescent Cell Viability Assay (Promega) was used to directly measure cellular ATP levels. The kit contains a luciferin and a luciferase; the luciferin undergoes luciferase catalysed mono-oxygenation in the presence of ATP, O_2 and Mg^{2+}. The luciferase reaction produces light in amounts proportional to ATP levels. The CellTiter-Glo solution was prepared according to manufacturer's instructions and added to treatment media in 96-well plates (100 μL). Plate contents were mixed for 2 min using an orbital shaker and luminescence signal allowed to stabilise for 10 min at RT before reading.

Protease activity

Following the pairwise KD screen cellular viability was estimated using the CellTiter-Fluor Cell Viability Assay (Promega) in 96-well plates. Solutions were prepared according to manufacturer's instructions. The cell permeable GF-AFC substrate undergoes protease mediated cleavage in live cells to generate a fluorescent molecule and can therefore be used as a measure of live-cell protease activity. The GF-AFC solution (100 μL) was added to treatment media and

incubated for 1 h, fluorescence (400 nM excitation, 505 nM emission) was measured as a marker of live cell protease activity.

2.1.4 Immunocytomchemistry

Coverglasses (13 mm) were sterilised with EtOH in 24-well plates and coated in poly-*L*-lysine. Cells were grown in the absence or presence (100 μM) of MPP^+, with or without transfections. Cells were washed once with PBS and then fixed using 4% v/v paraformaldehyde for 10 min before washing a further two times. Cells were blocked and permeabilised for 3 h at RT in PBS (10 % goat serum v/v, 0.1% v/v Triton-X 100), then incubated with primary antibodies overnight at 4 °C in PBS (1% v/v goat serum, 0.1% v/v Triton-X 100) (*Table 2.1*). Cells on coverglasses were then washed three times with PBS (0.1% v/v Triton-X100) and incubated with the appropriate 488, 594 or 647 nm fluorophore conjugated rabbit and mouse secondary antibodies for 1 h at RT, protected from light. Coverglasses were washed once with PBS (0.1% v/v Triton-X 100) then incubated with DAPI (4',6-diamidino-2-phenylindole) (1:2000) for 10 min and finally washed again with PBS. Coverglasses were mounted on slides using FluorSave (Calbiochem) and stored at 4 °C protected from light. Cells for caspase-3 activation analysis following MPP^+ treatment were viewed using Nikon Eclipse TC2000-U at (20 x magnification) and photographed using DAPI and green fluorescence filters. The images were merged and file names randomised to allow blind counting. The cells used to investigate autophagic processes following the combined protein OE were imaged using EVOS FL Auto (60 x magnification), using filters for DAPI, GFP (green fluorescent protein), Tx-Red and Cy5. All images were merged.

2.1.5 Flow cytometry

Cells were treated with MPP^+ in 12-well plates as detailed above. After 48 h cells were washed with PBS and then incubated with 500 μL of trypsin for 5 min. The trypsin was neutralised with 500 μL of FBS supplemented OM and the cell suspension was transferred to an eppendorf and pelleted by centrifugation at 2,000 RPM for 5 min. The supernatant was removed and cells were washed three times with ice cold PBS (500 μL). Cells were resuspended in 100 μL of binding buffer (Beckman Coulter), and 10 μL of annexin-V-FITC (Beckman Coulter) was added. Cells were incubated for 30 min on ice, protected from light. A further 400 μL of binding buffer and 10 μL of 7-aminoactinomycin D (7-AAD) (Beckman Coulter) was then added and the cells were incubated for a further 30 min on ice, protected from light. A Calibur flow cytometer

was used to separate the cells and the forward/side scatter plot was used to gate the intact cell population following consultation with the flow cytometer technician; 10,000 events in this region were collected.

2.1.6 siRNA (small interfering RNA) transfection

KD was achieved using siRNA (*Table 2.2*); ScramSN1 was used as a transfection control. Prevalidated siRNA (Life Technologies) were used with the exception of *SNCA* for which a sequence previously designed and validated within the Wade-Martin's laboratory was utilised [114]. An initial siRNA concentration of 50 nM and the transfection protocol had been previously optimised within the Wade-Martin's laboratory to maximise transfection efficiency and KD. Where this proved ineffective (as assessed by WB), siRNA concentration was increased to 100 nM to improve KD. KD of at least 52% was achieved for all proteins modulated in this thesis.

Procedures were initially carried out in 12-well plates, but later developed in 24-well plates with all volumes halved to achieve the same final concentrations. All siRNA transfections were conducted in an RNase and contamination free environment; RNase Zap (Sigma) was used to decontaminate all surfaces, equipment and unused pipette tips. Prior to transfection cells were washed three times with unsupplemented OM, then 700 μL of unsupplemented OM was added to each well. For each well to be transfected, 3 μL of LF2000 (Invitrogen) was resuspended in 150 μL of OM and incubated for 5 min at RT. Simultaneously, each siRNA was resuspended in 150 μL of OM for 5 min. The siRNA and LF2000 mixtures were subsequently combined and incubated at RT for 20 min to allow complex formation, 300 μL mixture was then added to cells in a drop-wise fashion. After 6 h at 37°C, 300 μL of OM with 30 % v/v FBS was added to the wells (no antibiotics). Then, 24 h after transfection the media was removed and replaced with 1 mL of OM supplemented with FBS and antibiotics. KD was assessed by WB 48 h after transfection. In the experiments where KD was combined with MPP^+ exposure, MPP^+ was added 24 h after transfection (approximately 36 h after initial cell seeding). Cell viability assays were conducted at the stated time points.

Pairwise KD

Pairwise KD were conducted in 96 well plates. Each row and column was assigned a protein so that the same proteins were targeted along the diagonal. The order of proteins was randomised between experiments to mitigate any edge effects. Cells were seeded on poly-*L*-lysine coated plates as above, and washed prior to transfection. For each well to be transfected, 375 nL

Gene	Protein	Conc. (nM)	Ambion product number	Sequence
ScramSN1	n/a	50	AM16106	GAGAAUAGGGAGGAGAACAtt
CALM1	Calmodulin	50	s2340	AGGCAUUCCGAGUCUUUGAtt
CALM2	Calmodulin	50	s2345	CAAAGAAGCUUUUUCACUAtt
CALM3	Calmodulin	50	s2346	AGAUGAUCAGGGAGGCUGAtt
FRAP1	mTOR	100	s603	CAUUCGCAUUCAGUCCAUAtt
GABARAP	GABARAP	50	s22362	AGAAGAUCCGAAAGAAAUAtt
IKBKG	Nemo	100	s16186	AAACAGGAGGUGAUCGAUAtt
MAP1LC3B	LC3B	50	s37748	AUGUCCGACUUAUUCGAGAtt
PPP2R2B	PPP2R2B	100	s10971	GGGACUACUUGACCGUCAAtt
SQSTM1	P62	50	s16962	CUUCCGAAUCUACAUUAAAtt
TP53	P53	50	s605	GUAAUCUACUGGGACGGAAtt
YWHAZ	14-3-3ζ	50	s14970	GGAGGGUCGUCUCAAGUAUtt

Table 2.2: **siRNA used for protein knockdown.** All siRNA were purchased from Life Technologies.

of LF2000 was resuspended in 15 μL of OM and incubated for 5 min at RT. Each siRNA was resuspended in 15 μL of OM per well and after 5 min, the siRNA and LF2000 mixtures were combined and incubated at RT for 20 min. The mixtures were subsequently diluted with OM to give a total volume of 50 μL per well. In a column-wise fashion, the final wash was removed from each set of wells and 50 μL of the relevant transfection mix added to each well. A second transfection mix was then added in a row-wise fashion (50 μL per well) so that each well contained two different siRNAs in 100 μL of OM (except along the diagonal). After 6h, 30 μL of OM with 30 % v/v FBS was added to the wells (no antibiotics) and from this point the protocol continued as in *Subsection 2.1.6*.

2.1.7 Preparation of plasmids

Preparation of Electrocompetent Cells

DH10B E-Coli bacteria were cultured in 1.5 mL of lysogeny broth [10 g/L NaCl, 10 g/L tryptone, 5 g/L yeast extract] at 37 °C overnight, shaken at 225 RPM. Cultures were then tipped into a further 100 mL of lysogeny broth and grown at 37 °C until optical density at 600 nm was between 0.35 and 0.36. Cultures were cooled to 0 °C for 40 min and then pelleted at 2400 g, 4 °C for 15 min. The pellet was washed three times with 100 mL of 10% v/v glycerol, following each wash the bacteria were pelleted at 4 °C and the following speeds for 15 min, 3500 g, 4700 g and 5400 g. After the final wash cells were resuspended in minimal glycerol and split into 50 μL aliquots which were snap frozen before storage at -80 °C.

Electroporation

Prior to electroporation, an aliquot of electrocompetent cells was slowly thawed on ice then 5 μL of DNA was added and the mixture was transferred to a 0.1 cm electroporation cuvette. Electroporation was conducted using a Gene Pulser Xcell (Bio Rad) at capacitance 35 μFD, resistance 20 Ω and voltage 1.8 kV. Immediately following electroporation, 450 μL of RT SOC medium (Invitrogen) was added and the mixture was incubated at 37 °C for 1 h. Bacteria were plated on agar plates with appropriate antibiotics and grown at 37 °C overnight.

Miniprep

A single culture was picked and grown in 1.5 mL of lysogeny broth overnight at 37 °C with shaking. The bacteria were pelleted by centrifugation at 2400 g for 10 min. The supernatant was aspirated and the pellet was resuspended in 70 μL of STET buffer [8% sucrose (w/v), 5% Triton X 100 (v/v), 50 mM EDTA, 50 mM Tris.Cl (pH 8)]. Bacteria were lysed using 200 μL of alkaline SDS [1% SDS (w/v), 0.2 M NaOH] solution and then neutralised with 150 μL of 7.5 M ammonium acetate. The neutralised lysate was cooled on ice for 5 min and then centrifuged at 16,200 g for 20 min at 4 °C. The supernatant was mixed with 250 μL of *iso*propanol and the DNA pelleted by 8 min centrifugation at 16,200 g. The DNA pellet was washed with 200 μL of 70% v/v ethanol and allowed to air dry. Finally, the DNA was resuspended in TE [10 mM Tris, 1 mM EDTA, pH 8] containing 5 μgml^{-1} RNase A (Qiagen).

Gel electrophoresis

Agar gels (1% w/v) with 0.004% v/v ethidium bromide were prepared and used with TE buffer. Plasmid DNA (200-400 ng) was incubated for 3 h at 37 °C with 0.2 μL of appropriate restriction endonucleases (New England Biolabs), 1.5 μL of appropriate 10x buffer (New England Biolabs) and 0.15 μL of 100x BSA (bovine serum albumin) (New England Biolabs) in a total volume of 15 μL. Following digestion, the products of each reaction were mixed with 7μL sample buffer [15% (v/v) Ficoll, 0.025% (v/v) xylene cyanol] and the entire volume loaded onto the gels. Gels were run for 2-6 h at 70 V and visualised using Chemidoc XRS. The molecular weight of each band was estimated using GeneRuler 1kb Plus DNA Ladder (Thermo Scientific).

Maxiprep

A maxiprep plasmid purification kit (Qiagen) was utilised to prepare larger amounts of DNA suitable for transfection. A single colony, whose identity had been confirmed by miniprep and subsequent digestion, was grown overnight in 250 mL of lysogeny broth at 37 °C, shaken at 300 RPM. Bacteria were pelleted by centrifugation at 5000 RPM for 10 min at 4 °C. Bacteria were completely resuspended in 15 mL of Resuspension Buffer + RNaseA. The suspension was then incubated for 5 min at RT with 15 mL of Lysis Buffer before neutralisation with 15 mL of Neutralisation Buffer. The suspension was mixed before loading onto an equilibrated NucleoBond Xtra Column and Filter and allowed to empty under gravity. The filter was washed with 15 mL of Equilibration Buffer and then discarded. The column was then washed with 25 mL of Wash Buffer before elution of the DNA using 15 mL of Elution Buffer. The DNA was precipitated with 10.5 mL of *iso*propanol and then pelleted by centrifugation at 14,000 RPM for 30 min at 4 °C. The pellet was washed with 5 mL of 70% v/v ethanol, centrifuged at 14,000 RPM for 30 min (4 °C) and allowed to dry at RT. Finally the DNA was resuspended in 300 μL of TE, DNA concentration was determined by measuring absorbance at 260 and 280 nm using the Nano Drop ND-1000 Spectrophotometer (Thermo Scientific) and samples stored at -20 °C.

2.1.8 DNA transfection

The following plasmids were cloned for transfection: HA-P62 (gift of Qing Zhong, Addgene plasmid # 28027), pEGFPc1-GABARAP, pEGFPc1-GBRL1 (GABARAP Like 1) and pEGFPc1-GBRL2 (GABARAP Like 2) (all gifts of Kunikazu Tanji). Procedures were carried out in 12-well plates, but later used in 24-well plates with all volumes halved to achieve the same final concentrations. Before transfection cells were washed three times with unsupplemented OM then 700 μL of unsupplemented μL of OM was added to each well. For each well to be transfected, 3 μL of LF2000 (Invitrogen) was resuspended in 150 μL of OM and incubated for 5 min at RT. Simultaneously, for each well to be transfected, 1.5 μg of each plasmid was resuspended in 150 μL of OM and incubated for 5 min at RT. Where combined transfections were utilised, all plasmids were mixed at this stage. Subsequently, the DNA and LF2000 mixtures were combined and incubated at RT for 20 min to allow complex formation and 300 μL of the mixture was added drop-wise to each well of cells. After 6 h at 37 °C, 300 μL OM supplemented with 30 % v/v FBS was added to the wells (no antibiotics). Then, 24 h after transfection, the media was removed and replaced with 1 mL of OM supplemented with FBS and antibiotics. OE was assessed by WB and fluorescence microscopy 48 h after transfection. Where OE was combined

with MPP^+ exposure, MPP^+ was added 24 h after transfection (approximately 36 h after initial cell seeding). Cell viability assays were conducted at the stated time points.

2.1.9 Preparation of RNA for microarrays

RNA was extracted from control and MPP^+ treated cells (100 μM, 24 h, 6-well plates) prior to microarray analysis using the RNeasy Mini Kit (Qiagen). Cells were washed once with PBS and lysed directly using Buffer RLT (600 μL per well). The lysate was collected using a rubber policeman, transferred to an eppendorf and pipetted to mix. The lysate was next transferred to the QIAshredder spin column, placed in a 2 mL spin column and collection tube and centrifuged for elution at 13000 g for 2 min. A solution of 70 % RNase free ethanol (600 μL) was added to the supernatant and pipetted to mix. The sample was transferred to an RNeasy spin column and placed in a 2 mL collection tube. The column and collection tube were centrifuged at 8000 g for 15 sec and flow-through discarded. A DNA digest was performed as follows: the column was washed with Buffer RW1 (350 μL) and centrifuged at 8000 g for 15 sec. The column was then treated with DNase 1 incubation mix [10 μL DNase 1 stock solution, 70 μL Buffer RDD] for 30 min at RT and finally the column was washed again with Buffer RW1 (350 μL) and centrifuged at 8000 g for 15 sec. Following DNA digestion, the column was washed with Buffer RPE (500 μL) and centrifuged at 8000 g for 15 sec and then again with Buffer RPE (500 μL) and centrifuged at 8000 g for 2 min. The RNeasy spin column was transferred to a new collection tube and centrifuged at 13,000 g for 1 min. To elute the RNA, the column was placed in a new spin column and RNase-free water added directly to the membrane and centrifuged at 8000 g for 1 min. Extracted RNA was stored at -80 °C prior to microarray analysis.

All further steps were performed by Dr. Sheen Lee. RNA integrity numbers (RIN) were calculated to assess the quality of the RNA. Where RIN values were satisfactory, expression analysis was performed using Affymetrix Human Gene 2.0 ST Arrays. The Probe Logarithmic Intensity ERror (PLIER) algorithm was used to calculate gene expression using a probe affinity parameter to correct for differing binding affinities. Expression values for each probe were calculated for each sample and average fold changes following MPP^+ treatment were found. P values were calculated using a multiple t-test with multiple testing corrections.

2.1.10 Radio-label pulse-chase assay for determination of autophagic flux

These methods were based on the protocol of Gronostajski and Pardee [287] which they used for 3T3 cells and are here also extended to M17 cells. 3T3 and M17 cells were seeded and maintained

in DMEM and OM respectively and grown in poly-*L*-lysine coated 6-well plates. The day after seeding, 5 μL of [14C]-valine(1.85 MBq/mL, 28 MBq/mmol final specific activity) was added to each well and the cells were cultured for an additional 48 h. Media containing [12C]-valine (1 mM) was prepared to prevent re-incorporation and the cells were maintained for an additional 24 h in the new media. Cells were washed three times with [12C]-valine media and 2 mL of fresh media added. At this point rapamycin treatment (1 μM) or serum starvation (0.5% FBS) was initiated. Aliquots of media (200 μL) were collected at 0.25, 0.5, 1, 1.5, 2.5, 4, 6 and 12 h. Media aliquots were precipitated by addition of ice cold trichloroacetic acid (TCA) (20% (w/v), 200 μL). Samples were centrifuged (10 min) and the supernatant transferred to scintillation vials for counting. After 12 h all remaining media was removed and cells were lysed using 400 μL NaOH (100 mM). The lysate was also transferred to scintillation vials for counting. All samples were counted using the Tri-Carb 2800 TR Liquid Scintillation Analyzer (Perkin Elmer) measuring counts with energies between 4 and 156 keV over a 5 min period. An estimation of the total counts released was subsequently calculated for each time point, and the percentage degradation was calculated based on lysate values.

The pulse-chase protocol was adapted to measure the effect of transfection on protein degradation. Cells were grown in 24-well plates overnight, then 1 μL [14C]-valine was then added to each well and cells cultured for a further 48 h. Antibiotic and FBS free media was supplemented with [12C]-valine (1 mM) and filtered. The [12C]-valine media was used to wash the cells, act as plating media and prepare transfection solutions as detailed in *Subsections 2.1.6* and *2.1.8*. OM supplemented with FBS, antibiotics and [12C]-valine (1 mM) was prepared. Cells were washed three times and 200 μL of the new media added to each well. After 12 h, all media was collected and precipitated with ice-cold TCA (200 μL). Cells were lysed with NaOH (200 μL) and both the media and lysate prepared for counting as detailed above. Counts from media and lysates were used to calculate protein degradation over the 12 h.

2.1.11 Dopamine high-performance liquid chromatography (HPLC)

High-performance liquid chromatography (HPLC) coupled with electrochemical detection were used to separate and identify DA and its metabolites using a protocol previously developed within the laboratory [116]. Cells were cultured on 6-well plates in the absence or presence of MPP^+ and AMPT. Prior to harvesting cells were washed with Hank's balanced salt solution, and then lysed using perchloric acid (PCA) (100 mM, 500 μL) before being snap frozen in brown eppendorfs to protect lysate from light. Samples were stored at -80 °C. Immediately prior to analysis lysates were homogenised using a needle, then 200 μL was loaded into a 0.22

μm centrifugal filter. The filter was centrifuged at 4000 RPM for 5 min at 4 °C and the flow through retained. Each sample (150 μL) was loaded into a brown sample vial for HPLC analysis.

To allow identification of peaks, 5 pM stock solutions of DA and metabolically related compounds (noradrenaline, DA, DOPAC, 5'hydroxyindole-3-acetic acid (5-HIAA), homovanillic acid (HVA) and *L*-DOPA) were prepared in PCA (100 μM). A combined sample containing all six compounds (5 pM, 100 μM PCA) was also prepared. Samples were separated using the mobile phase [13 % (v/v) methanol, 120 mM NaH_2PO_4, 800 μM EDTA, 3.2 mM 1-octanesulfonic acid (OSA), pH 3.43] with a flow rate of 1 mL/min and 50 μL injection per sample. Electrochemical peaks were recorded for 30 min after each sample injection. Standard samples were used to assign retention times to each metabolite. Lysates were run and peaks assigned based upon retention times.

2.2 Statistical analysis of experimental results

All statistical analysis was performed using GraphPad Prism 6.0. Experimental results were analysed using a 1 or 2-way analysis of variance (ANOVA) with Dunnett or Sidak multiple comparison test, two-tailed t-test or linear regression with R^2 values calculated. P values of less than 0.05 following multiple testing corrections were considered statistically significant. Throughout this thesis mean values are plotted with errors representing the standard error of the mean (SEM) either side of the mean value [key: * represents P$\leq$0.05, ** represents P$\leq$0.01, *** represents P$\leq$0.001 and **** represents P$\leq$0.0001]. The standard deviation and SEM of n values of sample x are defined as:

$$SD_x = \sqrt{\frac{1}{n-1}\sum_{i=1}^{n}(x_i - \bar{x})^2} \tag{2.1}$$

$$SE_x = \frac{SD_x}{\sqrt{n}} \tag{2.2}$$

The Dunnett test was used where each mean was to be compared to a control mean. This test assumes that each group will have the same variance. The scatter of all groups (not just the tested groups) are used to give a more precise value for scatter and increase the power of the test to detect small differences. The Dunnett test can be used to compare groups with equal or unequal n. The Holm-Sidak method is more general and was used where the means of all groups were to be compared for all other groups, here the Dunnett test is inappropriate. The Sidak test does not assume equal variance between groups and has less sensitivity to detect

small differences than the Dunnett method. The Sidak method is a straightforward test which considers the sign of the difference between each matched pair of scores with the assumption that where the null hypothesis is true, the number of positive and negative differences will be equal. Although this test has more power than a Bonferroni correction, confidence intervals cannot be calculated.

Statistical analysis of microarray data was performed by Dr. Sheena Lee using a moderated t-test and multiple testing corrections.

2.3 Network methods

2.3.1 Online resources utilised

iRefIndex

iRefIndex is a consolidated PPI database that was used throughout this thesis. A more extensive discussion of the creation and advantages of iRefIndex is given in *Subsection 4.1.4*. iRefIndex [288] was downloaded on 19th July 2012, the non-human interactions were removed and an ID conversion table was created using iRefR [289, 290] to provide the key dataset used throughout this thesis. Datasets containing only experimental (excluding OPHID data) and only low-throughput results were constructed. Low-throughput was defined as interactions where the lowest pubmed re-use (LPR) value was under 10. Each MITAB table was converted to an edge list and then a graph. For each of the datasets four graphs were constructed: binary, bipartite, spoke and matrix.

DAPPLE

Disease Association Protein-Protein Link Evaluator (DAPPLE) was used identify significant connectivity within a PPIN generated from the MPP^+ seedlist [291]. DAPPLE utilises the In-Web database containing 169,810 high confidence, pair wise interactions between 12,793 human proteins [292] and has previously been validated in the contexts of rheumatoid arthritis and Crohn's disease [291] and autism spectrum disorders (ASD) [293]. The creators of DAPPLE generated a background population of 50,000 random networks (constructed via a within-degree node-label permutation with an additional switching step for nodes with a unique degree) to assess statistical significance of network connectivity values. For this thesis, a PPIN was constructed to include all direct interactions between the seeds (proteins were converted to gene ID

before entry into the web interface) and then common interactors (proteins interacting with two or more seeds) were included to form an indirect network. Four metrics were calculated for the resulting PPIN: the total number of edges in the direct network, the degree of each seed in the direct and indirect networks and the degree of common interactors in the indirect network (note that edges between common interactors are not included). Mean and individual values were calculated for node metrics. The mean values are reported along with expected values generated from 10,000 random permutations, and P values were calculated based on the background population. P values for each individual common interactor and seed were also calculated. For those seeds appearing in both the direct and in-direct network, two P values for connectivity were calculated and a Bonferroni correction performed for the two tests and the smaller P value selected. All node P values were then Bonferroni corrected to allow for multiple testing across the PPIN. Corrected P values of less than 0.05 were considered statistically significant.

Uniprot

Uniprot provides a comprehensive, cross referenced, knowledge-base of all known proteins [294]. Information available for each entry includes: alternative protein names, name of corresponding gene, protein function, protein sequence, subcellular localisation of the protein, protein tissue specificity, any known involvement in diseases, ontologies of protein and corresponding gene, and binary PPI. Uniprot was used to interconvert protein names and IDs as well as to collect information about proteins identified through PPIN analysis.

Kyoto Encyclopaedia of Genes and Genomes (KEGG)

Kyoto Encyclopaedia of Genes and Genomes (KEGG) is a series of hand curated diagrams illustrating the key processes and species implicated in metabolism, genetic information processing, environmental information processing, cellular processes, organismal systems and human diseases (including PD) [295]. Genes whose mutations are known to lead to familial diseases are highlighted and the pathways are linked so that the user can identify all pathways in which a species is involved. KEGG pathways were used as a reference source in generating seed lists.

Online Mendelian Inheritance in Man (OMIM)

The Online Mendelian Inheritance in Man (OMIM) database provides a comprehensive list of genes involved in human diseases including mutations that result in heritable cases and SNPs that increase susceptibility [296]. Each entry includes information in some or all of the following

categories: gene structure and function, clinical features, pathologic findings, mapping, genetics, modifier genes and animal models. The OMIM database was used as a reference source in generating seed lists.

GO annotations

GO annotations provide a controlled, unified language to describe genes and proteins in eukaryotic organisms [297]. Annotations are divided into three categories: biological process, molecular function and cellular component. Each descriptor is hierarchical such that a gene may be described by a very general term and, in addition, a more specific term from the same family. The Uniprot web interface was used to export the GO annotations [297] for each node in the 1-hop and shortest-path experimental binary PPIN

DAVID

The Database for Annotation, Visualization and Integrated Discovery (DAVID) [298] was used to detect GO annotational enrichment within groups of proteins. DAVID has been widely used to detect functional enrichment within groups of genes or proteins in the context of network analysis [299–302]. Within this thesis, lists of community members were exported from R. The Uniprot protein ID were entered into the DAVID web interface and converted to Entrez Gene ID. The resulting gene list was input into the annotation enrichment tool (with all the nodes in the relevant PPIN used as the background population) and genes were mapped to GO identifiers. The percentage of genes within the input group (community) with each GO annotation was found and a fold enrichment (compared to the background population) was calculated. P values were calculated using a modified Fisher's exact test (EASE score) for each GO annotation, and were Bonferroni corrected for multiple comparisons, P values of less than 0.05 were considered to indicate statistically significant annotational enrichment.

2.3.2 Seed selection

Putative seeds were collected by accumulating data from the OMIM database [17], KEGG pathways [295], PDGene [31], published experimental microarray analyses following neurotoxins [303–308] and a thorough review of the PD literature. The key criteria for inclusion as a seed was that the protein had been independently and experimentally, demonstrated to be involved in MPP^+ or MPTP pathology. The criteria were assessed by conducting a PubMed search with the criteria: 'seed' AND 'MPP^+' OR 'MPTP'. The resulting publications were

reviewed to determine whether they did indeed offer experimental validation. All seeds on the resulting seedlist were screened using Cytoscape and the BisoGenet plugin and those with a human protein-protein interaction degree exceeding 100 were excluded. The role of all potential seeds was also investigated by literature review and those documented to be involved in the latter stages of cell death, e.g. the caspases were excluded. Based on Uniprot entries [294], gene ontology (GO) annotations and literature reviews each protein was assigned to one of six categories. The categories contain systems-level biological processes known to be involved in MPP^+ and PD pathology: apoptosis, autophagy, DA homeostasis, mitochondrial dysfunction, oxidative stress and the synuclein family. The protein seeds were converted to uniprot ID and the list imported into R where uniprot ID were converted to ROGID (redundant object group identifier) using the conversion table generated above (*Subsection 2.3.1*).

2.3.3 Sampling

The sampling of networks to create relevant, and computationally tractable, subgraphs is a technique which has been widely applied across biological systems. Typically a network is 'grown' from a predefined list of seeds [283, 293, 299–301, 309–314]. In PPIN, sampling relies on the increased likelihood of interaction between proteins with common functions, 'guilt by association' [95, 274]. In *Chapter 4* 1-hop [315] and shortest path sampling [309, 310, 316] were utilised; these techniques have previously been used to create disease-related networks [309, 314].

The MPP^+ seedlist was used to sample each of the 12 data sets (all data, all experimental data and all low-throughput data with binary, bipartite, spoke and matrix representations of interactions between more than two proteins) using both 1-hop (snowball) and shortest path sampling approaches. Under the 1-hop sampling approach each seed and all of its neighbours were included in the sampled graph, and all edges between these nodes (including cross links between two non-seed species) were also included. In the shortest-path approach, the shortest-path between each possible pair of seeds (861 combinations) was found and all nodes on the path were included in the induced subgraph. In cases of multiple shortest-paths between two seeds, all of the nodes on all of the shortest paths were included. All edges between the selected nodes were included, again including all cross links between two non-seed proteins. Where seeds were not connected to the main network they were excluded from the resultant sampled graph.

2.3.4 Network characterisation

The iRefR and igraph packages were used within R [317] to characterise PPIN. The total number of nodes and edges, density, network transitivity, average shortest path length, network diameter and average node degree were calculated for each PPIN. It should be noted that all networks were connected. The betweenness centrality (BC) of all nodes was calculated, nodes ranked and the top 10 nodes identified for sampled networks. Node ID were converted to ROGID and then to Uniprot ID (using the conversation table generated above). The Uniprot web interface was used to find protein names for Uniprot ID identified.

The igraph spin-glass community detection function (γ=1) was used to determine communities and all nodes were labelled with their membership.

For visualisation, graph files were exported in gml format and imported to Gephi [318]. Node BC were recalculated in Gephi and used to size nodes as appropriate. Nodes were coloured according to community membership as exported from R. All graph layouts were determined by the Gephi force atlas algorithm. Node labelling was performed manually.

2.3.5 Steiner analysis

A minimum spanning tree connects a set of seeds using the minimum total path length, resulting in a subgraph containing all of the seeds (where they can be connected) and a subset of the original network edges [299, 319]. Steiner trees are an extension of minimum spanning trees [320]. In addition to the seeds supplied by the user, additional nodes (Steiner nodes) may be included to minimise total path length. Where only two seeds are used, the Steiner tree is simply the shortest path and where all network nodes are included in the seedlist, the Steiner tree is the minimal spanning tree with all nodes used as seeds [320]. The Steiner tree problem is computationally expensive; however, Dreyfus and Wagner developed an efficient algorithm for its approximate solution [321]. Their approach utilises the decomposition of the seedlist into a series of smaller sets of seeds and solving the Steiner problem for each subset. Only optimal solutions to the subsets are retained such that non-optimal solutions are only considered once [321]. In an extension of Steiner analysis, nodes may be weighted and the total weight of the Steiner tree minimised [309]; algorithms for the approximate solution of such problems have also been developed [320, 322, 323] and the software tool *Steiner Package* [320] has been made available.

The PPIN formed by 1-hop and shortest-path sampling of the experimental binary dataset

were exported as edgelists. Systems-level processes were defined using the respective MPP$^+$ seedlists (*Tables 4.2, 4.3, 4.4, 4.5, 4.6 and 4.7*) and these nodes acted as the terminals for Steiner analysis. The user supplied inputs for the Steiner analysis were the relevant edge lists, terminals and (where appropriate) weighting factors for all nodes. The *Steiner Package* then generated a list of Steiner nodes which linked the user-supplied terminals with a minimum total path length and minimum total weighting, where weighting factors were included. Edge lists for the Steiner networks were also generated and used to draw networks in Gephi. Node degree and BC were used as weighting factors for some analyses. Once the Steiner network's nodes had been identified (supplied nodes plus Steiner nodes) all edges between these nodes were included.

2.3.6 Betweenness centrality based analysis

Definition of betweenness centrality

The betweenness cetrality (BC) is a measure of a node's importance in the transmission of information across a network. BC is defined as the proportion of all shortest paths across a network which any single node appears in:

$$BC(v) = \sum_{\substack{a \neq b \neq v \\ a,b,v \in V}} \frac{\gamma_{ab}(v)}{\gamma_{ab}} \tag{2.3}$$

Where V is the set of nodes in the network, $\gamma_{ab}(v)$ is the number of shortest paths between nodes a and b that pass through node i and γ_{ab} is the total number of shortest paths between nodes a and b.

Bridging centrality

Hwang *et al.* identify bridging nodes as rate limiting points within the network and they suggest that such nodes in PPIN are potential drug targets [324]. The bridging centrality (C_R) for each node within the experimental binary PPIN formed by shortest-path and 1-hop sampling was calculated in R according to the equation described by Hwang *et al.* [324]. The C_R is defined as the product of a node's BC and its bridging coefficient (C_B):

$$C_R(v) = BC(v) \times C_B(v) \tag{2.4}$$

$$C_B(v) = \frac{d(v)^{-1}}{\sum_{i \in N_v} \frac{1}{d(i)}} \tag{2.5}$$

Where $d(v)$ is the degree of node v and $N(v)$ is the set of neighbours of node v. Nodes were ranked according to bridging centrality and the top node ID were converted to protein names. The cut off for top bridging centrality nodes was defined as 200 for the 1-hop network, and 90 for the shortest-path network, to give approximately 20 proteins for each.

Subgraph analysis

Subgraph analysis identified proteins with a particularly high BC when the union of two smaller subgraphs was formed. Two subgraphs were created using shortest-path sampling on the experimental, binary PPIN with either the autophagy or mitochondrial dysfunction seeds (*Tables 4.3 and 4.5*). Ubiquitin was deleted and the BCs of each protein in each of the subgraphs and the union graph were calculated . In order to measure the importance of proteins in the cross-talk between mitochondrial dysfunction and autophagy the ΔBC was calculated. ΔBC was defined as follows:

$$\Delta BC = BC_{Total} - BC_{Auto} - BC_{Mito} \tag{2.6}$$

Where BC_{Auto} is the BC of each node in the autophagy subgraph, BC_{Mito} is the BC of each node in the mitochondrial subgraph and BC_{Total} is the BC of each node in the union graph. More generally the ΔBC of node v can be expressed as:

$$\Delta BC(v) = BC_{A \cup B}(v) - (BC_A(v) + BC_B(v)) \tag{2.7}$$

Each subgraph and the union graph were visualised in Gephi and networks were manually annotated with the names of the highest centrality proteins.

Selective betweenness centrality analysis

The selective BC aimed to identify nodes which were important in connecting the proteins associated with autophagy and mitochondrial dysfunction in the MPP^+ PPIN as a whole, in contrast to the subgraph analysis (*2.3.6*), which considered the relationships between the smaller subgraphs corresponding to particular biological processes.

Under the selective BC only the shortest paths between pairs of a particular subset of the networks nodes (i.e. a, b $\subset$ V) were considered to contribute to BC. Subsets were determined by the GO annotations for example, autophagy, such that only shortest paths between pairs of nodes with the GO annotation autophagy were considered to contribute towards node v's selective BC. More generally:

$$SelectiveBC(v) = \sum_{\substack{a \neq b \neq v \\ v \in V \\ a,b \subset V}} \frac{\gamma_{ab}(v)}{\gamma_{ab}} \tag{2.8}$$

The selective BC of all nodes in the two PPIN following the removal of ubiquitin was calculated. a, b were sequentially defined as the:

1. Mitochondrial proteins.
2. Autophagy proteins.
3. MPP^+ proteins.
4. The combined list of mitochondrial and autophagy proteins.

GO annotations relating to mitochondrial dysfunction, autophagy and MPP^+ toxicity were defined (*Table 2.3*). The nodes within each PPIN which corresponded to each set of GO annotations were manually identified to generate three protein lists for each PPIN: mitochondrial, autophagy and MPP^+ related. The lists of Uniprot ID were then imported into R.

The selective BC_{Δ} was calculated as the difference between selective $BC_{mito \cup auto}$ and the sum of selective BC_{mito} and selective BC_{auto}. Values were normalised to the top scoring node for each metric and 'top hits' were defined as those with a selective BC value exceeding 30%.

2.3.7 Comparison of network results

A number of BC comparisons were formed:

1. Total BC before and after removal of ubiquitin from PPIN.
2. Total BC vs selective BC metric.
3. ΔBC values from subgraph analysis vs selective BC_{Δ}.

The different values for each node within the two PPIN were collected and exported to GraphPad Prism where x, y scatter plots were drawn, linear regression performed and R^2 values calculated to assess correlation.

Cellular Process	GO annotation
Mitochondria	
Mitochondrion organization	GO0007005
Mitochondrial inner membrane	GO0005743
Mitochondrial outer membrane	GO0005741
Mitochondrion	GO0005739
Autophagy	
Autophagy	GO0006914
Regulation of autophagy	GO0010506
Autophagic vacuole assembly	GO0000045
Atg8 ligase activity	GO0019776
Atg12 ligase activity	GO0019777
Negative regulation of macroautophagy	GO0016242
Positive regulation of macroautophagy	GO0016239
Negative regulation of autophagy	GO0010507
Positive regulation of autophagy	GO0010508
Processes involved in MPP^+ pathology	
Mitochondrial fragmentation involved in apoptotic processes	GO0043653
Mitochondrion morphogenesis	GO0070584
Release of cytochrome C from mitochondria	GO0001836
Apoptotic mitochondrial changes	GO0008637
Regulation of release of cytochrome C from mitochondria	GO0090199
Mitochondrion degradation	GO0000422
Regulation of reactive oxygen species metabolic process	GO2000377
Mitochondrial fusion	GO0008053
Mitochondrial fission	GO0000266
Regulation of mitochondrial membrane potential	GO0051881

Table 2.3: **The GO annotations used to select nodes for selective BC calculation.** Proteins with mitochondrial or autophagy annotations were used to define these processes. MPP^+ pathology was defined using a list of annotations which included many of the key aspects of neurotoxicity.

Chapter 3

The MPP^+ model of PD in the BE(2)-M17 cell line

3.1 Introduction

As discussed in *Chapter 1* the *in vitro* MPP^+ model of PD is viewed as the most appropriate for this thesis due to its excellent phenocopy of PD, well studied mechanism, ease of use and reproducibility of results. Below a more mechanistic description of the current understanding of the MPP^+ model is outlined focussing on cell death and the neurotoxin's effect on autophagy.

3.1.1 MPP^+ induced cell death

MPTP is able to cross the blood brain barrier where it is metabolised to MPP^+ by MAO-B within glial cells [69]. MPP^+ is not able to cross the blood brain barrier and therefore poses fewer risks in a laboratory environment. MPP^+ is taken up by DAT which accounts for selectivity for DA neurones [70].

Within cells, MPP^+ may be sequestered in synaptosomal vesicles by VMAT2, in a manner analogous to DA. DA sequestration is protective and it is thought that the ratio of DAT to VMAT2 expression predicts neuronal vulnerability to MPP^+ [325]. MPP^+ is actively transported into the mitochondria where it reaches high concentrations and blocks NADH oxidation at complex I [71–73]. Inhibition of the electron transport chain (ETC) leads to ATP depletion, a switch to glycolysis and consequent increase in lactate concentration [79, 88]. MPP^+ induced complex I inhibition also results in the generation of ROS [98, 190, 209]. ROS result in cellular oxidative stress characterised by oxidation of protein, lipids and DNA [98, 209, 213] and reminiscent of

that observed in the brains of PD patients. ROS are essential for MPP^+ induced cell death and antioxidants rescue MPP^+ cytotoxicity downstream of complex I inhibition [98, 204, 211].

In most experimental models MPP^+ induces cell death via an apoptotic mechanism. Nuclear condensation/fragmentation and caspase-3 cleavage occur downstream of mitochondrial damage [98, 209, 326] and caspase inhibitors protect against cell death [327, 328]. However, in some instances, necrotic cell death and caspase independent apoptosis have been demonstrated [190, 329, 330]. The discordance between these cell death mechanisms has not been fully explained, but may be due to different experimental models or variation in MPP^+ dosage regimes, in general higher doses appear to be associated with increased necrotic cell death.

Typical MPP^+ induced cell death is characterised by the upregulation of BAX, its translocation to the mitochondria, permeabilisation of the outer mitochondrial membrane and consequent release of cytochrome C or apoptosis inducing factor (AIF) [328, 331]. *Bax* KO mice are protected from MPTP induced neurodegeneration and BAX KD abrogates MPP^+ induced cytotoxicity *in vitro* [331]. Apoptosis regulator BCL-2 (BCL2) inhibits BAX mediated apoptosis, OE mice and cell lines are protected from MPTP induced cell death [332].

The mechanism by which MPP^+ results in BAX upregulation and translocation is a matter of debate but the process is thought to occur via ROS and downstream of complex I blockade [333]. Perier *et al.* suggested that the DNA damage caused by ROS resulted in activation of P53 and JNK causing upregulation and mitochondrial translocation of BAX, respectively [328]. ROS also cause peroxidation of cardiolipin, disrupting the binding of cytochrome C to the inner mitochondrial membrane and increasing the pool of readily releasable cytochrome C priming cells for BAX mediated apoptosis [213].

ROS led to further mitochondrial damage characterised by DRP1 dependent fragmentation, loss of motility and loss of membrane potential [190, 203, 204, 209]. This mitochondrial damage leads to further ROS production resulting in a vicious cycle of oxidative stress and mitochondrial dysfunction [204].

Increased levels of α-synuclein have been widely demonstrated following MPP^+ exposure [98–100]. Increased expression occurs downstream of ROS production and increased transcript levels indicate an increase in expression rather than only decreased protein breakdown [215]. This α-synuclein upregulation is mediated by the ERK pathway and Kalivendi *et al.* showed that MPP^+ exposure leads to alternative splicing leading to a shorter form of α-synuclein which has an increased propensity to aggregate [334]. α-Synuclein KD is protective against MPP^+ induced cell death and this occurs through reduced DAT mediated uptake [115] and diminished nNOS

(neuronal nitric oxide synthase) activity [79].

Kalyanaraman and colleagues have conducted an extensive investigation into the role of intracellular iron in MPP^+ induced toxicity [98, 215, 334, 335]. They demonstrated transferrin dependent iron accumulation downstream of ROS production, but upstream of α-synuclein accumulation and cell death [98]. Further, iron influx resulted in decreased levels of tetrahydrobiopterin leading to decreased levels of the nNOS dimer and increased ROS production, exacerbating the oxidative stress induced by MPP^+ exposure [335].

3.1.2 Cellular models

BE(2)-M17 (M17) is a human, DA producing, neuroblastoma cell line [284]. Other commonly used neuronal cell lines include PC12, SH-SY5Y and MN9D. However, the M17 line offers the key advantages of being both human derived and DA producing [116], it has been suggested that DA may play a contributory role in cell death in PD and PD models [220]. Previous work in the laboratory demonstrated that M17 cells express TH, AADC, VMAT and the A9 marker GIRK2 in addition to DA [116]. The M17 cell line has been used by this laboratory, and others, to investigate PD related pathways and MPP^+ vulnerability [79, 111, 116, 220, 336, 337]. However, MPP^+ induced processes have not been as thoroughly characterised as in alternative cell lines. The key disadvantage of the M17 line is its resistance to retinoic acid induced differentiation [338].

3.1.3 Microarray data

In principle, for microarray analysis cellular mRNA is extracted, the mRNA reverse transcribed to cDNA and fluorescently labelled. The microarray contains probes for both coding and non-coding mRNA and through complementary binding, levels of cDNA can be measured [339]. Microarray analysis has been used to investigate differential gene expression following MPP^+ exposure in mice [303], SH-SY5Y cells [304], Neuro-2a cells [305], PC12 cells [306] and MN9D cells [307] as well as autopsy samples from PD patients [308]. However, previous investigations have produced somewhat divergent results and there has been no such study in M17 cells.

cDNA microarray analysis in SH-SY5Y identified 48 genes with a twofold, or greater, change in expression following MPP^+ treatment [304]. Half of these genes belonged to one of three categories: transcription proteins, cell cycle proteins or kinase activators/inhibitors. However, only three of the results were confirmed by real-time polymerase chain reaction (GADD153, Myc proto-oncogene and RNA binding protein 3), with the other genes not tested or no significant

difference found. Although the differentially expressed genes were specific to MPP^+ exposure, they were not consistent following retinoic acid induced differentiation.

Illustrating the variability in expression analysis results, Miller *et al.* investigated altered gene expression in MPTP treated mice using two time points, two array platforms and three data mining methods [303]. The authors reported divergent results depending on the technology and time point used; 24 h after MPTP lesion 138 genes were identified as differentially expressed using Affymetrix Arrays and 425 using Amersham CodeLink plates, but only 11 of the genes were common between the two arrays. However, a list of 19 genes whose expression was consistently altered across both arrays was generated. The authors also identified changes across groups of genes corresponding to cytoskeletal stability and maintenance, synaptic integrity, cell cycle and apoptosis.

Elstner *et al.* demonstrated better overlap between microarray studies when pathways, as opposed to genes were compared [308]. The authors used laser capture microdissection to isolate individual DA neurones from the SNpc of PD patients, and avoid contamination with glial cells. Over 1000 transcripts whose expression was significantly changed in PD patients were identified and, although only 8% of the genes overlapped with a previously published study [340], there was excellent overlap in the pathways enriched in significantly altered genes between the two datasets. Elstner *et al.*'s study suggested that mitochondrial dysfunction, oxidative phosphorylation and the protein ubiquitination pathway were central to PD pathology.

It is not clear whether the inconsistent set of genes identified to have altered expression is a result of variations in cell type and MPP^+ dosage or of the various microarray systems used for analysis. Therefore this thesis contains such an investigation in the M17 cell line with the aim that microarray data could be used to inform the construction of PPIN.

In other disease models the results of such microarray experiments have been used to construct PPIN. Genes whose expression is altered are used as the seeds for network construction and further genes that are close in network space are hypothesised to have relevance in such disease models [341, 342].

3.1.4 Cellular viability assays

A large number of assays are used to estimate cellular viability. The choice of assay will depend upon a number of factors including the mechanism of cell death, experimental system, cost and time constraints.

The reduction of tetrazolium salts (including MTT and MTS) to highly coloured formazens are a widely used measure of cell viability [343]. Reduction depends on the presence of NAD(P)H and is largely dependent on glycolysis, rather than the ETC [344]. It has been demonstrated that MPP^+ treatment leads to a short term upregulation of glycolysis [79], as a response to ETC inhibition, therefore, such assays should be used with caution in the context of MPP^+ induced cell death.

Neutral red is a lysosomal stain which passes freely through the cytoplasm, but is protonated and therefore trapped in the lysosome. Uptake is proportional to cell and lysosome number, but also depends on the proton gradient across the lysosomal membrane. The proton gradient relies on ATP and therefore, neutral red absorbance has been used to estimate cellular viability [286, 345] and, across a wide range of test reagents, there is good agreement between readouts from the MTT and neutral red assays [345]. Neutral red absorbance has occasionally been used to measure MPP^+ toxicity *in vitro* and there was a significant decrease absorbance when PC12 cell were incubated with MPP^+ (1.5 mM, 24 h) [346].

Apoptotic cell death is characterised by caspase mediated protein cleavage. Caspases are sequentially activated by cleavage and therefore levels of cleaved caspases can be used to measure apoptotic cell death [343]. Caspase-3 is an initiator caspase and therefore, is widely used as a marker of cell death [343]. Cleavage can be monitored using WB or (with antibodies specific for the cleaved form) by immunocytochemistry (ICC) or flow cytometry [327].

Annexin-V binds to the cell membrane protein phosphatidylserine (PS). Normally PS remains within the cells interior. However, upon the initiation of apoptosis PS is exposed leading to annexin-V binding [343]. Annexin-V staining is performed in live (non-fixed) cells and is normally conducted in conjunction with a strong nuclear stain (7-AAD or propidium iodide (PI)) to mark any cells whose membranes have been permeabilised. Combined annexin-V and 7AAD/PI staining can therefore distinguish between healthy (unstained), early apoptotic (annexin-V stained), late apoptotic (annexin-V and 7AAD stained) and necrotic (7AAD stained) cells. Such analysis is typically performed by flow cytometry [188] and MPP^+ treatment (1 mM, 24 h) results in increased annexin-V staining in PC12 cells [347].

Rhodium dyes, including TMRM, accumulate in the mitochondria and their fluorescence depends on the size of the mitochondrial membrane potential [348]. Therefore, they can be used to identify mitochondrial membrane depolarisation. Such dyes are widely used for fluorescence microscopy investigations, but have also been applied to higher throughput plate reader and flow cytometry assays [209, 349]. A flow cytometry study in SH-SY5Y confirmed that TMRM

fluorescence is decreased after only 13 h MPP^+ treatment (5 mM) [209].

3.1.5 Measures of autophagy

As discussed previously (*Subsection 1.4.2*), autophagy is the process of cellular self-digestion by which long lived proteins and organelles are degraded and their constituents recycled. A number of methods are commonly used to estimate the rate of autophagic turnover in cellular systems. The most widely used approaches centre around protein markers, most notably LC3B and to a lesser extent P62 [350]. Unprocessed LC3B is cytoplasmic however, the protein is conjugated to phosphatidylethanolamine (PE) in the autophagosome membrane by ATG7 and remains attached throughout the maturation process until, following cargo degradation, LC3B is recycled by ATG4 [149]. LC3B lipidation can be monitored by WB as a distinct band with lower apparent molecular weight is detected corresponding to the lipidated form [350]. Alternatively, the conjugation of LC3B to the autophagosome can be observed by fluorescence microscopy as the formation of puncta using either a fluorescently tagged form of the protein or ICC [351]. However, cytosolic form of LC3B will also be detected. Once the puncta corresponding to autophagosomes have been identified, their colocalisation with lysosomes (identified using lysosomal dyes such as lysotracker or antibodies for lysosomal proteins) can be used to measure lysosomal fusion [350]. P62 acts as a molecular adaptor targeting ubiquitinated cargo for degradation, and is rapidly degraded following lysosomal fusion [352]. Therefore decreased P62 levels have been used in conjunction with LC3B to measure autophagosome numbers [353]. In a manner similar to LC3B, autophagosomes can be identified as P62 positive puncta using ICC or fluorescently tagged proteins [353].

While such methods are widely used they must be treated with a degree of caution. An accumulation of LC3B-II may either represent an overall increase in autophagic flux or a blockage in flux leading to the accumulation of autophagosomes due to trafficking defects, problems with lysosomal fusion or protein degradation. Therefore, control experiments should be conducted using compounds capable of blocking autophagosome degradation for example bafilomycin A1 or chloroquine both of which inhibit lysosomal acidification [350]. If increased LC3B lipidation/puncta formation is as a result of increased autophagic flux then treatment with bafilomycin A1 or chloroquine will result in a further increase in LC3B-II levels [350]. Where no change is observed upon treatment, it is likely that LC3B-II accumulation is as a result of blocked autophagic flux rather than an increased rate of initiation [350], although where basal levels of lipidated LC3 are high a ceiling effect may prevent further increase [164].

Where available, electron microscopy (EM) is an excellent tool for autophagic investigations. Autophagosomes can be identified by their double lipid membrane and in many cases organelles (including mitochondria) can be detected within the autophagosomes [350]. However, the same caveats apply as to measurement of LC3B, accumulation of autophagosomes may reflect a block in autophagic flux rather than an increased initiation of autophagy [350].

Pulse-chase assays offer an alternative method of autophagy detection. Such methods involve the incubation of cells in radio-labelled media (typically either 14C or 3H labelled valine or leucine) so that radio-labelled proteins are accumulated [287, 354, 355]. The cells are then incubated in non-labelled (cold) media and as proteins are broken down through autophagy, the constituent amino acids can diffuse across the cell membrane and into the media. Aliquots of media can be collected and the levels of radio-labelled amino acid measured to calculate the rate of protein degradation. However, some caution must be exercised when using leucine for radio-labelling as high concentrations of leucine act as a potent inhibitor of autophagy [354]. Such approaches have been widely employed in hepatocytic tissue, but are less well explored in neuronal cell lines [355].

3.1.6 Effect of MPP^+ on autophagy

The effects of MPP^+ on autophagy have been investigated by a number of groups. There are some discrepancies in published studies, but the majority of reports indicate that MPP^+ treatment leads to increased LC3B lipidation and autophagosome accumulation downstream of mitochondrial damage [99, 100, 159, 186, 186, 188, 190, 204, 351, 356]. Whether autophagosome accumulation is a result of increased autophagic flux or a blockage of lysosome fusion is a matter of some debate and may depend upon the experimental system. There are also contradictory reports as to whether autophagy is protective or deleterious in conjunction with MPP^+ exposure and this may depend upon the MPP^+ dosage and cell line used.

MPP^+ as a stimulator of autophagy

Zhu *et al.* conducted a thorough investigation of the effects of MPP^+ treatment in the SH-SY5Y cell line and primary midbrain DA neurones [152]. They reported increased autophagy in response to MPP^+ using EM to observe increased autophagosome numbers, MDC (monodansylcadaverine) staining to measure late stage autophagosomes and WB to follow LC3B lipidation. However, they saw no change upon treatment with phosphatidylinositol 4,5-bisphosphate 3-Kinase (PI3K) inhibitors 3-methyladenine and wortmannin nor with Beclin-1 siRNA mediated

KD. They suggested that MPP^+ induced autophagy occurred via a PI3K independent pathway and proposed that the neurotoxin induced autophagy via the ERK pathway. ERK activation occurred within 8 h of MPP^+ exposure and preceded changes in autophagy [186]. Treatment with UO126, an inhibitor of the upstream dual specificity mitogen-activated protein kinase kinase 1 (MAPKK1), ablated MPP^+ induced autophagy and prevented cell death. Interestingly, transient OE of ERK2 was sufficient to induce autophagy and mitochondrial degradation (in the absence of neurotoxins) and led to increased cell death [153].

Zhu *et al.* extended their earlier work to investigate chronic MPP^+ exposure using repeated doses, over 2 weeks, in differentiated SH-SY5Y cells [203]. The chronic treatment regime led to significant cell death, changes to mitochondrial morphology and autophagy (as measured by electron microscopy, MDC staining and LC3B lipidation) with ERK activation peaking after each MPP^+ treatment. By inhibiting ERK activation they were able to prevent the changes to mitochondrial morphology, protein expression and respiratory capacity otherwise induced by MPP^+ exposure. However, while inhibition of autophagy via ATG7 or LC3B siRNA prevented some changes to mitochondrial morphology the blockage of autophagy was insufficient for protection and the authors suggested that in the chronic model ERK activation resulted in cell death by pathways other than autophagy.

Other groups have demonstrated an upregulation of autophagy following MPP^+ treatment [356, 357]. Rodriguez-Blanco *et al.* reported caspase-independent cell death following MPP^+ treatment in differentiated PC12 cells and upregulation of autophagy [357]. However, although the authors reported ERK activation following MPP^+ exposure, they did not see any change to autophagy or cell death upon co-treatment with MAPK inhibitors and suggested that ERK activation is 'merely a protective response upon stress'. Verhaar *et al.* also reported MPP^+ induced autophagy in differentiated SH-SY5Y with marked accumulation of Beclin1 at the ER [356] in contrast to Zhu *et al.* who demonstrated Beclin1 independent autophagy following MPP^+ treatment [152].

MPP^+ as an inhibitor of autophagy

In contrast to the above results, others have demonstrated that MPP^+ treatment leads to decreased autophagic flux, despite the accumulation of autophagosomes [159, 186–188]. A thorough investigation of autophagy in PD models came from Dehay *et al.* who studied the effect of MPTP in mice, MPP^+ in the M17 cell line and autopsy samples from PD patients and concluded that lysosomal damage was central to PD the aetiology [159]. The authors detected

increased autophagosome levels (measured using LC3) and decreased lysosomal levels (measured using LAMP1) across all three models; further, human LB were shown to be LC3B immunoreactive. Additional mechanistic studies were conducted in the M17 cell line where the authors demonstrated damaged mitochondria (by EM) and lysosomal membrane permeabilisation. The lysosomal permeabilisation prevented autophagosome fusion and led to the release of lysosomal enzymes into the cytoplasm. Further they confirmed that lysosomal damage occurred via ROS and at time points preceding cell death. Supporting the role of lysosomal dysfunction in blocking autophagic flux, Li *et al.* demonstrated decreased lysosomal activity following MPP^+ treatment [186].

3.1.7 Effect of autophagy on MPP^+ toxicity

Beyond the debate about the effect of MPP^+ on the rate of autophagic flux, there are conflicting reports as to whether autophagy is protective or deleterious in the context of MPP^+ toxicity.

The concept of autophagic stress suggests that excessive autophagy (such as that induced by neurotoxins) is, in itself, harmful as the cells ability for regenerative protein synthesis is exceeded by the rate of protein breakdown [154, 357]. Chu *et al.* reported that rapamycin treatment potentiated MPP^+ induced cell death in SH-SY5Y and that ATG7 siRNA mediated KD was protective in MPP^+ infused rats [154]. Further, Rodriguez-Blanco *et al.* demonstrated that the inhibition of autophagy (via bafilomycin A1 treatment) rescued MPP^+ neurotoxicity [357].

However, others have demonstrated that upregulating autophagy is protective in combination with MPP^+ treatment. Garcia-Garcia *et al.* demonstrated caspase dependent cell death upon MPP^+ exposure that is exacerbated upon blocking autophagy [188]. The authors blocked autophagy by OE of the dominant-negative form of ATG5, a system that they suggested was superior to pharmacological interventions or siRNA mediated KD.

In direct contrast to the results of Chu, Dehay *et al.* demonstrated that TFEB OE increased autophagic flux and prevented MPP^+ induced cell death in M17 cells [159]. The authors also showed that rapamycin treatment was protective against MPP^+ neurotoxicity and acted by upregulating lysosome biogenesis and increasing autophagosome clearance.

Other systems used to induce protective autophagy in an MPP^+ context include:

- The use of 3-*N*-butylphthalide (a natural product derived from *Apium graveolens* (celery) and used to treat stroke victims) to induce autophagy and promote α-synuclein breakdown in PC12 cells [358].

- Lanosterol (a cholesterol precursor depleted in the striatum of MPTP treated mice) treatment to protect DA neurones in MPTP treated mice or MPP^+ treated primary cultures. The lanosterol co-treatment led to increased number of autophagosomes and their increased association with mitochondria [359].
- Paeoniflorin (the active component of the traditional medicine *Paeoniae alba*) co-treatment rescued MPP^+ treated PC12 cells, increasing LC3B-II levels and α-synuclein degradation [347].
- Co-treatment with modified Yeoldahanso-tang (a traditional Korean dried herb mixture) in MPTP treated mice led to preservation of DA neurones with increased levels of the autophagic proteins Beclin1 and LC3B [360].
- Sublethal hypoxic preconditioning in SH-SY5Y led to a transient increase in LC3B lipidation and MDC staining which occurred via ROS formation. Pre-conditioning decreased MPP^+ induced cell death, caspase-3 cleavage and MPP^+ induced autophagy. When the preconditioning was combined with autophagy blocker 3MA the protective effect was ablated [361].

3.1.8 Aims of chapter

This chapter is centred on the characterisation of the MPP^+ model in the M17 cell line. It is essential that the model is accurately characterised and sensitive assays are developed so that small alternations following protein modulations can be detected. With this broad aim in mind, this chapter has four specific goals:

1. To determine a suitable MPP^+ treatment regime in M17 cells to facilitate the investigation of the effects of protein modulation on MPP^+ vulnerability.
2. To characterise MPP^+ induced cell death in M17 cells and optimise a series of assays for measuring cell death.
3. To investigate the effect of MPP^+ on autophagy in M17 cells and optimise assays for measurement of autophagic flux.
4. To explore the hypothesis that cellular DA contributes to MPP^+ sensitivity in M17 cells.

3.2 Results

3.2.1 Optimisation of MPP^+ treatment regime

Although MPP^+ is a widely used neurotoxin, a wide range of doses and administration times have been used experimentally. Therefore, MPP^+ induced cell death in the M17 cell line was characterised.

MTS

MTS reduction was used to estimate cellular viability following MPP^+ treatment (*Figure 3.1*). After 48 h treatment with MPP^+ (20 nM - 200 μM), MTS reduction was decreased in a dose dependent fashion for doses exceeding 10 μM; there was no significant decrease in MTS reduction at earlier time points or lower doses.

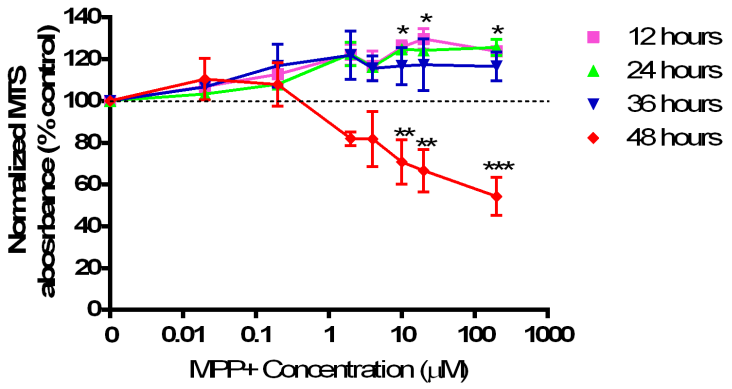

Figure 3.1: **MPP^+ treatment decreases MTS reduction in a dose dependent fashion.** Cells were treated with doses of MPP^+ from 20 nM to 200 μM for 12 - 48 h. MTS reduction was measured for triplicate wells and normalised to untreated controls (average unnormalised control absorbances were 0.592, 0.783, 0.630 and 0.861 for 12, 24, 36 and 48 h respectively). Data points represent means ± SEM (n=3), ** represents P≤0.01, *** represents P≤0.001 compared to 100% normalised control. Data were analysed using a 2-way ANOVA with Dunnett multiple comparison test.

Cell counts

As a comparison to MTS reduction, cell counts were performed for a range of MPP^+ doses and treatment times. Cells were imaged 24, 36 and 48 h after MPP^+ treatment (1-2000 μM), blinded images were counted for morphologically normal cells and normalised to untreated controls (*Figure 3.2*). Following 48 h treatment, there was a dose dependent, statistically significant decrease in cell number for MPP^+ concentrations exceeding 5 μM. There was also significant cell loss following 36 h treatment with 500 μM and 2 mM MPP^+. Given cell count and MTT

results, 100 μM MPP^+ was selected for further experiments (at a range of time points) as this dose of MPP^+ led to approximately 50% cell loss after 48 h therefore, allowing for both increases and decreases in cellular viability. It was not viable to continue experiments beyond 48 h due to the proliferation of untreated control cells.

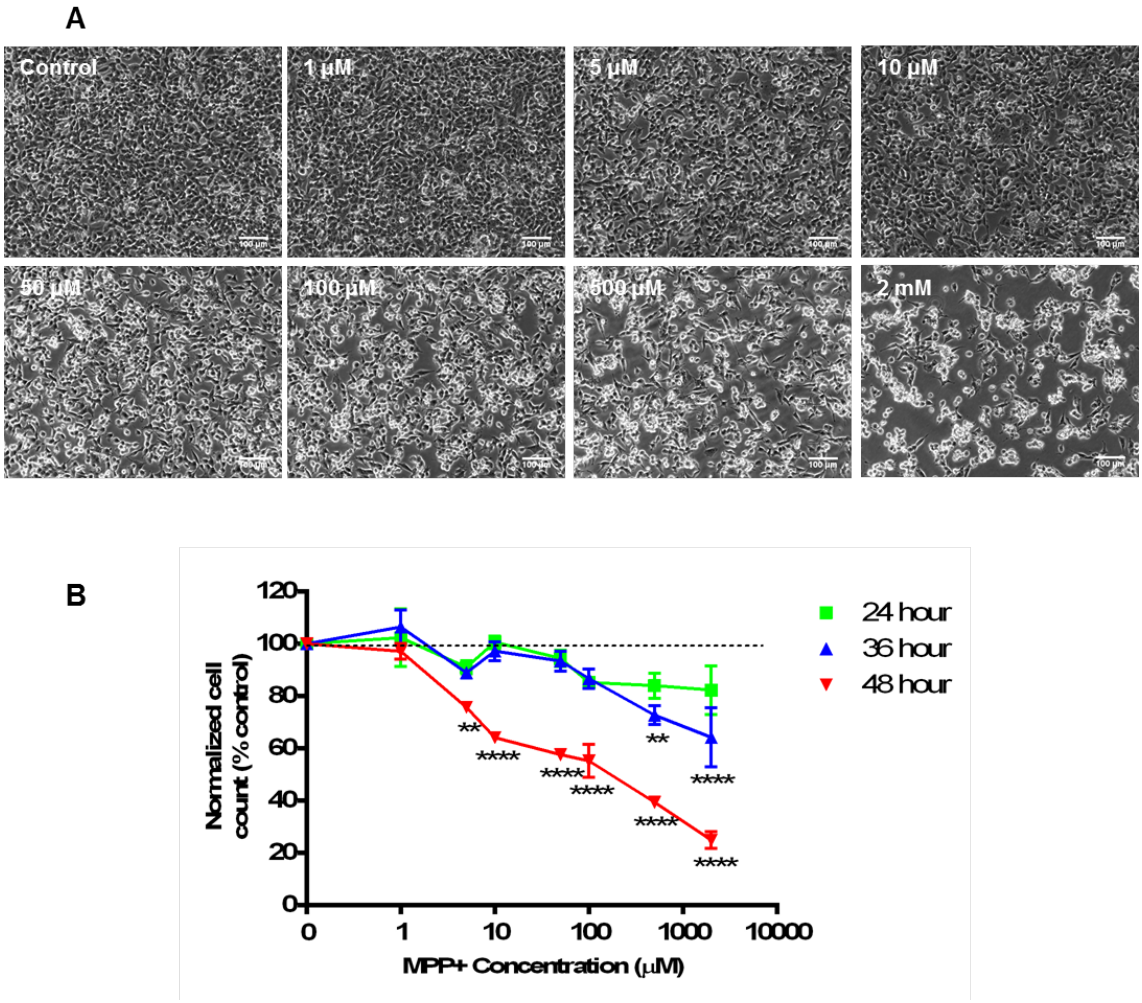

Figure 3.2: **MPP^+ decreases the number of live cells in a time and dose dependent fashion.** Cells were treated with doses of MPP^+ from 1 μM to 2 mM for 24 - 48 h. Bright-field images were collected for triplicate wells at 20 x magnification (scale bars are 100 μm). **A** Example images of cells following 48 h treatment with MPP^+. **B** The number of live cells were counted, all counting was conducted blind. Counts were normalised to untreated controls (average unnormalised counts were 59.1, 66.8 and 113.5 cells at 24, 36 and 48 h respectively). Data points represent means ± SEM (n=3), ** represents P≤0.01, *** represents P≤0.001 compared to 100% control. Data were analysed using 2-way ANOVA with a Dunnett multiple comparison test.

ATP depletion

MPP^+ is a complex I inhibitor and has previously been demonstrated to cause ATP depletion [362]. ATP levels were measured using the CellTiter-Glo®kit following treatment with MPP^+ (100 μM) and the potent complex III inhibitor antimycin A (10 μM - a concentration previously optimised in the Wade-Martins laboratory); antimycin A was utilised as a positive control,

known to impede ADP phosphorylation [363]. After normalisation to untreated cells, there was a significant decrease in ATP levels after 17 h treatment with antimycin A and 30 h treatment with MPP^+ (*Figure 3.3A*).

ATP depletion experiments were repeated in low glucose/high galactose media to confirm that ATP depletion occurred as a result of blockade of the ETC, rather than inhibition of glycolysis (*Figure 3.3B*). Under low glucose conditions, 3 h treatment with antimycin A and 17 h treatment with MPP^+ were sufficient to result in a significant decrease in ATP levels. ADP phosphorylation was completely ablated after 42 h treatment with either toxin.

It is acknowledged that ATP levels were not corrected for cell number. Although cell counts (*Figure 3.2*) demonstrated no significant change in cell number following 36 h treatment with 100 μM MPP^+, reduction in cell numbers were seen at later time points. Therefore, the ATP depletion observed at 42 and 48 h is likely to be partially due to a decrease in the number of live cells as a result of both increased apoptosis and decreased proliferation. Further, cell counts were not conducted in galactose media and it is possible that low glucose conditions reduced cellular proliferation and this may have affected the results for the ATP assay.

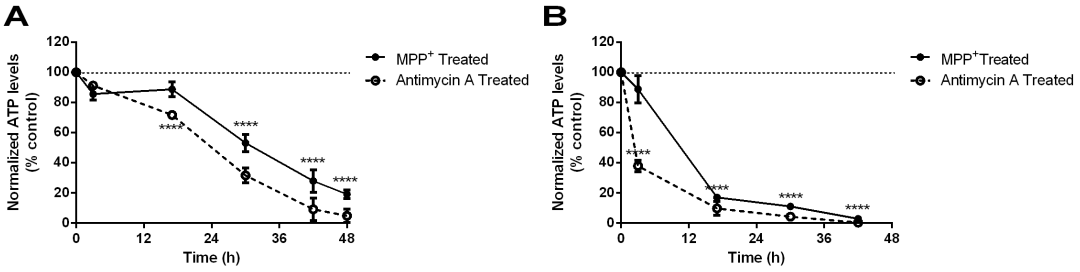

Figure 3.3: **MPP^+ and antimycin A decrease cellular ATP levels by ETC blockade.** Cells were treated with MPP^+ (100 μM) or antimycin A (10 μM) for 3 to 48 h in normal (**A**) or low glucose (**B**) media. Cellular ATP levels were measured for triplicate wells and values were normalised to untreated control cells. Unnormalised controls were 7.50, 6.84, 6.32, 8.82 and 10.17 RLU in glucose media and in galactose media 3.21, 395, 4.33 and 4.48 RLU in galactose media. Data points represent means ± SEM (n=3), **** represents P≤0.0001 compared to 100% control. Data were analysed using a 2-way ANOVA with a Dunnett multiple comparison test.

Neutral red absorbance

The lysosomal stain neutral red was used to characterise MPP^+ induced cell death. Under normal conditions neutral red diffuses into the lysosome where it is protonated and becomes trapped. Having demonstrated that MPP^+ treatment results in ATP depletion, it was hypothesised that it would also result in decreased neutral red accumulation.

After 6-48 h MPP^+ treatment (100 and 5 μM), neutral red absorbance was measured and these

values normalised to the absorbance from untreated cells (*Figure 3.4*). MPP^+ treatment led to significant decreases in neutral red accumulation after 36 h (79% control for 5 μM and 50% control for 100 μM). A number of further experiments were then conducted to explore neutral red absorbance as a marker of cellular ATP levels.

First, it was confirmed that the changes in neutral red uptake were not due to a change in overall lysosomal numbers. Therefore LAMP1 (a lysosomal marker) levels were measured by WB at a series of time points (2-48 h) following MPP^+ exposure (100 μM). There were no changes to LAMP1 protein levels at any time point indicating no alteration to overall lysosome numbers (*Figure 3.5*).

Next, it was confirmed that known ETC inhibitors also reduced neutral red accumulation. The potent complex III inhibitor antimycin A (10 μM) was compared to MPP^+ treatment (100 μM) (*Figure 3.6A*). Both treatments resulted in significant decreases in neutral red accumulation with lower absorbances recorded for antimycin A treatment at all time points. MPP^+ treatment resulted in 65% control absorbance after 30 h treatment.

In order to confirm that the deacidification of lysosomes was sufficient to prevent neutral red accumulation and that neutral red was not accumulated in organelles other than lysosomes, absorbance was measured after 5 h treatment with the vacuolar-type H^+-ATPase inhibitor bafilomycin A1 (50 nM) (*Figure 3.7*). Bafilomycin A1 treatment resulted in 24 % control neutral red absorbance compared to a 79 % absorbance following MPP^+ treatment. The effect of bafilomycin A1 confirmed that neutral red was accumulated specifically in the lysosomes and that this was dependent on low pH.

Finally, to confirm that the reduced neutral red uptake was as a result of ETC blockade, MPP^+ and antimycin A treatment were repeated in low-glucose/high-galactose media (*Figure 3.6B*). Under low-glucose conditions, MPP^+ treatment resulted in decreased neutral red absorbance after 17 h with 68% control absorbance after 30 h. Antimycin A treatment resulted in decreased neutral red absorbance at all time points with 27% control absorbance after 30 h. When the two media conditions were compared (*Figures 3.6 C* and *D*), a significant difference was observed after 42 h treatment with MPP^+ (*Figures 3.6 C*) or antimycin A (*Figures 3.6 D*). Low glucose conditions potentiated the loss of neutral red accumulation, indicating that ATP depletion was as a result of ETC blockade.

In combination these experiments demonstrated that neutral red absorbance was decreased following MPP^+ treatment as a result ATP depletion due to ETC inhibition. For further investigations the neutral red was utilised following 36 h MPP^+ treatment as a significant decrease

in absorbance was seen even in the most variable experiments conducted.

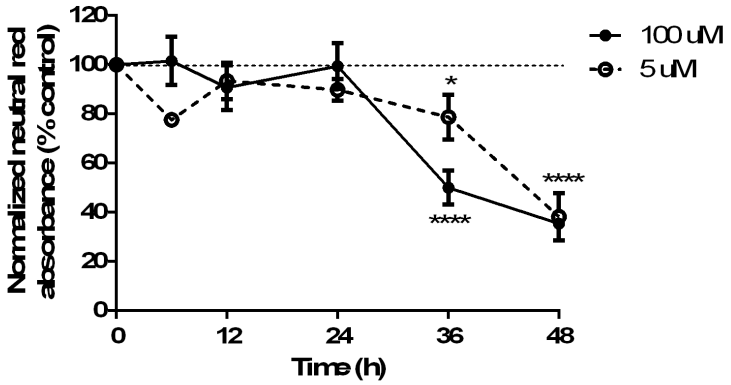

Figure 3.4: **MPP$^+$ treatment decreases cellular neutral red accumulation.** Cells were treated with MPP$^+$ (5 or 100 μM) for 6 to 48 h. Cells were then treated with neutral red reagent and absorbance measured at 540 nm for triplicate wells. Values were normalised to untreated control cells (average unnormalised control absorbances were 0.312, 0.439, 0.299, 0.218 and 0.236). Data points represent means ± SEM (n=3), * represents P≤0.05 and **** represents P≤0.0001 compared to 100% control. Data were analysed using a 2-way ANOVA with a Dunnett multiple comparison test.

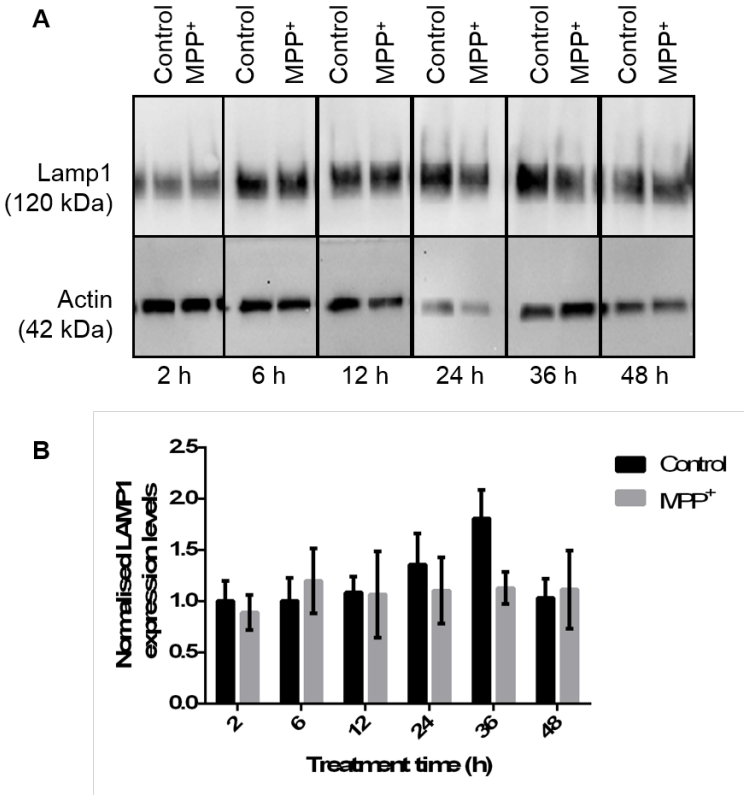

Figure 3.5: **Lysosome levels are unchanged following MPP$^+$ treatment.** Cells were treated with 100 μM MPP$^+$ for 2 - 48 h and LAMP1 levels measured by WB and normalised to actin loading control. Bars represent means ± SEM (n=3). Data were analysed using a 2-way ANOVA with a Sidak multiple comparison test.

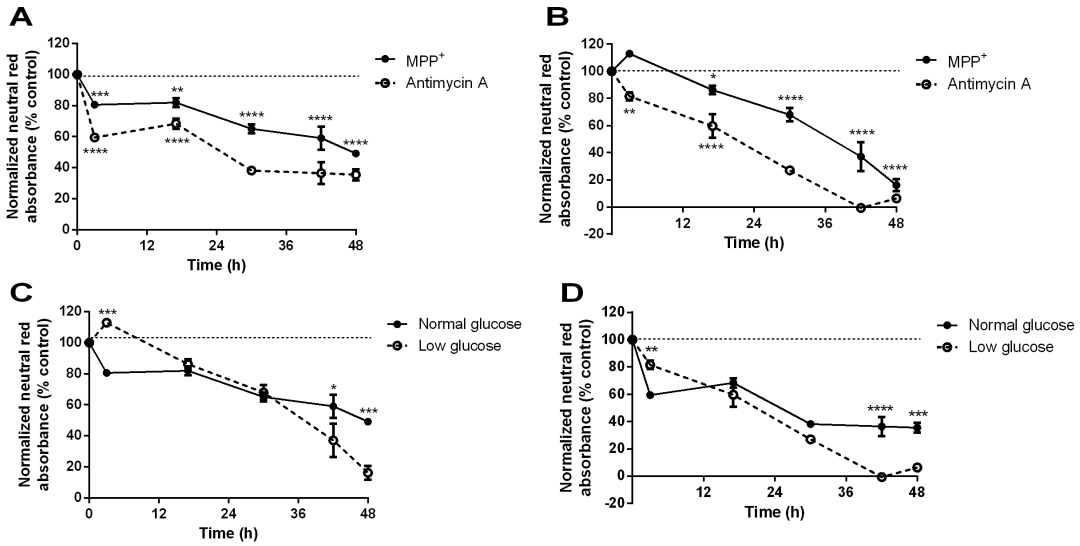

Figure 3.6: **Decreased neutral red accumulation is a result of ETC blockade.** Cells were treated with MPP^+ (100 μM) or antimycin A (10 μM) for 3 to 48 h in normal (**A**) or low glucose (**B**) media. Cells were then treated with neutral red reagent and absorbance measured at 540 nm for triplicate wells. Values were normalised to untreated control cells (average unnormalised control absorbances were 0.397, 0.214, 0.408, 0.312 and 0.469 in normal media and 0.350, 0.304, 0.204, 0.302 and 0.310 in low glucose media). Data points represent means ± SEM (n=3), ** represents P≤0.01, *** represents P≤0.001 and **** represents P≤0.0001 compared to normalised control. Data were analysed using a 2-way ANOVA with Dunnett multiple comparison test. **C** and **D** show the same data, but allow a comparison of the different media conditions for MPP^+ (**C**) and antimycin A (**D**). Data points represent means ± SEM (n=3), * represents P≤0.05, ** represents P≤0.01, *** represents P≤0.001 and **** represents P≤0.0001 between the two media conditions. Data were analysed using 2-way ANOVA with a Sidak multiple comparison test.

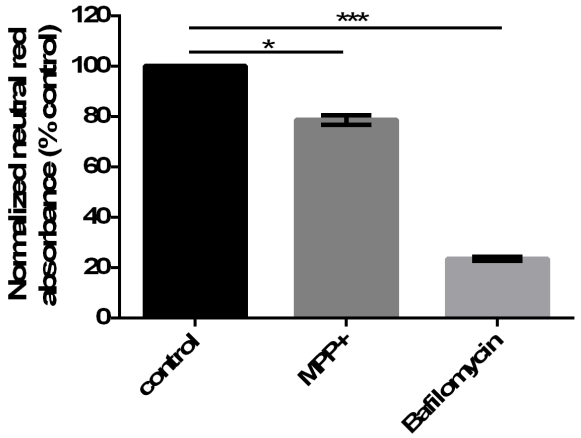

Figure 3.7: **Neutral red absorbance is dependent on lysosome acidification.** Cells were treated with MPP^+ (100 μM) or bafilomycin A1 (50 nM) for 5 h. Cells were then treated with neutral red reagent and absorbance measured at 540 nm for triplicate wells. Values were normalised to untreated control cells. Bars represent means ± SEM (n=3), * represents P≤0.05 and *** represents P≤0.001 compared to normalised control (unnormalised average control absorbance was 0.164). Data were analysed using a 1-way ANOVA with a Dunnett multiple comparison test.

TMRM fluorescence

TMRM fluorescence was used to measure mitochondrial membrane potential following MPP^+ treatment (5 and 100 μ M) and normalised to untreated cells (*Figure 3.8*). Cells treated with MPP^+ for 24 h displayed significantly decreased fluorescence; 100 μM MPP^+ led to a 40% normal fluorescence and 5 μM MPP^+ resulted in 83% normal fluorescence.

The potent mitochondrial toxin CCCP was used to confirm that TMRM was selectively accumulated in the mitochondria and that its fluorescence was dependent on mitochondrial membrane potential. Cells were treated with MPP^+ (100 μM) or CCCP (10 nM to 10 μM) for 2 h and then measured TMRM fluorescence and normalised these values to untreated controls (*Figure 3.9*). There was no change in TMRM fluorescence following 2 h MPP^+ treatment but doses of CCCP exceeding 100 nM resulted in significant decrease in fluorescence and treatment with 10 μM CCCP led to 19% normal TMRM fluorescence.

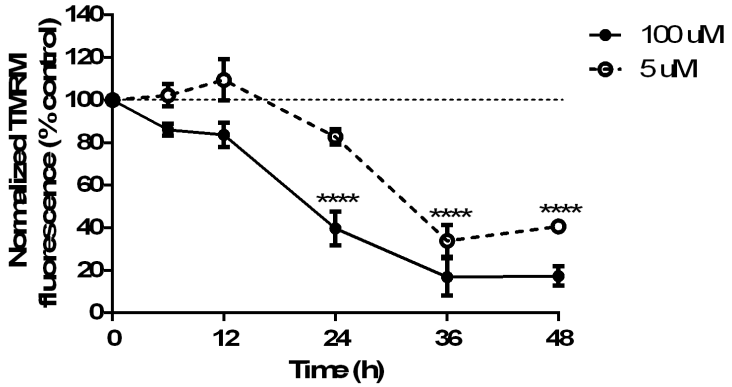

Figure 3.8: **MPP^+ treatment decreases mitochondrial membrane potential.** Cells were treated with MPP^+ (5 or 100 μM) for 6 to 48 h. TMRM (150 nM) fluorescence was measured (excitation 544 nm and emission 590 nm) for triplicate wells. Values were normalised to untreated control cells (average unnormalised control fluorescences were: 7021, 8087, 8792, 10825 and 14858 RFU). Data points represent means ± SEM (n=4), **** represents P≤0.0001 compared to normalised control. Data were analysed using a 2-way ANOVA with a Dunnett multiple comparison test.

Brief MPP^+ exposure

It has been previously demonstrated that MPP^+ induced cell death occurs over 24-72 h [199, 201, 209] however, it has not been established whether continuous MPP^+ exposure is required to induce cell death or whether an inevitable chain of events is set in motion by even a brief MPP^+ exposure. Cells were exposed to MPP^+ (100 μM) for 2, 4 or 10 h and then the media was replaced to remove any remaining toxin. TMRM and neutral red assays were used to assess the impact of MPP^+ treatment and data are also shown for cells exposed to MPP^+ continuously

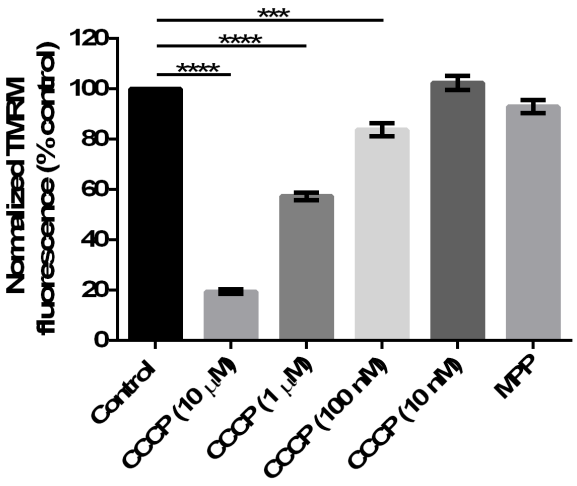

Figure 3.9: **TMRM fluorescence is dependent on mitochondrial membrane potential.** Cells were treated with CCCP (10 nM to 10 μM) or MPP^+ (100 μM) for 2 h. TMRM fluorescence was measured (excitation 544 nm and emission 590 nm) for triplicate wells. Values were normalised to untreated control cells (average unnormalised control fluorescence was 1165 RFU). Bars represent means ± SEM (n=3), *** represents P≤0.001 and **** represents P≤0.0001 compared to normalised control. Data was analysed using a 1-way ANOVA with a Dunnett multiple comparison test.

for 48 h (*Figure 3.10A*).

MPP^+ exposure resulted in an early decrease in neutral red absorbance (72% control after 2 h compared to untreated cells) and after 36 h treatment uptake was decreased to 46 % of that for untreated cells. The alternative MPP^+ regimes also decreased neutral red uptake and when the four regimes were compared at the 36 h time point, each regime induced a significant decrease in absorbance (*Figure 3.10B*). Further, cells treated with MPP^+ for 36 h had lower neutral red uptake than those treated for 2-10 h. However, there was no significant difference between neutral red absorbance with 2, 4 or 10 h exposure to MPP^+.

A similar analysis was conducted using TMRM fluorescence as a marker of mitochondrial membrane potential with 24 h selected as the key time point for comparison (*Figure 3.10C and D*). At the 24 h time point both constant and 4 h exposure led to a significant decrease in fluorescence (54% and 70% control fluorescence respectively). When the brief exposures were compared to constant exposure, significantly less depolarisation was seen with 2 and 10 h MPP^+ exposure, but there was no significant difference between 4 h and constant exposure.

Therefore, it was concluded that a brief MPP^+ exposure was sufficient to induce cell death with deleterious effects observed after 2 h and continuing after the removal of the neurotoxin, but that longer MPP^+ exposure times resulted in additional cellular damage.

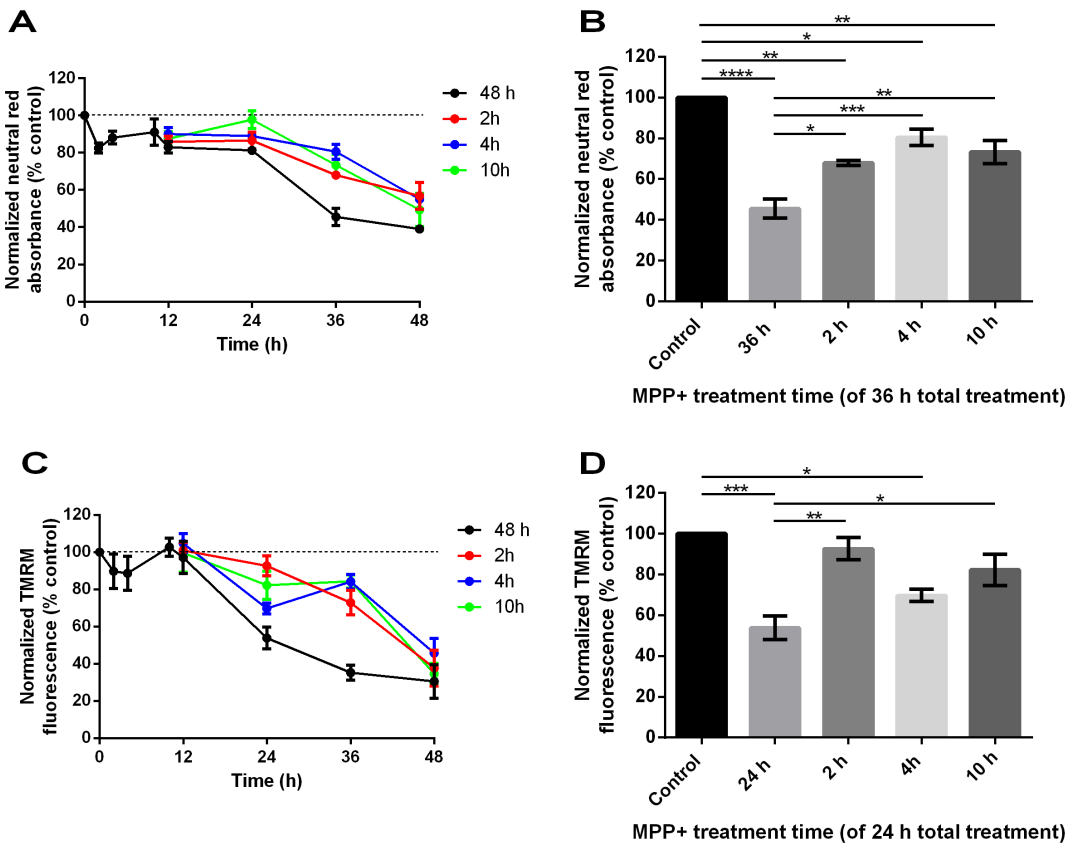

Figure 3.10: **Short term (2 h) MPP^+ exposure is sufficient to initiate cytotoxicity.** Cells were treated with MPP^+ (100 μM) for 2, 4 or 10 h and then the media replaced, data are also shown for cells subjected to constant MPP^+ exposure. Cells were cultured for a total of 2-48 h from the initial MPP^+ treatment. **A** and **B** cells were then treated with neutral red reagent and absorbance measured at 540 nm for triplicate wells, values were normalised to untreated control cells at each time point (average unnormalised control absorbances were 0.272, 0.246, 0.264, 0.273, 0.305, 0.284, 0.374). **B** neutral red data for 36 h total treatment time. **C** and **D** TMRM fluorescence was measured (excitation 544 nm and emission 590 nm) for triplicate wells. Values were normalised to untreated control cells (average unnormalised control fluorescences were 3649, 4681, 5798, 1743, 3462, 5015 and 4360 RFU). **D** TMRM data for 24 h total treatment time. Data points and bars represent means ± SEM (n=3), * represents P≤0.05, ** represents P≤0.01, *** represents P≤0.001 and **** represents P≤0.0001. Data analysed using 1-way ANOVA with Sidak multiple comparison test.

3.2.2 MPP^+ induced apoptosis

There have been divergent reports as to whether MPP^+ induces cell death by an apoptotic, autophagic or necrotic mechanism [98, 154, 328, 330]; however, the mechanism of cell death has not yet been explored in M17 cells.

Annexin-V and 7AAD staining

Annexin-V and 7AAD staining in conjunction with flow cytometry was used to identify healthy, apoptotic, late apoptotic and necrotic cells (*Figure 3.11*). Following consultation with the flow

cytometer technician, a population of intact cells was gated based on side and forward scatter. Forward scatter is a crude measure of cell size and side scatter a crude measure of internal complexity. Therefore, gating was used to exclude small cell fragments and clumps of cells; the gate was also established to select for as homogeneous cellular population as possible to facilitate comparisons. All analysis was conducted on only this gated population. Unstained control cells were used to establish the thresholds for postive annexin-V and 7AAD staining. Following 36 h MPP^+ treatment (100 μM), increased annexin-V staining was observed and the proportion of gated cells in the early stages of apoptosis increased from 10 to 42%.

Caspase-3 cleavage

Caspase-3 cleavage is a key marker of apoptosis and staining is performed on fixed cells. Cells were stained with a conjugated fluorescent antibody specific to the cleaved form of caspase-3 and then flow cytometry used to measure the proportion of stained cells within the intact cell gated region following MPP^+ treatment (100 μM 36 h). As for annexin-V/7AAD flow cytometry, a sample of unstained cells was used to establish a parameter for positive cleaved caspase-3 staining. Exposure to MPP^+ led to a significant increase in the percentage of gated cells staining for cleaved caspase-3; following treatment 82% cells stained positive compared to 65% of control cells (*Figure 3.12*). The proportion of cells staining positive for cleaved caspase-3 under control conditions was higher than expected so the experiments were repeated (36 h, 100 μM MPP^+) with the same antibody, but using ICC to measure the proportion of stained cells (*Figure 3.13*). The ICC analysis indicated that the proportion of cells staining positive had increased from 7 to 94% following MPP^+ treatment. Although both methods showed a significant increase in cleaved caspase-3 the values for control cells was more plausible following ICC.

3.2.3 Effect of MPP^+ on autophagy

Analysis of autophagy by WB

Lipidated LC3B is a key marker of autophagosomes and its levels are widely used as a measure of autophagy. It was confirmed that MPP^+ treatment (48 h, 100 μM) resulted in increased LC3B lipidation as previously reported in other cell lines (*Figure 3.14 A*) [100, 159, 188]. However, there was no significant difference between LC3B lipidation in cells treated with the vacuolar-type H^+-ATPase inhibitor bafilomycin A1 (50 nM) and MPP^+ when compared to bafilomycin A1 alone indicating that MPP^+-induced LC3B-II accumulation was as a result of blocked autophagic flux.

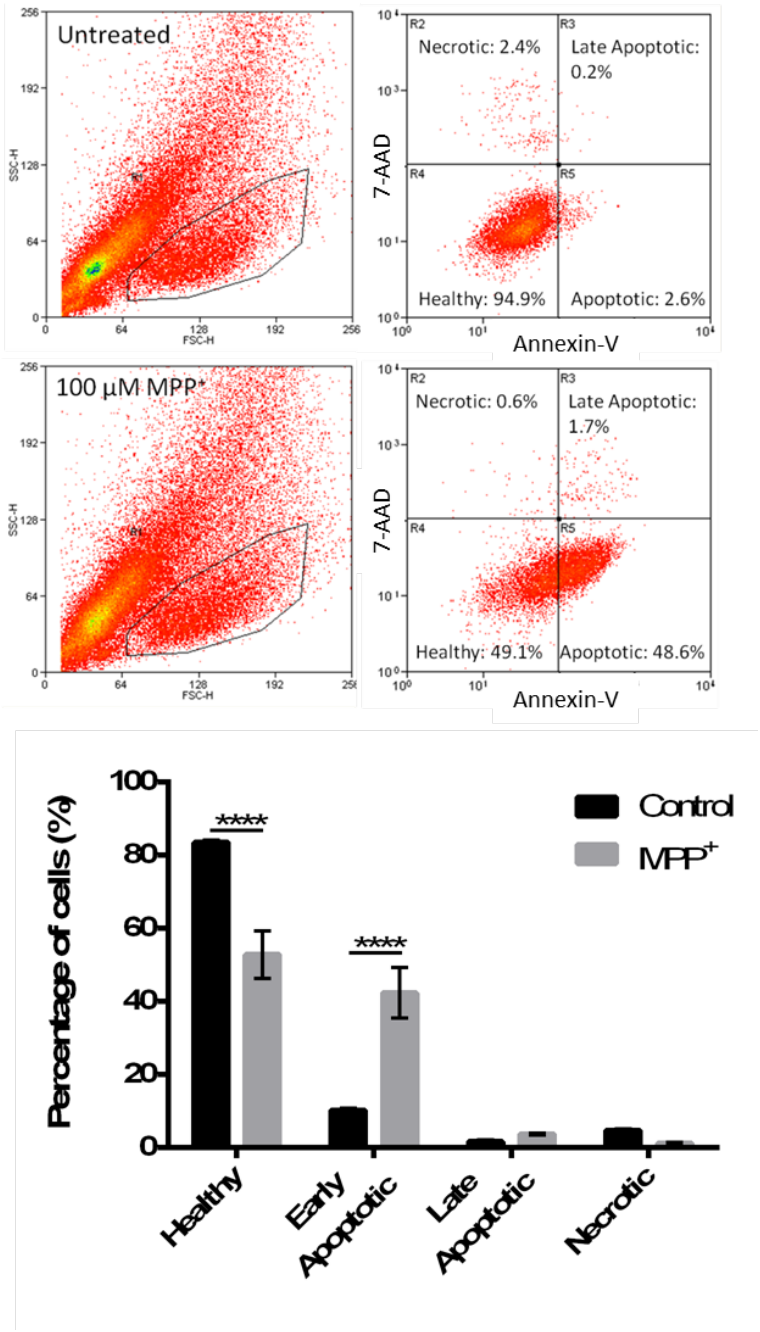

Figure 3.11: **MPP$^+$ treatment initiates apoptosis.** Cells were treated with MPP$^+$ (100 μM) for 36 h and stained with annexin-V-FITC and 7-AAD, flow cytometry was performed and 10,000 events in the gated region were collected. Annexin-V and 7-AAD labelling was used to categorise cells as healthy, early apoptotic, late apoptotic or necrotic. Bars represent means ± SEM (n=3), **** represents P≤0.0001. Data were analysed using a 2-way ANOVA with Sidak multiple comparison test.

LC3B lipidation was also measured after 24 h exposure to MPP$^+$ (100 μM) (*Figure 3.14B*); at this time point there was no difference in LC3B lipidation upon MPP$^+$ treatment in either the absence or presence of bafilomycin A1.

It has been suggested that disruptions to CMA may result in altered autophagic flux as a compensatory mechanism [165]. Therefore LAMP2A was used as a marker of CMA and levels of LAMP2A were measured following 24 and 48 h treatment with MPP$^+$ (100 μM) (*Figure 3.15*).

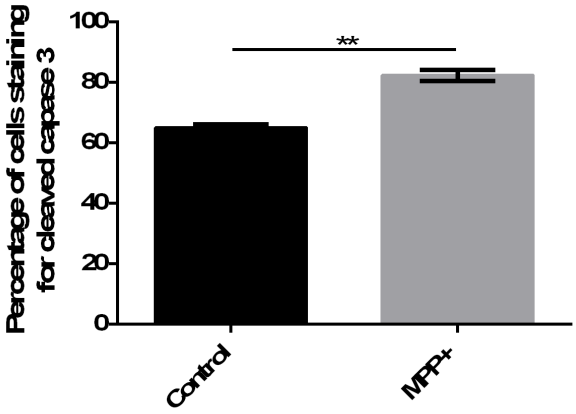

Figure 3.12: **MPP$^+$ treatment leads to caspase-3 cleavage as assessed by flow cytometry.** Cells were treated with MPP$^+$ (100 μM) for 36 h and then fixed with paraformaldehyde. Cells were stained for cleaved capase 3 then flow cytometry was performed and 10,000 events in gated region were collected. Unstained cells were used to determine gating parameters for caspase staining and the proportion of stained cells was calculated. Bars represent means ± SEM (n=3), data were analysed using a 2-tailed t test, ** represents P≤0.01.

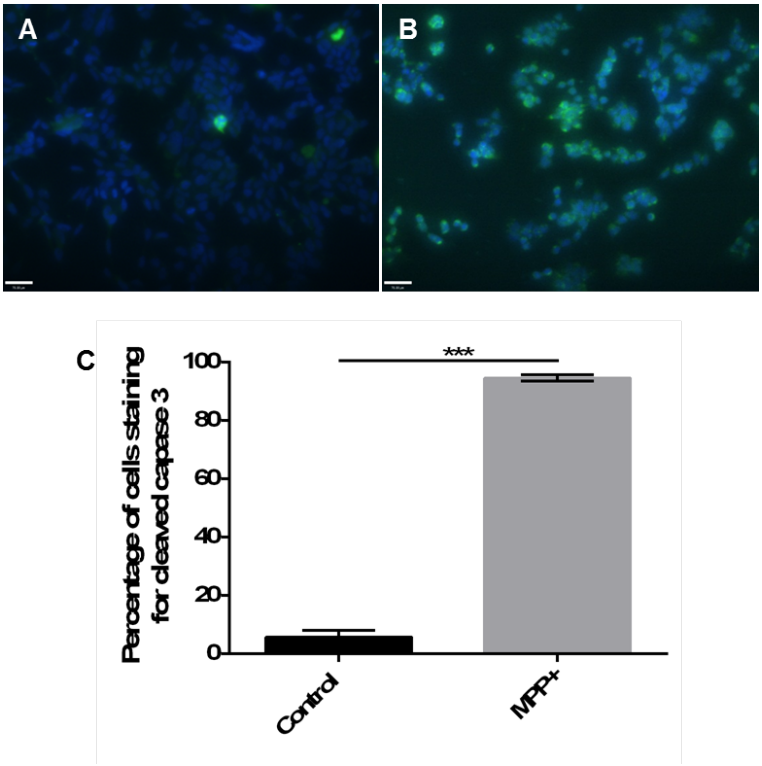

Figure 3.13: **MPP$^+$ treatment leads to caspase-3 cleavage assessed by immunocytochemistry.** Cells were cultured on coverslips and treated with MPP$^+$ (100 μM) (**A**) or control media (**B**) for 36 h. Cells were fixed and stained for cleaved caspase-3 and nuclei costained with DAPI. Fluorescence images were collected for triplicate wells at 20 x magnification (scale bar is 70 μm). The number of cleaved caspase-3 positive and negative cells in each image was counted (**C**), all counting was conducted blind. Bars represent means ± SEM (n=3), data analysed using a 2-tailed t test, *** represents P≤0.001. Data were analysed using 2-tailed t test.

No change in LAMP2A level was seen at either time point. LAMP2A levels have previously been used as a measure of CMA activity as the protein corresponds to the rate-limiting step in this process [168, 171, 350, 364]. However, unaltered levels of LAMP2A may not provide conclusive

evidence of unaltered CMA if other stages of the process are defective. Therefore, although this data provides no evidence of changes to CMA, it cannot be unequivocally established that the process is unaffected by MPP^+ treatment.

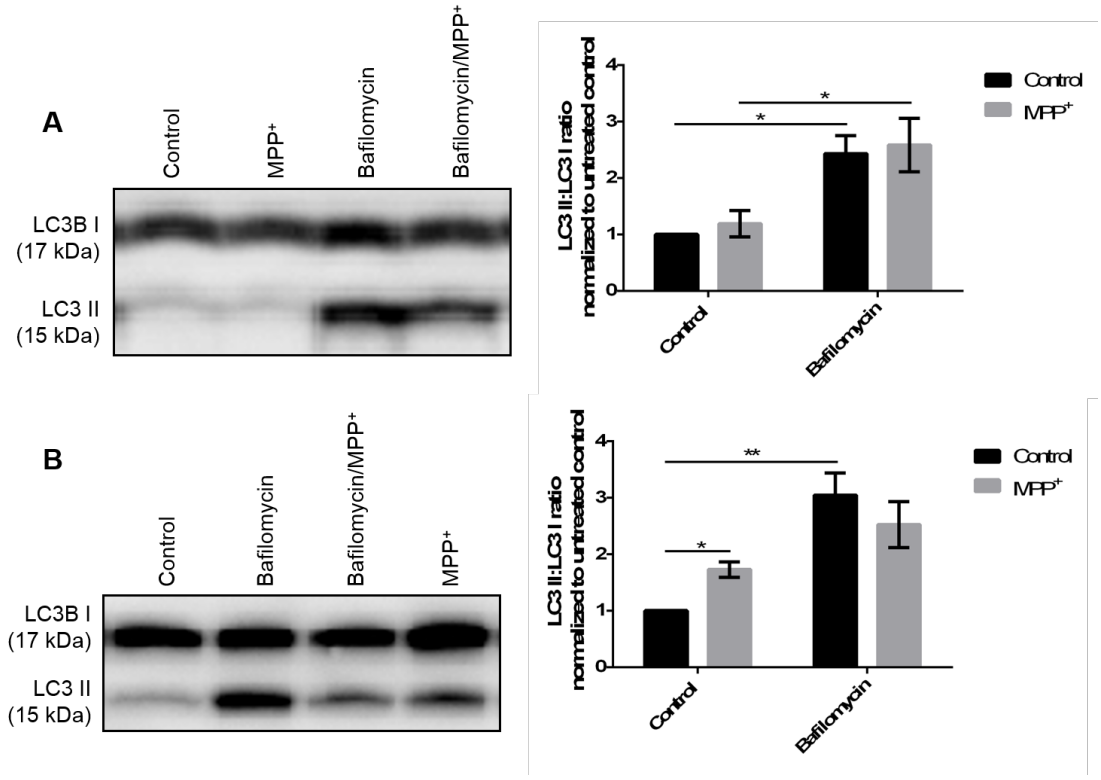

Figure 3.14: **MPP^+ treatment results in increased LC3B lipidation which is not further increased by bafilomycin A1 co-treatment.** Cells were treated with MPP^+ (100 μM) and bafilomycin A1 (50 nM) for 24 (**A**) or 48 h (**B**). LC3B levels were measured by WB, the ratio of LC3B-II to LC3B-I was then calculated and normalised to untreated controls. Bars represent means ± SEM (n=3), data were analysed using a 2-way ANOVA with a Sidak multiple comparison test, * represents P≤0.05 and **represents P≤0.01.

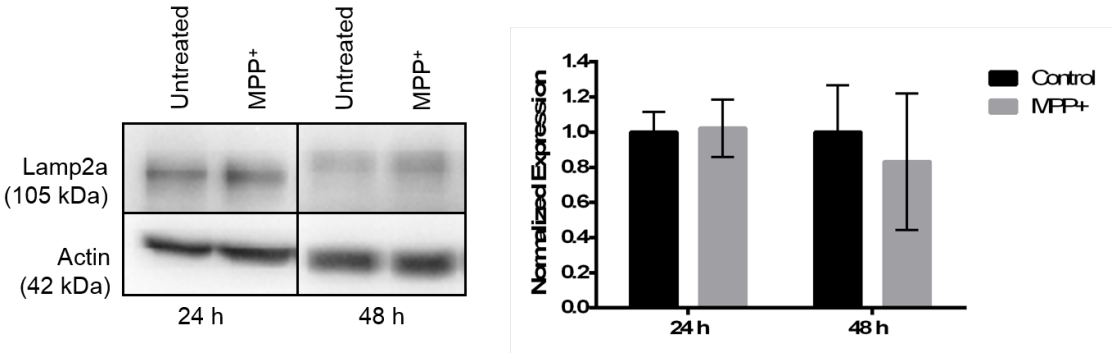

Figure 3.15: **Chaperone mediated autophagy is not affected by MPP^+ treatment in M17 cells.** Cells were treated with MPP^+ (100 μM) for 24 or 48 h, LAMP2A levels measured by WB and normalised to untreated controls. Bars represent means ± SEM (n=3). Data were analysed using a 2-way ANOVA with a Sidak multiple comparison test.

Analysis of autophagy using pulse-chase experiments

Radio labelled pulse-chase assays are considered the 'gold standard' for measuring autophagic flux [350] and were used as a comparison to the analysis conducted by WB. Initially, previously published results in the 3T3 cell line [287] were replicated (*Figure 3.16A*). At each time point a sample of media was collected, activity measured and the amount of radioactivity in the entire media was estimated. Cumulative values were used to calculate the total amount of radioactivity released into the media at each time point. At the end of the experiment, the cells were lysed and radioactivity remaining in the cells was calculated. These data were used to calculate the percentage of total radioactivity released into the media at each time point. Radioactivity released was assumed to correspond to protein breakdown, as the 24 h chase period ensured that all of the radio-labelled amino acid was incorporated in long lived proteins and the excess of cold valine ensured that the radio-labelled amino acid was not reabsorbed following diffusion across the cell membrane.

In accordance with published results, a linear rate of protein degradation was observed and the rate of protein degradation was significantly increased following serum starvation. In the 3T3 cell line protein degradation over 6 h was increased from 6.6 to 11.4% upon starvation. The protocol was then extended to the M17 cell line where a smaller increase, from 6.1 to 7.9% was seen over the same time period (*Figure 3.16B*).

A similar protocol, with the final timepoint extended to 12 h, was used to investigate the effect of established autophagy inducer, rapamycin, and MPP^+ on the M17 cell line (*Figure 3.17*). Rapamycin treatment (1 μM) significantly increased protein breakdown with an increase from 4.4 to 5.2% breakdown after 6 h and from 8.1 to 9.8% after 12 h. However, following 12 h treatment with MPP^+ (100 μM) protein degradation was significantly decreased from 8.1 to 7.0%.

Following the observation that 12 h MPP^+ treatment decreased autophagic flux, autophagy was measured following MPP^+ treatment times up to 48 h omitting the 24 h chase period (*Figure 3.18*). In untreated cells the rate of protein breakdown was non-linear due to the initial breakdown of short lived proteins. MPP^+ treatment resulted in decreased cumulative protein degradation after 24 h (18.5 compared to 21.3%) and after 48 h treatment the total protein turnover was decreased from 35.5 to 25.1%. This decreased autophagic flux is consistent with the lysosome deacidification previously observed (*Figures 3.4, 3.6 and 3.7*) because functional acidic lysosomes are required for protease mediated protein breakdown.

To facilitate a comparison between WB and pulse-chase methods, LC3B lipidation was measured

in M17 cells following 12 h treatment with starvation (0.5 % serum) or rapamycin (1 μM) in the presence and absence of bafilomycin A1 (50 nM) (*Figure 3.19*). Significant increases in LC3B lipidation was seen upon bafilomycin A1 treatment under all experimental conditions. Rapamycin treatment also resulted in an increase in LC3B lipidation compared to controls when coupled with bafilomycin A1 treatment. However, no difference was observed following serum starvation indicating that the pulse-chase technique had higher sensitivity.

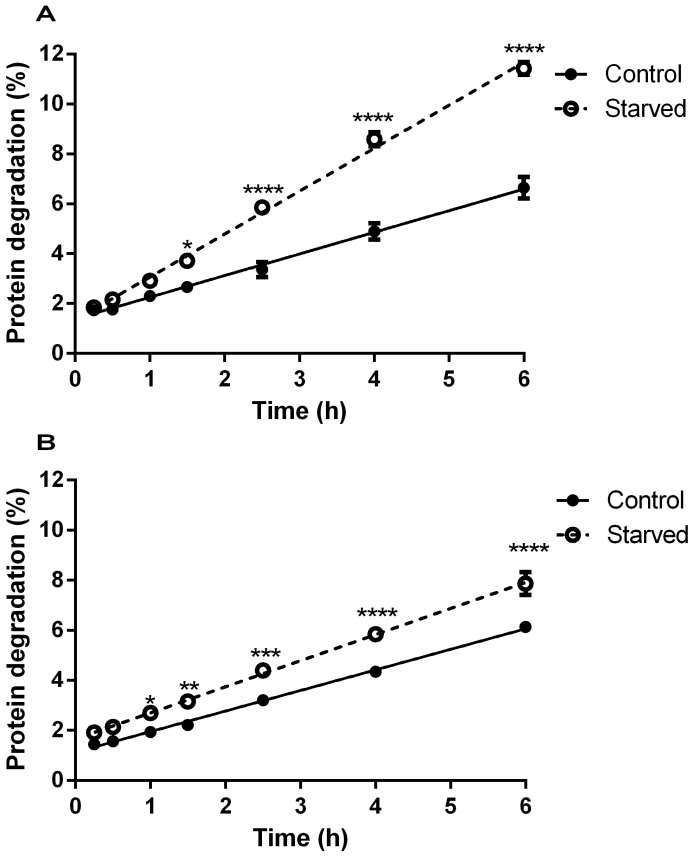

Figure 3.16: **Serum starvation increases autophagic flux in 3T3 and M17 cells.** 3T3 (**A**) and M17 (**B**) cells were labelled with 14C-valine for 48 h and then maintained in cold media (1 mM valine) for a further 24 h. The media was then replaced with either normal (10 % FBS, 1 mM valine) or starvation (0.5% FBS, 1 mM valine) media. Aliquots were taken at time points from 15 min to 6 h and precipitated with TCA. Radiation in the supernatant was measured by scintillation count and protein degradation calculated using scintillation counts from lysed remaining cells (6 h). Data points represent means ± SEM (n=3), * represents P≤0.05, ** represents P≤0.01, *** represents P≤0.001 and **** represents P≤0.0001 compared to controls. Linear regression was performed and data were analysed using a 2-way ANOVA with a Sidak multiple comparison test.

3.2.4 Effect of dopamine on MPP^+ toxicity

To establish the importance of DA in MPP^+ induced cell death in M17, AMPT was used to deplete cellular DA.

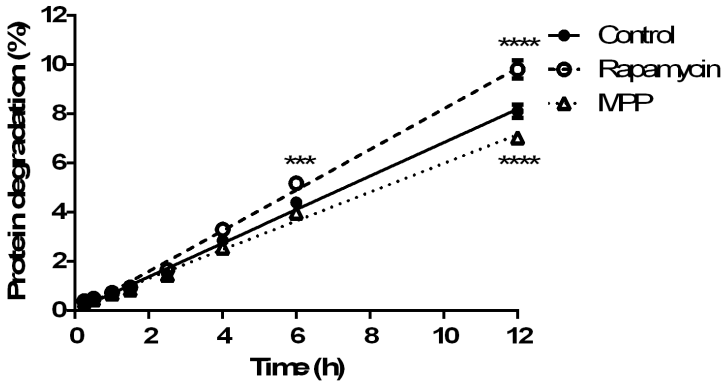

Figure 3.17: **Rapamycin and MPP$^+$ have opposite effects on autophagy in M17 cells.** M17 cells were labelled with 14C-valine for 48 h and then maintained in cold media (1 mM valine) for a further 24 h. The media was replaced and cells were treated with rapamycin (1 μM) and MPP$^+$ (100 μM). Aliquots were taken at time points from 15 min to 12 h and precipitated with TCA. Radiation in the supernatant was measured by scintillation count and protein degradation calculated using scintillation counts from lysed remaining cells (12 h). Data points represent means ± SEM (n=3), *** represents P≤0.001 and **** represents P≤0.0001 compared to controls. Linear regression was performed and data were analysed using a 2-way ANOVA with a Sidak multiple comparison test.

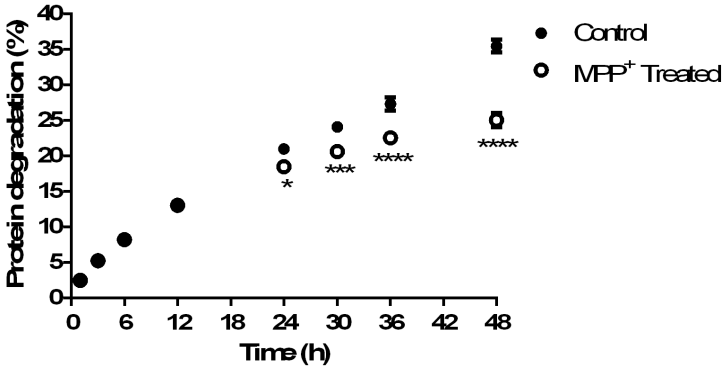

Figure 3.18: **MPP$^+$ treatment further decreases autophagic flux at time points up to 48h.** M17 cells were labelled with 14C-valine for 48 h. The media was replaced (fresh media contained 1 mM valine) and cells were treated with 100 μM MPP$^+$. Aliquots were taken at time points from 1 to 48 h and precipitated with TCA. Radiation in the supernatant was measured by scintillation count and protein degradation calculated using scintillation counts from lysed remaining cells (48 h). Data points represent means ± SEM (n=3), * represents P≤0.05, *** represents P≤0.001 and **** represents P≤0.0001 compared to controls. Data were analysed using a 2-way ANOVA with a Sidak multiple comparison test

Optimisation of HPLC

DA and its metabolites were detected using HPLC coupled with electrochemical detection. Standard solutions (100 nM) of *L*-DOPA, DA, DOPAC, Noradrenaline, HVA and 5-HIAA were prepared in PCA (100 μM), the retention time of each compound was measured and it was confirmed that the peaks could be separated in a mixed solution (*Figure 3.20*).

Serial dilutions of the mixed solution were prepared and the HPLC traces analysed (*Figure 3.21*).

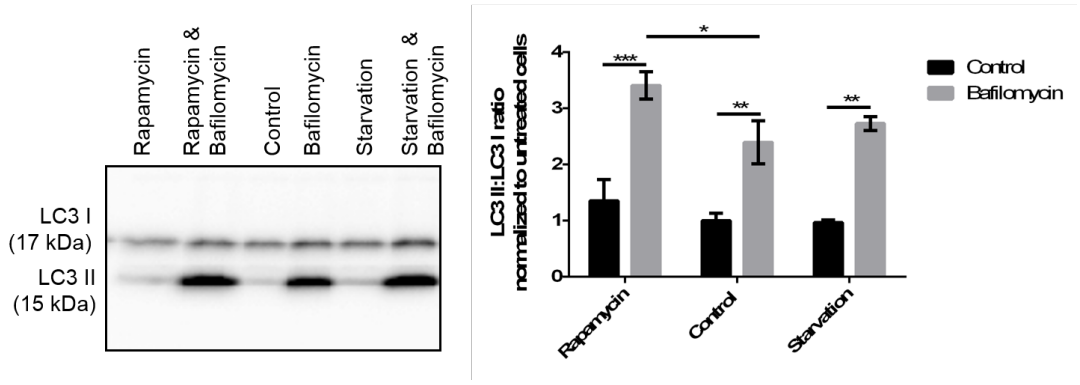

Figure 3.19: **Pulse-chase assay is a more sensitive measure of autophagy than LC3B lipidation.** Cells were treated with bafilomycin A1 (50 nM) for 12 h in normal media (10% FBS), rapamycin treated media (1 μM) or starvation media (0.5% FBS). Protein (10 μg) was separated by electrophoresis and probed for LC3, the ratio of LC3B-II to LC3B-I was then calculated and normalised to untreated controls. Bars represent means ± SEM (n=3). Data analysed using 2-way ANOVA with Sidak multiple comparison test

Each compound could be detected in the range of 5 to 100 nM and peak area was proportional to concentration for each compound. Linear regression was performed for each compound and the following R^2 values were calculated: *L*-DOPA - 0.994, NA - 0.997, DOPAC - 0.9995, 5HIAA - 0.9956, DA - 0.9891, HVA - 0.9929. Finally, it was confirmed that DA could be detected in M17 cells and that the DA peak could be distinguished from other peaks (*Figure 3.22*).

Optimisation of AMPT treatment

A preliminary HPLC experiment confirmed that 24 h treatment with AMPT (500 μM) resulted in approximately 90% DA depletion and that at a higher concentration (1 mM) the cells were almost entirely DA free (*Figure 3.23A*).

However, cellular viability as estimated by neutral red absorbance was significantly compromised following 48 h AMPT treatment (500 μM or 1 mM) (*Figure 3.23 B*). In standard OM, 1 mM AMPT led to 63 % control neutral red absorbance; with 500 μM AMPT concentration neutral red absorbance was increased to 66% control, but there was no significant difference between 1 mM and 500 μM AMPT. HEPES (4-(2-hydroxyethyl)-1-piperazineethanesulfonic acid) buffered media was employed to prevent AMPT mediated acidification; however AMPT treatment still resulted in significantly decreased neutral red absorbance to 81% and 78% HEPES control for 500 μM and 1 mM AMPT respectively.

In order to optimise AMPT treatment, the dose dependence of DA depletion (24 h post treatment) and loss of cellular viability (48 h post treatment) were explored (*Figure 3.23C*). Over this range of concentration (5 - 500 μM), AMPT had a dose dependent effect on both neutral

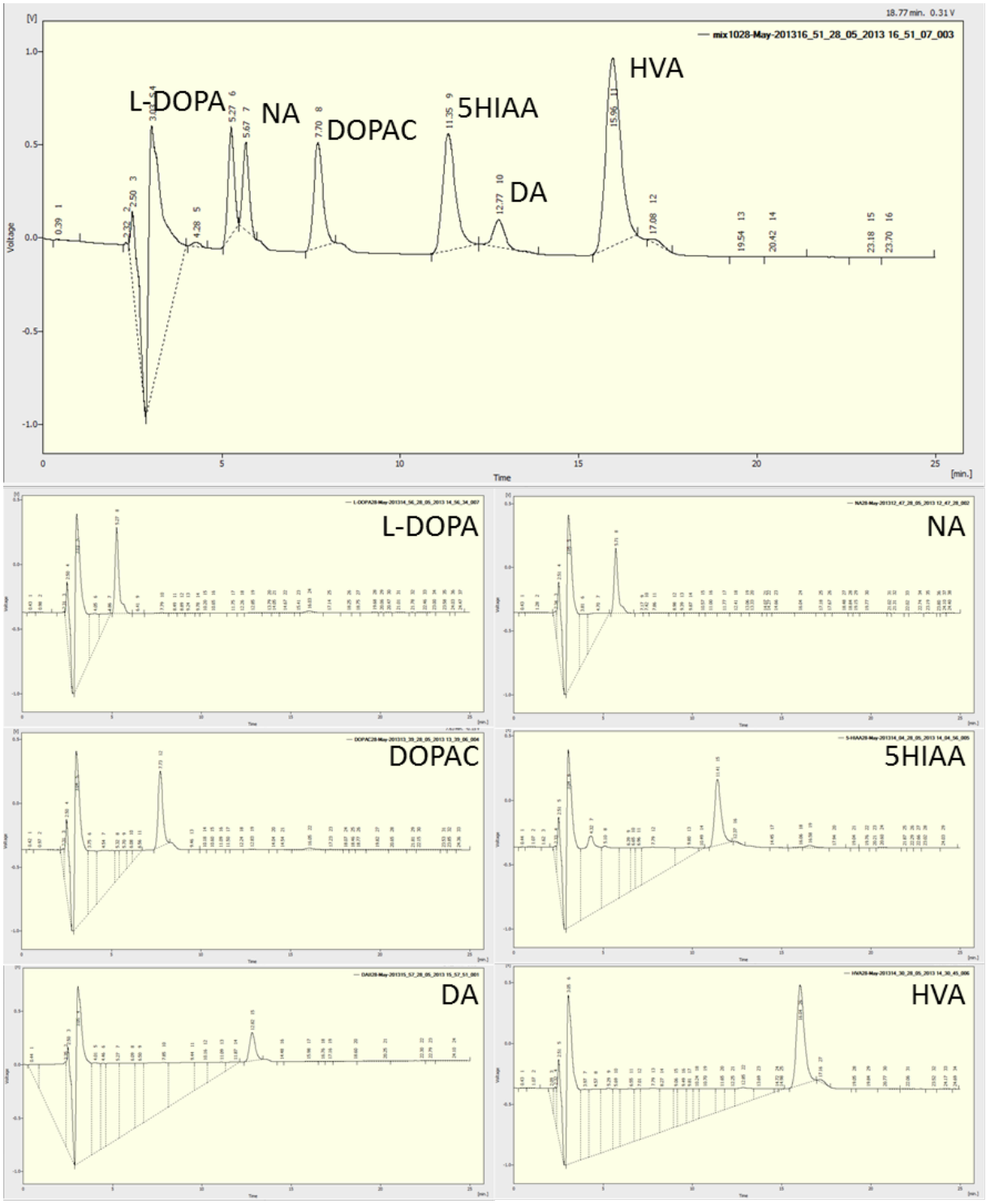

Figure 3.20: **Dopamine metabolites can be separated by HPLC.** 100 nM solutions of DA and metabolites were prepared (in 100 μM PCA), samples were separated by HPLC and detected electrochemically. A mixed solution was also compared (100 nM for each compound) and subjected to HPLC analysis.

red absorption and DA depletion; 100 μM AMPT was selected as a dose for further experiments as this resulted in 38% control DA and 89% control neutral red absorption.

The optimised regime (AMPT 48 h, 100 μM) was used to measure the effect of DA depletion on MPP^+ vulnerability (100 μM, 36 h, neutral red accumulation) (*Figure 3.23D*). DA depletion (via AMPT treatment) had no significant effect on neutral red uptake either in the absence, or

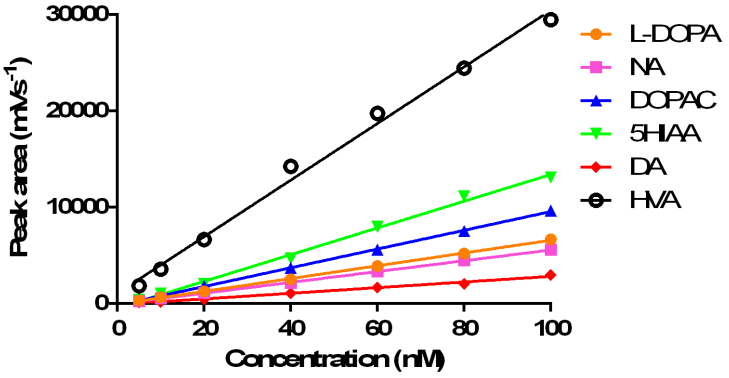

Figure 3.21: **Dopamine metabolite HPLC peak area depends upon concentration.** A series of mixed solutions of DA and metabolically related compounds (each 5 to 100 nM) were prepared in 100 μM PCA, separated by HPLC and detected electrochemically. Each peak was identified by its retention time and peak area measured. Linear regression was performed.

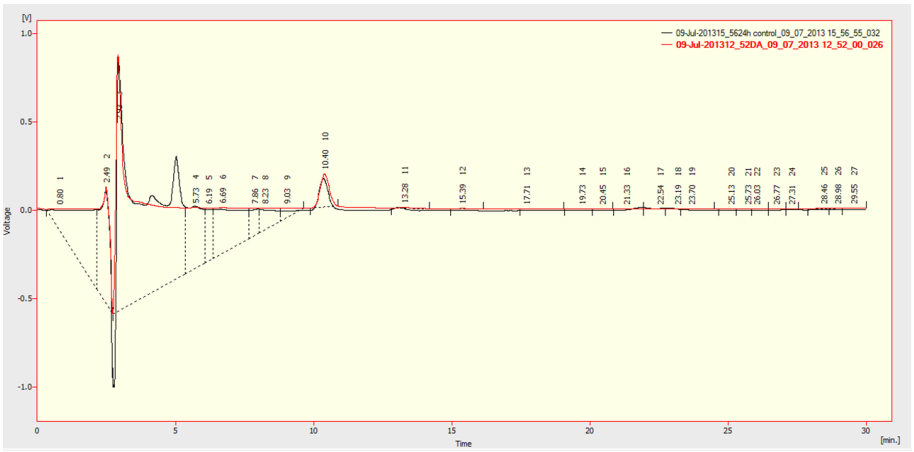

Figure 3.22: **M17 cells contain dopamine.** M17 cells were trypsinised and resuspended in PCA (100 μM) to achieve lysis. The solution was subjected to HPLC analysis and the DA peak identified based on retention time compared to standard solution (100 nM).

presence, of MPP^+ suggesting that DA did not potentiate MPP^+ cytotoxicity in M17 cells.

3.2.5 Microarray data

Previous reports have shown altered gene expression *in vitro* following MPP^+exposure [303–307]. To analyse gene expression in M17 cells RNA samples were prepared from M17 cells following 24 h exposure to MPP^+ (100 μM), control samples were also prepared. Microarrays were run by Dr. Sheena Lee using Affymetrix Human Gene 2.0 ST Arrays, Dr. Lee also performed data analysis. Following PLIER normalisation and multiple t tests, 220 differentially expressed genes were identified. However, no genes remained significant following correction for multiple testing. Therefore, testing for pathway/functional enrichment was not considered appropriate. Probe signals for selected genes with significant altered expression (before multiple testing correction) are shown in *Figures 3.24*.

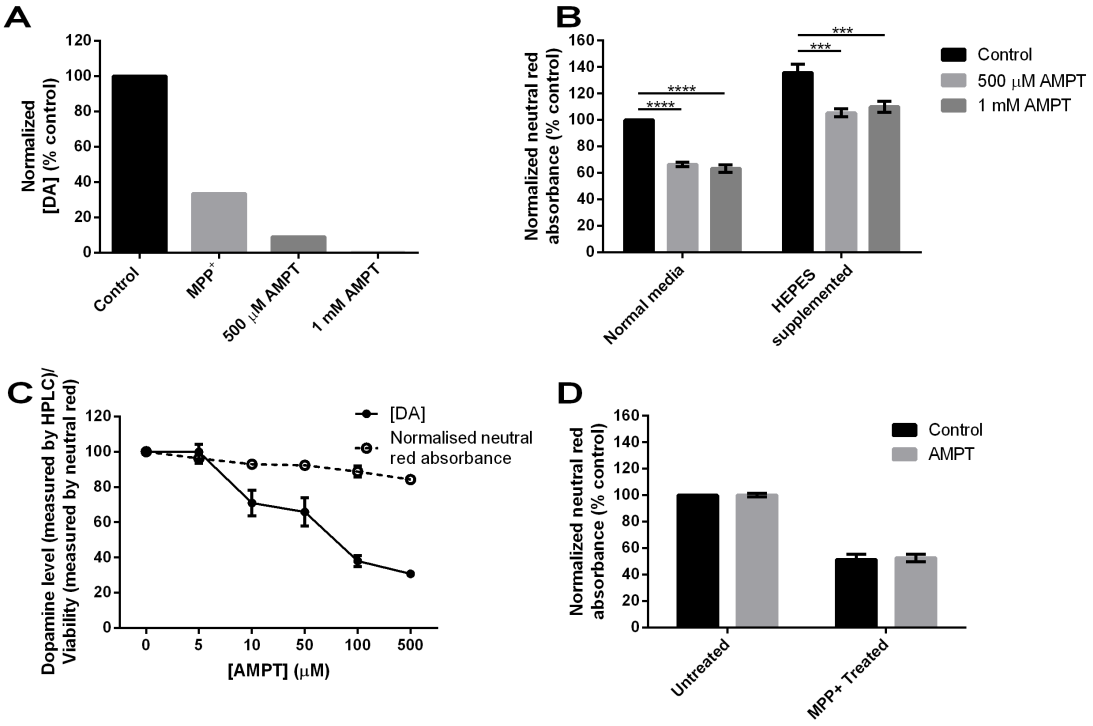

Figure 3.23: **Dopamine depletion does not affect cellular vulnerability to MPP$^+$ in M17 cells A** Cells were treated with MPP$^+$ (100 μM) or AMPT (500 μM or 1 mM) for 24 h, trypsinised and resuspended in PCA. Solutions were separated by HPLC followed by electrochemical detection. Peak size was normalised to protein concentration and then normalised to untreated cells (unnormalised control absorbance was 0.394). Bars show a single experiment. **B** Cells were treated with AMPT (500 μM or 1 mM) for 48 h in either normal (OM) media or media supplemented with HEPES. Cells were then treated with neutral red reagent for 2 h, washed, lysed and absorbance measured at 540 nm for triplicate wells. Values were normalised to untreated control cells (unnormalised control absorbance was 0.490). Data points represent means ± SEM (n=3), *** represents P≤0.001 and **** represents P≤0.0001 compared to untreated control for each media condition. Data were analysed using a 2-way ANOVA with a Dunnett multiple comparison test. **C** Cells were treated with AMPT (5 - 500 μM). After 24 h cellular DA levels were measured by HPLC and electrochemical detection (as above) and after 48 h cellular viability was assessed by neutral red uptake (as above) (unnormalised control absorbance was 0.239). Data points represent means ± SEM (n=3). **D** Cells were treated with AMPT (100 μM) for 48 h and MPP$^+$ (100 μM) for 36h. Cellular viability was assessed using neutral red uptake (as above) and values normalised to untreated controls (unnormalised control absorbance was 0.923) . Bars represent means ± SEM (n=3). Data were analysed using a 2-way ANOVA with a Sidak multiple comparison test.

In order to compare the results from this thesis to other MPP$^+$ *in vitro* microarray studies a subset of genes with a differential expression of at least 1.5 fold and a p value equal or less to 0.05 were identified. Such an approach has previously been reported by Simunociv *et al.* [340] and in their study of MPP$^+$ treated PC12 cells Xu *et al.* highlighted genes with at least a twofold change in expression without further statistical analyses [306]. When the data generated for this thesis was analysed in this way, 41 genes had at least a 1.5 fold average change in expression, none had a twofold change. The 41 genes were compared to the results from published *in vitro* microarray studies following MPP$^+$ treatment in SH-SY5Y [304], Neuro-2a [305], PC12 [306]

and MN9D [307] cells. Four genes (CHAC1, GPT2, SLC6A9 and TRIB3) upregulated in Neuro-2a [305] following MPP^+ treatment also appeared in the M17 list and one of the genes (TRIB3) also appeared in the PC12 study [306]; there was no overlap with the SH-SY5Y [304] or MN9D [307] studies.

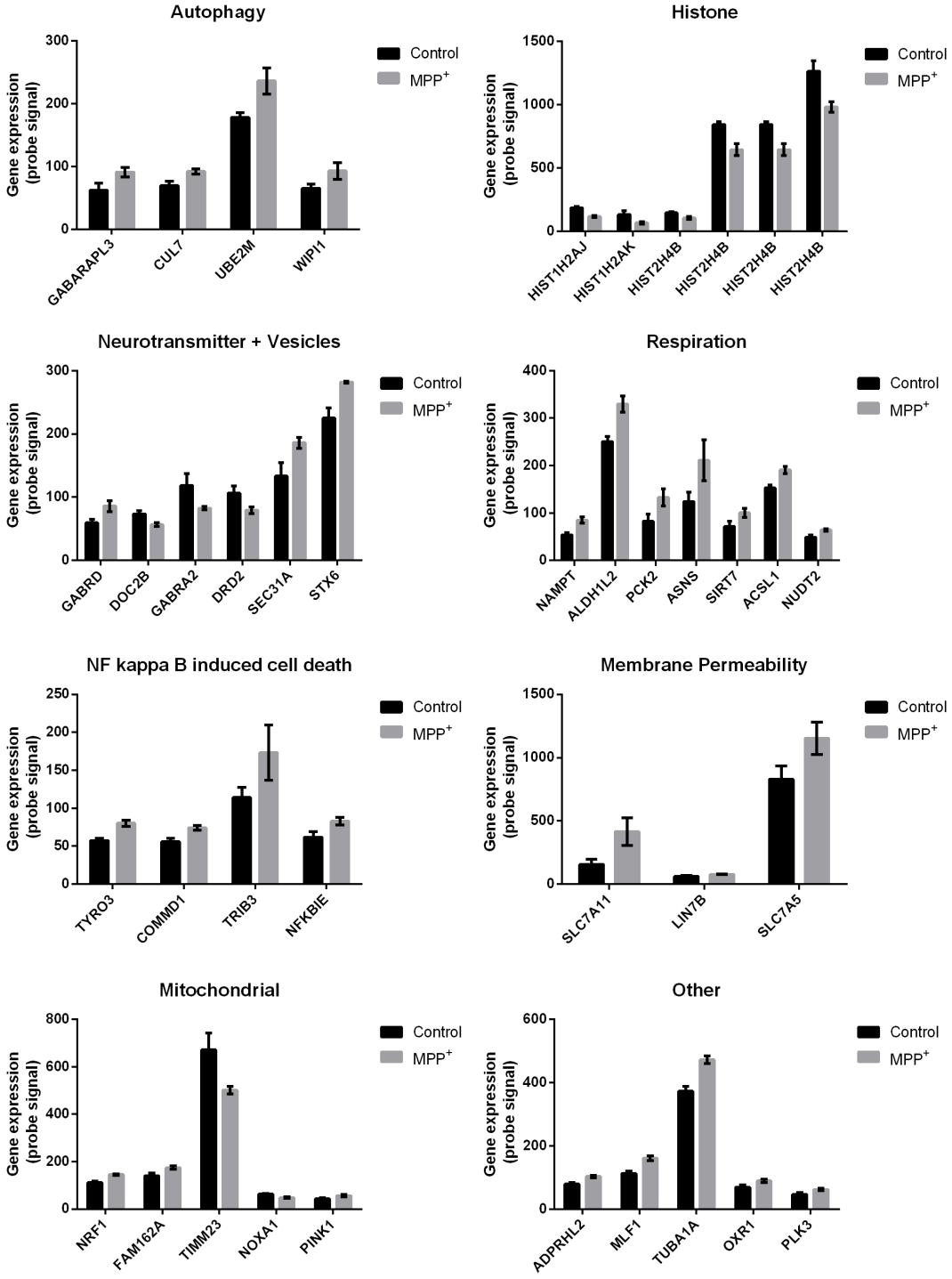

Figure 3.24: **Microarray analysis shows no statistically significant alteration to gene expression in M17 cells following MPP^+ treatment.** Cells were treated with MPP^+ (100 μM) for 24 h. RNA was extracted and analysed using Human Gene 2.0 ST Arrays. Genes were grouped manually according to process and average probe signal is shown. Bars represent means $\pm$ SEM (n=3).

3.3 Discussion

3.3.1 MPP^+ induced cell death in M17 cells

This chapter focussed on the characterisation of MPP^+ induced cell death in the M17 cell line and the development of sensitive assays. MPP^+ was shown to induce cell death in a time and dose dependent manner as measured by decreased MTS reduction and cell counts, lower sensitivity was observed using the MTS assay.

The doses of MPP^+ required to induce cell death in M17 cells were lower than typically used in PC12 [99, 100, 306, 347] or SH-SY5Y [98, 100, 114, 188, 199, 209, 304, 356, 361, 365] cell lines; however, the dose response was similar to that reported in the published studies of MPP^+ exposure in M17 cells [79, 201, 336]. The higher vulnerability better reflects that observed in primary neuronal tissue [190, 221, 327, 366] and may indicate that the M17 cell line is a more physiological model. The greater MPP^+ vulnerability may reflect the DA nature of M17 cells or the ratio of DAT to VMAT. A regime of 100 μM MPP^+ was used for further investigations as it resulted in approximately 50% cell death after 48 h. The longest possible treatment time with a lower dose of MPP^+ was considered optimal to better mimic the chronic nature of PD. However, the mitotic division of M17 cells limited the time for which cells could be cultured and M17 cells are resistant to retinoic acid induced differentiation [338].

In accordance with previously published results, MPP^+ induced ATP depletion; antimycin A was used as a positive control for ATP depletion. For both toxins, ATP depletion was potentiated by the use of low glucose/high galactose media. Although galactose can be used as a substrate for respiration, there is no net release of ATP from its conversion to pyruvate [104]. The decreased ATP levels in galactose media indicate that MPP^+ and antimycin A cause ATP depletion by blockade of the ETC and not inhibition of glycolysis. These results are in accordance with MPP^+ being a complex I inhibitor, as previously reported [71–73].

Neutral red is a lysosomal dye which is trapped in the lysosome upon protonation. Accumulation depends upon the maintenance of a proton gradient across the membrane, and is ATP dependent [286, 345]. Neutral red is established as a cellular viability assay and results correlate with MTS reduction [345]; however, the assay has not been widely used in the context of MPP^+ induced cell death. MPP^+ treatment led to a decrease in neutral red absorbance with no change to overall lysosomal levels (measured by LAMP1 levels). Absorbance was also decreased following treatment with antimycin A - known to cause potent ATP depletion. The effects of both MPP^+ and antimycin A were exacerbated in low glucose/high galactose media consistent with an

increase in lysosomal pH via cellular ATP depletion as a result of ETC blockade. Treatment with the vacuolar-type H^+-ATPase inhibitor bafilomycin A1 led to a rapid and profound decrease in neutral red absorbance demonstrating that an increase in lysosomal pH was sufficient to prevent neutral red accumulation and that neutral red was selectively concentrated in the lysosomes.

The fluorescence of TMRM, and other rhodium dyes, has been widely used to measure the loss of mitochondrial membrane potential following MPP^+ exposure and other mitochondrial insults [204, 209, 327]. However, TMRM fluorescence is generally measured on a single cell basis and is not frequently optimised for use on a plate reader. It was demonstrated that MPP^+ treatment (100 μM) led to a significant decrease in TMRM fluorescence after 24 h. The results in this thesis are in accordance with those of Fall and Bennett who demonstrated that MPP^+ treatment (5 mM, 13 h) led to decreased TMRM fluorescence in SH-SY5Y [209]. CCCP is known to collapse mitochondrial membrane potential and acted as a positive control for the TMRM assay [348]. CCCP exposure was shown to lead to loss of TMRM fluorescence in a dose dependent manner following 2 h treatment demonstrating that TMRM fluorescence was dependent on mitochondrial membrane potential and not accumulation elsewhere within the cell. The optimisation of the neutral red and TMRM assays provided a system by which MPP^+ induced cell death could be followed in a sensitive, yet medium-throughput fashion.

Flow cytometry in conjunction with annexin-V and 7AAD staining was used to determine the mechanism of cell death in M17 cells. Despite the caveat of possibly inaccuracies in gating, the results indicated increased annexin-V binding characteristic of apoptotic cell death following MPP^+ treatment. Increased caspase-3 cleavage was observed using both flow cytometry and ICC supporting apoptosis as the mechanism for cell death in M17 cells following MPP^+ exposure. ICC provided superior results as the use of the conjugated antibody in conjunction with flow cytometry led to an anomalously high degree of straining in control cells most likely due to the exclusion of healthy cells through flawed gating. However, the increased capase-3 cleavage detected by both flow cytometry and ICC is in accordance with previously published reports of MPP^+ induced apoptosis in other cell lines [98, 209, 211, 326], although there has been little investigation of the mechanism of cell death in the M17 line.

Having characterised an MPP^+ regime based on constant exposure, the effects of brief MPP^+ exposure were investigated. It was demonstrated that as little as 2 h exposure to MPP^+ was sufficient to cause significant loss of cell viability and mitochondrial damage, athough these effects were not fully realised until later time points. Damage was not observed until after the neurotoxin was removed, indicating that initial MPP^+ exposure set in motion an inevitable process of cell death that could not be reversed by toxin removal. However, increased deleterious

effects were observed for longer exposures to MPP^+ suggesting that further damage was caused throughout the exposure window.

3.3.2 Effects of MPP^+ on autophagy in M17 cells

The effects of MPP^+ on autophagy are a matter of debate and it is likely that they depend upon experimental system and dosage of MPP^+. Published results indicate the MPP^+ exposure leads to an accumulation of autophagosomes as measured by LC3B lipidation, the detection of LC3B positive puncta by fluorescence microscopy and the identification of autophagosomes by electron microscopy [99, 100, 159, 186, 186, 188, 190, 204, 351, 356]. However, there is conflicting evidence as to whether autophagosome accumulation reflects an increased rate of autophagic flux or a blockage in the fusion of autophagosomes with lysosomes or subsequent cargo degradation.

In accordance with published results, an increase in LC3B lipidation was detected following 48 h MPP^+ treatment. However, no change in LC3B lipidation was observed after 24 h MPP^+ treatment, although by this time point cell death is inevitable. No further change to lipidated LC3B levels was seen upon co-treatment with bafilomycin A1 indicating that autophagosome accumulation occurred as a result of blocked degradation rather than increased initiation of autophagy.

It has been suggested that blockage of CMA may lead to alterations in macroautophagy as a compensatory process [165, 168]. Therefore, levels of LAMP2A, an established marker corresponding to the rate limiting step of CMA [168, 170, 171, 350, 364], were investigated. No changes to LAMP2A levels were seen after either 24 or 48 h MPP^+ treatment suggesting that there were no alterations to CMA in the M17 MPP^+ model. However, it is acknowledged that were other stages of CMA impeded, CMA flux could be reduced in the absence of changes to LAMP2A levels. Others have demonstrated changes in lysosome levels following MPP^+ treatment [159], however, no change in the levels of LAMP1 were observed in this thesis, indicating no change in overall lysosome number. Decreased neutral red uptake indicated an increase in lysosomal pH consistent with ATP depletion. It is proposed that ATP depletion results in the loss of the proton gradient across the lysosomal membrane leading to a blockage in autophagic flux. Alternatively, ROS may damage the lysosomal membrane; however, the potentiation of decreased neutral red uptake in galactose media indicates that ATP depletion is the trigger for lysosomal dysfunction. This could be further established by repeating experiments with anti-oxidant cotreatment to counteract the effects of ROS.

To measure the overall rate of autophagic flux a pulse-chase assay was developed. Although such

assays are established in hepatocytic tissue [354] they are less widely used in immortalised cell lines [287, 355] and they have seldom been utilised in neuronal models. Previously published results in 3T3 cells [287] were replicated and it was demonstrated that autophagy could be induced in M17 cells following 6-12 h serum starvation or rapamycin treatment. Interestingly, the increases in overall protein degradation in M17 cells were smaller than those in the 3T3 cell line, indicating that M17 cells were less sensitive to the induction of autophagy.

LC3B WB were performed following identical conditions (serum starvation or rapamycin treatment) and no change in lipidation levels was seen following starvation in the presence or absence of bafilomycin A1. Although the lack of increased LC3B lipidation following starvation in M17 cells is plausible given the pulse-chase data (where only a small increase in degradation was observed), it is in contrast to that reported in other cell lines [152, 367, 368]. This discrepancy highlights the variations between different cell lines and indicates that the M17 line may not respond to autophagic stimuli in an entirely typical fashion; this may be a limitation in using M17 cells to explore autophagic processes. The unaltered LC3B lipidation following starvation also indicated that the pulse-chase assay had higher sensitivity than LC3B WB.

MPP^+ treatment resulted in the slowed breakdown of long lived proteins after 12 h (as measured by the pulse-chase assay), a time point preceding any changes to LC3B lipidation, further supporting the idea of higher sensitivity in the pulse-chase assay. Where cells were cultured for 48 h in the presence of MPP^+ there was a further, dramatic decrease in the rate of protein breakdown consistent with further cellular dysfunction and eventual death. The pulse-chase data demonstrated that the accumulation of lipidated LC3B observed in the M17 cell model was as a result of blocked autophagic flux, a previous area of contention. This effect is consistent with the lysosomal dysfunction observed as without functional acidic lysosomes, protein degradation cannot occur. Therefore, any treatment which led to lysosome deacidification would be expected to result in the build-up of autophagosomes and a lower rate of autophagic flux.

An intriguing comparison can be drawn between the results in this thesis and the result reported by Dehay *et al.* who also explored the effects of MPP^+ on autophagy in the M17 cell line [159]. Dehay *et al.* reported an accumulation of autophagosomes as a result of decreased autophagic flux. Lysosomal dysfunction was suggested to be the cause of this blockage. In contrast to the results in this thesis, the authors reported decreased lysosome numbers and lysosomal membrane permeabilisation by mitochondrially produced ROS. However, this thesis and the work of Dehay *et al.* are in agreement that MPP^+ treatment results in decreased autophagic flux in M17 cells as a result of lysosomal dysfunction.

3.3.3 Effect of dopamine on MPP^+ vulnerability in M17 cells

It was hypothesised that the M17 line's vulnerability to MPP^+ was potentiated by the presence of endogenous DA. The SH-SY5Y cell line exhibits a lower sensitivity and the laboratory has previously demonstrated that SH-SY5Y cells do not express TH or DA [79]. Further, DA is known to be cytotoxic and a potential cause of oxidative stress [220, 222]. Some investigations into the effect of DA on neurotoxin vulnerability have previously been conducted [226, 227], but not in the M17 cell line. Although AMPT induced DA depletion does not alter rotenone vulnerability [226, 227], DA and non-DA cell lines do exhibit differential DA vulnerability [226] and methamphetamine co-treatment potentiates rotenone vulnerability [227].

AMPT was used to deplete DA in M17 cells and a dosage regime was optimised to minimise toxicity. However, no change to MPP^+ vulnerability was seen upon DA depletion, indicating that DA did not alter MPP^+ vulnerability in M17 cells. The ratio of DAT to VMAT2 may explain the M17 line's higher sensitivity to MPP^+ when compared to SH-SY5Y and PC12 cells. Levels of DAT control the uptake of the neurotoxin and VMAT2 mediates MPP^+'s sequestration into cellular vesicles. Further, MPP^+ toxicity is proportional to the levels of DAT and VMAT2 [325]. This hypothesis could be explored by KD and OE of DAT and VMAT2 in the M17 line and an exploration of MPP^+ sensitivity.

3.3.4 Microarray data following MPP^+ treatment in M17 cells

Microarray studies have been performed in other cell lines (although not M17) to investigate the altered expression of proteins following MPP^+ exposure [304–307]. Further, in other disease areas differentially expressed genes (identified by microarray analysis) have been used as seeds in the construction of disease related PPIN [341, 342]. Therefore, microarray analysis was conducted to identify differentially expressed genes in M17 cells following MPP^+ treatment.

Although 220 genes were initially identified, none remained statistically significant after correction for multiple testing - a procedure which is essential in the analysis microarray data [369]. The lack of significant results was surprising as, although three replicates provided limited statistical power, published studies in other MPP^+ *in vitro* models with similar replicate numbers had identified differentially expressed genes. Further, the MPP^+ treatment regime employed (24 h, 100 μM) had already been shown to cause apoptotic cell death in M17 cells within this thesis.

In order to compare the results obtained in this thesis to published studies the 41 genes with at

least a 1.5 fold change in expression were highlighted, although it is acknowledged that no genes exhibit statistically significant differential expression. The greatest overlap (four genes) was found with Mazzio *et al.*'s study in Neuro-2a cells which identified 287 differentially expressed genes. It should be acknowledged that the number of genes reported in the Neuro-2a study is higher than that in the other studies (287 compared to 106 for PC12, 51 for MN9D and 48 for SH-SY5Y studies), which may explain the greater overlap.

Although the degree of overlap with other studies was low, it should be noted that overlap between published microarray studies from post mortem PD samples is also low [308]. Additionally, when Miller *et al* studied identical MPTP treated mouse SNpc samples using two different arrays systems, only approximately 2% of the genes identified were significantly altered on both arrays [303]. None of the published *in vitro* MPP^+ studies were conducted using Affymetrix arrays used in this thesis and only one was conducted in a human cell line [304].

Regardless, the microarray data will be an invaluable resource for further investigations. Transcript levels of individual proteins can be extracted from the dataset and expression predicted, proteins with very low transcript levels are unlikely to be present at the protein level. Although not investigated in this thesis, the data on the expression of non-coding mRNAs following MPP^+ treatment has not previously been collected and may be valuable to others.

3.3.5 Limitations and biases of assays

Viability assays

As with all assays, the viability assays employed in this thesis had a number of limitations. As experiments were performed on dividing cells it was impossible to distinguish between cell death and reduced cell proliferation. To address this issue, experiments would need to be repeated on differentiated cells.

Further, many of the assays (in particular the ATP, TMRM, neutral red and MTT/MTS assays) were performed using a plate reader and therefore, values are for the entire well rather than an individual cell. Consequently, any decrease in cell number would lead to lower readout values even if 'per-cell' values were constant. No significant change in cell number was seen until after 36 h MPP^+ treatment; however, decreases in viability reported at later time points are likely to be partially due to lower cell numbers. Further, cell counts were not repeated in galactose media and therefore, the reported potentiation of ATP depletion and diminished neutral red uptake may have been partially due to lower cell numbers. Variations in cell numbers could be allowed

for by preparing duplicate plates and estimating cell number with a BCA assay.

Beyond, these general considerations, the neutral red assay had several further limitations. Any increase/decrease in lysosome levels will result increased/decreased neutral red uptake even if there is no change to lysosome acidification [286]. LAMP1 levels were shown to be unaltered following MPP^+ treatment. However, WB have limited sensitivity and is remains possible that lysosome levels were altered. Additionally, it was demonstrated that Bafilomycin A1 treatment resulted in decreased neutral red uptake with no change to cellular ATP levels. Therefore, although ATP depletion results in decreased neutral red uptake, diminished neutral red absorbance cannot be entirely reliably used as an indicator of ATP depletion.

MTS/MTT reduction is dependent upon glycolysis, which is upregulated immediately following MPP^+ exposure [79, 88]. Therefore, these assays may underestimate cell death, particularly at early time points and should be used in conjunction with other viability assays.

Flow cytometry

Although flow cytometry analysis was conducted with the assistance of the flow cytometer technician it is accepted that there may have been flaws in this analysis. The forward/side scatter plot was gated to select only intact cells. However, any inaccuracies in this gating would result in erroneous results. Such gating errors would explain the anomalously high proportion of cells detected as stained for cleaved caspase 3 if many healthy cells were excluded by gating. It would be helpful to repeat such analysis on non-gated data to investigate the effects of gating on the conclusions drawn.

The use of live cells for flow cytometry proved problematic as the cell populations on the fluorescence plot shifted during in the time taken to run medium to large numbers of samples (2 to 4 h). It is considered likely that this is due to cell death caused by the trypsinisation, resuspension and staining protocol. It was for this reason that cleaved caspase 3 staining in fixed cells was also explored.

However, any clumping of cells would lead to them being excluded from analysis and if healthy or apoptotic cells had different propensities to clump this would bias the estimations of the extent of cell death under both the caspase-3 and the annexin-V/7AAD protocols. Due to these limitations, flow cytometry was not further used in this thesis. As a point of interest, it is noted that initial flow cytometry experiments with SH-SY5Y cells resulted in considerably more homogenous cell populations as assessed by forward/side scatter.

Autophagy assays

As discussed extensively, LC3B lipidation is an imperfect measure of autophagic flux. Even when conducted with a Bafilomycin A1 control, this assay does not provide information about the amounts of proteins/organelles contained with autophagosomes [350]. Further, there is considerably redundancy in the LC3 subfamily and other proteins may substitute for LC3B [353, 370].

The identification of puncta by ICC has similar limitations as this technique provides no information about the content of the puncta. Further, such data can only provide static 'snap shots' of a dynamic process. The data in this thesis was further limited by the failure to detect autophagosomal and lysosomal puncta colocalisation and the diffuse nature of the LC3B staining.

Although superior, pulse-chase assays also have limitations. The data provided does not allow for the distinction between CMA and macroautophagy. Due to the TCA precipitation any secreted intact proteins would have be excluded from the analysis [287]. Additionally, it was assumed that the excess of cold valine in culture media would not affect the rate of autophagy, although this was not tested.

It is further acknowledged that all experiments were conducted in mitotic cells, post-mitotic cells might be expected to respond differently to autophagic stimuli as damaged proteins and organelles cannot be diluted by cell division.

Other assays

Although used extensively, WB remain a semi-quantitative technique and small changes to protein levels may not have been sensitively detected; improved results could be achieved using ELISA assays. Due to variations in antibody binding affinity, intensities could not be compared for different proteins. Further, variations in antibody or HRP activity or incubation time limited the comparison of intensities between different blots necessitating the use of normalised data.

Although HPLC allowed accurate measurement of DA and its metabolites, many of these compounds (including DA) are unstable and light sensitive. Despite all precautions, it is likely that such breakdown occured and this would have introduced error into the measurement of DA levels, possibly leading to an overestimate of the extent of DA depletion achieved.

3.3.6 Summary

In summary, an MPP^+ treatment for the M17 cell line was optimised. It was demonstrated that cell death occurred via an apoptotic mechanism and that ATP depletion was as a result of blockade of the ETC in accordance with previously published results [73, 79, 209]. However, depletion of endogenous DA did not affect MPP^+ vulnerability in M17 cells. Notwithstanding the limitations dicussed above, the TMRM and neutral red assays were optimised to allow characterisation of cell damage in a medium-throughput manner. A pulse-chase assay was also optimised for use in the M17 cell line and shown to exhibit higher sensitivity than LC3B lipidation levels as measured by WB. MPP^+ treatment led to a decreased rate of autophagic flux with no evidence of alteration to overall lysosome levels or CMA. TMRM, neutral red and pulse-chase assays will be used to measure alterations to MPP^+ induced cytotoxicity following the modulation of target proteins. Protein targets will be identified through network analysis and centred around the role of mitochondrial dysfunction and altered autophagy in the context of MPP^+ induced cell death.

Chapter 4

Protein-protein interaction networks

4.1 Introduction

Network science is a rapidly evolving area of research and offers a possible route for the analysis of large amounts of complex data in fields as diverse as biology, computer science and social interactions [95, 371]. As discussed in *Chapter 1*, biological systems can be modelled using PPIN and this thesis aims to use such networks to identify potential points for therapeutic intervention. PPIN are viewed as the most pertinent network model because changes to protein structure or abundance may result in pathology in the absence of genetic abnormality. The majority of currently approved drugs, target proteins which do not correspond to disease causing genes [273]. Further, in PPIN, edges represent experimentally testable, physical interactions rather than less well defined relationships or influences. Below follows an introduction to the key concepts of biological networks.

4.1.1 Key network concepts

A network is a graph made up of nodes (vertices) connected by edges, more mathematically $G = (V, E)$ where V is the set of nodes (vertices) and E is the set of edges. The degree of a node is defined as the number of non-self edges it has, that is the number of other nodes it is connected to [371]. In the context of this thesis, a node represents a protein and an edge signifies a physical interaction between two proteins. An illustrative network is shown in *Figure 4.1.* A path is a series of edges which may be traversed to move from one node to another (such that an edge exists between each node and its successor) and path length is the minimum number of steps separating two nodes [371]. The average shortest path length of a connected network is the average of the lengths of the shortest paths connecting all possible pairs of nodes [371].

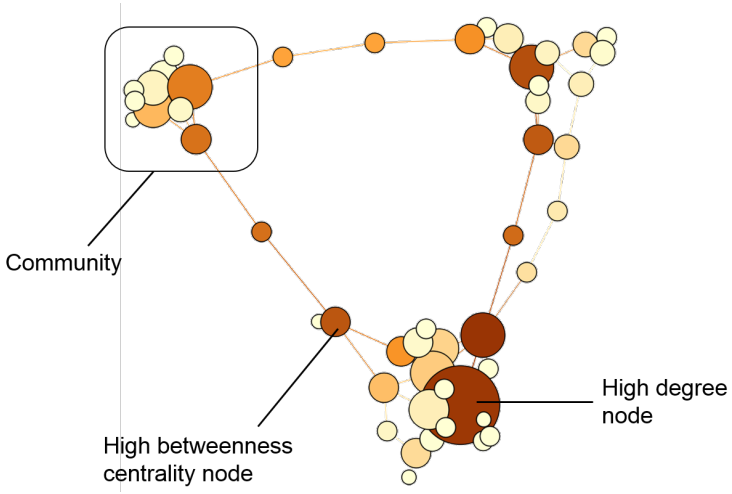

Figure 4.1: **An illustrative network.** In the case of a PPIN the nodes would represent proteins and the edges would represent physical interactions between two proteins. Nodes are sized according to degree; a hub has a high degree and therefore a large size. Nodes are coloured according to betweenness centrality (BC); the darker the colour, the higher the centrality of a node. Communities are groups of nodes which interact more strongly with each other than the network as a whole. In the illustrative network the edges are unweighted and undirected.

The diameter of a network is the longest, shortest path between any two connected nodes - it can be thought of as the distance from one side of the network to the other [95]. The density of a network is the proportion of all possible edges which exist. Where every node is connected to every other node the density is one and where there are no edges then density is zero. Many real-world networks, including most currently available PPIN, are sparse [371].

Networks may be weighted or unweighted. In an unweighted network all edges are equivalent, but in a weighted network, some edges are more important than others [371]. Edge weighting may represent the volume of interaction (for example the number of flights between two airports) or, the confidence that an edge is accurate [265]. Edges may also be directed, representing an interaction that only occurs in one direction [371].

Communities within networks

PPIN, in common with many other types of networks, exhibit a modular structure. Some groups of nodes are more strongly connected to each other than the rest of the network; these groups are termed communities. In yeast, communities within PPIN typically represent protein complexes (groups of proteins that simultaneously interact to form multi molecular machinery) or functional modules [372]. The extent of clustering across a network gives the probability that two nodes, both connected to a common node, also share an edge. Clustering may be heterogeneous across PPIN and highly connected groups of old proteins are observed in yeast PPIN [373].

Numerous methods have been developed for identifying communities within networks [374]. This thesis utilised the Potts method for community detection [375] as it has previously been shown to be effective in PPIN [376] and a package is available for use in R. Lewis *et al.* used the Potts method within the yeast PPIN to identify communities and demonstrated that they displayed significant GO annotational enrichment [376]. Further, the authors showed that, by altering the resolution parameter (γ), different biological processes could be identified and that the optimal value of γ depended upon the process that was to be identified. The mean clustering coefficient of a community was shown to act as a good predictor of its functional homogeneity [376]. Annotational enrichment offers a route to ascribing biological function to PPIN communities. However, care must be taken as GO annotations may be predicted on the basis of interactions and the annotation of the proteome is uneven, with some proteins more fully annotated than others [376].

Degree distribution

Real-world networks have several initially surprising properties. The average shortest path length across connected networks is low, such that any node can be connected to any other node in only a few steps - termed the 'small-world' property [371]. Further, interactions are not evenly distributed with most nodes having a low degree, but a few (termed hubs) having a very high degree [95, 371]. A number of theoretical network models have been applied to try and explain the properties of real-world networks.

One of the first network models developed was the Erdos-Renyi random graph model in which all possible edges have an equal probability [377]. The Erdos-Renyi model results in an average shortest path length for connected networks proportional to the total number of network nodes ($l \propto logN$) - explaining the small world behaviour observed. However, this model predicts an binomial degree distribution (frequently approximated as a Poisson distribution) which cannot explain the occurrence of hubs [95, 371].

An alternative model of 'scale-free' networks is characterised by degree distributions obeying power laws ($P(k) \propto k^{\theta}$) [371]. The 'scale-free' model predicts the occurrence of hub nodes and (for values of θ between two and three) ultra-small world behaviour ($l \propto loglogN$). It has been suggested that scale-free networks are universal [371], and that biological networks are scale free [95, 378, 379]. The Barabasi-Albert model accounts for the development of scale-free networks due to network growth (addition of new nodes) and preferential attachment (new nodes are more likely to attach to highly connected nodes) [371]; in a biological context a scale-free

network might be predicted by gene-duplication [371].

However, more recent work has called the scale-free hypothesis into question and suggested that assignments of power laws had been made without sufficient statistical rigour or when lacking data over a sufficient range [380, 381]. Further, Stumpf and Porter suggested that the assignment of power laws where there is no mechanism to explain their occurrence may be of limited use [382].

Although none of the available network models fully recapitulate the features of PPIN [383, 384], hubs remain an important feature of biological networks. Hubs may either be assortative or disassortative, that is hubs are more or less likely than random to be connected to other hubs. Both phenomena are observed in real-world networks, but PPIN are generally disassortative [385]. Further, real-world networks, including biological networks, typically exhibit small world properties [95, 386] such that a perturbation in one part of the network can rapidly effect the entire system [386].

Centrality

The concept of centrality measures the importance of a given node for the overall integrity of the network. One, widely used, measure is the betweenness centrality (BC) (*Subsection 2.3.6*), which can be thought of as the number of shortest paths which would be disrupted were a given node deleted [387]. Numerous extensions of the BC metric have been proposed and algorithms developed for their efficient calculation including those only considering a subset of paths and/or nodes [387, 388].

4.1.2 Robustness of PPIN

PPIN (along with other real-world networks) are robust to random deletions, but vulnerable to targeted attacks [269, 371]. Scale-free networks are predicted to be robust, but a network does not need to exactly obey the power-law to be robust [371]. The disruptive effect of node deletions can be measured by network fragmentation which is maximised where nodes are selected for removal based on their degree or centrality [269, 371, 385]. In experimental systems, such deletions can be achieved using KO or KD. Theoretical results have been replicated in yeast, and while some deletions are lethal, the majority of proteins appear to be non-essential, this is not fully explained by the presence of duplicate copies of genes [389–391].

Although there is considerable redundancy in biological systems under optimal conditions, when

deletions are combined with stress or low nutrient conditions deleterious effects are more common. Hillenmeyer *et al.* showed that 97% of yeast gene KOs have a growth phenotype under suboptimal experimental conditions [392]. The concept of synthetic lethality is that when perturbations are combined with an external stress or genes deleted in combination they are more likely to affect viability [389, 393]. Although biological systems display considerable redundancy under optimal conditions, they may not be robust under all conditions nor to multiple deletions.

Such biological redundancy can intuitively be understood; there are alternative pathways for many biological functions - such that if one is damaged the process can still be completed and modularity can prevent an attack in one module from effecting the entire system [394].

Currently, the extent to which biological essentiality can be predicted by network topology is not clear. Jeong *et al.* demonstrated a correlation between node degree and essentiality in yeast [395] and others have shown that essentiality (across a number of model organisms) is related to node centrality in PPIN [396–398]. However there is still debate as to the biological explanation behind the 'centrality-lethality rule' and others question the predictive value of a node's topology [399].

4.1.3 PPI data

Recent developments in high-throughput techniques have led to the availability of large amounts of PPI data, both facilitating and necessitating systems biology approaches [95, 400]. There are two main types of high-throughput experiment used to collect PPI data: yeast two hybrid (Y2H) and tandem affinity purification (TAP) [384, 401].

In a Y2H approach, a yeast transcription factor is divided in two with one protein of interest attached to the DNA binding domain and the other attached to the transcription activating domain [274]. Only when the two proteins interact is a complete transcription factor formed, resulting in transcription of a reporter gene. Y2H is an *in vitro* technique which allows transient and unstable interactions to be detected [384]. However, all interactions must occur in the nucleus (not the physiological environment for many proteins), the proteins are expressed at above physiological levels and only two proteins may be tested at a time [402]. Further, Y2H may report interactions between proteins that would not come into contact under normal conditions, due to sub-cellular localisation or temporally different expression [403]. Increasing the utility of such approaches, the split ubiquitin based system, allows cytosolic and membrane based interactions to be detected in yeast [302]. An interaction between the two fusion proteins allows

ubiquitin binding protease mediated cleavage, the release of a transcription factor and subsequent expression of a reporter gene.

In a TAP experiment a bait protein is tagged and used to purify an entire complex; the members of the complex are then identified by mass spectrometry. TAP is able to detect complex multimeric species and the purification procedure decreases nonspecific binding compared to other affinity-based techniques [401, 402]. However, complexes must be able to survive the purification process, the technique is less able to detect transient interactions and is biased towards proteins with a high abundance [384, 401, 402]. Additionally, it is difficult to determine which interactions are direct and which will not occur in the absence of other complex members [403].

An alternative approach to PPI data is the curation and compilation of large numbers of publications reporting interactions detected low-throughput methods. However, such databases exhibit poor reliability and are more vulnerable to experimenter bias [400]. Scientists are more likely to investigate proteins that they are interested in, primarily those that are thought to play important roles in cellular pathways or disease mechanisms, and as more experiments are conducted with such proteins more interactions are likely to be uncovered. Therefore, proteins at the centre of active research are likely to have a higher reported number of interaction partners which will increase their degree, and most likely, centrality in PPIN [276, 400, 404–406].

Although high-throughput PPI data would ideally be validated using low-throughput techniques (such as confocal microscopy to detect colocalisation, co-immunoprecipitation, surface plasma resonance studies or spectroscopic studies) [401], they remain a valuable resource and should not necessarily be considered inferior to that generated through low-throughput methods [276, 406]. It must be acknowledged that although a large amount such of data have been collected, the human PPIN is far from complete [407]. However, this thesis hypothesises that sufficient data are available to allow the generation of biologically relevant models.

4.1.4 iRefIndex as a consolidated PPI database

Consolidated databases are created by combining multiple primary PPI databases, providing the obvious advantage of increasing the quantity of PPI data available in a single place, and therefore coverage of the underlying PPIN. Increased data coverage is particularly valuable given the relatively low overlap in the interactions reported from common publications across different databases [405]. iRefIndex is a consolidated database [288] containing data from BIND [408], BioGRID [409], CORUM [410], DIP [411], HPRD [412], InnateDB [413], IntAct [414], MatrixDB, MINT [415], MPact [416], MPIDB [417], MPPI [418] and OPHID [419]. iRefIndex was created

in four major steps [288]:

1. Each protein (within each database) was assigned a sequence globally unique identifier (SEGUID) based on its amino acid sequence.

2. Interaction data from the multiple databases was compiled, references for each interaction were retrieved. Interactions between two partners (binary) or representing complexes were included.

3. Each protein species was mapped to a redundant object group (ROG). Initially the primary reference was used to make an assignment, failing this any secondary references and, finally, the amino acid sequence were used; 96% of interactors were unambiguously assigned to a ROG, 1.2% were assigned with some ambiguity and 2.8% were not assigned.

4. Each interaction was mapped to a redundant interaction group (RIG) based on concatenation of the ROGID for the two species.

At the time of initial release iRefIndex had 21,615 unique human ROGID with 112,466 interactions [288], these numbers have subsequently increased. Significant support for iRefIndex is provided in the form of the R package iRefR [290]. iRefR, in combination with igraph [289], facilitates the construction of PPIN, the conversion of ROGID to Uniprot ID, the calculation of key network properties, the identification of communities and the exportation of data in gml format.

A key advantage of iRefIndex is the use of canonical identifiers to map all protein isoforms (including splice variants and differential post translationally modifications) to a common identifiers. Combining data relating to different isoforms removes what has been identified as a key source of divergence in the underlying databases [420] and is important as proteins with multiple splice variants frequently occupy central network positions [421]. The importance of using a consolidated interaction database was highlighted by the work of Turinsky *et al.* who reported that, where two databases cite a common publication, the average overlap in reported human proteins (nodes) and human PPI (edges) as 58% and 37% respectively [405]. The authors identified the assignment of interactions to different protein isoforms as a key contributor to this variation and this problem is eliminated in iRefIndex.

iRefIndex also allows for the consolidation of complex data (interactions involving more than two partners) from TAP experiments and binary data from pairwise experiments. The reporting of complex data is a potential source of error in PPIN. Whereas some databases report complex interactions as a list of all proteins identified in the complex, others report the complex

interaction as a series of binary interactions with a single bait species (spoke expansion) [405]. Such an approach has the risk of reporting proteins to have anomalously high degrees creating artificial shortcuts across resultant PPIN [420]. Although iRefIndex inherits from its underlying databases some of the problems relating to the binary expansion of complex interaction data, a study conducted by Stojmirovic and Yu reported that such spoke expanded complexes were less prevalent in the iRefIndex human PPI data than that for other species [420]. Where lists of multiple interacting species are retained, iRefR and igraph provide four methods for representing complex data:

- Binary - All complex species excluded and only binary interactions included, each node represents a protein and each edge demonstrates an experimentally proven or predicted interaction between two proteins.
- Bipartite - Complexes are represented as distinct node type, where a protein has been shown to form part of a complex an edge is added between the protein node and the complex node.
- Spoke - The prey node is identified and edges are added between this node and all other proteins in the complex. The prey node is usually defined as the protein used as bait during experiments, for example the protein immunoprecipitated. No other edges are added between complex members unless there is further evidence of an interaction.
- Matrix - All members of the complex are assumed to interact and edges are added between every complex member and every other complex member.

The flexibility in the use of complex data is a key advantage of iRefIndex as a source of PPI data. However, retaining only binary interactions may increase the reliability of PPI data. Turinsky *et al.* reported an average overlap in reported PPI interactions (across all species) between PPI databases as 72% for binary data and 29% for complex data where a common citation was given [405].

Concerns have been raised about the reliability of PPI data [403, 422, 423] and this has resulted in numerous algorithms to predict the reliability of interactions computationally [422, 424, 425]. However in 2012, Mora and Donaldson demonstrated better predictive power in PPIN generated from all data contained within iRefIndex than when using, supposedly, more reliable datasets [426] and weak links have been proposed to play a critical role in stabilising networks [427]. Further, Hakes *et al.* suggested that creating high confidence datasets may introduce additional bias and alter key topological features of the resulting network [406]. The authors proposed that although high confidence interaction sets may be reliable, they are unlikely to be representative

of the underlying network [406].

4.1.5 Applications of biological networks

There have already been some successes in the biomedical applications of network science, most prominently in the identification of disease causing genes and the investigation of the properties of existing drugs [265].

Cancer

Network approaches have gained particular traction in the field of oncology as cancers rapidly develop resistance and therefore multi-targeted approaches are essential [265]. Further, the concept of synthetic lethality (*Subsection 4.1.2*) allows tumours to be sensitised to treatments based on their differential gene expression patterns [393]; siRNA screens have been conducted to identify mutations that sensitise cancers to a given drug [404, 428].

Folger *et al.* constructed a generic cancer metabolic network by sampling a general metabolic network using a seedlist of metabolic enzyme-coding genes that are highly expressed across cancer cell lines [283]. The authors identified enzymes whose deletion was expected to be selectively toxic in cancer cells (compared to non-dividing human cells) and showed that this set of enzymes was significantly enriched in targets of FDA approved metabolic anti-cancer drugs. Further, pairs of enzymes predicted to be synthetically lethal were identified and pairs where one enzyme was selectively inactivated in some cancer lines were identified, in such cases it was predicted that an inhibitor of the other half the pair would be selectively toxic to cancer cells [283].

PPIN have also been used, in conjunction with gene expression data, to predict survival and identify biomarkers in breast cancer patients [299, 429]. Taylor *et al.* identified hubs within a human PPIN and classified hubs as inter (co-expressed with partners in a tissue specific manner) and intramodular (co-expressed with partners across all tissues). The removal of intermodular hubs had a greater effect on network topology and mutation of these proteins was more commonly associated with cancer [429]. The hubs were then studied in a cohort of breast cancer patients. Although expression levels of hubs were not altered, the differences in their correlation patterns were used to build a prognostic signature predicting patient survival. For example, BRCA1 expression is strongly correlated with that of its interaction partners only in patients with good outcomes [429].

Jahid *et al.* used a Steiner approach to connect genes differentially expressed in breast cancers within a PPIN [299]. By altering network weighting, a series of random Steiner networks were generated and consistent non-leaf nodes corresponding to differentially expressed proteins were identified. These potential biomarkers were then used to train classifiers to separate metastatic and non-metastatic patients [299].

Identification of disease genes

It has been demonstrated that proteins corresponding to genes related to the same diseases are more likely to interact, share common GO annotations and tissue expression patterns [291, 398]. These groups of related proteins have been termed 'disease modules' [96], and the proteins connecting disease modules suggested as potential intervention points [430]. Disease genes do not seem to be associated with genes encoding essential proteins nor are they more likely to be hubs than would be expected at random [398]. A possible explanation is that mutations in essential genes typically result in embryonic lethality and therefore, are not associated with observed diseases. Further, disease related genes tend to be tissue specific [398].

Numerous network methods have been used to identify disease related genes or prioritise long lists of potential targets resulting from GWAS or microarray studies [265, 431]. Integrated networks, built using multiple forms of data (edges based on co-expression, PPI, interactions in KEGG pathways and common GO annotations) have been constructed and novel disease genes identified based on their closeness to groups of known disease genes [432, 433]. Alternative approaches have considered random walks starting at known disease genes [434], rather than shortest paths and Navlakha and Kingsford created an algorithm that combined random-walk, clustering and neighbourhood metrics to determine disease causing genes based on known genes in PPIN [435]. In a different approach, gene lists were prioritised based on their centrality in networks integrating genomic and phenomic data from a number of disease related sources [311].

A recent alternative to 'guilt by association' methods involved comparing the gene co-expression networks of Crohn's disease patients and controls to prioritise GWAS signals [436]. Similarly to the work of Taylor *et al.* [429] in breast cancer, the authors demonstrated that disease related genes are more likely to show altered co-expression behaviour in patients than controls - a phenomenon labelled 'guilt by rewiring' [436].

Moving beyond the idea of single causative genes, Noh *et al.* demonstrated genetic epistasis in ASD [293]. The authors generated an ASD PPIN centred on causal copy number variants whose mouse KO models had phenotypes related to ASD. The ASD network showed increased

connectivity (compared to random models) and most patients had copy number variations in multiple ASD network proteins. Epistatic diseases, where multiple mutations lead to a phenotype, further undermine the concept of a pharmaceutical 'magic bullet' targeting a single site.

Drug networks

Drug networks connect proteins based on their interaction with common drugs, or drugs based on common protein targets. Although not conducted as a network analysis, the work of Borisy *et al.* demonstrated that drugs may have synergistic effects that are not seen when either drug is administered in isolation [277], the next logical step would be to design treatments based around multiple interventions.

Drug networks have demonstrated that promiscuity of current drugs, in one such analysis 35% of the drug like molecules were found to bind to multiple proteins [437]. Additionally, protein drug targets are enriched in GO annotations corresponding to membrane proteins, receptors, transcription factors and cell signalling components [438], these protein classes are commonly considered druggable by the pharmaceutical industry [271]. Yildrim *et al.* created a network of FDA approved drug, linked where they shared common targets [273]. Of the 890 drugs included, 476 existed in a common component demonstrating that currently approved drugs show a high degree of overlap in their protein targets. Through a comparison with disease genes the authors demonstrated that the majority of drugs are palliative, rather than etiological - that is the targeted proteins are not the underlying cause of the disease [273]. Keiser *et al.* extended their drug networks to include experimental validation of their predictions. Having used a network approach to predict off target effects of 3665 FDA approved or investigational drugs, they experimentally confirmed 23 new drug target interactions [439].

Target identification from PPIN

In their comprehensive review of molecular networks for drug discovery, Csermely *et al.* describe PPIN as 'one of the most promising network types to identify new drug targets' [265]. Much work has been conducted characterising the topological properties of current drug targets within PPIN and it has been suggested that future drug targets will have similar properties [273]. There is some disagreement as to what the ideal topological properties of a drug are, but the majority of reports suggest that drug targets have a somewhat higher degree and higher centrality than other proteins within the network [426, 440].

The 2012 work of Mora and Donaldson is particularly pertinent to this thesis [426]. The authors used iRefIndex to investigate whether topological features of nodes are good predictors for current drug targets. Their results confirmed previous studies and indicated that degree and centrality are both predictors for drug targets within PPIN. PPIN constructed using all the data contained within iRefIndex gave better prediction results than any of the PPIN constructed from supposedly more reliable data including low-throughput, non-predicted and annotation based scoring methods. Further, the form of complex representation (binary, spoke or matrix) did not affect their conclusions. Drug targets for oncology drugs appeared to have a different behaviour to drug targets as a whole and the authors cautioned that predictive value of node topology may vary according to disease area. Finally, the targets of withdrawn drugs had higher centralities than drug targets as a whole and the authors suggested that high degree may correspond to an increased risk of side effects [426].

Beyond oncology, most studies identifying drug targets using PPIN analysis has been focussed on infectious species (i.e. bacteria, fungi and viruses) [265]. Ideal therapeutics for these disease achieve maximum disruption and lethality (of the infectious agent) which can be modelled as network disruption, denoted the 'central hit strategy' by Csermely *et al.* [265]. Therefore hub proteins are suitable targets and these are readily identified through network analysis [281]. Following the identification of central nodes in PPIN, drug targets in *Mycobacterium tuberculosis* [279, 280], *Pseudomonas aeruginosa* [441] and methicillin-resistant *Staphylococcus aureus* (MRSA) [281] have been suggested, although there has been little experimental validation of network predictions. Raman *et al.*'s work in *Mycobacterium tuberculosis* is particularly exciting as the authors identified multiple proteins whose combined deletion was predicted to have maximal network impact [280]. Although the edges in their network represented metabolic relationships (rather than physical interactions), Raman *et al.*'s results demonstrated that combinations of protein deletions may have non-synergistic effects.

Beyond the fields of cancer and antibiotics, drugs must strike a balance between targeting central (often essential) proteins and peripheral nodes whose modulation will have little effect on the system as a whole [265]. It has been demonstrated that bridging and intermodular nodes are primary transmitters of network perturbations and such nodes have been suggested as ideal intervention points [442]. Hwang *et al.* developed, and patented, the bridging centrality (C_R) metric which they suggested would identify suitable drug targets [324, 443] (*Subsection 2.3.6*). While many centrality metrics strongly favour nodes with high degrees, the C_R was designed to identify nodes which act as critical connection points between highly connected communities, but may not have a high degrees themselves [324]. Hwang *et al.* demonstrated that their metric was

capable of identifying bridging nodes in a range biological networks, that removal of bridging nodes caused significant disruption to real-world networks (as measured by average shortest path length) and that removal of top bridging nodes allowed the identification of communities [324]. The authors explored their metric in the context of a yeast PPIN and demonstrated that bridging nodes connect sub-regions of the network associated with particular biological functions [443]. The removal of bridging nodes was less likely to be lethal than those with the highest BC and they had less correlated gene expression. Therefore, the authors proposed that bridging nodes, identified by their network topology, represented potential drug targets and the authors were able to, retrospectively, identify drug targets within disease networks [443].

PPIN for neurodegenerative disorders

While much disease-network analysis has focussed on the fields of oncology and infectious agents there are some examples of networks modelling neurodegenerative disorders. Network techniques have received particular attention in the field of Alzheimer's disease (AD), although most studies have focussed on the disease's aetiology, rather than identifying potential sites for therapeutic interventions.

The first studies focussed on building networks between genes differentially expressed in the brains of AD patients. Ray *et al.* used differentially expressed genes to build a gene network and then identified communities [300]. One of these communities was enriched in genes implicated in cardiovascular disease; the authors suggested that cardiovascular disease and AD are linked by common biochemical pathways [300]. A similar study, using genes with altered expression in the hippocampus of AD patients, was able to identify the transcription factor CREB as a key regulator of genes with altered expression in AD [312].

More recent studies have combined such microarray analysis with PPIN to identify underlying disease pathways. Hallock *et al.* generated an AD PPIN around a set of seed proteins known to be implicated in AD. The authors then added gene expression data and identified cluster of differentially regulated proteins within their network. Two such clusters were identified corresponding to the MAPK/ ERK pathway and clathrin-mediated receptor endocytosis, the authors suggested that these pathways were key to AD aetiology [313]. In a similar study it was shown that genes differentially expressed in AD had higher BC in PPIN than their neighbours [444], demonstrating that topological properties may have disease relevance.

In an alternative approach to the use of microarray data, Liang *et al.* identified genes with differential expression in six brain regions of AD patients (following laser microdissection of

neurones) and used these genes to form induced subgraphs corresponding to each of the brain regions sampled [301]. Hubs were identified in each subgraphs and the hub proteins were shown to form a connected network across the six brain regions. The proteins in the hub network were specifically perturbed in AD (microarray data was used to compare expression in other neurodegenerative diseases), enriched in proteins known to be constituents of amyloid plaques and neurofibrillary tangles and the expression of genes corresponding to these hub proteins was correlated with AD progression. Further, the authors reported that the hub network was enriched in targets for rapamycin and curcumin and that these molecules should be considered as potential AD therapeutics targeting multiple disease related proteins [301].

A further study based on identifying potential drug targets was conducted by Rao *et al.* who generated an AD PPIN based on sampling from a set of 136 disease related proteins [282]. The authors identified the nodes with the highest degree and suggested that these proteins might be suitable drug targets.

Surprisingly, network approaches have been little utilised for neurodegenerative disorders beyond AD [265]. However, Limviphuvadh *et al.* created PPIN to model six neurodegenerative disorders (including PD) starting from 13 causative genes (some neurodegenerative disorders have multiple associated genes and there is also overlap between the diseases) and used HPRD and a hand curated set of PPIs to extend their network [314]. The six PPIN were overlaid and common proteins were identified. The 14-3-3 family proteins were significantly enriched in the combined PPIN and the authors suggested that these proteins may play an important role in neurodegenerative disorders; however, there was no experimental validation of the paper's predictions [314].

Relating specifically to PD, the 2012 thesis of Matthias Konn centred on the construction of a PPIN around α-synuclein with the goals of elucidating protein function and identifying potential therapeutic targets [302]. The author used a number of Y2H and TAP based approaches to validate PPI for WT and mutant forms of the protein resulting in a set of 135 high confidence interactors that had been validated using at least two techniques, only eight of these interactions been previously published. The author then identified interactors which had been previously shown to modulate α-synuclein toxicity in model organisms and identified 33 human proteins whose expression in *S.cerevisiae* altered α-synuclein toxicity - many of the proteins identified had roles in cellular transport. Konn's study has a number of important implications for this thesis. First, proteins capable of modulating *in vitro* PD models can be identified through PPI. Second, high-throughput PPI data can be validated and gives biologically relevant results (the author demonstrated relevant GO annotational enrichment in lists of α-synuclein interactors).

Finally, even around well studied proteins, PPI data is incomplete with many interactions still to be recovered; the most complete set of interactions may be generated using data from multiple techniques [302]. A similar approach was taken by Beilina *et al.* who screened for LRRK2 interactors and through PPI data were able to elucidate a role for LRRK2 in the clearance of trans-Golgi derived vesicles [445].

Finally, in August 2014, Rakshit *et al.* published a studying using PPIN to identify potential PD biomarkers [446]. PPIN were constructed where nodes represented proteins differentially expressed in the brains of PD patients and edges were derived from a compilation of experimental PPIN databases. The authors identified critical genes based on their topology (high degree, or low degree in combination with high BC), clique membership and association with neurotransmitters. Based on their analysis, 12 proteins not previously associated as PD were suggested as potential biomarkers [446].

Both this thesis and the work of Rakshit *et al.* identify critical proteins in PD related PPIN through a combination of topological network analysis and biological intuition. However, there are key distinctions. Rakshit *et al.* aimed to identify biomarkers in a PD network sampled from a long list of proteins corresponding to differentially expressed genes. In contrast, this thesis was centred on the analysis of MPP^+ PPIN generated by sampling from a shorter manually created list of proteins known to have a role in the early stages of MPP^+ pathology. Further, the goal of this thesis was to identify intervention points regardless of whether these proteins had altered expression levels following MPP^+ treatment. Although Rakshit *et al.* generated a list of suggested biomarkers, there is no experimental validation of their work; a key goal of this thesis is to test the predictions of network analysis *in vitro*.

Experimental validation of network approaches

Many disease related network analyses have lacked experimental validation. However, there are some exciting exceptions which highlight the potential opportunities.

Behrends *et al.* generated a PPIN of the human autophagy system [447]. The authors elucidated, and confirmed, all the PPIs of 32 proteins linked to autophagy using TAP and generated a PPIN with 409 nodes. Within the resulting PPIN the authors demonstrated a significant enrichment in GO terms relating to vesicle transport, proteolysis, signal transduction and phosphorylation. Proteins within the PPIN were KD using siRNA and for some, but not all, nodes KD resulted in altered autophagic flux. Although the proteins for modulation were not selected on the basis of network analysis, this publication formed an important precedent for this thesis which aims

to identify proteins whose modulation might result in altered behaviour.

An example of experimental validation of target identification from PPIN analysis comes from Li *et al.*'s work in oncology [448]. The authors found that known cancer genes had distinct topology in PPIN compared to other genes, with increased average degrees and clustering coefficients and shorter average shortest path lengths to other known cancer genes [448]. The authors used topological network properties, along with GO enrichments and sequence information to construct a machine learning algorithm able to identify new cancer genes and validated their predictions through a siRNA KD screen; KD of predicted cancer genes led to decreased viability in a cancer cell line. The authors suggested that these genes could act as future therapeutic targets [448].

However, there are no examples of protein targets, identified through network analysis, being validated in experimental models of neurodegenerative disorders.

4.1.6 Aims of chapter

The key objective of this chapter was to use a network approach to identify proteins whose modulation was expected to alter neurotoxicity in an MPP^+ model of PD. In order to achieve this objective there were a number of subsidiary aims:

1. Development of a suitable seedlist of MPP^+ relevant proteins.
2. Use of the seedlist and publically available PPI data to sample MPP^+ relevant PPIN.
3. Characterisation of the resultant PPIN including the identification of central nodes and biologically relevant communities.
4. Comparison of the PPIN resulting from different sampling techniques and datasets.
5. Testing of previously reported methods for target identification by network analysis.
6. Development of novel techniques for network analysis to facilitate the identification of multiple proteins predicted to modulate biological cross talk between systems-level processes involved in MPP^+ toxicity.

Andrew Elliott (a fellow DPhil student) has conducted extensive research into PD related PPIN from a more theoretical perspective. His work has centred on the bias induced by sampling in PPIN and how this affects community detection. In collaboration with Andrew, pairs of nodes whose deletion was predicted to have maximal network impact were identified.

4.2 Results

4.2.1 iRefIndex as a source of PPI data

iRefIndex was downloaded and used to generate binary, bipartite, spoke and matrix PPIN including all, all experimental and all low-throughput data as outlined in *Subsection 2.3.1.* The number of nodes, edges and the network density were calculated for each PPIN and are shown in *Table 4.1.* As data (either predictive or high-throughput) were excluded the number of nodes, edges and density all decreased. Bipartite PPIN had more nodes than other forms of complex representation, as an additional node was introduced for each complex species. Binary PPIN had a similar number of nodes to other forms of complex representations, but fewer edges as interaction-data relating to complex species were excluded. The PPIN constructed using the matrix method had 3-4 times as many edges as when other complex representations were used, as an edge was added between each complex member.

Dataset	Complex Representation	Nodes	Edges	Density
All interactions	binary	16334	117056	$8.8x10^{-4}$
Experimental interactions	binary	15298	90628	$7.7x10^{-4}$
Low-throughput interactions	binary	10353	42319	$7.9x10^{-4}$
All interactions	bipartite	23217	159670	$5.9x10^{-4}$
Experimental interactions	bipartite	22292	133242	$5.4x10^{-4}$
Low-throughput interactions	bipartite	14353	57771	$5.6x10^{-4}$
All interactions	spoke	17105	133350	$9.1x10^{-4}$
Experimental interactions	spoke	16180	107249	$8.2x10^{-4}$
Low-throughput interactions	spoke	11203	48801	$7.8x10^{-4}$
All interactions	matrix	17105	422455	$2.9x10^{-3}$
Experimental interactions	matrix	16180	398380	$3.0x10^{-3}$
Low-throughput interactions	matrix	11203	154459	$2.5x10^{-3}$

Table 4.1: **iRefIndex can be used to form human PPIN.** A series of datasets was constructed by removing first predicted and then high-throughput data and then used to generate PPIN using different methods to represent data pertaining to complex interactions. Binary PPIN do not include data from complex interactions. In the bipartite PPIN a second type of node is introduced to represent complex species. The spoke model links all members of the complex to the prey species and the matrix model links all members of the complex to each other.

4.2.2 Seedlist construction

A systems-level model of MPP^+ induced toxicity and PD was constructed following a thorough literature review (*Section 1.4*) and exploration of relevant KEGG pathways [295]. *Figure 4.2* illustrates the interplay between the systems-level processes implicated in PD and MPP^+ toxicity, resulting in eventual cell death. Whereas PD can be triggered by dysfunction is several systems-

level processes (mitochondrial dysfunction, α-synuclein, autophagy), MPP^+ toxicity is triggered by mitochondrial insult, with all other cellular dysfunction lying downstream. Potential seeds for each systems level process were identified as outlined in *Subsection 2.3.2*. High degree seeds were excluded as such proteins are likely to be important to generic cellular processes rather than bringing particular insights to MPP^+ pathology and a single high degree seed can have a disproportionate effect on the sampled PPIN. Only a small number of putative seeds had a degree exceeding 100 (*Figure 4.3*), but the following were removed: ABL1, JNK, Caspase-3, Caspase-8, Akt, BCL-2, MAPK, PARP1, P53 and GSK-3β. Putative seeds involved in the later stages of apoptosis were also removed as this thesis was most interested in interventions at the earliest stages of toxicity leading to the removal of: Caspase-9, ASK1, Daxx, AIF and Puma. The final seedlist of 40 proteins was divided into six systems-level biological processes corresponding to those identified as central in MPP^+ toxicity (*Tables 4.2, 4.3, 4.4, 4.5, 4.6 and 4.7*).

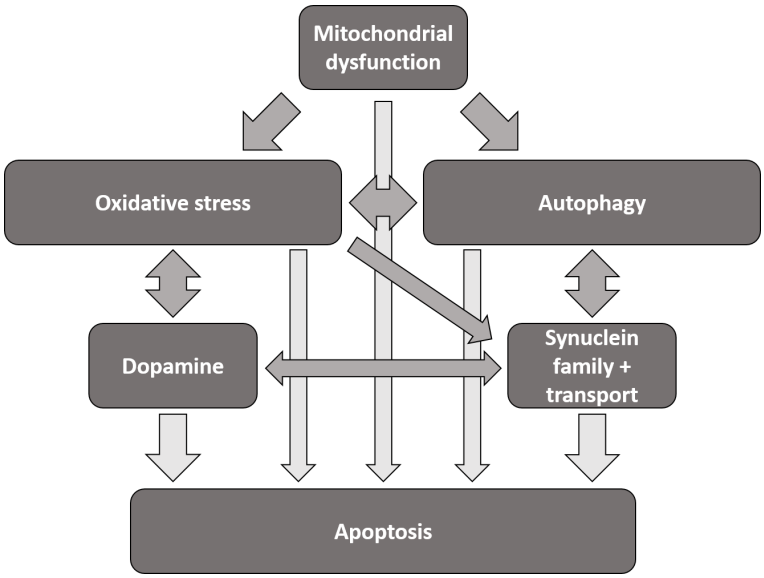

Figure 4.2: **MPP^+ pathology and Parkinson's disease (PD) can be viewed as the interplay of systems-level processes.** Systems-level processes are represented by boxes and the interplay between processes is shown through arrows. Familial PD can be triggered by mutations in genes in several systems-level processes (mitochondrial (PINK1, parkin), autophagy (GBA, ATP13A2), α-synuclein & MAPT) sporadic PD is thought to be due to the interplay of these processes. In MPP^+ models of PD, all cellular dysfunction lies downstream of initial mitochondrial insult. However, many of the systems-level dysfunctions associated with PD are replicated in the MPP^+ model.

4.2.3 Use of DAPPLE to validate the seedlist

DAPPLE (*Subsection 2.3.1*) was used to test whether the seedlist proteins were more connected than would be expected at random. It should be noted that although this PPIN shared a common seedlist with the networks analysed later in this thesis, the DAPPLE network was sampled from

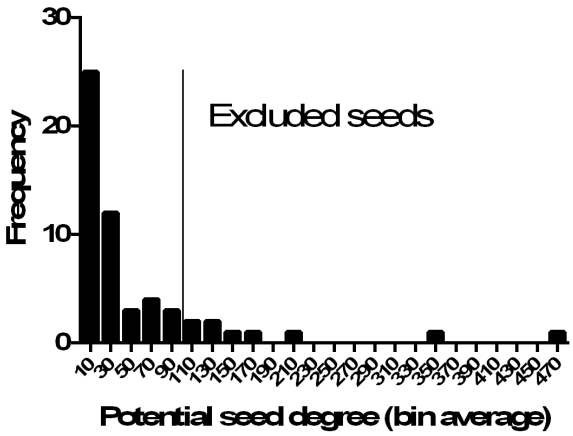

Figure 4.3: **Most putative seed proteins have a low degree.** Degree of potential seeds was measured using Cytoscape, potential seeds with a degree exceeding 100 were excluded from the final seedlist.

Protein	UniprotID	Function	References	UniprotKB
Dual specificity mitogen-activated protein kinase kinase 4 (MAPKK4)	MP2K4	Apoptosis regulation. Part of MAPK/ERK pathway. Phosphorylated by LRRK2 and ASK1.	[152, 203]	P45985
Apoptotic protease-activating factor 1 (APAF1)	APAF	Regulates apoptosis. Downstream of cytochrome C release.	[449]	O14727
BH3-interacting domain death agonist (BID)	BID	Proapoptotic. BCL-2 family. Interacts with BAX leading to its insertion into membranes and cytochrome C release.	[213, 328, 331, 450]	P55957
Apoptosis regulator BAX	BAX	Proapoptotic. Normally found in cytosol and then insets into membranes upon apoptotic stimuli allowing cytochrome C release form the mitochondria. Regulated by P53.	[213, 328, 331, 450]	Q07812

Table 4.2: **Apoptosis seed proteins.** Proteins which have been, independently, experimentally shown to be involved in the apoptotic stage of MPP^+ induced cell death. References give evidence of each protein's involvement in MPP^+/MPTP pathology. No protein with a degree exceeding 100 is included and proteins involved in the later stages of apoptosis have been excluded. The seedlist was used to sample from iRefIndex to create, smaller, PPIN enriched in MPP^+ relevant processes.

the InWeb PPI database (not iRefIndex) and did not include cross links between non-seed nodes (*Figure 4.4*). The direct edge count, seed direct mean degree, seed indirect mean degree and common interactors mean degree were all higher than expected based on random PPIN and corrected P values indicated statistically significant increased connectivity in the seedlist PPIN

Protein	UniprotID	Function	References	UniprotKB
Microtubule-associated proteins 1A/1B light chain 3B (LC3B)	MLP3B	PE conjugation allows autophagosomal maturation and autophagic cargo targeting. MPP^+ leads to dephosphorylation. Higher levels in PD patient brains.	[149, 351]	Q9GZQ8
LAMP2A	LAMP2	Essential for CMA. Blocked by mutant forms of α-syn or DA modified α-syn. Decreased levels of LAMP2A increase the lifetime of α-syn.	[347]	P13473
Heat shock cognate protein of 70 kDa (HSC70)	HSP7C	Recognises pentapeptide sequence to target molecules for CMA.	[189, 451]	P50502
Activating molecule in BECN1-regulated autophagy protein 1 (AMBRA1)	AMRA1	Activates autophagy. Interacts with Parkin. Induces mitophagy.	[452]	Q9C0C7
Beclin1	BECN1	Autophagy initiation.	[357, 361]	Q14457
Ubiquitin carboxyl-terminal hydrolase isozyme L1	UCHL1 (UCHL1)	Deubiquitinates. Trafficking. Mutations lead to recessive familial PD.	[453]	P09936
Interleukin-12 subunit α (IL12A)	IL12A	Proteasome mediated MPP^+ induced cell death.	[454]	P29459

Table 4.3: **Autophagy seed proteins.** Proteins which have been, independently, experimentally shown to be involved in autophagy following MPP^+/MPTP treatment, references give evidence for each protein's involvement. No protein with a degree exceeding 100 is included. The seedlist was used to sample from iRefIndex to create, smaller, PPIN enriched in MPP^+ relevant processes.

(*Table 4.8*). The increased connectivity was consistent with the seed proteins being involved in a single disease process, although not conclusive of such a relationship. However, evidence of increased connectivity may be somewhat circular as proteins involved in the same disease are more likely to be investigated simultaneously and their interactions exposed.

Following initial analysis, corrected P values for the indirect and direct degrees of each of the seed in the DAPPLE PPIN were calculated using DAPPLE, the lowest corrected P value is reported. Of the seed proteins, 14 had corrected P values of less than 0.05 indicating that they had higher degrees than would be expected at random (*Table 4.9*). A number of common interactors also had degrees with corrected P values of less than 0.05 in the indirect DAPPLE

Protein	UniprotID	Function	References	UniprotKB
Aromatic-L-amino-acid decarboxylase (AADC)	DDC	Conversion of *L*-DOPA to DA.	[455]	P20711
Tyrosine 3-monooxygenase (TH)	TY3H	Converts tyrosine to *L*-DOPA, rate limiting step in DA synthesis.	[456]	P07101
Synaptic vesicular amine transporter (VMAT2)	SLC18A2	Packages DA and MPP^+ into vesicles. Relative levels of VMAT and DAT are thought to explain differential neurone vulnerability.	[115, 325]	Q05940
Sodium-dependent dopamine transporter (DAT)	SC6A3	Uptake of DA and MPP^+. Relative levels of VMAT and DAT are thought to explain differential neurone vulnerability.	[114, 115, 325]	Q01959

Table 4.4: **Dopamine seed proteins.** Proteins which have been, independently, experimentally shown to be involved in DA homeostasis, following MPP^+/MPTP treatment, references give evidence for each protein's involvement. No protein with a degree exceeding 100 is included. The seedlist was used to sample from iRefIndex to create, smaller, PPIN enriched in MPP^+ relevant processes

PPIN (*Table 4.10*). Those not previously considered as seeds were investigated using PubMed, but no additional experimental evidence of their involvement in MPP^+ pathology was found. Caspase-8 and BCL2 had already been rejected as potential seeds due to their high degree.

4.2.4 Sampling of PPIN

Using the set of underlying PPIN (*Table 4.1*) and the seedlist of 40 MPP^+ related proteins, sampling was conducted as outlined in *Subsection 2.3.3* to construct smaller PPIN enriched in MPP^+ relevant processes. Two sampling methods (shortest-path and the 1-hop) were used to construct PPIN to facilitate a comparison between sampling approaches. Sampling was repeated for the same seedlist for each of the 12 underlying PPIN reflecting the four different approaches for dealing with complex interactions (binary, bipartite, spoke or matrix) and the three different datasets (all data, all experimental, all low-throughput) resulting in twelve PPIN for each sampling approach (*Tables 4.11* and *4.12*). All sampled networks were connected. The degree distributions of the PPIN generated by both 1-hop and shortest-path sampling using the underlying experimental binary PPIN are also shown (*Figure 4.5*).

As seen in the underlying PPIN, exclusion of predictive and high-throughput data led to a decrease in the number of nodes and edges. Data exclusion also resulted in an increase in

Protein	UniprotID	Function	References	UniprotKB
Heat shock protein 75 kDa	TRAP1	Phosphorylated by PINK1. Maintains mitochondrial function and polarisation. Mitochondrial analogue of Hsp90, binds to TNF type 1 receptor associated protein.	[457, 458]	Q12931
Dynamin-1-like protein (DRP1)	DNM1L	Mitochondrial fission.	[201, 203, 204]	O00429
Transcription factor A, mitochondrial (TFAM)	TFAM	Mitochondrial transcription factor. Pro-survival. Decreases ROS production.	[199, 203]	Q00059
BAX	BAX	Proapoptotic. Normally found in cytosol and then insets into membranes upon apoptotic stimuli allowing cytochrome C release form the mitochondria. Regulated by P53.	[213, 331]	Q07812
E3 ubiquitin-protein ligase parkin	PRKN2	Ubiquitin ligase. Lies downstream of PINK1 in targeting depolarised mitochondria for mitophagy. Important for mitochondrial fission. Mutations lead to familial recessive PD.	[365]	O60260
Protein DJ-1	PARK7	Removes reactive oxygen species. Involved of regulation of mitochondrial dynamics through DRP1. Degraded by MMP3. Mutations lead to familial recessive PD.	[201]	Q99497
Serine protease HTRA2l	HTRA2	Normally mitochondrial. Relocates to cytosol. Leads to MMP-3 activation.	[328, 459]	O43464
Voltage-dependent anion-selective channel protein 1 (VDAC1)	VDAC1	Forms a channel through the mitochondrial outer membrane and also the plasma membrane.	[328, 451]	P21796
PTEN-induced putative kinase protein 1 (PINK1)l	PINK1	Kinase, recruits parkin to depolarised mitochondria. Involved in mitochondrial quality control. Familial mutations lead to familial recessive PD.	[457, 458]	Q9BXM7

Table 4.5: **Mitochondrial seed proteins.** Proteins which have been, independently, experimentally shown to be involved in mitochondrial dysfunction following MPP^+/MPTP treatment, references give evidence for each protein's involvement. No protein with a degree exceeding 100 is included. The seedlist was used to sample from iRefIndex to create, smaller, PPIN enriched in MPP^+ relevant processes

average shortest path length and decrease in average node degree. Average PPIN transitivity was lowest for PPIN constructed using only experimental data indicating decreased global clustering.

Protein	UniprotID	Function	References	UniprotKB
Sepiapterin reductase	SPRE	Catalyses final step of tetrahydrobiopterin synthesis.	[79, 335, 460]	P35270
Nitric oxide synthase, brain	NOS1	NO is a radical scavenger. Antioxidant. Regulated by BH4.	[115, 335, 366]	P29475
Catalase	CATA	Decomposition of peroxides. Protects cells against oxidative stress.	[461]	P04040
Glutathione peroxidase 1	GPX1	Antioxidant. Catalyses reaction of GSH with hydrogen peroxide.	[98, 210, 461]	P07203
Glutamate-cysteine ligase	GSH1	Glutathione biosynthesis.	[210]	P48506
Glutathione synthetase	GSHB	Glutathione biosynthesis.	[210]	P48637
Glutathione reductase	GSHR	Reduction of oxidised glutathione.	[210, 461]	P00390
GTPCH	GCH1	Synthesis of tetrahydrobiopterin.	[79, 215, 460]	P30793
Aconitate hydratase (Aconitase)	ACON	Inactivated by ROS. Stimulates iron uptake. Mitochondrial stress. Required for cell death following MPP^+ stress.	[98, 211, 215, 460]	Q99798
Serotransferrin	TRFE	Transferrin receptor facilitates uptake of iron loaded transferrin. MPP^+ upregulates TfR expression leading to oxidative stress.	[98, 215, 460]	P02787
Superoxide dismutase [Cu-Zn]	SOD1	Removes free radicals - cytosolic.	[145, 189, 212, 461]	P00441
Superoxide dismutase [Mn]	SOD2	Removes free radicals - mitochondrial.	[189, 461]	P04179

Table 4.6: **Oxidative stress seed proteins.** Proteins which have been, independently, experimentally shown to be involved in oxidative stress following MPP^+/MPTP treatment, references give evidence for each protein's involvement. No protein with a degree exceeding 100 is included. The seedlist was used to sample from iRefIndex to create, smaller, PPIN enriched in MPP^+ relevant processes

Predicted interactions are likely to increase clustering as proteins with common interaction partners will be predicted to interact. In contrast, high-throughput experiments are more likely to reveal interactions between proteins which were previously thought to be unrelated (due to the less hypothesis driven nature of high-throughput experiments). The exclusion of predicted data and inclusion of high-throughput PPI would be expected to result in lower clustering within experimental PPIN.

The PPIN constructed using the matrix method had considerably higher average degrees, den-

Protein	UniprotID	Function	References	UniprotKB
Stromelysin-1	MMP3	Truncates C terminal of α-syn. Colocalises with LB.	[104, 459, 462]	P08254
α-Synuclein	SYUA	Membrane protein, involved in DA transport and release. Major component of LB. Mutations and duplications/triplications lead to familial dominant PD. KD protects against MPP^+ toxicity.	[97, 99, 100, 114, 115, 215, 463]	P37840
β-Synuclein	SYUB	Found in pre-synaptic terminals, has significant similarity with α-synuclein and may have overlapping function.	[464]	Q16143
γ-Synuclein	SYUG	Found in pre-synaptic terminals, has significant similarity with α-synuclein and may have overlapping function.	[465]	O76070
Microtubule-associated protein tau	TAU	GWAS studies link SNPs within the MAPT locus with an increased risk of PD. Stabilises microtubules. Encourages α-synuclein fibrillisation.	[130, 131, 463]	P10636

Table 4.7: **Synuclein seed proteins.** Proteins which have been, independently, experimentally shown to be related to the synuclein family in the context of MPP^+/MPTP toxicity, references give evidence of each protein's involvement. No protein with a degree exceeding 100 is included. The seedlist was used to sample from iRefIndex to create, smaller, PPIN enriched in MPP^+ relevant processes

Parameter	Observed	Expected	P Value
Direct edges count	16.0	2.6	0.0001
Seed direct degrees mean	1.6	1.0	0.0272
Seed indirect degrees mean	22.0	13.6	0.0051
Common interactors degrees mean	2.62	2.2	0.0003

Table 4.8: **A DAPPLE PPIN generated from the seedlist is more connected than would be expected at random.** Statistics for direct and indirect DAPPLE PPIN constructed from seed nodes using DAPPLE to sample from the InWeb database. P values were calculated based on 10,000 permutations from a background population of DAPPLE PPIN generated by within-degree node-permutations.

sities and transitivities and lower average shortest path lengths than other networks due to the addition of edges between all complex members. The matrix networks were not used for further analysis. The PPIN formed through other forms of complex representation were broadly similar though the bipartite PPIN had additional nodes and consequent lower densities and average degrees.

PPIN sampled using the shortest-path approach had more nodes and edges than those generated by 1-hop sampling. Shortest-path PPIN typically exhibited a higher average degree and density and shorter average shortest path lengths. Shortest-path sampling is based around the minimisation of path lengths between seed nodes and therefore smaller average shortest path lengths

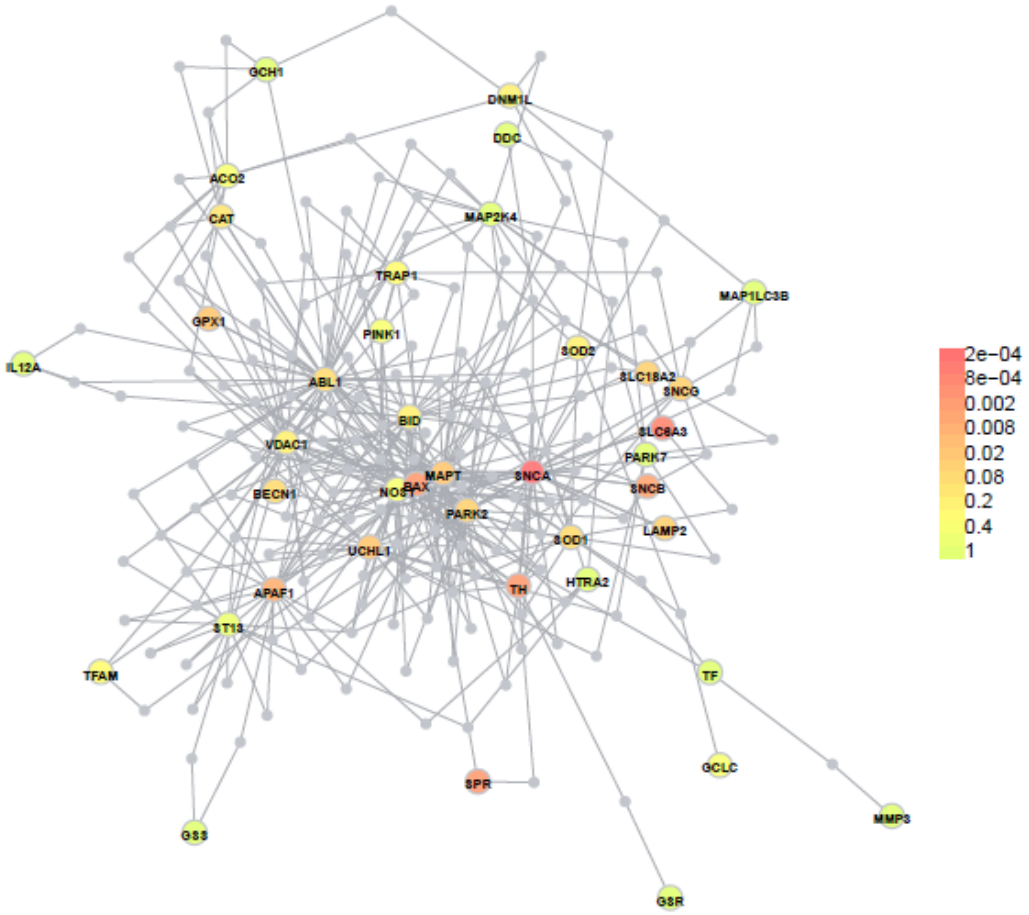

Figure 4.4: **A PPIN can be generated from the seedlist using DAPPLE.** A PPIN was constructed from the InWeb databvase using DAPPLE to sample from the seedlist. Seed proteins are coloured according to P values for their connectivity. Common interactors (non-seed nodes) are coloured grey.

were expected. Only seed nodes can exist as 'leaf' nodes following shortest-path sampling and increased densities and average degrees are, therefore, a consequence of shortest-path sampling. As can be seen in *Figure 4.5*, a higher proportion of nodes within the 1-hop PPIN had a very low degree. Neither PPIN had a linear relationship between log node degree and log frequency, indicating that the sampled PPIN were not scale-free. Although the majority of nodes had a low degree, both PPIN contained hub proteins with very high degrees.

1-Hop PPIN had higher transitivities than their shortest-path sampled counterparts as the neighbours of all seeds are always included in the resultant PPIN, generating small clusters. Despite the differences in the results, both forms of sampling were able to generate PPIN of a tractable size with low average shortest path lengths compatible with the small world properties expected in biological networks [466].

Gene	Protein	Corrected P value
SNCA	α-Synuclein	2.0010^{-4}
SLC6A3	DAT	6.0010^{-4}
TH	TH	1.4010^{-3}
BAX	BAX	1.6010^{-3}
SPR	Sepiapterin reductase	1.8010^{-3}
SNCB	β-Synuclein	3.8010^{-3}
APAF1	APAF1	$5.80\text{x}10^{-3}$
MAPT	Tau	$1.28\text{x}10^{-2}$
GPX1	Glutathione peroxidase 1	$1.34\text{x}10^{-2}$
UCHL1	UCHL1	$1.38\text{x}10^{-2}$
PARK2	Parkin	$2.60\text{x}10^{-2}$
LAMP2	LAMP2	$2.98\text{x}10^{-2}$
SLC18A2	VMAT2	$3.12\text{x}10^{-2}$
SNCG	γ-Synuclein	$4.14\text{x}10^{-2}$
SOD1	SOD1	$5.35\text{x}10^{-2}$
BECN1	Beclin1	$6.51\text{x}10^{-2}$
CAT	Catalase	$8.51\text{x}10^{-2}$
VDAC1	VDAC1	$1.25\text{x}10^{-1}$
SOD2	SOD2	$1.26\text{x}10^{-1}$
BID	BID	$1.33\text{x}10^{-1}$
DNM1L	DRP1	$1.51\text{x}10^{-1}$
TRAP1	TRAP1	$2.15\text{x}10^{-1}$
TFAM	TFAM	$2.73\text{x}10^{-1}$
PINK1	PINK1	$3.14\text{x}10^{-1}$
ACO2	Aconitase	$3.21\text{x}10^{-1}$
NOS1	nNOS	$3.33\text{x}10^{-1}$
GCLC	Glutamate-cysteine ligase	$3.37\text{x}10^{-1}$
HSPA8	HSC70	$4.67\text{x}10^{-1}$
HTRA2	HTRA2	$5.65\text{x}10^{-1}$
GSS	Glutathione synthetase	$5.67\text{x}10^{-1}$
GCH1	GTP cyclohydrolase 1	$6.14\text{x}10^{-1}$
DDC	AADC	$6.52\text{x}10^{-1}$
MAP1LC3B	LC3B	$7.28\text{x}10^{-1}$
MAP2K4	MAPKK4	$7.29\text{x}10^{-1}$
TF	Serotransferrin	$8.78\text{x}10^{-1}$
GSR	Glutathione reductasel	$9.55\text{x}10^{-1}$
PARK7	DJ1	$9.71\text{x}10^{-1}$
IL12A	IL12A	$9.97\text{x}10^{-1}$
MMP3	Stromelysin-1	$9.97\text{x}10^{-1}$

Table 4.9: **Fourteen seeds are more connected than would be expected at random in the DAPPLE PPIN.** P values for seed degree based on 10,000 permutations from a background population of DAPPLE PPIN generated by within-degree node-permutations. Where seeds have a direct and indirect degree a Bonferroni correction was performed for the two tests and the lowest P value selected. A Bonferroni correction was applied to account for multiple testing.

Gene	Protein	Corrected P value
PRKACA	cAMP-dependent protein kinase catalytic subunit alpha	$1.64\text{x}10^{-2}$
MCL1	Induced myeloid leukaemia cell differentiation protein Mcl-1	$1.64\text{x}10^{-2}$
CASP8	Caspase-8	$1.64\text{x}10^{-2}$
MAPK3	Mitogen-activated protein kinase 3	$1.64\text{x}10^{-2}$
PRKCE	Protein kinase Cϵ type	$1.64\text{x}10^{-2}$
BCL2L1	BCL-2-like protein 1	$1.64\text{x}10^{-2}$
ATP6V1B2	V-type proton ATPase subunit B, brain isoform	$1.64\text{x}10^{-2}$
BAK1	BCL-2 homologous antagonist/killer	$1.64\text{x}10^{-2}$
GRK5	G protein-coupled receptor kinase 5	$1.64\text{x}10^{-2}$
BCL2	Apoptosis regulator BCL-2	$1.64\text{x}10^{-2}$
ARID4B	AT-rich interactive domain-containing protein 4B	$1.64\text{x}10^{-2}$
GSTZ1	Maleylacetoacetate isomerase	$3.25\text{x}10^{-2}$

Table 4.10: **Twelve common interactors are more connected than would be expected at random in the DAPPLE PPIN.** Common interactors are proteins which interact with two or more of the network seeds. The degree of common interactors in the indirect DAPPLE PPIN were measured and P values calculated based on 10,000 permutations from a background population of DAPPLE PPIN generated by within-degree node-permutations. P values were Bonferroni corrected for multiple testing and proteins with a P value of less than 0.05 are shown.

Network	Nodes	Edges	Density	Transitivity	Average shortest path length	Diameter	Average degree
All data, binary complex representation	1164	12162	$1.80\text{x}10^{-2}$	$2.18\text{x}10^{-1}$	2.82	6	20.9
All data, bipartite complex representation	1341	13092	$1.46\text{x}10^{-2}$	$2.09\text{x}10^{-1}$	2.92	6	19.5
All data, matrix complex representation	2521	137321	$4.32\text{x}10^{-2}$	$4.59\text{x}10^{-1}$	2.36	6	
All data, spoke complex representation	1302	14755	$1.74\text{x}10^{-2}$	$1.94\text{x}10^{-1}$	2.77	6	22.7
Experimental data, binary complex representation	947	7005	$1.56\text{x}10^{-2}$	$1.09\text{x}10^{-1}$	2.88	6	14.8
Experimental data, bipartite complex representation	1171	7884	$1.15\text{x}10^{-2}$	$1.06\text{x}10^{-1}$	3.02	6	13.5
Experimental data, matrix complex representation	2359	125959	$4.53\text{x}10^{-2}$	$4.80\text{x}10^{-1}$	2.37	6	107
Experimental data, spoke complex representation	1092	9271	$1.56\text{x}10^{-2}$	$1.14\text{x}10^{-1}$	2.83	6	17.0
Low-throughput data, binary complex representation	508	2592	$2.01\text{x}10^{-2}$	$1.30\text{x}10^{-1}$	3.07	7	10.2
Low-throughput data, bipartite complex representation	585	2818	$1.65\text{x}10^{-2}$	$1.26\text{x}10^{-1}$	3.18	7	9.63
Low-throughput data, matrix complex representation	1080	34337	$5.89\text{x}10^{-2}$	$7.37\text{x}10^{-1}$	2.60	6	63.6
Low-throughput data, spoke complex representation	533	2948	$2.08\text{x}10^{-2}$	$1.37\text{x}10^{-1}$	3.04	7	11.1

Table 4.11: **PPIN were generated through 1-hop sampling.** Key topological features for PPIN sampled from iRefIndex using a seedlist of 40 MPP^+ relevant proteins and a 1-hop sampling approach. Twelve different underlying PPIN were used for sampling including only low-throughput data, only experimental data or all data and using a binary, bipartite, matrix or spoke complex representation.

Network	Nodes	Edges	Density	Transitivity	Average shortest path length	Diameter	Average degree
All data, binary complex representation	1454	21331	$2.02\text{x}10^{-2}$	$1.63\text{x}10^{-1}$	2.57	5	29.3
All data, bipartite complex representation	1615	19790	$2.02\text{x}10^{-2}$	$1.66\text{x}10^{-1}$	2.61	5	28.9
All data, matrix complex representation	1960	112191	$5.84\text{x}10^{-2}$	$4.13\text{x}10^{-1}$	2.20	5	
All data, spoke complex representation	1416	22150	$2.21\text{x}10^{-2}$	$1.62\text{x}10^{-1}$	2.55	5	31.3
Experimental data, binary complex representation	1195	14014	$1.96\text{x}10^{-2}$	$1.15\text{x}10^{-1}$	2.61	5	23.5
Experimental data, bipartite complex representation	1306	15396	$1.81\text{x}10^{-2}$	$1.10\text{x}10^{-1}$	2.64	5	23.6
Experimental data, matrix complex representation	1837	97211	$5.76\text{x}10^{-2}$	$4.11\text{x}10^{-1}$	2.21	5	105.8
Experimental data, spoke complex representation	1265	16874	$2.11\text{x}10^{-2}$	$1.19\text{x}10^{-1}$	2.56	5	26.7
Low-throughput data, binary complex representation	667	5751	$2.40\text{x}10^{-2}$	$1.47\text{x}10^{-1}$	2.75	6	16.2
Low-throughput data, bipartite complex representation	785	6058	$1.92\text{x}10^{-2}$	$1.37\text{x}10^{-1}$	2.87	6	15.4
Low-throughput data, matrix complex representation	913	20881	$4.96\text{x}10^{-2}$	$5.03\text{x}10^{-1}$	2.45	6	45.7
Low-throughput data, spoke complex representation	699	6555	$2.35\text{x}10^{-2}$	$1.47\text{xx}10^{-1}$	2.74	7	17.0

Table 4.12: **PPIN were generated through shortest-path sampling.** Key topological features for PPIN sampled from iRefIndex using a seedlist of 40 MPP^{+} relevant proteins and a shortest-path sampling approach. Twelve different underlying PPIN were used for sampling including only low-throughput data, only experimental data or all data and using a binary, bipartite, matrix or spoke complex representation.

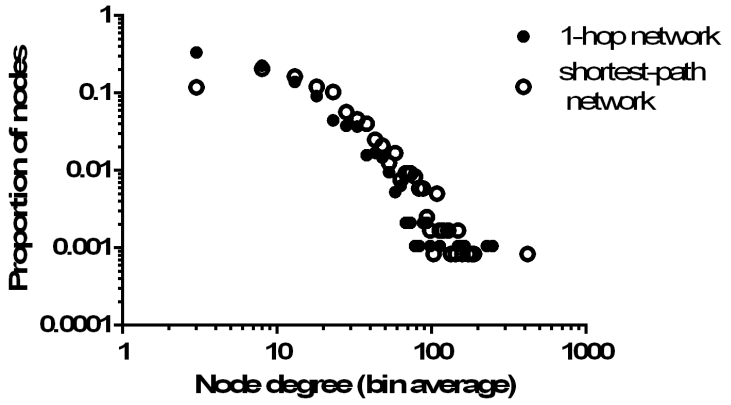

Figure 4.5: **Sampled PPIN do not have a scale-free degree distributions.** The seedlist of 40 MPP^+ relevant proteins was used to sample the experimental, binary underlying PPIN and the degree distributions of the two resulting PPIN were plotted. Node degree and the proportion of network nodes both displayed using a logarithmic scale.

4.2.5 Nodes with the highest centrality

Following the construction of sampled PPIN, the ten proteins with highest BC within each 1-hop sampled PPIN were identified (*Table 4.13*); such nodes are critical for the communication of information across the network and are expected to be biologically important [396, 397]. The proteins identified were largely consistent across all the 1-hop sampled PPIN with seven proteins appearing repeatedly (although their ranking varied between the PPIN): polyubiquitin, tyrosine-protein kinases ABL1, Src and Fyn, growth-factor receptor-bound protein 2, 14-3-3ζ, TNF receptor associated factor 6 (TRAF6). Additionally, eight of the 40 original seed proteins used for sampling (parkin, tau, nNOS, α-synuclein, MMP3, BAX, Beclin1, transferrin) appeared as high BC nodes with α-synuclein and parkin appearing across all of the networks. The PPIN sampled using only low-throughput data had a particular tendency to include seed proteins as high centrality nodes with at least six of the top ten nodes being seed proteins for each of these PPIN. The reoccurrence of seed proteins may be a result of the 1-hop sampling technique as all of the seed proteins neighbours are included in each sampled PPIN. Alternatively, the high centrality may reflect their pivotal role in MPP^+ networks either as a result of genuine biological importance or due to a surfeit of experimental data across a wide range of interaction partners.

The central nodes appeared robust to the method of complex representation and the binary PPIN were used for further analysis as each node represented a biologically targetable species (unlike in a bipartite PPIN) and each edge represented an experimentally validated PPI. Further, binary data is more reliably recorded in PPI databases [405] and the spoke representation of complexes has been shown to distort network properties [420]. Given the relative paucity of

data, illustrated by the low number of nodes in sampled low-throughput PPIN and the high proportion of seeds identified as central nodes within these PPIN, the purely low-throughput PPIN were not further investigated.

In order to investigate the effect of sampling method, the nodes with highest BC were identified for the PPIN formed using both shortest-path and 1-hop sampling on the underlying PPIN including all data and the underlying PPIN including all experimental data (*Table 4.14*). A number of the same proteins appeared regardless of sampling method: polyubiquitin , 14-3-3ζ, growth factor receptor-bound protein 2, TRAF6, ABL1 and Src. However, the rank order of the nodes was different dependent on sampling method with ABL1 being relatively less central in the shortest-path PPIN. Additionally, inhibitor of nuclear factor κB kinase subunitϵ (IKKE) and SMAD 2 appeared as central proteins only when shortest-path sampling was utilised; SMAD2 is a signal transducer regulating multiple pathways [467] and IKKE plays a crucial role in the NF-κB pathway [468]. It should be noted that ubiquitin had the highest BC in all PPIN investigated in this thesis.

The inclusion of predicted data did not have a large effect on the most central seeds, but there were important differences based on sampling technique. Therefore, the binary, experimental PPIN generated by the 1-hop and shortest-path sampling approaches were further investigated to allow for a comparison of the sampling techniques. The experimental dataset was selected because of concerns relating to predictive data, a decision consistent with the approach taken in PPI-trim to process the iRefIndex database [420]. The two PPIN are described as the 1-hop and shortest-path PPIN for the remainder of this thesis.

BC ranking	All data, binary complex model	All data, bipartite complex model	All data, spoke complex model	Experimental data, binary complex model	Experimental data, bipartite complex model	Experimental data, spoke complex model	LTP data, binary complex model	LTP data, biparite complex model	LTP data, spoke complex model
1	Polyubiquitin-C	Polyubiquitin-C	Polyubiquitin-C	Polyubiquitin-C	Polyubiquitin-C	Polyubiquitin-C	Polyubiquitin-C	Polyubiquitin-C	Polyubiquitin-C
2	Tyrosine-protein kinase ABL1	ABL1	Growth factor receptor-bound protein 2 (GRB2)	ABL1	ABL1	ABL1	ABL1	ABL1	ABL1
3	GRB2	GRB2	ABL1	GRB2	*α-Synuclein*	GRB2	*Tau*	*Tau*	*Parkin*
4	Tyrosine-protein kinase Fyn	*α-synuclein*	*Transferrin*	Fyn	GBR2	*Transferrin*	*Parkin*	*Parkin*	*Tau*
5	Src	Fyn	Fyn	Src	Fyn	Fyn	*nNOS*	*α-Synuclein*	*nNOS*
6	*α-Synuclein*	*Parkin*	*α-synuclein*	*α-synuclein*	Src	*α-synuclein*	*α-synuclein*	*nNOS*	*α-synuclein*
7	14-3-3ζ	Src	14-3-3ζ	*Parkin*	*Parkin*	Src	*MMP-3*	*BAX*	*MMP-3*
8	*Parkin*	14-3-3ζ	Src	Epidermal growth factor receptor	*Beclin1*	*Parkin*	Caspase-3	Cellular tumour antigen P53	Myc proto-oncogene protein
9	TNF receptor-associated factor 6 (TRAF6)	*Beclin-1*	TRAF6	14-3-3ζ	14-3-3ζ	14-3-3ζ	P53	Caspase-3	Caspase-3
10	GTP cyclohydrolase 1	TRAF6	*Parkin*	P53	*Tau*	P53	Src	*MMP-3*	Src

Table 4.13: **Consistent proteins show high centrality across 1-hop sampled PPIN based on different datasets.** The nodes with the highest BC in each PPIN were identified and the iCROGID converted to protein names. Comparisons can be made on the data included (all, experimental or low-throughput (LTP)) and the type of complex representation (binary, bipartite or spoke). Seed proteins are highlighted using *italic* font.

PPIN				
Rank	**All Data - Path**	**Experimental Data - Path**	**All Data - Hop**	**Experimental Data - Hop**
1	Polyubiquitin-C	Polyubiquitin-C	Polyubiquitin-C	Polyubiquitin-C
2	14-3-3ζ	GRB2	ABL1	ABL1
3	GRB2	14-3-3ζ	GRB2	GRB2
4	TRAF6	TRAF6	Fyn	Fyn
5	Inhibitor of nuclear factor κB kinase subunitϵ (IKKE)	IKKE	Src	Src
6	SMAD2	SMAD2	*α-Synuclein*	*α-Synuclein*
7	ABL1	ABL1	14-3-3ζ	*Parkin*
8	Colorectal mutant cancer protein	Src	*Parkin*	Epidermal growth factor receptor
9	Src	P53	TRAF6	14-3-3ζ
10	P53	Retinoblastoma-associated protein	GTP cyclohydrolase 1	P53

Table 4.14: **The sampling method employed affects the most central nodes in PPIN.** PPIN were sampled using the shortest-path and 1-hop approaches and underlying PPIN containing only binary data with the inclusion or exclusion of predictive data from the OPHID database. The nodes with the highest BC in each PPIN were identified and the iCROGID converted to protein names. Seed proteins are highlighted using *italic* font.

4.2.6 Community detection

Having characterised proteins with high centrality across the PPIN, communities corresponding to biological processes were identified. Identification of systems-level processes implicated in MPP^+ would provide support for the validity of the PPIN as models of the *in vitro* system. A spin-glass algorithm can be used to detect communities within PPIN and it has been demonstrated that such communities correlate with biological, systems-level process [376]. This algorithm was applied to the 1-hop and shortest-path PPIN and a list of the proteins in each community was extracted. DAVID (*Subsection 2.3.1*) [298] was then used to identify GO annotational enrichment within each community. The entire PPIN were used as the background population for each analysis, to avoid false enrichment values for annotations enriched across the entire sampled PPIN e.g. neuronal proteins. The details of the most significantly enriched GO annotation for each community are given where the Bonferroni corrected values were less than 0.05 (*Table 4.15*). Major, systems-level biological processes including autophagy, plasma membrane, translation and cell death were identified in both the 1-hop and shortest-path PPIN and the communities are visualised in *Figures 4.6 and 4.7*.

1-Hop network				
Community	Number of proteins	Most enriched GO annotation	P value	Fold enrichment
0	19			
1	1			
2	210	Translation	$1.70\text{x}10^{-4}$	3.1
3	5	Cytokine binding	$2.30\text{x}10^{-7}$	79.8
4	38			
5	5	Peroxisome fission	$2.10\text{x}10^{-5}$	184.2
6	107	Mitochondrial outer membrane	$1.90\text{x}10^{-2}$	4.2
7	323	Cell death	$7.40\text{x}10^{-15}$	1.9
8	275	Plasma membrane	$6.90\text{x}10^{-21}$	1.9
9	4			
10	2			
11	72	Autophagy	$2.40\text{x}10^{-8}$	12.5
Shortest-path network				
Community	Number of proteins	Most enriched GO annotation	P value	Fold enrichment
0	5	Cytokine Binding	$1.20\text{x}10^{-2}$	52.4
1	60	Regulation of autophagy	$1.10\text{x}10^{-9}$	26.2
2	324	Plasma membrane	$2.40\text{x}10^{-36}$	2.1
3	32	RNA processing	$2.20\text{x}10^{-20}$	12.8
4	226	Proteasome complex	$6.40\text{x}10^{-13}$	5.1
5	237	Translation	$9.2\text{x}10^{-12}$	3.3
6	230	Apoptosis	$1.90\text{x}10^{-16}$	2.6
7	302	DNA binding	$2.70\text{x}10^{-63}$	3.1

Table 4.15: **Communities corresponding to biological processes can be identified in PPIN.** The seedlists (*Tables 4.2, 4.3, 4.4, 4.5, 4.6 and 4.7*) were used with the binary experimental PPIN formed from iRefIndex and a 1-hop or shortest-path sampling approach to construct the PPIN. Communities were detected using a spin-glass algorithm (γ=1) and biological functions were assigned using enrichments in GO annotations according to DAVID. For each community, where there was a significant annotational enrichment, the top enrichment is given along with its Bonferroni corrected P value and fold enrichment value.

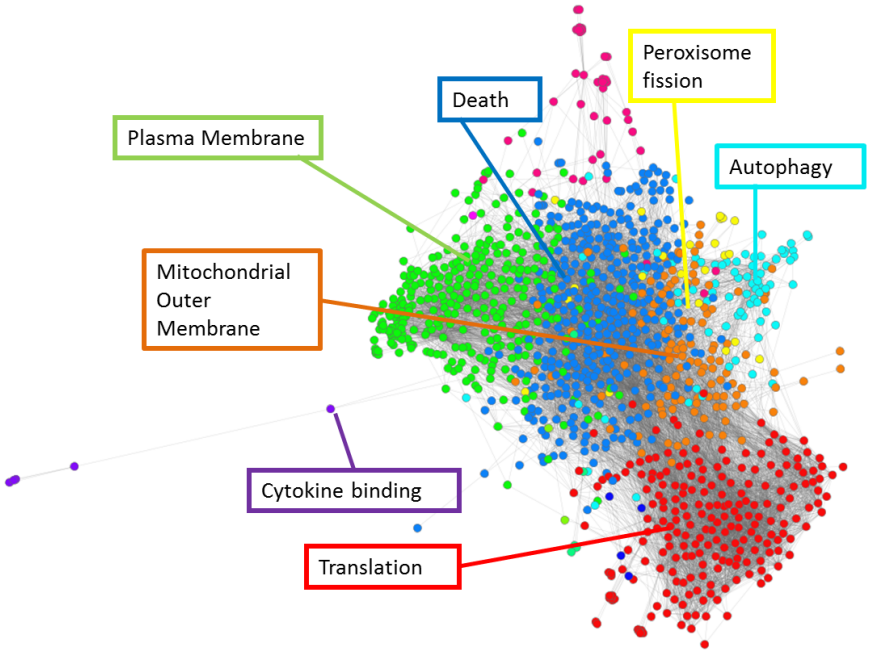

Figure 4.6: **Communities corresponding to biological processes can be identified in 1-hop PPIN.** The seedlists (*Tables 4.2, 4.3, 4.4, 4.5, 4.6 and 4.7*) were used with experimental binary iRefIndex PPIN and 1-hop sampling to construct a PPIN, non-binary interaction data were discarded. Communities were detected using a spin-glass algorithm (γ=1) and biological functions were assigned using enrichments in GO annotations according to DAVID.

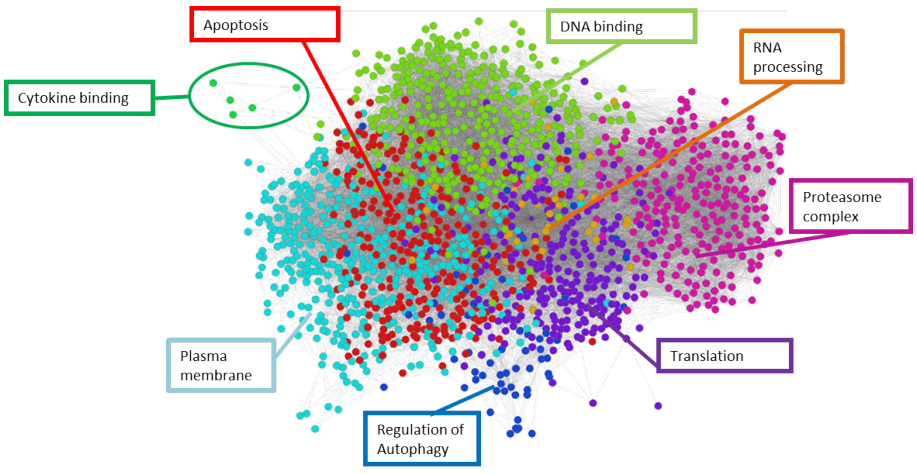

Figure 4.7: **Communities corresponding to biological processes can be identified in shortest-path PPIN.** The seedlists (*Tables 4.2, 4.3, 4.4, 4.5, 4.6 and 4.7*) were used with experimental binary iRefIndex PPIN and shortest-path sampling to construct a PPIN. Communities were detected using a spin-glass algorithm (γ=1) and biological functions were assigned using enrichments in GO annotations according to DAVID.

4.2.7 Target identification

The goal of this thesis was to identify protein targets whose experimental modulation could alter MPP^+ toxicity in an *in vitro* system. High BC has been shown to correlate with essentiality [396, 397] and so more extensive analysis was used to identify proteins that could perturb the PPIN in a more subtle fashion, altering the flow of information between different cellular processes.

4.2.8 Bridging centrality

Hwang's bridging centrality has been proposed as a method to identify suitable drug targets [324, 443] (*Subsection 2.3.6*). The metric was calculated for all proteins in the shortest-path and 1-hop PPIN and the top scoring nodes were identified (*Table 4.16*). Some of the bridging nodes (e.g. PINK1 [457] and glutathione synthetase [210]) have a documented role in MPP^+ cytotoxicity. However, most of the highlighted proteins are relatively unknown in the context of MPP^+/PD pathology. Proteins, such as α-synuclein have a proven role in MPP^+ toxicity [114] and therefore act as 'positive controls' for future analyses. The failure to recover such proteins from the bridging centrality analysis was a key concern. There were also concerns about the metric's methodology which heavily favours nodes with low degrees.

4.2.9 Mitochondrial dysfunction and its interaction with autophagy

Given concerns about the veracity of the results recovered using the bridging centrality metric, further target identification was conducted in a more hypothesis driven fashion to identify proteins involved in the cross talk between mitochondrial dysfunction and changes to autophagy in the context of MPP^+ toxicity. Mitochondrial insult initiates MPP^+ toxicity and is also an important systems-level process in PD aetiology [246, 247, 328] (*Subsection 1.4.3*). Autophagy is essential in long-lived cells such as neurones and the blockage of autophagy leads to neurodegeneration (*Subsection 1.4.2*), familial cases of PD have been linked to alterations in autophagy [142, 160]. It was hypothesised that by modulating the cross-talk between the two systems-level processes cell survival could be promoted following MPP^+ treatment.

4.2.10 Steiner analysis

Steiner analysis allows critical pathways to be extracted from a far larger PPIN (*Subsection 2.3.5*). Such an analysis was conducted on both the shortest-path and the 1-hop PPIN. The

Steiner nodes identified from the two PPIN were very similar (*Table 4.17 and Figure 4.8A and B*). In both cases, the number of Steiner nodes was much higher for the oxidative stress seeds than for other systems-level processes.

All of the initial analyses identified ubiquitin as a Steiner node, ubiquitin plays a key role in labelling proteins for degradation. Weighting factors (based on degree and BC) were utilised in an attempt to identify Steiner nodes beyond ubiquitin as had previously been reported by White and Ma'ayan [309]. Although weighting led to the selection of alternative Steiner nodes, ubiquitin remained a critical linking node across all analyses (*Table 4.18, Figure 4.8 C and D*). In order to further investigate the role of proteins other than ubiquitin in connecting the seeds, two alternative PPIN (one corresponding to each sampling method) were created with ubiquitin deleted. The same seeds were used on the adjusted networks and Steiner nodes identified (*Table 4.19, Figures 4.8E and F*). Following deletion of ubiquitin there was a greater divergence of results between the 1-hop and shortest-path PPIN. Steiner analysis successfully recovered proteins known to be important in MPP^+ toxicity/PD including SNAP25, NEDD4 and α-synuclein.

The Steiner analysis was helpful in identifying critical 'linking' nodes. However, Steiner analysis results in a binary measure, nodes are either Steiner nodes or they are not. Therefore, further metrics were investigated in order to generate a metric for all nodes, to allow the ranking of proteins and facilitate comparisons between different analyses.

4.2.11 Betweenness centrality between subgraphs

The goal of this section of work was to extend the investigation into proteins critical in the cross talk between mitochondrial dysfunction and autophagy, but to give a metric for a larger range of nodes than was possible using the Steiner-type analysis. Subgraph ΔBC analysis (*Subsection 2.3.6*) was performed on shortest-path networks corresponding to autophagy and mitochondrial dysfunction. The shortest-path sampling approach was selected here to investigate the transmission of information between the systems-level biological processes. BC in both graphs, the union sungraph and ΔBC were calculated (*Figure 4.9*) and the nodes with highest ΔBC were identified (*Table 4.20*). In most cases the ΔBC value was positive, as with the expansion of the network, nodes occurred in more shortest paths; however, in a few cases ΔBC was negative, illustrating cases where the union created alternative shortest routes.

The ΔBC calculation was used to identify proteins which were particularly important for the cross-talk between the autophagy and the mitochondrial dysfunction rather than identifying

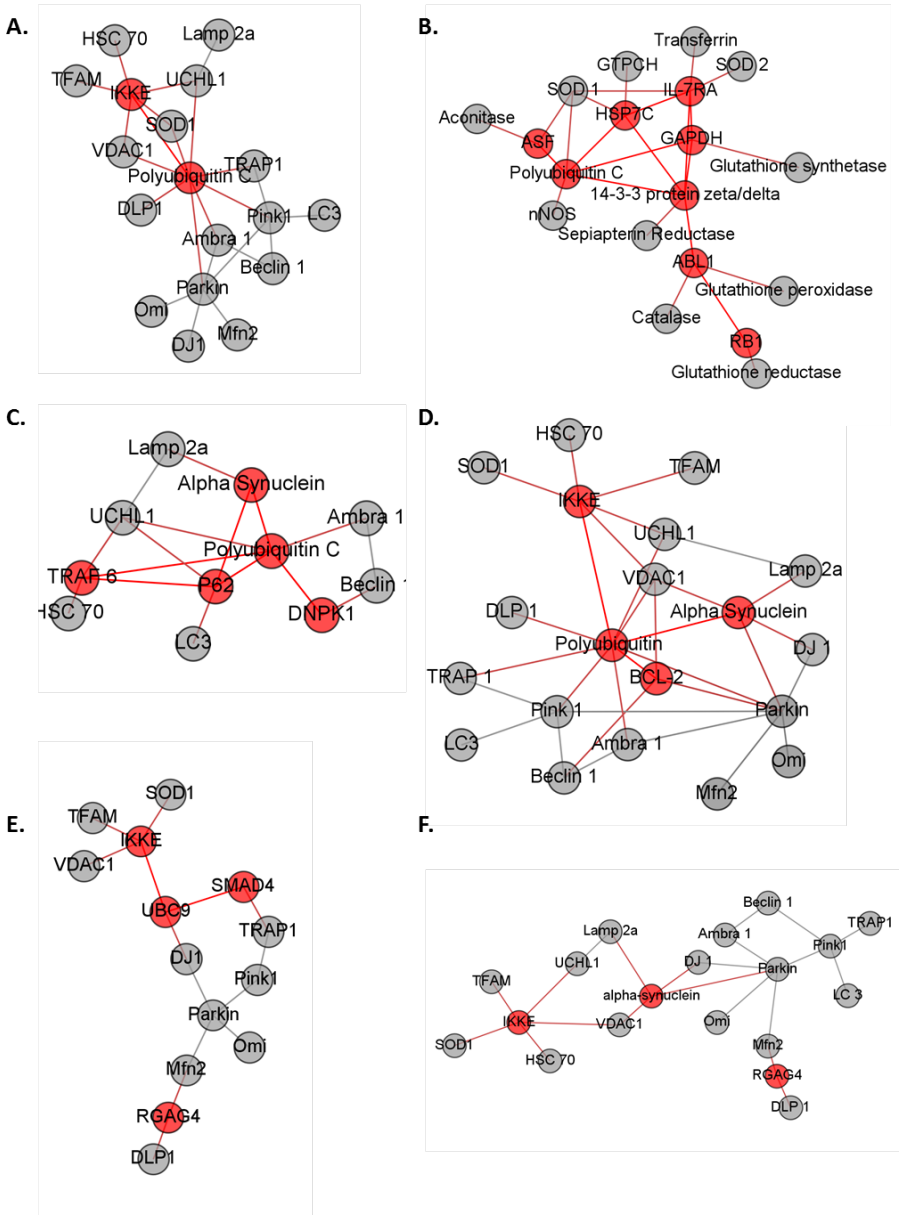

Figure 4.8: **Steiner analysis allows the identification of key nodes in MPP$^+$ PPIN.** Steiner type analysis was performed on both the shortest-path and 1-hop PPIN using sets of the initial seed nodes (*Tables 4.2, 4.3, 4.4, 4.5, 4.6 and 4.7*) as Steiner terminals. **A** Mitochondrial and autophagy seeds used as terminals. **B** Oxidative stress seeds used as terminals in 1-hop PPIN. **C** Autophagy seeds used as terminals in the shortest-path PPIN with weighting by degree. **D** Mitochondrial and autophagy seeds used as terminals in the 1-hop PPIN with weighting by degree. **E** Mitochondrial seeds used as terminals in the shortest-path PPIN with ubiquitin removed. **F** Mitochondrial and autophagy seeds used in 1-hop PPIN with ubiquitin removed. Steiner nodes (those not defined as initial seeds) are coloured red. All edges between nodes within the Steiner graphs are shown.

proteins which were central to one or other systems-level processes. Therefore, a protein which transmitted no additional information in the union graph, when compared to the sum of the two subgraphs, would have had a ΔBC of nought. Eight of the top ten proteins were the same when ΔBC and total BC (for the union graph) were compared (*Figure 4.9*). However, ESR1 and P53 were replaced with VDAC1 and GABARAP under the ΔBC measure. Having identified proteins particularly important in the interplay between autophagy and mitochondrial dysfunction the

next step was to investigate whether the same results would be achieved when the systems-level processes were considered in the context of the entire sampled PPIN.

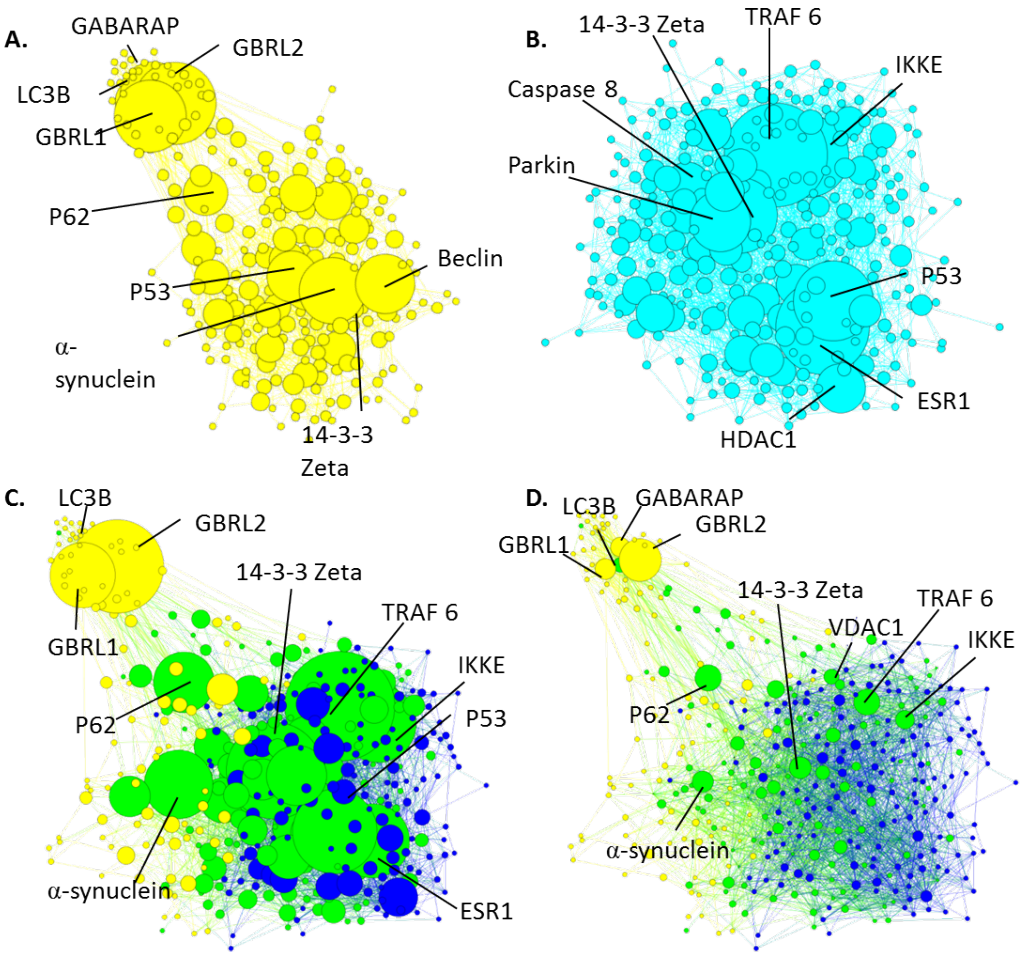

Figure 4.9: **Subgraph analysis identifies proteins predicted to be important for the cross-talk between autophagy and mitochondrial dysfunction.** **A** and **B** Subgraphs formed using shortest-path sampling of the experimental, binary PPIN derived from iRefIndex with ubiquitin removed and the autophagy (**A**) and mitochondrial (**B**) seeds in *Tables 4.3 and 4.5*; nodes are sized according to BC in the subgraph. **C** and **D** Union of the two subgraphs, yellow nodes appear only in the autophagy subgraph, blue nodes only in the mitochondrial dysfunction subgraph and green nodes are common to the two subgraphs; nodes are sized according to total (**C**) or Δ (**D**) BC.

4.2.12 Identification of optimal pairwise combinations

Given the robust nature of biological networks and the need to make multiple interventions it was important to identify combinations of proteins whose simultaneous modulation was expected to have the largest effect on the system. This work was conducted in collaboration with Andrew Elliott with all code written and executed by Andrew. The BC is a measure of the number of shortest paths that would be affected by the deletion of a node. Here, this work was extended

to consider the number of paths that would be disrupted by deleting a combination of nodes. The number of shortest paths affected following the removal of nodes a and b was defined as the number of shortest paths involving a plus the number of shortest paths involving b minus the number of shortest paths involving a and b. The detailed results from this analysis are presented in the *Appendix B*. However, in summary, the most effective pairs and trebles of nodes were the combinations of the individual top ranked nodes. Therefore, this thesis focussed on identifying top individual nodes with the goal of combining individual proteins for *in vitro* experiments.

4.2.13 Effect of deletion of ubiquitin

To assess the impact of the removal of ubiquitin the total BC of each node in the shortest-path PPIN was calculated both with, and without, ubiquitin and the correlation calculated (*Figure 4.10*), $R^2 = 0.9918$. Given the very high correlation coefficient the removal of ubiquitin was not expected to have a large effect on BC analysis and therefore further analyses were conducted on PPIN from which ubiquitin had been deleted.

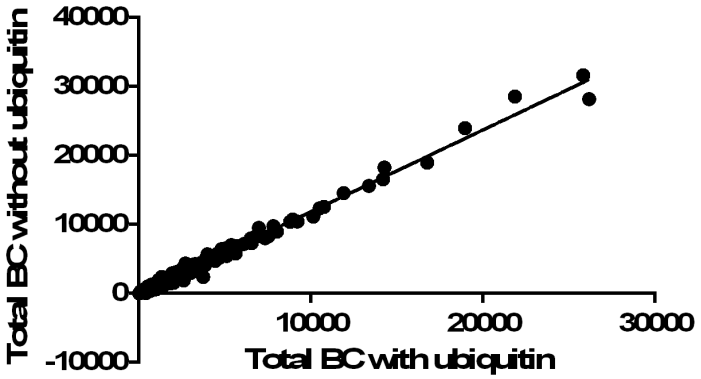

Figure 4.10: **Deletion of ubiquitin does not affect the identification of other high centrality nodes.** The BC of all nodes in the shortest-path PPIN was calculated. Ubiquitin was removed from the sampled PPIN and the BC of all nodes in the new PPIN was calculated. The BC for each node before and after the deletion of ubiquitin is displayed. Linear regression was performed and the R^2 correlation coefficient calculated.

4.2.14 Selective betweenness centrality

The selective BC (*Subsection 2.3.6*) was calculated for all nodes in the shortest-path PPIN using only mitochondrial paths (Selective BC_{mito}) and only MPP^+ paths (Selective BC_{MPP^+}). Additionally, the selective BC_{Δ} was calculated to consider the crosstalk between autophagy and mitochondrial dysfunction (*Table 4.21* shows the top hits). The top scoring nodes included a number of proteins that have independently been shown to modulate MPP^+ toxicity:

α-synuclein, ABL1 and parkin. Additionally, there were a number of results that had been highlighted by previous network analyses: 14-3-3ζ, IKKE, GBRL2, P62, P53 and BCL2.

The correlation between the selective BCs and overall BC was calculated to understand whether the selective measures did more than represent a node's overall properties within the PPIN (*Figure 4.11*). Although there was some correlation with overall BC the R^2 values demonstrated that the selective BC measure contained additional information.

In order to compare the results from the subgraph (*Subsection 4.2.11*) and the selective BC approaches, the ΔBC and the Selective BC_{Δ} were compared (*Figure 4.12*). Although there was correlation between the two metrics this was not complete.

The 'top hits' for selective BC from the 1-hop PPIN were calculated in a similar fashion (*Table 4.22*).

The selective BC analyses highlighted a number of possible target nodes. Some of the nodes had already been identified via other network analyses: α-synuclein, GABRARAP, GBRL1, GBRL2, P62, ABL1, Beclin1 and LC3B. However, some targets were unique to the selective BC analyses. Over the six selective BC analyses (across both PPIN), 28 proteins were identified as potential targets. Twelve of the proteins were common to the two PPIN with, seven only identified in the shortest-path PPIN and nine only in the 1-hop PPIN, and some nodes were identified by multiple analyses. The identification of different target proteins in the two networks demonstrated the impact of sampling method.

Although network analyses identified biologically plausible critical nodes the only way to validate the predictions was by testing them in an experimental system. Given the number of targets identified, experimental validation of all nodes was not feasible. Therefore, the results from the subgraph analysis (*Subsection 4.2.11*) and the selective BC analysis (*Subsection 4.2.14*) were prioritised with a particular focus on the proteins predicted to be important for the cross talk between autophagy and mitochondrial dysfunction as identified through the ΔBC and Selective BC_{Δ} analyses.

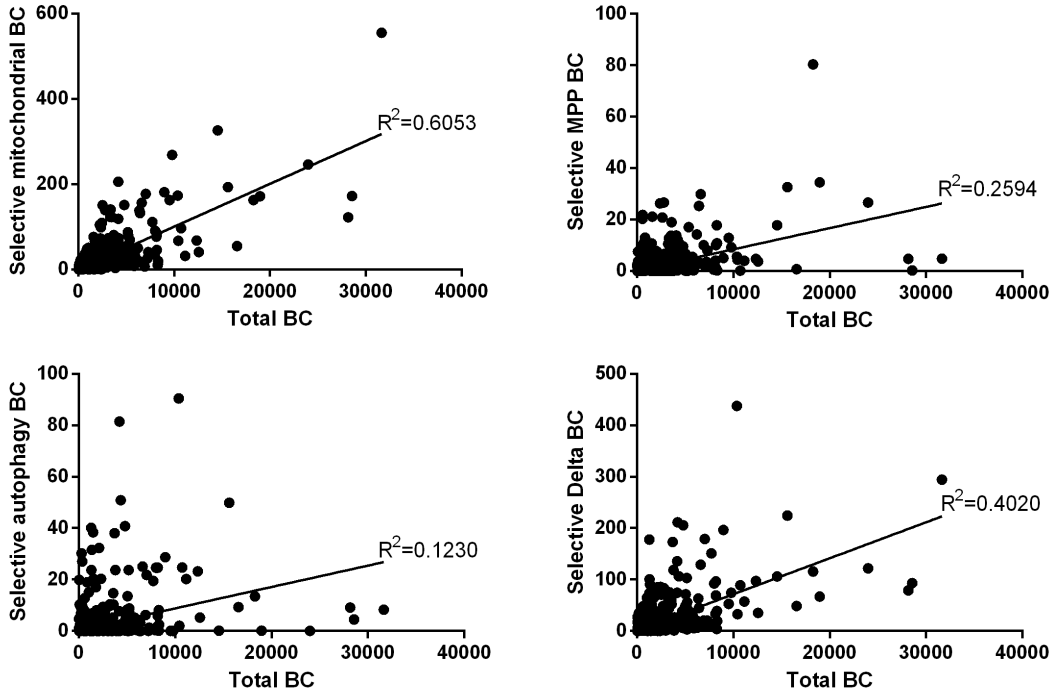

Figure 4.11: **Selective betweenness centrality (BC) contains additional informational information compared to total BC.** The total BC of all nodes in the shortest-path PPIN was calculated. The selective BC of each node was then calculated using subsets of nodes defined by their GO terms as involved in autophagy, mitochondria or MPP^+ pathology. The Selective BC_Δ for mitochondrial and autophagic processes was also calculated. Selective BC was plotted for total BC for each node, linear regression performed and the R^2 correlation coefficient calculated.

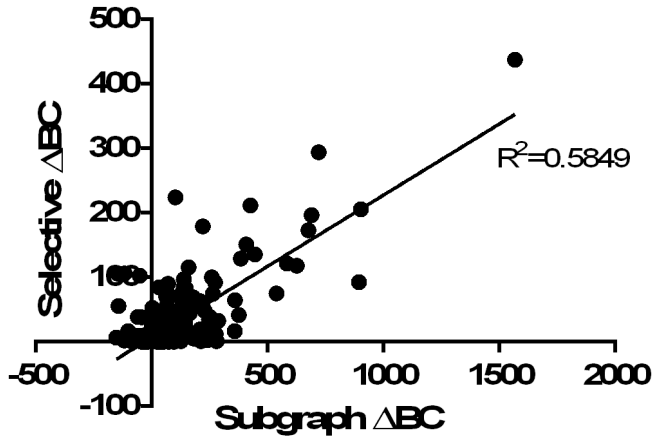

Figure 4.12: **There is some correlation between ΔBC and Selective BC_Δ.** ΔBC for each node in the subgraph analysis (*4.2.11*) was plotted against its selective BC_Δ (*Figure 4.11*). Linear regression performed and the R^2 correlation coefficient calculated.

1-Hop network		
CROGID	Protein	Bridging centrality
1409948	TNF11	2172.4
3561944	TIMP3	1047.6
1001745	Osteopontin	794.8
948452	TraB domain-containing protein	780.9
711280	Testican-1	445.3
4247195	Brevican core protein	439.4
222771	Decorin	398.0
3557303	PINK1l	395.4
1053734	Osteonectin	358.5
4635868	Oxysterol-binding protein-related protein 5	340.9
2318708	Nucleoporin SEH1	301.9
4092105	Dedicator of cytokinesis protein 1	299.3
5071329	E3 ubiquitin-protein ligase Praja-1	298.9
4227441	Cutaneous T-cell lymphoma-associated antigen 5	295.5
2113118	Glutathione synthetase	286.9
5832396	Secernin-1	282.6
2985525	Active breakpoint cluster region-related protein	260.8
3407738	PR domain zinc finger protein 2	256.7
815051	Glutathione reductase, mitochondrial	233.7
3976973	Lamina-associated polypeptide 2, isoforms β/γ	203.4
Shortest-path network		
CROGID	Protein	Bridging centrality
1314473	Golgi-associated PDZ and coiled-coil motif-containing protein	212.8
1045744	C-C chemokine receptor type 10	177.4
5083336	Laminin subunit α-1	158.3
2508904	Proteinase-activated receptor 2	149.9
2296687	Rab-3-interacting protein 2	141.5
3841000	snRNA-activating protein complex subunit 3	132.3
2394559	Heterogeneous nuclear ribonucleoprotein H3	131.5
1987115	E3 ubiquitin-protein ligase RNF123	131.2
3803247	Small glutamine-rich tetratricopeptide repeat-containing protein α	122.1
1409948	Tumour necrosis factor ligand superfamily member 11	121.8
281045	Phosphoserine aminotransferase	118.8
1401730	Ras-related protein Rap-1b	114.2
1870582	Elongation factor Ts, mitochondrial	112.6
5406757	Trans-Golgi network integral membrane protein 2	106.1
4474494	Amyloid protein-binding protein 2	104.1
403028	ATPase family AAA domain-containing protein 3B	103.5
5406611	General transcription factor 3C polypeptide 1	99.1
4750819	Pterin-4-α-carbinolamine dehydratase	96.6
4092105	Dedicator of cytokinesis protein 1	91.0
3976973	Lamina-associated polypeptide 2, isoforms β/γ	90.9

Table 4.16: **Hwang's metric identifies 'bridging nodes' in MPP$^+$ PPIN.** Bridging centrality was calculated for all nodes according to Hwang's equation. All proteins with a bridging centrality exceeding 200 for the 1-hop PPIN and 90 for the shortest-path PPIN are listed in the table.

Terminals	Network	Steiner nodes
Mitochondrial seeds	Hop	IKKE, Polyubiquitin C
Mitochondrial seeds	Path	IKKE, Polyubiquitin C
Autophagy seeds	Hop	IKKE, Polyubiquitin C, PINK1
Autophagy seeds	Path	IKKE, Polyubiquitin C, PINK1
Oxidative stress seeds	Hop	GAPDH, Polyubiquitin C, RB1, ABL1, 14-3-3ζ, HSP7C, IL-7RA, ASF
Oxidative stress seeds	Path	GAPDH, SRRM2, Polyubiquitin C, RB1, ABL1, 14-3-3ζ, HSP7C, IL-7RA
Mitochondrial and autophagy seeds	Hop	IKKE, Polyubiquitin C
Mitochondrial and autophagy seeds	Path	IKKE, Polyubiquitin C
Mitochondrial and apoptosis seeds	Hop	IKKE, Polyubiquitin C, Caspase-9
Mitochondrial and apoptosis seeds	Path	IKKE, Polyubiquitin C, Caspase-8, MAPK14

Table 4.17: **Similar Steiner nodes are identified in 1-hop and shortest-path sampled MPP$^+$ PPIN.** Steiner type analysis was performed on both the shortest-path and 1-hop PPIN using subsets of the initial seed nodes as Steiner terminals. The additional nodes required to connect all of the terminals (with a minimal path length) are termed Steiner nodes.

Terminals	Network	Weighting factor	Steiner nodes
Mitochondrial seeds	Hop	Degree	IKKE, Polyubiquitin C
Mitochondrial seeds	Path	Degree	IKKE, Polyubiquitin C, SMAD2, HDAC1
Mitochondrial seeds	Hop	BC	IKKE, Polyubiquitin C
Mitochondrial seeds	Path	BC	IKKE, Polyubiquitin C, Amyloid βA4, Androgen receptor, SMAD2
Autophagy seeds	Hop	Degree	P62, BCL2, α-synuclein, TRAF6, Polyubiquitin C
Autophagy seeds	Path	Degree	P62, α-synuclein, DNPK1, TRAF6, Polyubiquitin C
Autophagy seeds	Hop	BC	BCL-X, P62, TRAF6, Polyubiquitin C, EDFR, ABL1
Autophagy seeds	Path	BC	BCL-2, P62, TRAF6, Polyubiquitin C
Mitochondrial and autophagy seeds	Hop	Degree	BCL-2, α-synuclein, IKKE, Polyubiquitin C
Mitochondrial and autophagy seeds	Path	Degree	α-Synuclein, DNPK1, TRAF2, HDAC1, SMAD2, IKKE, Polyubiquitin C
Mitochondrial and autophagy seeds	Hop	BC	UBC9, SMAD2, MK14, BCL-X, P62, IKKE, TRAF6, Polyubiquitin C
Mitochondrial and autophagy seeds	Path	BC	BCL-2, P62, Amyloid βA4, Androgen receptor, SMAD2, IKKE, Polyubiquitin C
Mitochondrial and apoptosis seeds	Hop	Degree	Polyubiquitin C, IKKE, MPK14, ATK1
Mitochondrial and apoptosis seeds	Path	Degree	MAPK14, Caspase-3, HDAC1, SMAD2, IKKE, Polyubiquitin C
Mitochondrial and apoptosis seeds	Hop	BC	UBC9, SMAD2, MAPK14, Caspase-8, IKKE, Polyubiquitin C
Mitochondrial and apoptosis seeds	Path	BC	MAPK14, Caspase-3, Amyloid βA4, Androgen Receptor, SMAD2, IKKE, Polyubiquitin C

Table 4.18: **Weighting of Steiner analyses does not prevent the selection of ubiquitin as a Steiner node.** Steiner type analysis was performed on both PPIN using subsets of the initial seed nodes as Steiner terminals. The additional nodes required to connect all of the terminals (with a minimal path length) are termed Steiner nodes. Nodes were weighted for inclusion by their degree or BC.

Terminals	Network	Steiner Nodes
Mitochondrial seeds	Hop	RGAG4, SMAD4, UBC9
Mitochondrial seeds	Path	SNAP25, IKKE
Autophagy seeds	Hop	BCL-X, P53, IKKE, MAP1B
Autophagy seeds	Path	NEDD4, DAPK1, SNAP25
Mitochondrial and autophagy seeds	Hop	IKKE, α-synuclein
Mitochondrial and autophagy seeds	Path	SNAP25, IKKE
Mitochondrial and apoptosis seeds	Hop	RGAG4, SMAD4, UBC9, BCL-X, IKKE
Mitochondrial and apoptosis seeds	Path	MAPK14, Caspase-8, IKKE, SNAP25

Table 4.19: **Deletion of ubiquitin allows the identification additional of critical linking nodes in MPP$^+$ PPIN through Steiner analysis.** Steiner type analysis was performed on both PPIN (following removal of ubiquitin) using subsets of the initial seed nodes as Steiner terminals. The additional nodes required to connect all of the terminals (with a minimal path length) are termed Steiner nodes.

Protein	**ΔBC**	**Total BC**	**Mito BC**	**Auto BC**
GBRL2	1568	3761	0	2192
P62	902	2382	378	1103
TRAF6	894	4466	2644	927
14-3-3ζ	720	3891	1870	1301
α-synuclein	690	2713	293	1729
GBRL1	675	2576	0	1901
GABARAP	625	1671	0	1045
IKKE	583	3097	2050	464
VDAC1	538	1337	475	324
LC3B	425	2508	375	1708

Table 4.20: **Nodes with highest Δ betweenness centrality (BC) are predicted to be important for the cross-talk between autophagy and mitochondrial dysfunction.** The BC of each protein in the autophagy and mitochondrial dysfunction subgraphs, the union graph and the overall ΔBC (*Figure 4.9*). Nodes are ranked according to ΔBC.

Selective BC$_{mito}$		
Protein	Selective BC$_{mito}$	Normalised selective BC$_{mito}$ (%)
14-3-3ζ	555.2	100.0
RB	326.4	58.8
CRCM	268.5	48.4
IKKE	246.1	44.3
PPP2R2B	205.9	37.1
P53	193.2	34.8
α-Synuclein	181.1	32.6
Nemo	177.1	31.9
GBRL2	173.0	31.2
TRAF6	172.1	31.0
SMAD2	171.8	30.9
Selective BC$_{MPP+}$		
Protein	Selective BC$_{MPP+}$	Normalised selective BC$_{MPP+}$ (%)
ABL1	80.3	100.0
SMAD2	34.5	42.9
P53	32.7	40.6
Parkin	29.9	37.2
BCL2	26.6	33.2
IKKE	26.6	33.1
VIME	25.3	31.5
Selective BC$_{\Delta}$		
Protein	Selective BC$_{\Delta}$	Normalised selective BC$_{\Delta}$ (%)
GBRL2	437.7	100.0
14-3-3ζ	294.4	67.3
P53	224.2	51.2
LC3B	211.6	48.3
P62	205.7	47.0
α-syn	196.6	44.9
Nemo	179.1	40.9
mTOR	177.6	40.6
GBRL1	173.3	39.6
Calmodulin	151.2	34.5
PPP2R2B	135.5	31.0

Table 4.21: **Nodes with highest selective BC from shortest-path PPIN are expected to be critical for MPP$^+$ toxicity.** Selective BC only considering paths between specific nodes (as defined by GO annotation) within the shortest-path PPIN. Selective BC_{Δ} considered the difference between the combined autophagy/mitochondrial selective BC and the sum of the two separate selective BCs. All values were normalised to the top selective BC and proteins with a normalised value exceeding 30% are included in the table.

Selective BC$_{mito}$		
Protein	Selective BC$_{mito}$	Normalised selective BC$_{mito}$ (%)
ABL1	491.1	100.0
α-Synuclein	391.8	79.8
14-3-3ζ	236.1	48.1
RB	215.6	43.9
Tau	196.0	39.9
TNR1A	187.5	38.2
VIME	181.1	36.9
BCL2	176.0	35.8
Parkin	165.4	33.7
P53	164.1	33.4
Selective BC$_{MPP+}$		
Protein	Selective BC$_{MPP+}$	Normalised selective BC$_{MPP+}$ (%)
Parkin	87.7	100.0
ABL1	65.1	74.2
BCL2	64.1	73.1
VDAC1	56.6	64.6
BAX	46.8	53.4
Beclin1	36.9	42.1
TNR1A	36.1	41.2
MCL1	35.9	40.9
B2CL1	29.0	33.0
Selective BC$_{\Delta}$		
Protein	Selective BC$_{\Delta}$	Normalised selective BC$_{\Delta}$ (%)
Beclin	382.5	100.0
α-Synuclein	358.2	93.6
GBRL2	324.2	84.8
LC3B	292.9	76.6
ABL1	271.9	71.1
GBRL1	242.0	63.3
P62	206.9	54.1
mTOR	200.3	52.4
B2CL1	173.1	45.2
Parkin	170.0	44.5
GABARAP	145.8	38.1
P53	134.0	35.0
14-3-3ζ	133.5	34.9
BCL2	117.4	30.7

Table 4.22: **Nodes with highest selective BC from 1-hop PPIN are expected to be critical for MPP$^+$ toxicity.** Selective BC only considering paths between specific nodes (as defined by GO annotation) within the 1-hop PPIN. Selective BC_{Δ} considers the difference between the combined autophagy/mitochondrial selective BC and the sum of two separate selective BC values. All values are normalised to the top selective BC and proteins with a normalised value exceeding 30% are included in the table.

4.3 Discussion

4.3.1 Network construction

PPIN from the iRefIndex database

iRefIndex was used as a source of human PPI data. Datasets containing all data, all experimental data and all low-throughput data were established and PPIN were constructed using binary, bipartite, complex and matrix methods for the representation of interactions between more than two partners. As data (either predictive or high-throughput) were excluded the network density decreased because interaction data are lost more rapidly than proteins which may still be involved in other PPI supported by experimental/low-throughput data. Bipartite complex representation led to an increased number of nodes as an additional node was included for each complex and matrix representations led to a three to four fold increase in the number of network edges as an edge was added between each member of the experimentally detected protein complex.

MPP^+ seedlist

In order to create PPIN pertinent to MPP^+ pathology a seedlist of 40 MPP^+ related proteins was constructed and used to sample the networks. It must be acknowledged that the list of proteins known to be involved in MPP^+ pathology will only increase as further experiments are constructed and the seedlist only reflects the evidence available at the time of its creation.

The concept of sampling relies on the principle of guilt by association, proteins are more likely to interact with proteins involved in similar cellular processes or pathologies [274]. Therefore, proteins closely connected to those already known to be involved in MPP^+ cell death are more likely to also be involved in MPP^+ pathology. It was hypothesised that by creating a network enriched in MPP^+ relevant processes, critical interactions/proteins could be identified despite the noise generated by non-relevant interactions.

DAPPLE was used to demonstrate that the seedlist as a whole generated a PPIN more connected than would be expected at random by a number of measures. Increased connectivity suggested that the seeds were involved in common pathways, although analysis did not demonstrate a specific link with PD or MPP^+ pathology. Further, there is some circularity in connectivity analysis with proteins implicated in a single disease more likely to be investigated in concert. Fourteen proteins within the DAPPLE network were identified as being significantly more con-

nected than expected at random. The list of highly connected seeds included all three synucleins (α-synuclein is central to PD pathology (*Subsection 1.4.1*), parkin and UCHL1, mutations in which lead to autosomally recessive PD [3] and tau, a risk locus identified through multiple GWAS [31]. Although the other seeds were not individually more connected than would be expected at random, the seedlist as a whole resulted in a network that was more connected than would be expected were the seeds not otherwise linked.

It is acknowledged that although the DAPPLE PPIN and the other PPIN used for network analysis were prepared using a common seedlist, they are sampled from different underlying PPI databases (InWeb and IRefIndex respectively) and the DAPPLE PPIN does not include cross links between non-seed nodes. Therefore, conclusions regarding the DAPPLE PPIN cannot automatically be extended to the other PPIN in this thesis. However, it was considered probable that the increased connectivity of the seeds would also be seen in the iRefIndex PPIN. The DAPPLE PPIN could have been used for further investigations. However, iRefIndex contains more recent PPI data, includes PPI from more databases, maps protein isoforms to single canonical identifier and offers more control over the data included and form of complex representation. Therefore, iRefIndex was considered a superior source of PPI data to the DAPPLE network.

Microarray experiments had been conducted with the goal of identifying differentially regulated genes that could be used as an alternative seedlist (*Subsection 3.2.5*). However, no genes showed statistically significant MPP^+ induced alterations to expression following corrections for multiple testing.

Sampled networks

Sampling was used to construct PPIN enriched in MPP^+ relevant processes. The gross properties of the resulting networks were explored and nodes with the highest BC were identified. PPIN containing only binary interaction data were selected for further analysis to ensure that each node represented a protein that could be biologically targeted (unlike a bipartite PPIN). Further, spoke representations have been shown to distort PPIN by generating artificial hubs within the network [405, 420]. Although the matrix method of complex representation was briefly trialled, this resulted in very high network densities and increased clustering based on each experiment.

The paucity of low-throughput PPI data resulted in sparse networks when high-throughput data were excluded. Further, low-throughput data is not necessarily more reliable than high-throughput and has an increased risk of experimental bias [276, 400, 404–406]. Therefore,

high-throughput data was considered a valuable component of MPP^+ PPIN. Although the networks including and excluding predicted data were broadly similar, experimental networks were selected as the focus for this thesis such that each edge represented a biologically validated interaction. As the networks were unweighted there was no possibility of including predictive data with a lower confidence. The exclusion of predictive data is consistent with the approach used by the PPI-trim to generate high-quality datasets from iRefIndex [420].

Identification of high centrality nodes in sampled networks

The nodes with highest BC were identified across the sampled PPIN. The high centrality of ubiquitin reflects the fact almost all proteins can be ubiquitinated. Interestingly, ABL1 also had a very high centrality; ABL1 is the target of STI-571 (imatinib) and treatment with STI-571 has been shown to decrease MPTP toxicity in animal models [365]. A number of other tyrosine protein-kinases also repeatedly appeared with high BC, in particular Src and Fyn, this may be due to an important role in MPP^+ pathology or alternatively reflect their high degree in the unsampled PPIN. GBR2 had high BC values and is another protein with many potential binding partners, involvement in multiple cellular functions and a critical linking role in initiating a cellular pathway (Ras signalling) [469]. TRAF6 had a high BC in some PPIN; expression of TRAF6 is raised in the brains of PD patients and the protein localises to LB [470]. The protein 14-3-3ζ repeatedly appeared as a central node in the PPIN.

A number of the seed proteins (parkin, tau, nNOS, α-synuclein, MMP3, BAX, Beclin1, transferrin) also appeared as high BC nodes, particularly in the networks formed using only the low-throughput data. Their centrality may have been due to their critical role in MPP^+ pathology, modulation of levels of both parkin and α-synuclein alter MPP^+ toxicity [114, 365]. Alternatively, their centrality may be a result of bias in the underlying PPI data. Proteins already known to be involved in disease pathology (including MPP^+ toxicity as a model of PD) are more extensively investigated and therefore more interaction partners reported leading to a higher degree than would otherwise be expected in the networks.

There were key differences between the 1-hop and shortest path PPINs. The 1-hop networks had a lower degree, higher transitivity and a larger average shortest path length. These differences could mostly be explained by the sampling method used to construct the networks, but there was also variation in the nodes identified as having highest BC. To facilitate a comparison of the two sampling techniques, a 1-hop and a shortest-path PPIN generated using all binary, experimental PPI data were used for further analyses. Neither network's degree distribution

followed a power law.

Community identification

A spin glass algorithm was used to identify communities within the PPIN and enrichment of GO annotations used to assign biological function. Communities corresponding to systems-level biological processes involved in MPP^+ pathology were identified within the sampled PPIN. Although different communities were identified in the two networks the key processes of autophagy, cell death, plasma membrane and protein translation appear in both. The detection of communities provided confidence that PPIN representing the underlying, systems-level processes in MPP^+ toxicity had been identified.

4.3.2 Target identification

Although the proteins identified as having the highest BC were critical for the topology of the networks, high degree in PPIN has been shown to be correlated with biological essentiality [396, 397]. Therefore further analyses were conducted to identify potential target nodes.

Bridging centrality

The first approach used to identify targets capable of subtly modifying the transmission of information through the network was Hwang's bridging centrality [324, 443]. The majority of proteins identified were little investigated and few of the known 'positive controls' i.e. proteins whose expression is known to alter MPP^+ toxicity (such as α-synuclein or parkin) appeared as central nodes under this metric. This analysis favoured proteins that had been subject to relatively little investigation due to the inverse node degree term. This bias caused concerns about the veracity of the results from the bridging centrality analysis.

Further target identification considered proteins expected to mediate the transmission of information between the systems-level processes of mitochondrial dysfunction and autophagy. MPP^+ is a mitochondrial toxin with all other cellular dysfunction lying downstream of initial insult [209]; mitochondrial dysfunction is also central to PD aetiology [246, 247, 328]. Autophagy is essential for neurones and autophagic dysfunctions have been implicated in numerous PD and MPP^+ models [142, 160]. It was hypothesised that cellular protection could be achieved by altering the interplay between these systems-level processes.

Steiner analysis

Steiner analysis was used to identify nodes critical in connecting seeds in the sampled networks, this approach had previously been utilised in a study of genes commonly mutated in colorectal cancer [309]. When the two sampling methods were compared the results were largely identical suggesting that the sampling method has little impact on the key connection between seeds. The high number of Steiner nodes for the oxidative stress seeds reflected the fact that oxidative stress proteins are typically connected by non-protein species, e.g. antioxidants, and therefore more Steiner nodes are required to connect all of the terminals. Ubiquitin is a key linking node in the networks and appeared as a Steiner node in all analyses even when node weighting was used to disfavour its inclusion. White and Ma'ayan report weighting nodes by their degree to avoid overrepresentation of hubs in their study [309], but weighting was insufficient to counteract the high centrality of ubiquitin. However, upon ubiquitin's deletion a number of other proteins were identified as important connectors many of which (including NEDD4, α-synuclein and SNAP25) had validated roles in PD pathology.

Subgraph analysis

Subgraphs representing mitochondrial dysfunction and autophagy were created, ubiquitin removed and their union formed. A number of the nodes which had a high BC in the total network also had a high centrality in the more focused subgraphs these included 14-3-3ζ, IKKE, P53 and TRAF6 - their overall centrality may have been driven by the autophagy and mitochondrial dysfunction components of the network. Further, two of the known positive controls (parkin and α-synuclein) had a high BC in one, or other, of the process specific graphs.

Three proteins from the GABARAP subfamily (GABARAP, GBRL1 and GBRL2) appear in the top ten results for ΔBC. The GABARAP subfamily proteins exhibit a high degree of sequence similarity and functional redundancy [353, 370]. Further, LC3B (ranked 10th for ΔBC) belongs to the same family of proteins, all are orthologs of the yeast protein ATG8. The GABARAP proteins did not have a particularly high total BC which indicated that the subgraph analysis contributed additional information and that a node's characteristics in the network as a whole may not accurately predict its importance in a more specific context. TRAF6, 14-3-3ζ, IKKE had also been identified as critical nodes by Steiner analysis.

Pairwise analysis

Pairwise analysis was conducted in conjunction with Andrew Elliott and identified pairs of nodes that when deleted in combination would disrupt maximal numbers of network shortest paths. This analysis correlated well with the summation of individual BC values and indicated that the most effective combinations were likely to be combinations of the nodes predicted to be individually important.

Selective betweenness centrality

This metric was developed to consider the contribution of a subset of the network's shortest paths to a node's BC. Only the shortest paths between proteins with a specific GO annotation were included to identify nodes which were important for the transmission of information in the context of specific cellular processes. Although there was some correlation between selective BC and the subgraph analysis there were significant differences. The different definitions of mitochondrial/autophagy nodes are likely to cause the divergent results: under the subgraph analysis processes were defined as proteins known to be involved in MPP^+ induced cell death whereas, in the selective BC approach processes were defined by GO annotations and so included proteins which are not involved in the cellular response to the neurotoxin. Further, the selective BC approach included paths that were outside the scope of the smaller union network formed in the subgraph approach. Using the selective BC analysis 26 proteins were identified as critical nodes across the two networks and six analyses.

4.3.3 Comparison to results from analysis other Parkinsons related PPIN

Three of the proteins (α-synuclein, P62 and 14-3-3ζ) identified through the network analysis in this thesis were also identified in Rakshit *et al.*'s PPIN study of potential PD biomarkers, although these proteins were not included in the authors' list of 12 high priority biomarkers [446]. Further, GABARAP, calmodulin, P62 and 14-3-3ζ were also identified in Konn's PPIN as α-synuclein interactors [302].

An interesting comparison can be drawn between the work in this thesis and the work of Rakshit *et al.* as both studies attempted to identify critical proteins through topological analysis of PD related networks. However, there are a number of important distinctions. Rakshit *et al.* constructed a PD network and aimed to identify biomarkers; in contrast this thesis generated an MPP^+ network with the goal of identifying optimal intervention points, even where these

proteins were unaltered following MPP^+ exposure. This thesis utilised a manually constructed list of seeds demonstrated to be involved in MPP^+ pathology in comparison, Rakshit *et al.* used a much larger list of proteins corresponding to differentially expressed genes in the brains of PD patients. It is interesting to note that Rakshit *et al.* do not reproduce the results of other studies using the same microarray data and the authors comment on the range of analytical approaches that can be used to investigate microarray data [446]. Both this study and the work of Rakshit *et al.* utilised BC based topological analyses in combination with biological intuition to identify critical nodes. Whereas this thesis developed BC analyses to identify proteins that had a specific role in connecting systems-level processes of interest (autophagy and mitochondrial dysfunction), Rakshit *et al.* used biological intuition to prioritise the nodes highlighted by less biologically driven topological analysis particularly those involved in cliques and with associations with neurotransmitters. Given, the considerable methodological differences between the two approaches, it is gratifying that common nodes are identified as critical to MPP^+ and PD pathology. However, the key advantage of the work presented in this thesis is the experimental validation of these predictions.

Konns study of α-synuclein took a different approach, aiming to identify interactors with a protein known to be central to PD pathology rather than considering the disease state as a whole [302]. Therefore, his work was predominantly based on the construction of a set of high confidence PPI, rather than the analysis of the topology of the resulting network. However, it is intriguing to note that α-synuclein interacts with several of the intervention points identified by the network analysis in this thesis; this perhaps further underlines the central role of α-synuclein in PD and MPP^+ pathology.

4.3.4 Biological roles of proteins identified by network analysis

Proteins relating to autophagy

A number of the proteins identified in this thesis are involved in autophagy. GABARAP, GBRL1, GBRL2 and LC3 are involved in autophagosome maturation and elongation [353, 471] and P62 acts as an adaptor, targeting ubiquitinated proteins and organelles for degradation [352]. Additionally, Beclin1 can induce autophagy [150], the inhibition of mTOR upregulates autophagy [472] and VDAC1 is required for PINK1/parkin dependent mitophagy [180]. Although mitophagy is one component of maintaining a population of healthy mitochondria, the balance of mitochondrial fission and fusion is also crucial; the protein PPP2R2B (serine/threonine-protein phosphatase 2A 55 kDa regulatory subunit Bβ isoform) is thought to help regulate mitochondrial

fission/fusion and undergoes mitochondrial translocation following cell stress [200, 201]. Steiner analysis also highlighted members of the BCL family, including BCL-2 and BCL-X which play an important role in the initiation of autophagy and have been shown to mediate MPP^+ toxicity [154, 332, 473].

Proteins relating to apoptosis

The selective BC results included a number of proteins involved in the regulation of apoptosis in particular mitochondrial membrane permeabilisation and cytochrome C release. BAX transcription (mediated by P53) and translocation to the mitochondria leads to membrane permeabilisation and cytochrome C release, whereas B2CL1 and BCL2 act as apoptotic inhibitors [328, 450]. MCL1 is a further BCL-2 family protein and is able to either promote cell death or cell survival [474]. VDAC1 (a mitochondrial membrane pore) plays a crucial role in maintaining the potential across the mitochondrial membrane, allows the exchange of metabolites and is essential for mitochondrial-mediated cell death [180]. TRAF6, IKKE and NEMO all play key roles in NFκB induced cell death [468] and TNR1A activates TNF mediated cell death [475].

Proteins relating to α-synuclein

α-Synuclein was identified as a critical node by subgraph, Selective BC and Steiner analyses, in the latter the protein had a critical briding position (*Figure 4.8F*). α-Synuclein is central to PD pathology [101], mutations and multiplications in the gene lead to genetic PD [19, 20] and α-synuclein is the major component of LB found in the surviving DA neurones of PD patients [9].

14-3-3ζ was also highlighted by a number of network analyses. This protein shows a high degree of homology to α-synuclein [476], binds to LRRK2 [477] (mutations in which lead to genetic PD) and activates TH [476] (the rate limiting enzyme in DA synthesis).

Both NEDD4 and were SNAP25 were highlighted by the Steiner type analysis. NEDD4 allows the ubiquitination of α-synuclein and therefore its degradation and in yeast models of PD drugs capable of ameliorating α-synuclein toxicity act via NEDD4 [93]. SNAP25 protein is part of the SNARE complex (α-synuclein is a SNARE chaperone) and is involved in vesicle fusion, alterations in the level of SNAP25 have been seen in α-synuclein OE models of PD [121].

Tau was identified through the Selective BC analysis. GWAS studies have demonstrated a significant association between variations in *MAPT* and increased risk of PD [31]. Tau's key function

is the stabilisation of microtubules, stabilisation is dependent upon tau's phosphorylation state and there is evidence of hyperphosphorylation in PD (and disease models) resulting in microtubule destabilisation [130, 131, 463]. Vimentin (also identified by Selective BC analysis) is also a key component of the cellular cytoskeleton found in mesenchymal cells [284], intensely vimentin positive staining astrocytes have been found in affected areas of the brains of AD, Pick's disease, amyotrophic lateral sclerosis, multiple sclerosis and, to a lesser extent, PD sufferers [478].

Other proteins identified by network analysis

Although calcium homeostasis was not specifically investigated in this thesis, calcium influx and buffering is thought to contribute to the high energy demands of the DA neurones [230, 231] and both calmodulin and the CRAC channel were shown to have high selective BC.

4.3.5 Summary

PPIN enriched in MPP^+ relevant processes were generated using the iRefIndex PPI database and sampling using seedlists of proteins known to be involved in MPP^+ pathology. Proteins predicted to be critical in mediating mitochondrial dysfunction and its interplay with autophagy were identified using a number of analyses. There was considerably overlap between the different methods of target identification and known positive controls were recovered.

To test the network predictions, an *in vitro* MPP^+ model will be used with protein KD to mimic node deletions. The subgraph and selective BC analyses on the shortest-path PPIN were prioritised for experimental validation (*Table 4.23*); these analyses had highlighted a number of biologically interesting targets. Given the goal of identifying proteins which could alter the crosstalk between mitochondrial dysfunction and autophagy, the ΔBC and selective BC_Δ results from the shortest-path PPIN were experimentally tested. To have maximal impact on the biological system (MPP^+ induced neurotoxicity) it was predicted that multiple interventions would be required.

To generate a **target list one** from the subgraph analysis, the top two network results (GBRL2 and P62) were selected. Given the redundancy previously reported in the GABARAP subfamily [353, 370] and the high network score of GABARAP and GBRL1, GABARAP and GBRL1 were also included in **target list one**. **Target list one** was restricted to four proteins to facilitate the testing of all combinations (singles, doubles, triples and quadruple) and so that all proteins could be both KD and OE.

As a comparison, less biological intuition was used to generate **target list two** from the network analysis. All proteins highlighted by the selective BC_{Δ} (between autophagy and mitochondrial dysfunction) were included in **target list two** with the goal of systematically testing this network analysis. For the longer **target list two**, KD was prioritised to better mimic node deletion and it was planned to limit KD combinations to all possible doubles.

Target list one	**Target list two**
GBRL2	GBRL2
P62	14-3-3ζ
GBRL1	P53
GABARAP	LC3B
	P62
	α-synuclein
	Nemo
	mTOR
	GBRL1
	Calmodulin
	PPP2R2B

Table 4.23: **Twelve protein targets (across two lists) were predicted to modulate MPP^+ toxicity. Target list one** was generated through subgraph analysis *Subsection 4.2.11* and **target list two** was generated through selective BC analysis *Subsection 4.2.14*.

Chapter 5

Validation of network targets

5.1 Introduction

The key processes underlying MPP^+ cytotoxicity and the principles behind the assays employed were previously outlined (*Section 3.1*). Following extensive network analysis a number of proteins predicted to have pivotal roles in an MPP^+ model of PD were identified (*Chapter 4*). The targets were divided into two lists: **target list one** (from subgraph analysis *Subsection 4.2.11*) and **target list two** (from selective BC analysis *Subsection 4.2.14*) (*Table 4.23*).

This chapter focuses on the validation *in silico* predictions in the *in vitro* MPP^+ model. The proteins on the shorter, **target list one** will be modulated in both directions with the effects of OE and KD explored. For the more extensive, **target list two**, KD will be studied to replicate the node deletions that were explored *in silico*.

5.1.1 Techniques for protein modulation

Various techniques are used to modulate protein levels *in vitro*. This thesis utilised expression constructs to achieve OE and siRNA mediated KD. OE relies upon the transfection of small plasmids containing an additional copy of a gene of interest under the control of a promoter. Successful transfection is followed by transcription and translation of the gene of interest by endogenous cellular machinery. Such proteins may be expressed as fusion products with molecular tags to allow endogenous and exogenous protein to be distinguished. siRNA mediated KD utilises the RNA interference (RNAi) phenomenon to selectively destroy mRNA corresponding to proteins of interest (*Figure 5.1*) [479]. Pre-validated siRNA targeting many human proteins are commercially available.

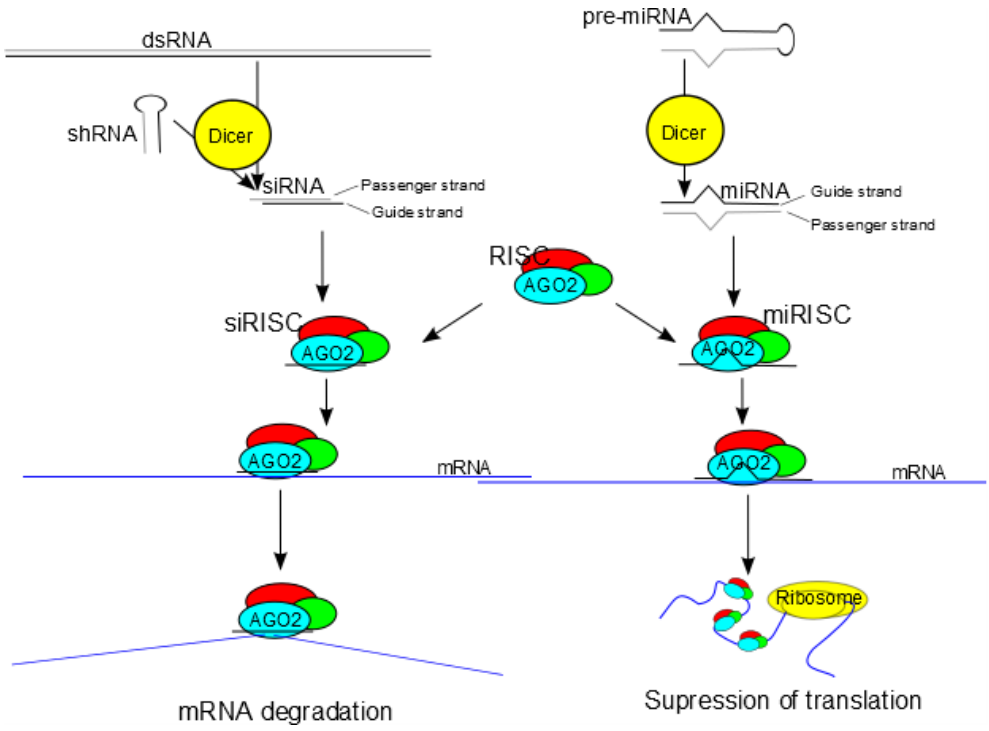

Figure 5.1: **The mechanism of RNA interference (RNAi).** The enzyme dicer cleaves long double stranded RNA (dsRNA) and short hairpin RNA (shRNA) following their export from the nucleus to generate small interfering RNA (siRNA); siRNA may also be exogenously introduced. In a similar fashion Dicer converts endogenous pre-micro RNA (miRNA) to form miRNA. siRNAs and miRNAs then interact with the RNA-induced silencing complex (RISC) to form siRISC and miRISC respectively. During siRISC/miRISC formation, the passenger RNA strand is destroyed leaving only the guide strand as part of the RISC complex; the guide strand has a complementary sequence to the targeted mRNA. Complementary binding between siRISC and mRNA results in argonaute2 (AGO2) mediated cleavage of the mRNA, and mRNA destruction. In the miRISC complex, complementary base pairing is not exact and so the binding of the miRISC complex to mRNA results in the suppression of translation, rather than mRNA degradation. Under experimental conditions, cells may be transfected with synthetically produced doubled stranded siRNA or plasmids expressing shRNAs.

5.1.2 Protein level modulations in MPP^+ models of Parkinson's disease

Protein level manipulations have previously been shown to modulate MPP^+ toxicity, particularly in the case of the proteins corresponding to mutated genes in familial PD. This laboratory has previously demonstrated that α-synuclein KD is protective against MPP^+ induced neurotoxicity [114, 115]. In contrast, depletion of PINK1 potentiates MPP^+ neurotoxicity in both *in vivo* and *in vitro* settings [457]. In a similar manner, parkin KD using shRNA resulted in increased MPP^+ vulnerability in the SH-SY5Y cell line [365]. OE models have also been utilised and the OE of WT, although not mutant, DJ1 was protective against MPP^+ induced neurotoxicity in the M17 cell line [201]. The deleterious effect of OE of mutant forms of DJ1 were reversed by KD of DRP1 [201].

Proteins not implicated in familial PD have also been experimentally modulated, further demonstrating that alteration of protein level can potentiate or ameliorate MPP^+ neurotoxicity. In Ko

et al.'s study into the role of parkin in MPP^+ toxicity, the authors demonstrated the critical role of proto-oncogene ABL1 (ABL1) mediated parkin phosphorylation in cell death and through ABL1 KD were able to protect cells [365]. Excitingly it was further shown that co-treatment with the ABL1 inhibitor STI-517 was able to replicate the effect of protein KD. Ko *et al.*'s work highlights how KD studies may be used as a precursor to pharmacological interventions, a possible continuation of this thesis.

Chu *et al.* demonstrated that both siRNA and shRNA mediated KD of AIF (release of AIF from the mitochondrial intermembrane space leads to caspase independent apoptosis) resulted in decreased MPP^+ toxicity [330]. Rescue was downstream of complex I inhibition and did not affect basal viability but decreased chromatin condensation and TUNEL staining after MPP^+ exposure. Admittedly under a somewhat different experimental paradigm, BAX and P53 KO mice are protected from MPTP induced neurodegeneration and those expressing the human form of BCL2 are protected from MPTP [331, 332, 480].

The proponents of the MPP^+ induced autophagic cell death theory have also used KD studies to support their arguments. Zhu *et al.*'s studies into the mechanism of MPP^+ toxicity highlighted the importance of ERK and its KD alleviated MPP^+ induced cell death [152]. The authors proposed an autophagic cell death pathway and to support their hypothesis demonstrated that LC3B, ATG5 and ATG7 KD were able to rescue neurotoxicity.

As a further example of RNAi approaches, shRNA mediated KD of cyclin-dependent kinase 5 activator 1, P35 (P35) led to decreased cell viability and increased vulnerability to MPP^+ whereas OE rescued neurotoxicity [454]. P35 is a neurone-specific activator of cyclin-dependent kinase 5 (CDK5), which has been implicated in cell death in neurodegenerative disorders and the complex is thought to be protective. Additionally, the siRNA mediated KD of MMP3 (known to cleave α-synuclein and contribute to its aggregation) protected cells from MPP^+ induced cell death [462].

Although the above do not provide an exhaustive account of all protein KD investigated in MPP^+ models of PD, this thesis aims to convince the reader that there is precedence of protein level modulation altering *in vitro* neurotoxicity. Protein level modulation is now extended to test the results of PPIN analysis. Here follows a brief introduction to the roles of each protein (in alphabetical order) modulated in this chapter; the role α-synuclein has already been extensively discussed in *Subsection 1.4.1.*

5.1.3 14-3-3ζ

The 14-3-3 family of proteins are ubiquitous and highly conserved, highest expression levels are found in the brain where they make up approximately 1% of soluble protein [476]. In mammals the family is made up of seven acidic 28-33 kDa proteins with five regions highly conserved between family members [476]. The 14-3-3 proteins self-assemble to form a range of homo- and hetero-dimers [481]. The dimers bind to a wide range of phosphorylated proteins, several hundred binding partners across a range of cellular processes have been identified and 14-3-3 proteins may be involved at multiple levels in cellular cascades [476, 481]. Binding of 14-3-3 proteins can alter protein structure, activity and localisation [476, 481].

The 14-3-3 family were first discovered as activators of TH and their binding to mitochondrial TH enhances DA production [111, 476]. Further, the 14-3-3 proteins bind to LRRK2 and binding is disrupted in mutant forms of LRRK2 leading to the formation of cytosolic pools of LRRK2 [477]. α-Synuclein has a high degree of sequence homology with 14-3-3 family proteins [476] and the two proteins interact. The 14-3-3 proteins are also anti-apoptotic, binding to BAX, BID and BAD and inhibiting their action [476]. Therefore, it has been suggested that OE of α-synuclein leads to sequestration of 14-3-3 proteins thereby promoting apoptosis [119, 336, 476]. The 14-3-3 proteins also colocalise with LB suggesting that they may have a role in α-synuclein aggregation [476].

Modulation of 14-3-3 protein levels has been shown to modulate α-synuclein, rotenone and MPP^+ toxicity. Yacoubain *et al.* demonstrated that pan-inhibition of 14-3-3 proteins potentiates MPP^+ and rotenone neurotoxicity and that selective OE of θ and ϵ (although not ζ) forms was protective [336]. Protection is thought to occur via increased 14-3-3 binding to BAX and the consequent inhibition of apoptosis [337]. KD of 14-3-3ϵ results in increased vulnerability to rotenone toxicity and α-synuclein aggregation and it has been suggested that increased vulnerability occurs via an autophagic mechanism [482]. Additionally, microarray data indicate differential expression of proteins involved in 14-3-3 signalling following MPP^+ exposure [304, 308].

Network analysis highlighted 14-3-3ζ as a protein of particular importance. Previously the modulation of 14-3-3ζ has not been shown to alter MPP^+ toxicity but the protein does colocalise with LB in PD brains [476].

5.1.4 ATG8 orthologs

The mammalian orthologs of ATG8 can be split into two subfamilies the LC3s and the GABARAPs with increased sequence homology within each subfamily [370]. ATG8 proteins are an essential part of the autophagic machinery and, following cleavage by ATG4 to expose a C-terminal glycine, are attached to the developing phagophore membrane via conjugation to PE [155]. There is significant functional redundancy within each subfamily but the two subfamilies have subtly different roles with the LC3s crucial for phagophore elongation and the GABARAPs involved in autophagosome maturation [353]. In addition to their role phagophore maturation, the ATG8 analogues play a critical role in recruiting cargo for degradation. Several cargo receptors have been identified (P62, NBR1 (Next to BRCA1 gene 1 protein) and optineurin) and interact with ATG8 analogues via the LIR (LC3 interacting region) motif [155]. The recruitment of P62 allows for the degradation of ubiquitinated cargo including large (up to 2 μm) P62 positive inclusion bodies [352]. Although the ATG8 analogues are all attached to the developing autophagosome and have similar roles in cargo recruitment, LC3B is classically used as marker of autophagosomes in investigations of autophagy [350, 483].

Three publications within the last year have emphasised the importance of the ATG8 family for autophagy [484]. Sawa-Makarska *et al.* demonstrated that ATG8 has multiple binding sites ensuring tight cargo binding to the phagophore and the exclusion of non-cargo material [485]. Nath *et al.* reported that the conjugation of ATG8 family proteins to PE is dependent on membrane curvature, ensuring a high concentration of the molecules on the leading edge of the phagophore and preventing the conjugation of ATG8 orthologs to mature autophagosomes [486]. Finally, Kaufmann *et al.* showed that conjugated ATG8s can act as a scaffold for the ATG5-ATG12-ATG16 complex stabilising membrane curvature to allow cargo recruitment [487].

Alterations to autophagy are implicated in PD and MPTP/MPP^+ models of the disease and changes in LC3B levels and lipidation are widely reported (*Subsection 3.1.6*). Both subfamilies are accumulated in LB in the brains of PD and dementia with LB patients [471]. Dephosphorylation of LC3s (although not GABARAPs) triggers their recruitment to autophagosomes in response to MPP^+ treatment [351]. The GABARAP subfamily has been less extensively explored. However, GABARAP is a NIX (NIP3-like protein X) binding partner allowing for possible crosstalk between apoptosis and autophagy [488].

5.1.5 Calmodulin

Calmodulin is a key, highly conserved ubiquitously expressed calcium binding protein. Calmodulin can bind to a wide range of proteins and thereby, regulate their activity in a calcium dependent fashion. As discussed in *Subsection 1.4.6*, large, poorly buffered calcium influx are thought to contribute to the vulnerability of the DA neurones on the SNpc in PD.

α-Synuclein and calmodulin have been shown to interact *in vivo* in a calcium dependent fashion and it has been suggested that this interaction may modulate α-synuclein aggregation [235]. α-Synuclein OE results in increased intracellular calcium levels which are capable of modulating the activity of numerous calmodulin binding partners [489]. Of particular relevance, Yang *et al.* recently demonstrated that the phosphoinhibition of PP2A, caused by α-synuclein is mediated by the kinase Src in a calmodulin dependent fashion [489].

There is some evidence of changes to calmodulin binding proteins in MPTP/MPP^+ models of the disease and treatment leads to increased intracellular Ca^{2+} levels [236]. Calmodulin antagonists trifluoperazine, W-7 and calmidazolium treatment leads to partial rescue of MPP^+ induced cell death and decrease the loss of mitochondrial membrane potential, cytochrome C release, ROS production and initiation of apoptosis [236].

5.1.6 mTOR

mTOR is a large kinase that plays a central role in the regulation of autophagy. mTOR forms two distinct protein complexes (each with several binding partners) mTORC1 and mTORC2. mTORC1 plays a pivotal role in the control of autophagy acting as the convergence points for the signalling pathways for amino acid levels, growth factors including insulin and three distinct glucose level signalling pathways [472]. Although mTORC2 was initially not thought to be involved in the control of autophagy, it has been shown to phosphorylate AKT, a protein which positively regulates mTORC1 activity and thereby supresses autophagy [490].

Under nutrient rich conditions mTORC1 phosphorylates ULK1/2 and ATG13 (both members of the ULK1/2 complex - the mammalian ortholog of the yeast ATG1 complex) [472]. However, under starvation conditions mTOR1 is inactivated and the loss of phosphorylation converts the ULK1/2 complex to its active form leading to its translocation to the autophagosomal membrane where the complex recruits other autophagy related proteins [472].

As discussed previously, some controversy exists as to whether such induction of autophagy is protective or deleterious in the context of MPP^+ toxicity (*Subsection 3.1.6*). However, follow-

ing MPP^+ treatment AKT mediated dephosphorylation of mTOR is observed resulting in the increased initiation of autophagosome formation [357].

5.1.7 NF-κB essential modifier (Nemo)

NF-κB transcription factors mediate cellular responses to external stress, inflammatory stimuli (including tumour necrosis factor-α (TNFα)) and interleukin-1 resulting in either cell survival or apoptosis. Under normal conditions the transcription factors are retained in the cytoplasm by inhibitors of NF-κB (IκBs). However, following external stimuli the IκBs are phosphorylated by the IκB kinase (IKK) complex targeting them for proteasomal degradation and leading to nuclear translocation of NF-κB [468]. Upon nuclear translocation the NF-κB transcription factors bind as dimers to κB sites in gene promoters and enhancers leading to increased transcription of target genes [468]. The IKK complex is made up of the catalytic subunits IKKα and IKKβ and multiple copies of the regulatory subunit, NF-κB essential modifier (Nemo) [468]. Activation of the IKK complex typically depends upon the ubiquitination of Nemo, allowing interactions between the complex and proteins containing ubiquitin binding domains [468].

Inflammation is thought to play a role in PD pathology and NFκB activation has been demonstrated in brain samples from PD patients, MPTP treated mice and primates and some MPP^+ *in vitro* models [491, 492]. In the SH-EP1 cell line NFκB activation partially mediates neurotoxin induced cell death via JNK activation [493].

Further, by preventing the activation of NFκB, MPTP induced neurodegeneration can be rescued in mouse and primate models [491]. However, in SH-SY5Y cells NFκB activation following MPP^+ treatment is pro-survival and in MN9D cells no activation is observed following MPP^+ treatment [493, 494]. Muller-Rischart *et al.* showed that parkin induces ubiquitination of Nemo resulting in increased expression of the mitochondrial protein OPA1 (optic atrophy 1), known to promote mitochondrial fusion, and thereby a protection from stress induced cell death [495]. The authors suggested that parkin has an adaptive role, activating an NFκB mediated pro-survival response in cases of moderate stress and mitophagy in instances of more severe mitochondrial stress [495].

5.1.8 P53

P53 is a key tumour suppressor gene and is widely mutated in tumours. The protein acts as a transcription factor and controls cell division or can activate apoptosis [496]. Under basal conditions proteins including MDM2 (E3 ubiquitin-protein ligase MDM2) negatively regulate

P53, promoting its degradation, blocking the protein's transcriptional activity and promoting the export of P53 from the nucleus [496]. Upon DNA damage P53 and MDM2 are both phosphorylated by ATM (ataxia telangiectasia mutated) preventing their interaction and activating P53. This leads to the translocation of P53 to the nucleus and the increased transcription of apoptotic proteins, including BAX and caspase-3 [496, 497].

P53 activation has been demonstrated in the context of MPP^+ toxicity and it is thought that ROS leads to the oxidation of nuclear DNA. It has further been shown that the effects of MPP^+ are ablated in P53 KO models [480]. P53 inhibitors protect MPTP treated mice from neurodegeneration and co-treatment of MPP^+ treated PC12 cells with P53 inhibitors decreases both BAX transcription and apoptotic cell death [498]. In a microarray study of PC12 cells, MPP^+ treatment led to increased transcription of the P53 regulated gene Ephrin A1 [306].

A number of PD related genes have been linked to P53 [499]. Parkin represses the transcriptional activity of P53 and protects cells from the caspase-3 mediated cell death induced by the neurotoxin 6-OHDA, an effect which is abrogated when mutant parkin is expressed [500]. The cyto-protective effects of DJ1 have also been linked to the repression of P53 transcriptional activity. OE of DJ1 results in decreased BAX expression and decreased caspase activation with the opposite results seen following KD [501]. The relationship between α-synuclein and P53 is somewhat more complex. Although α-synuclein OE models are generally toxic, it has been suggested that the protein has an anti-apoptotic activity through the negative regulation of P53 [502]. The interaction of P53 and α-synuclein has been explored *in vivo* and the motor-neurones of A53T-α-synuclein transgenic mice stain positively for P53 in a manner consistent with observed cell death, P53 also localises with the outer mitochondrial membrane in affected cells [503].

The involvement of P53 in both neurotoxin and genetic models of PD has even led to the suggestion that P53 may unify genetic and sporadic cases of PD by a single mechanism [504].

5.1.9 P62

P62 acts as an adaptor targeting ubiquitinated molecules for degradation by autophagy through interaction with ATG8 homologs (LC3 and GABARAP proteins) [352]. The colocalisation of P62 with autophagosomes is increased following treatment with MPP^+ [505].

P62 also plays a key role in the aggregation of ubiquitinated proteins where autophagy is impeded [352]. Komatsu *et al.* demonstrated that ablation of P62 prevented aggregate formation and the authors suggested that accumulation of P62 might, in itself, be deleterious [506]. However, LB

also contain considerable P62 which is thought to play a critical role in protective α-synuclein aggregation [507]. Where cells are treated with exogenous α-synuclein, P62 is required for the autophagic degradation of the inclusions formed [173].

Through its roles in aggregation and cargo targeting, P62 is essential for PINK1/parkin mediated mitophagy. Following mitochondrial depolarisation PINK1 recruits parkin to the damaged mitochondria where P62 in turn mediates the formation of polyubiquitinated chains - including the ubiquitination of VDAC1. Ubiquitination allows P62 binding, mitochondrial aggregation and targeting for autophagic degradation [180].

However, where autophagy is inhibited cytosolic levels of P62 are increased hindering the proteasomal breakdown of ubiquitinated molecules, by delaying their delivery to the proteasome and leading to their accumulation [508]. P53 is one such proteasomal substrate and its P62 dependent accumulation, following the inhibition of autophagy, may partially explain the deleterious effects of dimished autophagic flux [508].

The roles of P62 extend beyond the realm of autophagy and Moscat *et al.* have described, 'P62 at the crossroads of autophagy, apoptosis, and cancer' [509]. P62 is thought to mediate NFκB activation upstream of interleukin 1. Further, P62 in intracellular speckles interacts with TRAF6 and caspase-8 resulting in activation of NFκB or apoptosis respectively [509]. Thereby, P62 may determine whether cells undergo protective NFκB mediated responses or apoptosis following cellular stress. The accumulation of P62 also promotes tumorigenesis possibly mediated by increased ROS levels [510].

5.1.10 PPP2R2B

Protein phosphatase 2A (PP2A) is a highly conserved protein which acts to antagonise kinases and thereby regulate many cellular functions [511]. The protein is made up of three subunits: the ubiquitous catalytic and scaffold subunits and a variable regulatory subunit [511]. The regulatory subunit controls substrate specificity and subcellular localisation and there are 12 mammalian genes encoding variants of the protein [511]. The main neuronal regulatory subunit is encoded by the gene PPP2R2B which has two splice isoforms Bβ1 and Bβ2 [512]. Expansions of the CAG repeat in a non-coding portion of PPP2R2B lead to the neurodegenerative disease spinocerebellar ataxia type 12 (SCA12) and it is thought that this may occur via changes in the ratio of the two splice isoforms [513].

Of particular relevance to PD, PP2A is a key regulator of tau phosphorylation. The phosphatase dephosphorylates the protein with variable efficiency at the different sites and additionally PP2A

acts as an inhibitor of GSK-3β [514]. PP2A is also an important determinant of α-synuclein phosphorylation status and increased PP2A activity results in decreased α-synuclein aggregation and neurotoxicity [515]. However, aggregated α-synuclein increases the phosphoinhibition of PP2A resulting in further α-synuclein phosphorylation such that the pattern of phosphorylation and aggregation could be self-sustaining [489].

The two isoforms have different subcellular localisation, Bβ1 is primarily cytosolic whereas Bβ2 localises to the mitochondria [512, 516]. Bβ2 promotes apoptosis via mitochondrial fragmentation (via dephosphorylation of DRP1), increased ROS production and upregulation of mitophagy, particularly upon cellular stress (including rotenone treatment) [512, 513, 516]. However, partial rescue was achieved by inhibition of autophagy in PC12 cells OE Bβ2 [516].

5.1.11 Aims of chapter

Having characterised the MPP^+ model of PD in the BE(2)-M17 cell line (*Chapter 3*) a series of PPIN were built to model *in vitro* MPP^+ (*Chapter 4*). Analysis of these PPIN resulted in two lists of protein targets (**target lists one and two** (*Table 4.23*)). The key goal of this chapter was to validate *in silico* predictions *in vitro*. This task was divided into the following steps:

1. Modulation of the members of **target list one** (GBRL2, P62, GBRL1, GABARAP) via KD and OE.
2. Investigation of effects of modulation of the members of **target list one** on cellular viability and MPP^+ vulnerability.
3. KD of members of **target list two** (GBRL2, 14-3-3ζ, P53, LC3B, P62, α-synuclein, Nemo, mTOR, GBRL1, calmodulin, PPP2R2B).
4. Investigation of the effects of KD of members of **target list two** on cellular viability and MPP^+ vulnerability.
5. Study into the mechanisms of any neuroprotective effects.

KD was prioritised to model node deletion, KD is also more analogous to the effects that might be achieved via pharmacological interventions. However, OE was also tested for the members of the shorter **target list one**.

5.2 Results

5.2.1 Expression levels of target list one following MPP^+ treatment and KD

The previous microarray analysis (*Subsection 3.2.5*) was used to measure transcript levels corresponding to the members of **target list one** (*Figure 5.2*). There were no differences in transcript levels of any of the proteins following MPP^+ treatment. The microarray data suggested very low levels of the GBRL1 transcript.

Given the poor correlation between transcript and protein expression levels [517], protein levels were measured by WB (*Figure 5.3*). Endogenous levels of GBRL2 protein were too low to detect by WB, despite good antibody reactivity with transfected protein (*Figure 5.6*). The other three targets were detected by WB, no change to protein levels was seen following exposure to MPP^+. A second band corresponding to lipidated form GABARAP was detected; GABARAP-II corresponds to the autophagosomal form of the protein and is analogous to LC3B-II. However, in contrast to LC3B (*Figure 3.14*) there was no change in the ratio of GABARAP-II/GABARAP-I following MPP^+ treatment. Given that the GABARAP-II/GABARAP-I ratio was unaffected by MPP^+ treatment and the GABARAP-II band was faint, further WB were run without resolving the two bands.

Having confirmed endogenous expression of P62 and GABARAP, with protein levels unaffected by neurotoxin exposure, siRNA mediated KD was validated. KD was confirmed by WB with an average decrease in protein levels of 81% and 86% for P62 and GABARAP respectively. GBRL1 and GBRL2 KD was not attempted due to the low endogenous levels of these proteins.

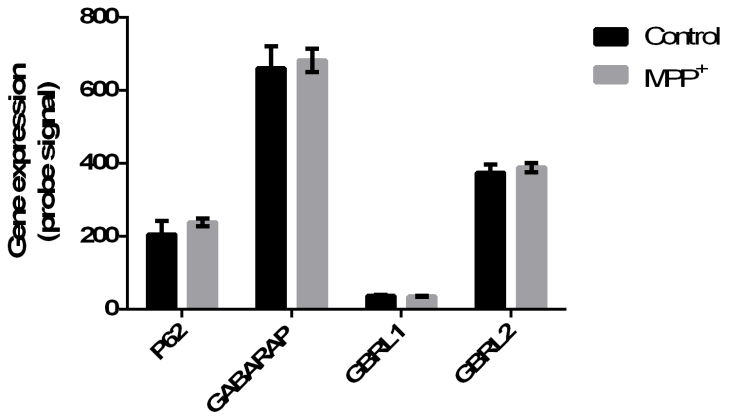

Figure 5.2: **mRNA levels of target list one are not affected by MPP^+ treatment.** Cells were treated with MPP^+ (100 μM) for 24 h. RNA was extracted and analysed using Human Gene 2.0 ST Arrays. Bars represent means ± SEM (n=3).

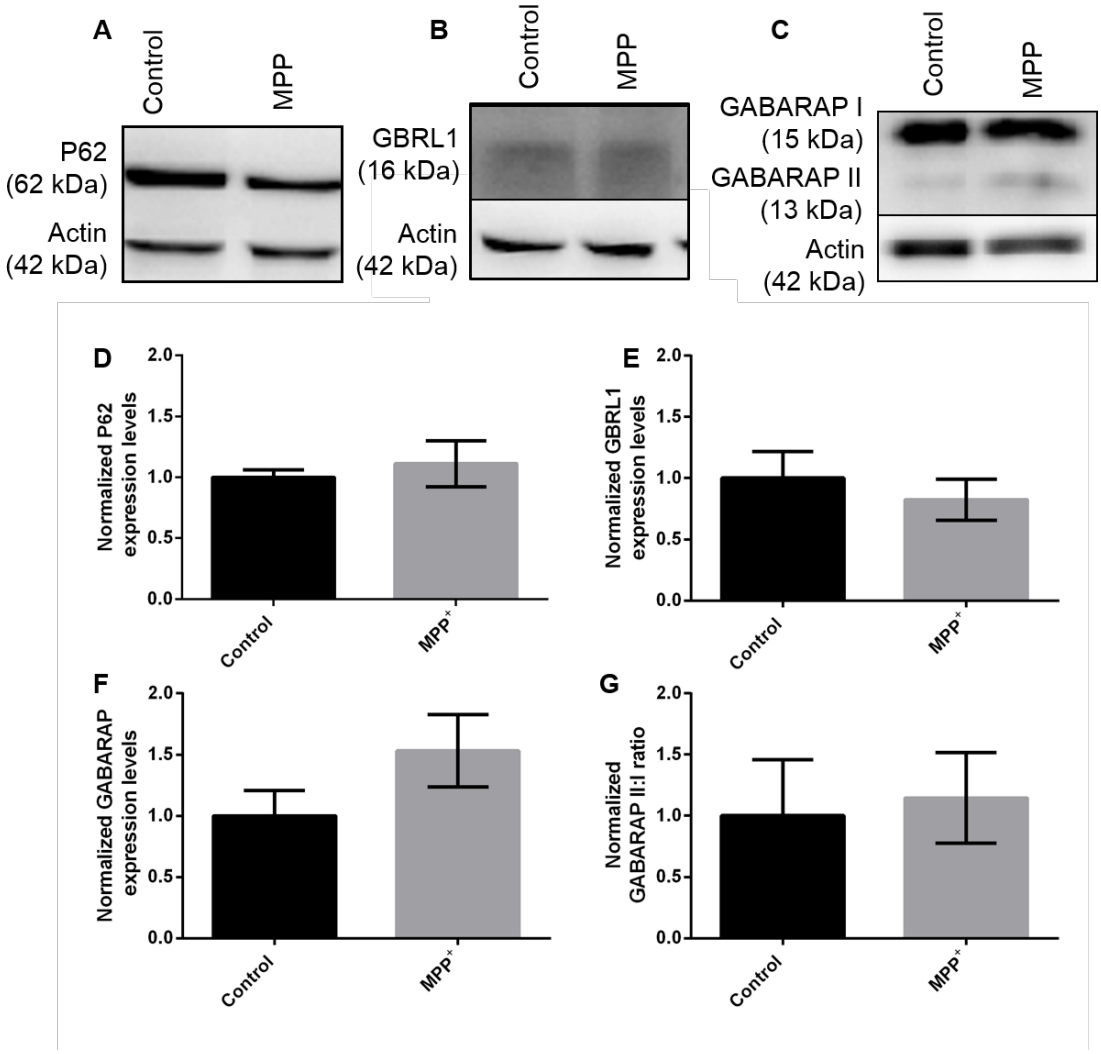

Figure 5.3: **Protein levels of target list one are not affected by MPP$^+$ treatment.** Cells were treated with MPP$^+$ for 48 h, protein levels measured by WB (**A** to **C**) and band density normalised relative to actin loading controls (**D** to **G**). Bars represent means ± SEM (n=3). Data were analysed using t tests.

5.2.2 Overexpression of target list one

Having achieved KD of the proteins expressed endogenously the OE of all four targets was optimised using previously validated expression constructs. Constructs were obtained, expressed in *E.coli*, purified and restrictions digests used to confirm plasmid identity and purity (*Figure 5.5*).

Cells were transfected with the purified plasmids and expression confirmed by WB and fluorescence microscopy for the EGFP fused GABARAP subfamily proteins (*Figure 5.6*). WB confirmed successful expression of the expression constructs. The transfected P62 was fused to an HA tag which led to little change in molecular mass and therefore the native and transfected proteins were not separated by WB (*Figure 5.6A*). In contrast, the GABARAP subfamily pro-

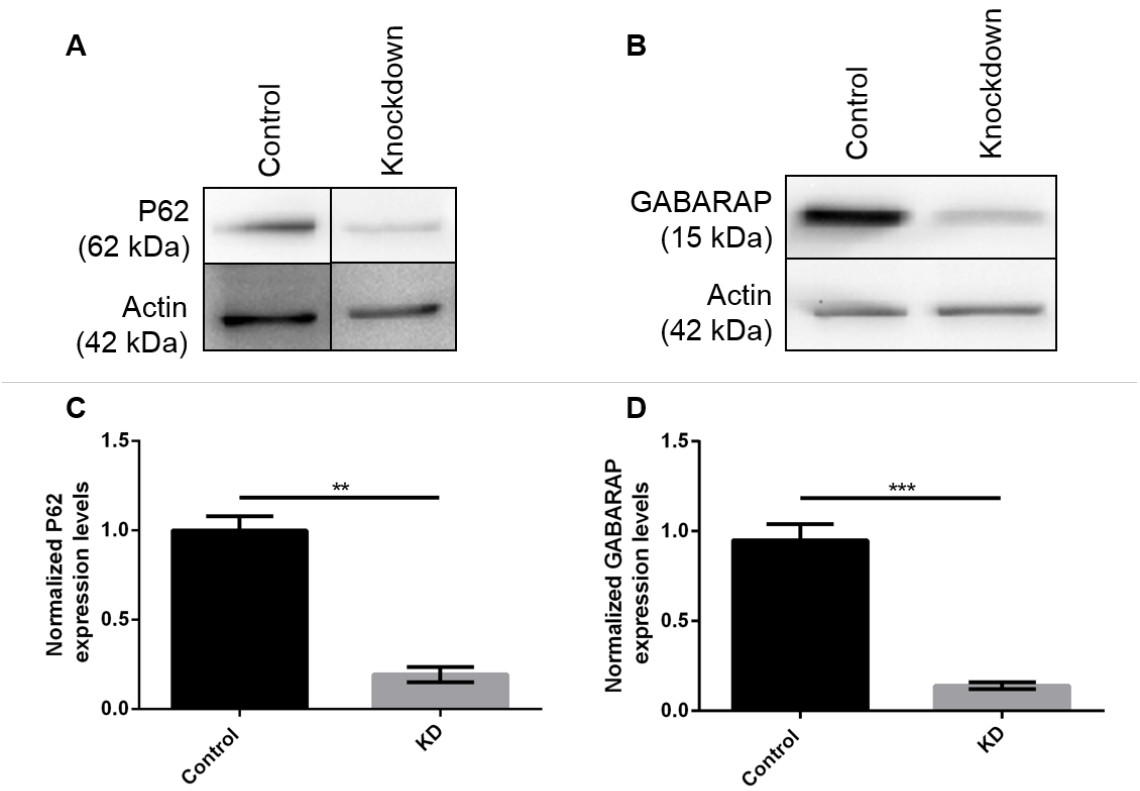

Figure 5.4: **GABARAP and P62 knockdown can be achieved using siRNA.** Cells were lipofected with appropriate siRNAs (50 nM); control cells were treated with a non-targeting siRNA. Cells were harvested 72 h after transfection and protein levels measured by WB (**A** and **B**) and band density normalised relative to actin load controls (**C** and **D**). Bars represent means ± SEM (n=3). Data were analysed using t tests, ** represents P≤0.01 and *** represents P≤0.001.

teins were fused to EGFP which led to a significant increase in molecular mass (*Figure 5.6B*). Some cross reactivity was observed between the GABARAP subfamily antibodies as has been previously reported [518]. Live-cell fluorescence microscopy confirmed expression of the fusion constructs when transfected individually (*Figure 5.6D-F*) or in concert (*Figure 5.6G*). It should be noted that only 20-30% cells were successfully transfected. There was no difference to the number of transfected cells when the three GABARAP proteins were overexpressed individually or simultaneously (*Figure 5.6G* and *H*).

5.2.3 Effect of modulation of target list one on vulnerability to MPP^+

Having optimised KD and OE of **target list one** the effects of protein modulation on cellular viability and MPP^+ vulnerability were explored. The cytotoxicity of MPP^+ was followed using TMRM fluorescence to measure mitochondrial membrane depolarisation, neutral red absorption as a marker of cellular ATP and cell counts to assess cell death. As noted in *Chapter 3* all three assays indicated significantly decreased cellular viability following MPP^+ exposure.

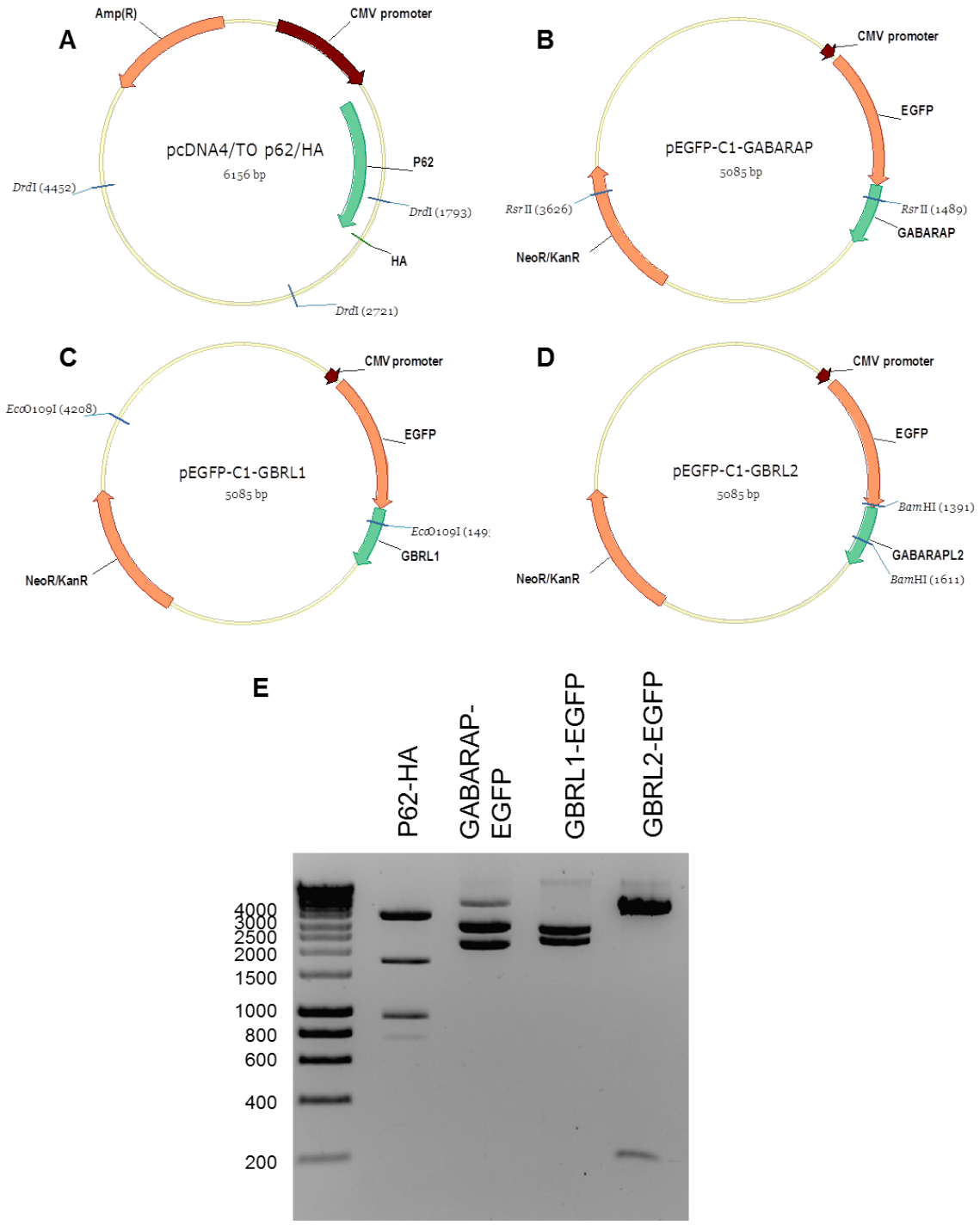

Figure 5.5: **Overexpression constructs corresponding to target list one were purified.** Vector maps of plasmids used to express P62-HA (**A**), EGFP-GABARAP (**B**), EGFP-GBRL1 (**C**) and EGFP-GBRL2 (**D**). **E** Gels following maxipreps and digestion with relevant enzymes to confirm plasmid identity. Restriction enzymes used and expected fragments: P62-HA: DrdI (921, 1731, 3497), EGFP-GABARAP: RsrII (2137, 2948), EGFP-GBRL1:Eco01091 (2713, 2372), EGFP-GBRL2: BamHI (220, 4865).

Following GABARAP and P62 KD no change was seen in TMRM fluorescence, neutral red absorption or cell counts in either the absence or presence of the neurotoxin MPP^+ (*Figure 5.7A*, *C* and *E*). However, when the two proteins were simultaneously KD decreased neutral red absorbance was observed in both the absence (89% control) and presence of MPP^+ (39% control compared to 63% without KD) (*Figure 5.7D*). Further, decreased cell counts (31% control

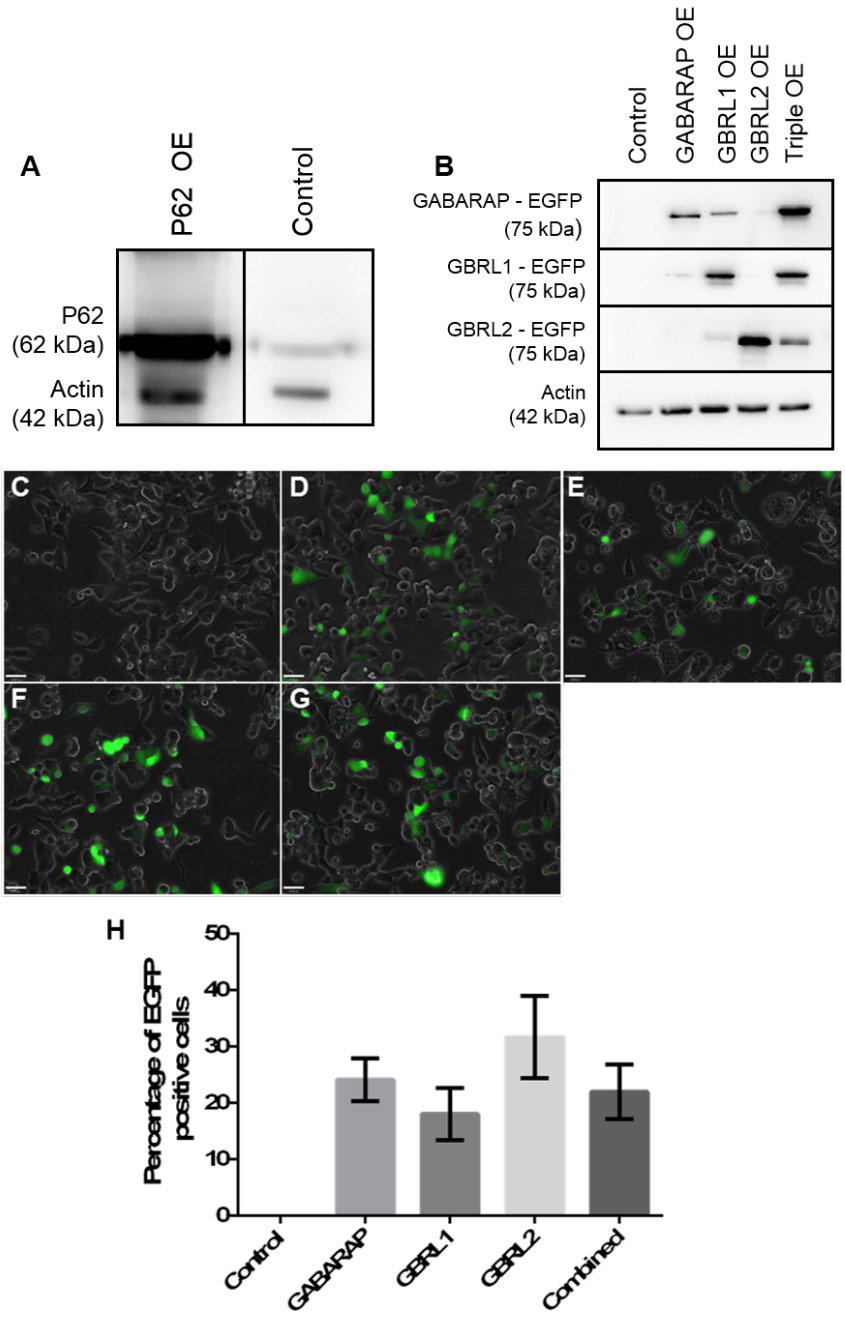

Figure 5.6: **Target list one proteins can be overexpressed *in vitro*** Cells were lipofected using 1.5 μg of plasmid DNA and 48 h after transfection cells were harvested for WB (**A** and **B**) or imaged using fluorescence microscopy (**C** to **G**). **A** OE of HA-P62 with actin loading control. **B** OE of GABARAP-EGFP, GBRL1-EGFP, GBRL2-EGFP or all three plasmids, each sample separately probed with each antibody. **C** to **G** Cells were transfected with control (**C**), GABARAP-EGFP (**D**), GBRL1-EGFP (**E**), GBRL2-EGFP (**F**) or combination of the three GABARAP constructs (**G**), cells are viewed at 20 x magnification (scale bars represent 70 μm) using appropriate filter to detect EGFP fluorescence. **H** the number of EGFP cells was counted to estimate transfection efficiency. Bars represent means ± SEM (n=3).

compared to 50% without KD) were seen following MPP^+ exposure (*Figure 5.7F*). These results indicated that the combined KD potentiated MPP^+ cytotoxicity. However, there was no change in TMRM fluorescence in either untreated or MPP^+ treated cells (*Figure 5.7B*).

Having determined that combined KD of **target list one** increased cellular vulnerability to

MPP^+, the effects of both single and combined OE were explored. None of the individual OE altered cellular viability in either the absence or presence of MPP^+ as measured by TMRM fluorescence, neutral red absorption or cell counts (*Figure 5.8A*, *C* and *E*). The combined OE had no effect on cellular viability in the absence of MPP^+ and there was no change in TMRM fluorescence following MPP^+ treatment (*Figure 5.8B*). However, the combined OE resulted in a rescue of MPP^+ induced neurotoxicity as measured by the neutral red assay and cell counts. Neutral red absorption was increased to 78% of control cells, compared to 56% without the OE (*Figure 5.8D*). In a similar fashion, cell counts were increased to 103% of control cells, compared to 67% without OE (*Figure 5.8F*).

Following the observation of a protective effect, the minimal effective OE set was determined. Each possible pair and triple of **target list one** was OE in concert and cellular vulnerability to MPP^+ measured (*Figure 5.9*). No rescue was observed in any of the combinations not containing P62. Additionally the combination of P62 and either GABARAP or GBRL2 was ineffective. However, P62 in combination with GBRL1 or any two member of the GABARAP subfamily resulted in protection from MPP^+ induced neurotoxicity. This suggested redundancy within the GABARAP subfamily, but also confirmed the need for multiple interventions.

5.2.4 An autophagic mechanism of protection for target list one

Given that each of the members of **target list one** has a role in autophagy (*Subsections 5.1.9* and *5.1.4*) and MPP^+ treatment was previously shown to decrease the rate of protein degradation (*Subsection 3.2.3*) it was hypothesised that the observed protective effect occurred via an autophagic mechanism.

LC3B lipidation was measured by WB following the protective combined OE in the absence and presence of MPP^+ (*Figure 5.10A*). Although MPP^+ treatment resulted in increased lipidation (as previously reported in *Subsection 3.2.3*) there was no difference in lipidation following the combined OE of **target list one** (*Figure 5.10B*).

The radio-label pulse-chase assay optimised in *Subsection 3.2.3* was used to measure the rate of protein degradation following the OE with a GFP expressing plasmid (pHGCX) used as a control plasmid to account for the effect of exogenous DNA on autophagy (*Figure 5.10C*). Although MPP^+ treatment resulted in decreased autophagic flux there was no difference following transfection with either the combination of **target list one** or the control plasmid.

ICC was then used to gain a better understanding of the effect of the combined OE on autophagy. Prior to investigation of autophagy following OE of **target list one**, the identification of LC3B

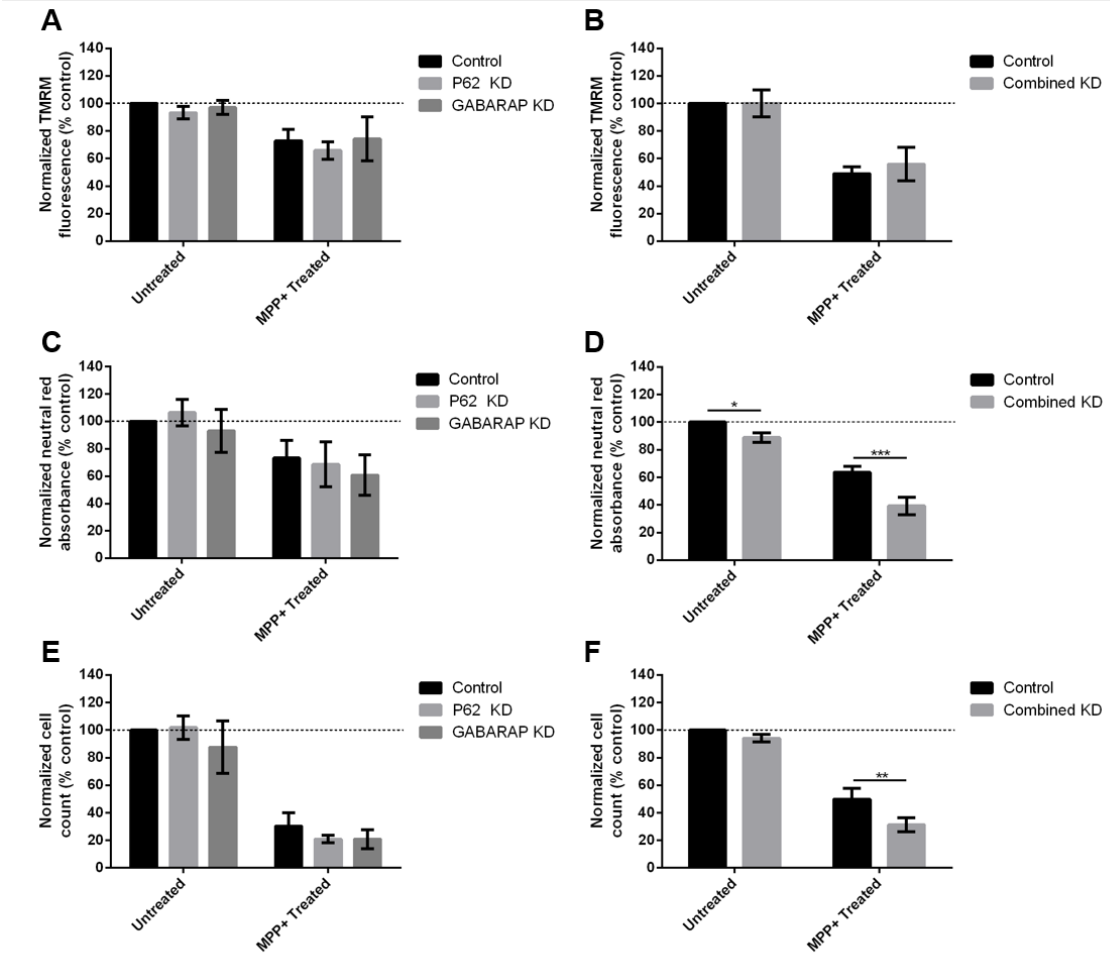

Figure 5.7: **Combined KD of target list one potentiates MPP$^+$ toxicity.** Cells were transfected with appropriate siRNAs (50 nM); control cells were treated with a non-targeting siRNA. Combined KD indicates simultaneous P62 and GABARAP KD. Then, 24 h after lipofection, cells were treated with MPP$^+$ (100 μM). **A** and **B** mitochondrial membrane polarisation was measured using via TMRM fluorescence 24 h after MPP$^+$ treatment (average unnormalised control fluorescences were 11246 and 841 RFU for **A** and **B** respectively). **C** and **D** cell viability was estimated using neutral red uptake 36 h after MPP$^+$ treatment (average unnormalised control absorbances were 0.532 and 0.369 for **C** and **D** respectively). **E** and **F** cell death was assessed by counting the number of morphologically normal cells in bright field images 48 h after MPP$^+$ treatment (average unnormalised cell counts were 180 and 130 for **E** and **F** respectively). Bars represent mean ± SEM (n=3), data were analysed using a 2-way ANOVA with Sidak multiple comparison test * represents P $\leq$0.05, ** represents P$\leq$0.01 and *** represents P$\leq$0.001.

and LAMP1 puncta was optimised in control cells (*Figure 5.11*). Although LC3B staining was reasonably diffuse, both LC3B and LAMP1 puncta were detected in control and MPP$^+$ treated cells. Under neither condition could extensive colocalisation be detected by eye and, despite several attempts, automatic puncta identification remained unsuccessful in the M17 cells. Following 36 h MPP$^+$ treatment, significant changes to cellular morphology, consistent with apoptotic cell death, were detected complicating assessment of changes to puncta numbers or staining intensity.

Following transfection, P62 and EGFP positive puncta were identified in some cells. Coverglasses

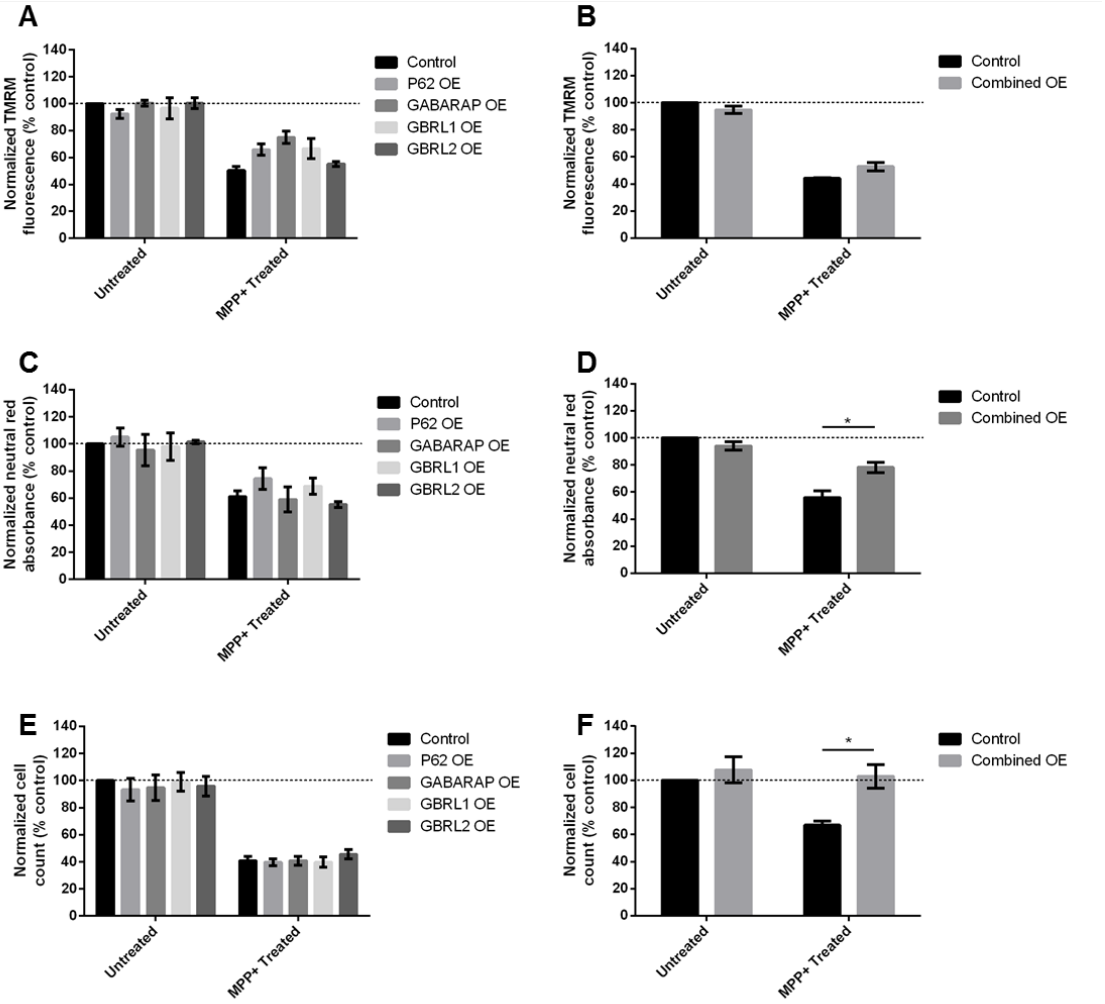

Figure 5.8: **Combined OE of target list one rescues MPP^+ toxicity.** Cells were transfected with DNA (1.5 g); 24 h after transfection cells were treated with MPP^+ (100 μM). Combined OE indicates the combined OE of P62, GABARAP, GBRL1 and GBRL2. **A** and **B** mitochondrial membrane polarisation was measured using via TMRM fluorescence 24 h after MPP^+ treatment (average unnormalised control fluorescences were 6002 and 5985 RFU for **A** and **B** respectively). **C** and **D** cell viability was estimated using neutral red uptake 36 h after MPP^+ treatment (average unnormalised control absorbances were 0.418 and 0.435 for **C** and **D** respectively). **E** and **F** cell death was assessed by counting the number of morphologically normal cells in bright field images 48 h after MPP^+ treatment (average unnormalised cell counts were 173 and 82 for **E** and **F** respectively). Bars represent mean ± SEM (n=3), data were analysed using a 2-way ANOVA with Sidak multiple comparison test * represents P $\leq$0.05 and ** represents P$\leq$0.01.

were costained with antibodies against GABARAP, GBRL1 and GBRL2 to confirm that the EGFP puncta represented the fusion proteins (*Figures 5.12*). In each case, puncta positive for P62, EGFP and the relevant GABARAP subfamily antibody were identified. Background staining was observed when using the GABARAP and GBRL2 antibodies which may have been due to endogenous protein, although native GBRL2 was not detected by WB. Although no P62 staining was seen in non-transfected cells under the microscope settings used to collect images, when exposure time was extended and light intensity increased, the endogenous protein could be detected (results not shown).

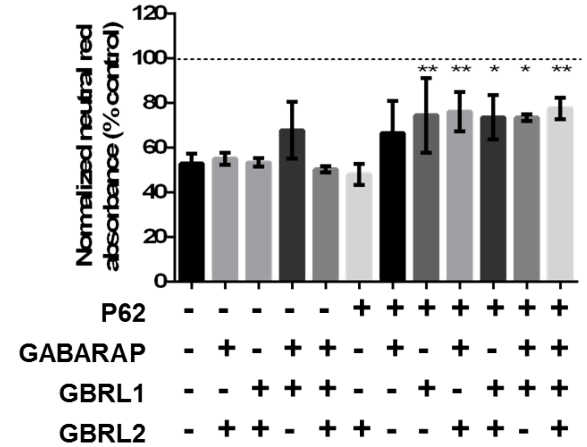

Figure 5.9: **The minimal effective OE set of target list one contains P62 and members of the GABARAP subfamily.** Cells were transfected with of DNA (1.5 g); 24 h after transfection cells were treated with MPP^+ (100 μM) and 36h later cellular viability was estimated using neutral red uptake. A minimal OE set was determined by sequentially testing each pair and triple combination of OE. Bars represent mean ± SEM (n=3), 1-way ANOVA with Dunnett multiple comparison test to MPP^+ control (average unnormalised control absorbance was 0.507), * represents P$\leq$ 0.05, ** represents P$\leq$0.01.

Having confirmed that the EGFP signal mirrored GABARAP subfamily staining, the EGFP signal was used for further puncta identification. The P62/GABARAP subfamily puncta were shown to colocalise with the autophagosomal marker LC3B under both control and MPP^+ treatment conditions indicating the formation of autophagosomes (*Figure 5.13*).

However, the puncta did not colocalise with the mitochondrial protein Tom20 under either control or MPP^+ treatment conditions (*Figure 5.14*), therefore, the images do not provide evidence of mitophagy. The P62/GABARAP subfamily puncta also did not colocalise with LAMP1 puncta under either control or MPP^+ treatment conditions (*Figure 3.5*). The LAMP1 puncta are lysosomes and the fusion of autophagosomes and lysosomes allows for the degradation of the autophagosome's contents. There is no evidence of such fusion between the GABARAP puncta and lysosomes in these ICC experiments.

5.2.5 Expression of target list two following MPP^+ treatment and KD

Following initial success with **target list one**, investigations were extended to the more extensive **target list two** elucidated by the selective BC analysis (*Subsection 4.2.14*). This section of work focussed on the KD of targets as node deletion better replicates the *in silico* analysis. Given that endogenous levels of GBRL1 and GBRL2 were too low for KD (*Subsection 5.2.1*) attention was focussed on the following members of **target list two**: α-synuclein, 14-3-3ζ, calmodulin, LC3B, mTOR, Nemo, P53, P62 and PPP2R2B.

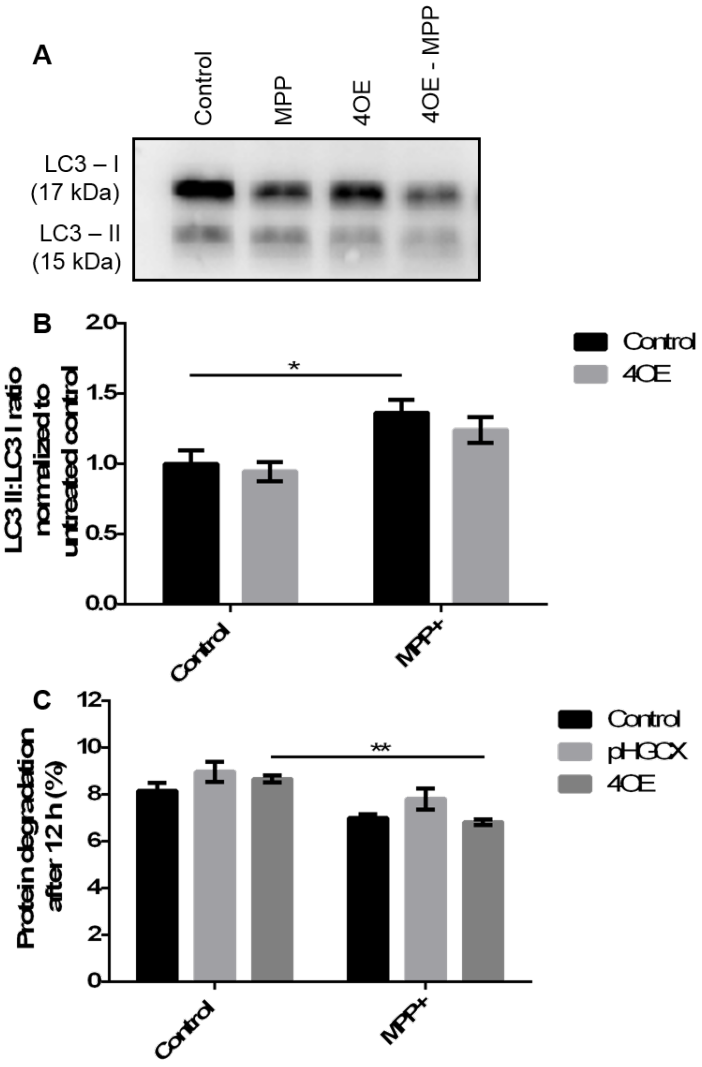

Figure 5.10: **Combined OE of target list one does not affect autophagic flux. A** Cells were transfected with the combined plasmid set and then treated with MPP^+ (100 μM), LC3B lipidation was measured by WB and the ratio of lipidated to unlipidated protein calculated (**B**). **C** Radio-labelled cells were transfected with combined plasmid set or control (pHGCX) plasmid, 24 h post transfection the amount of protein breakdown in a 12 h window was calculated using the pulse-chase assay in both presence and absence of MPP^+ (100 μM). Bars represent mean ± SEM (n=3), data were analysed with 2-way ANOVA with Sidak's multiple comparison test to control, * represents P≤0.05 and ** represents P≤0.01

Again, the microarray data (*Subsection 3.2.5*) were used to measure the levels of transcripts corresponding to each target protein (*Figure 5.16*). There were two order of magnitude differences between the expression levels of the different genes, however, there was no difference in the transcript levels of any of the members of **target list two** following MPP^+ treatment. The human protein calmodulin is encoded for by three distinct genes across three different chromosomes. Therefore, the Affymetrix Human ST 2.0 gene array contains a number of probes and the signal for each of probe is shown in *Figure 5.16B*.

Following optimisation of antibodies, the protein expression level of each member of **target list two** was measured by WB in the absence and presence of MPP^+ (*Figure 5.17*). Very low

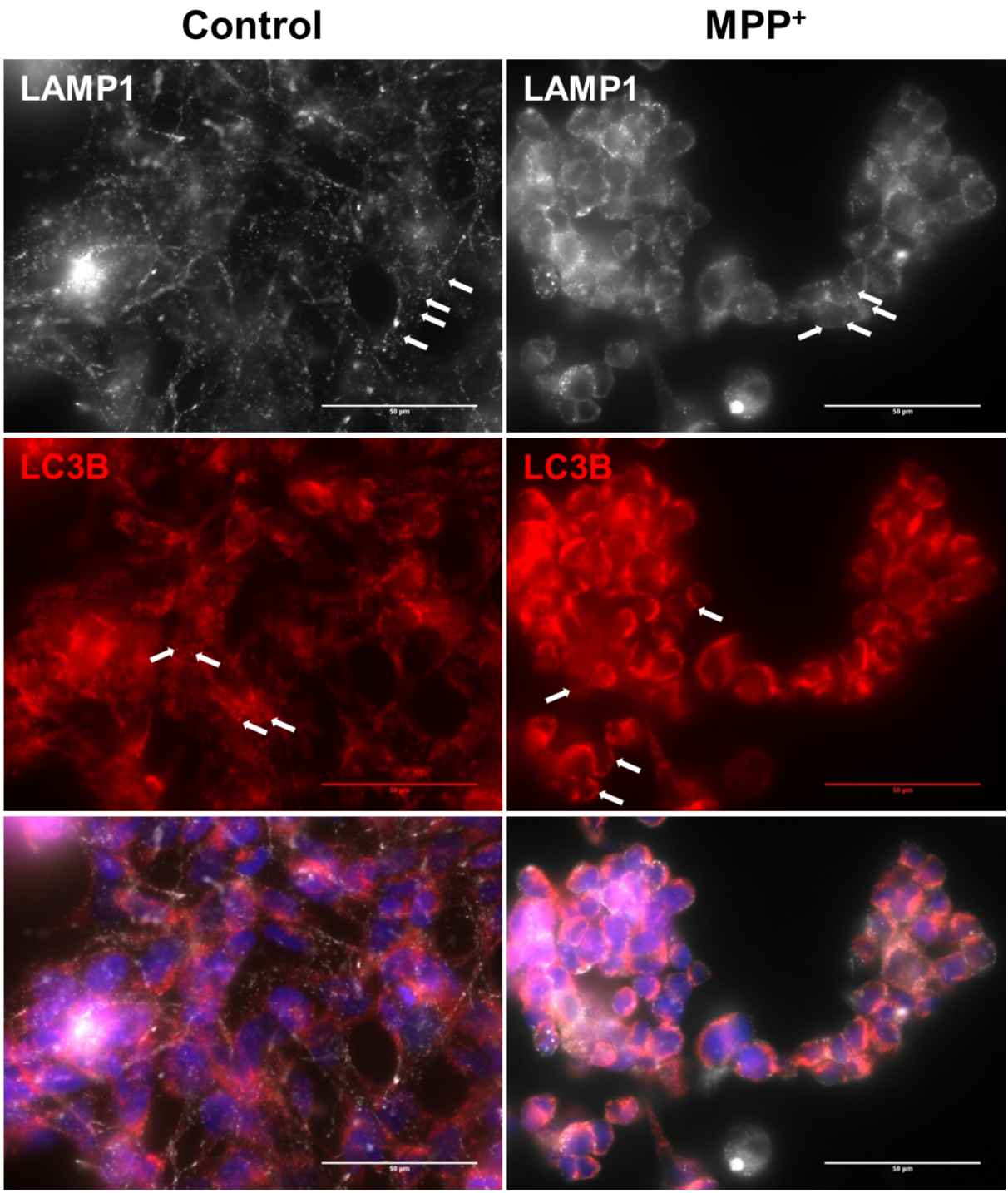

Figure 5.11: **LC3B and LAMP1 puncta can be detected in untransfected cell.** Control and MPP^+ treated (36 h, 100 μM) cells were fixed and immunocytochemistry used to detect LC3B and LAMP1. Cells were imaged at 60 x magnification, scale bar represents 50 μm. Illustrative puncta are shown with arrows.

protein levels of α-synuclein were observed, despite the use of three antibodies and several lysate preparation methods. However, a band was eventually detected with the assistance of a positive control (lysate from brain of *SNCA* overexpressing mouse [121]). There were no changes to protein levels of 14-3-3ζ, LC3B, mTOR, PPP2R2B, α-synuclein or calmodulin following 48 h MPP^+ treatment (*Figure 5.18A*, *B*, *C*, *G*, *H* and *I*). However, the protein levels of P62, P53 and Nemo were significantly decreased at this time point (*Figure 5.18D*, *E* and *F*). Given the role

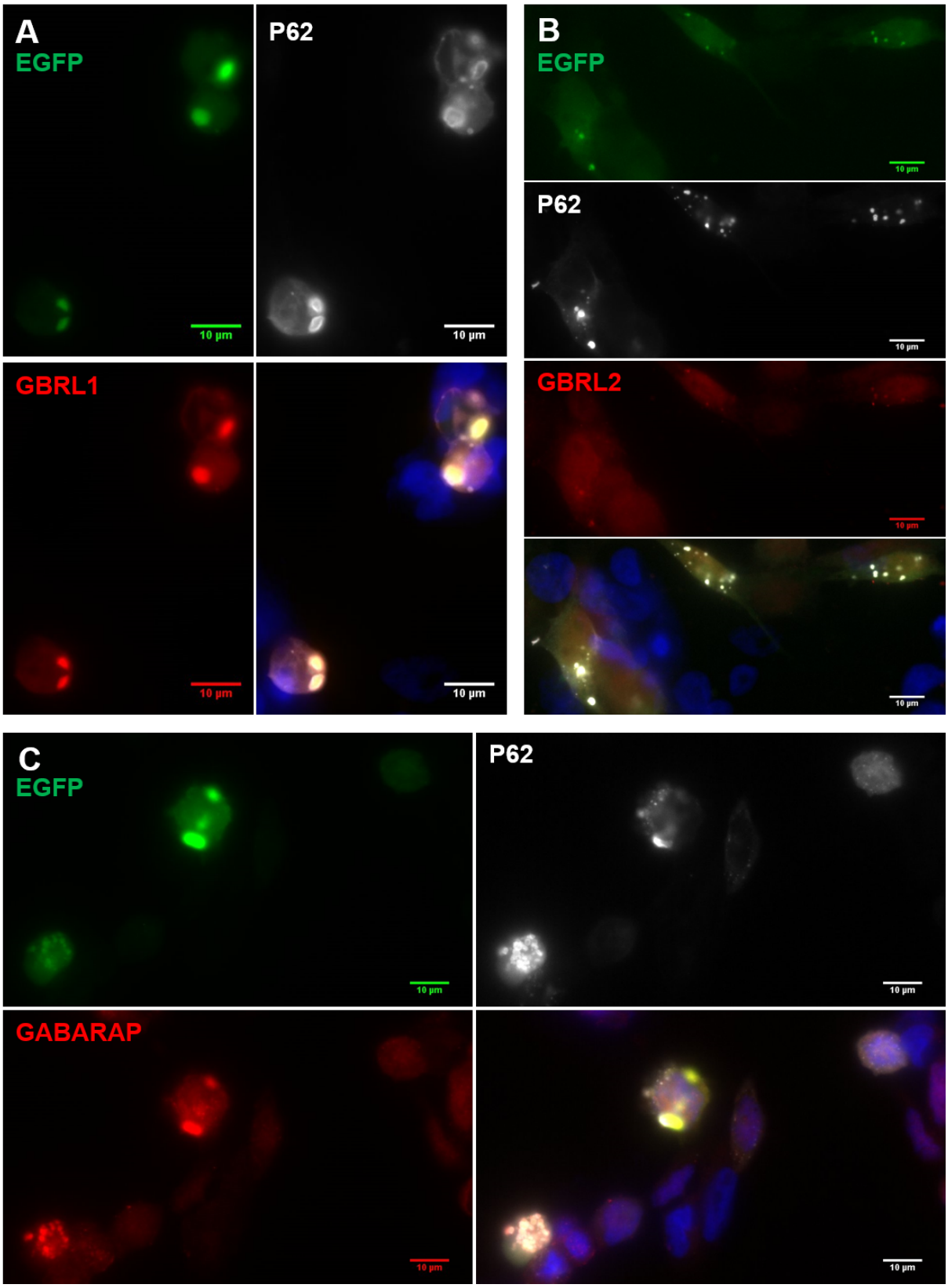

Figure 5.12: **EGFP signal and GABARAP subfamily proteins colocalise.** Cells were transfected with the combined plasmid set and 48 h later cells were fixed and immunocytochemistry used to detect GBRL1 (**A**), GBRL2 (**B**) or GABARAP (**C**) and P62. Cells were imaged at 60 x magnification, scale bar represents 10 μm.

of the proteins in MPP^+ induced cell death (*Subsections 5.1.8* and *5.1.7*), the decreased levels of P53 and Nemo were somewhat unexpected. Therefore, the level of each of the three proteins showing altered expression at 48 h was investigated at earlier timepoints. Following 6, 12, 24 or

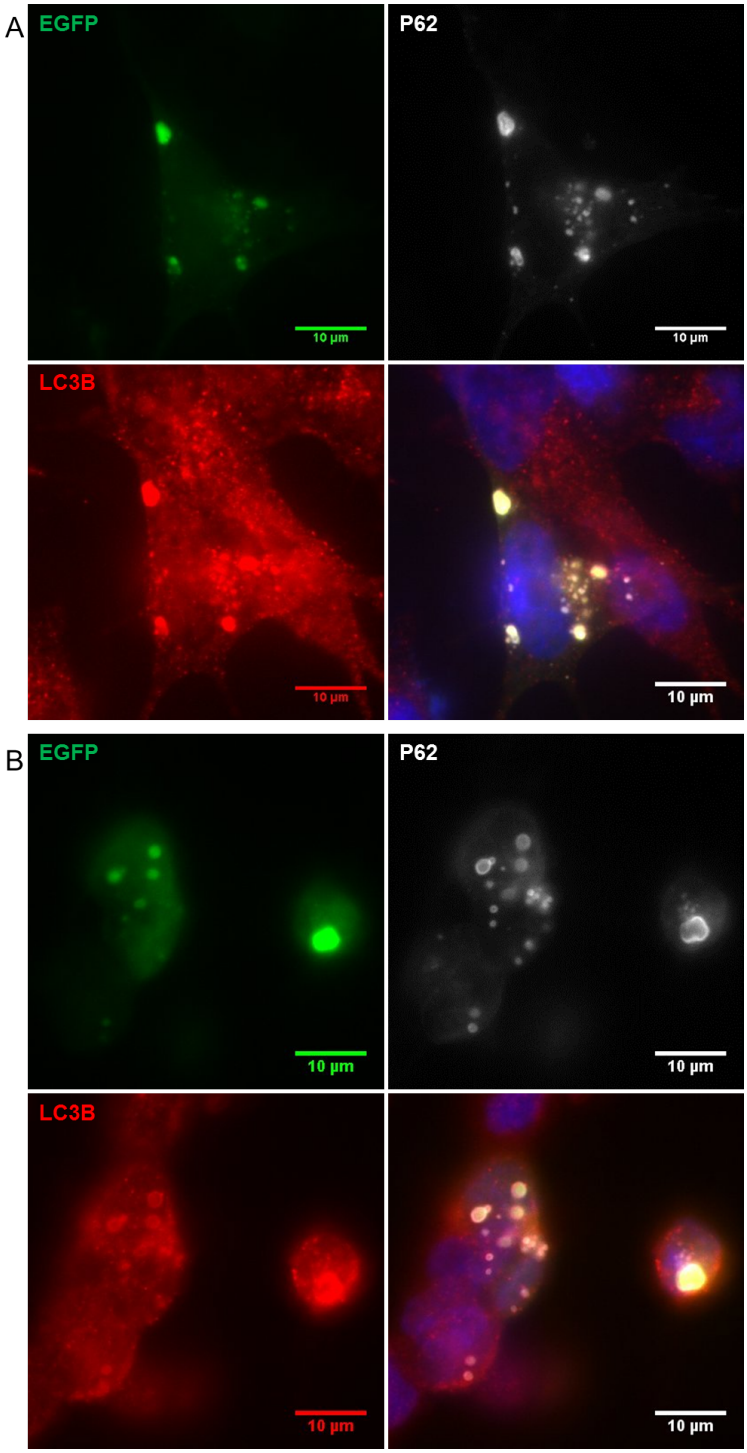

Figure 5.13: **Target list one puncta colocalise with LC3B.** Cells were transfected with the combined plasmid set and 24 h later cells were treated with control media (**A**) or MPP^+ (100 μM) (**B**). After a further 24 h, cells were fixed and immunocytochemistry used to detect P62 and LC3B (EGFP signal was used to detect GABARAP subfamily proteins). Cells were imaged at 60x magnification, scale bar represents 10 μm.

36 h MPP^+ treatment there was no change to the expression level of P62, P53 or Nemo (*Figure 5.19*). However, P53 and P62 expression levels were dependent on culture time.

Having measured protein expression levels, siRNA mediated KD of each member of **target list two** was optimised (*Figure 5.20* and *Figure 5.21*). The following average KD were achieved: 14-3-3ζ - 66%, LC3B - 63%, mTOR - 69%, P62 - 68%, P53 - 77%, Nemo - 53%, PPP2R2B -

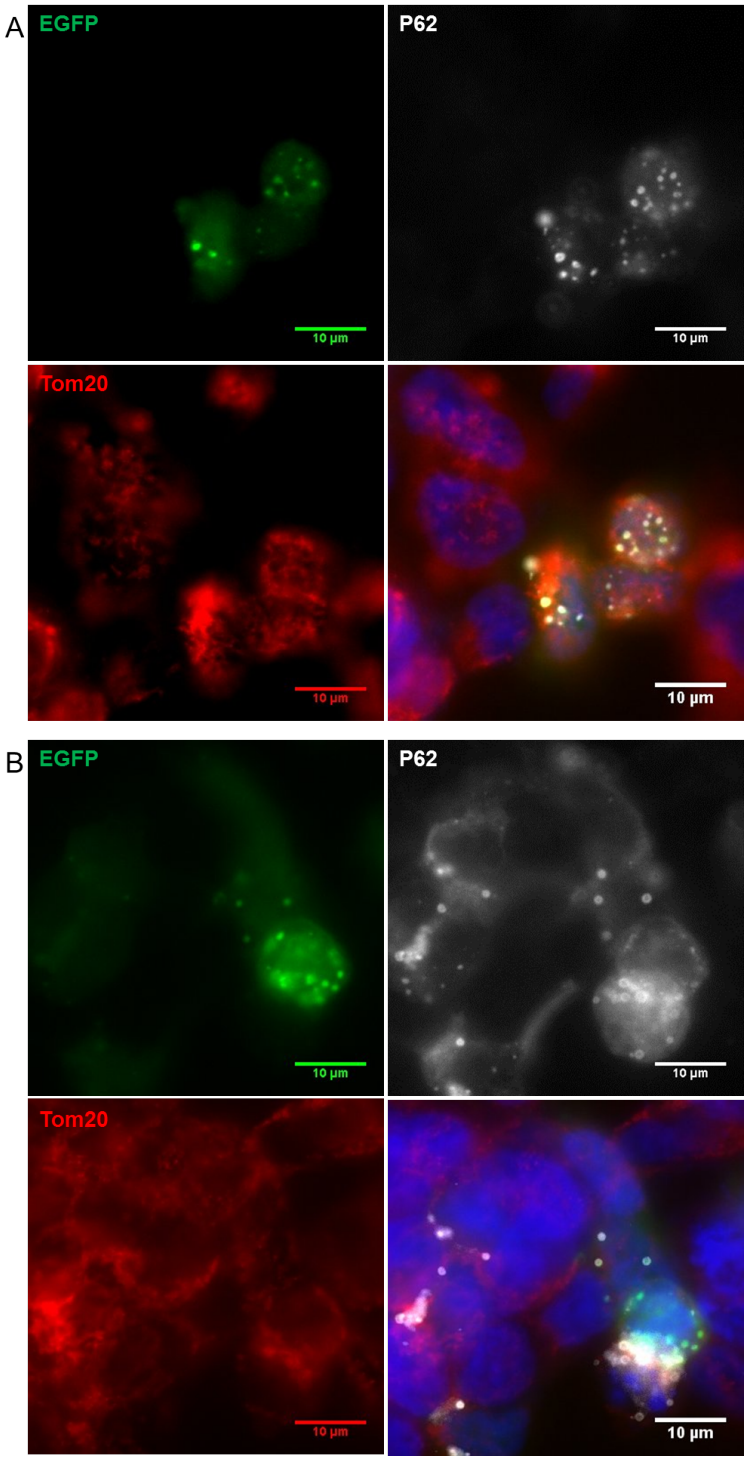

Figure 5.14: **Target list one puncta do not colocalise with Tom20.** Cells were transfected with the combined plasmid set and 24 h later cells were treated with control media (**A**) or MPP^+ (100 μM) (**B**). After a further 24 h, cells were fixed and immunocytochemistry used to detect P62 and Tom20 (EGFP signal was used to detect GABARAP subfamily proteins). Cells were imaged at 60 x magnification, scale bar represents 10 μm.

53%, α-synuclein - 58% and calmodulin - 52%. Calmodulin KD required a pool of three siRNA, one targeting each of the genes.

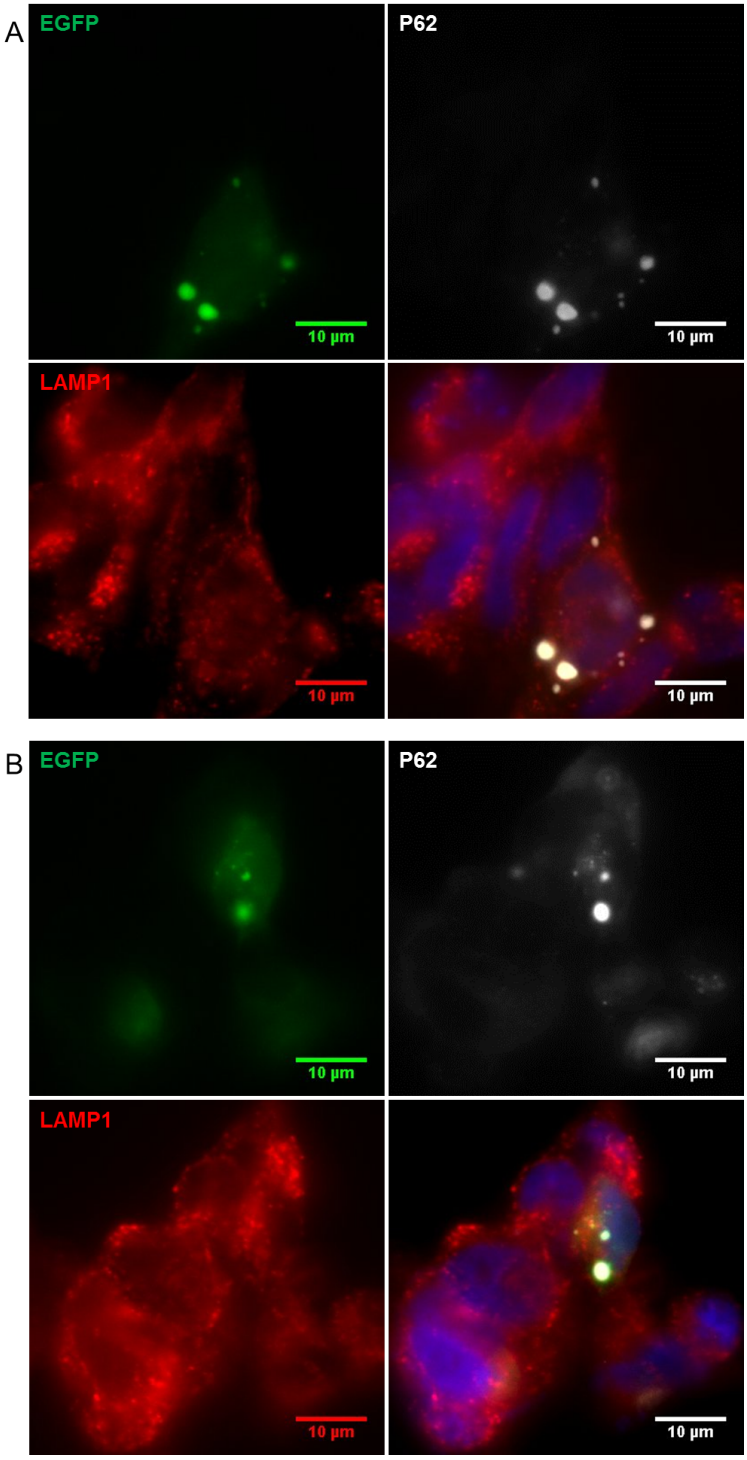

Figure 5.15: **Target list one puncta do not colocalise with LAMP1.** Cells were transfected with the combined plasmid set and 24 h later were treated with control media (**A**) or MPP^+ (100 μM) (**B**). After a further 24 h, cells were fixed and immunocytochemistry used to detect P62 and LAMP1 (EGFP signal was used to detect GABARAP subfamily proteins). Cells were imaged at 60 x magnification, scale bar represents 10 μm.

5.2.6 Effect of knockdown of target list two on cellular viability and autophagy

Having optimised the siRNA mediated KD of **target list two**, the effect of KD on cellular viability was investigated. Given the need for multiple testing corrections, a power calculation

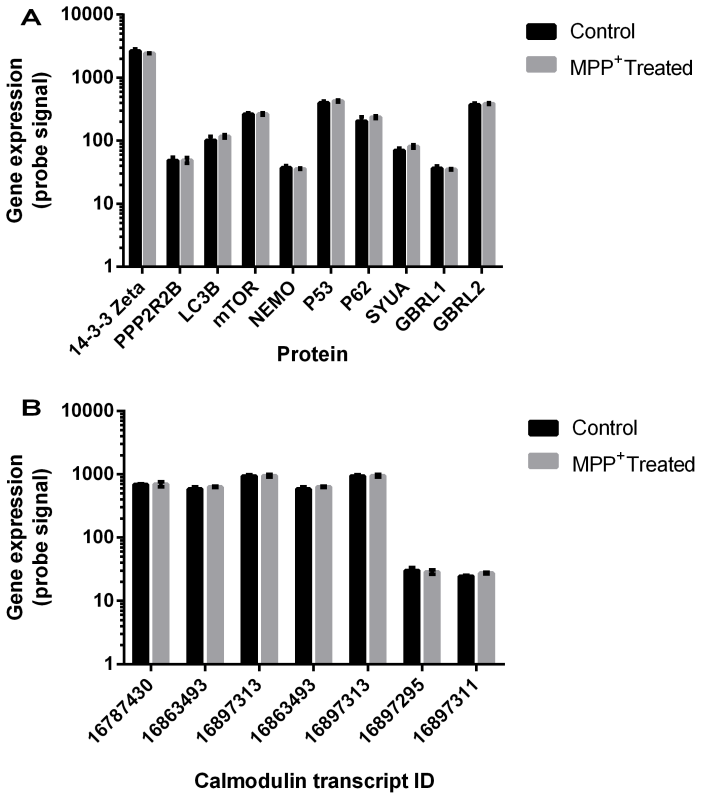

Figure 5.16: **mRNA levels of target list two are not affected by MPP$^+$ treatment.** Cells were treated with MPP$^+$ (100 μM) for 24 h. RNA was extracted and analysed using Human Gene 2.0 ST Arrays. **B:** Calmodulin gene expression based on the seven different probes. Bars represent means ± SEM (n=3).

was performed to determine the number of repeats required to see a medium sized effect with a P value of 0.05 and a power of 0.8. To achieve these parameters, seven independent repeats of each experiment was performed.

Cellular viability was estimated using neutral red absorbance (a measure of cellular ATP), TMRM fluorescence (a measure of mitochondrial membrane depolarisation) and MTT reduction (*Figure 5.22A-C*). The radio-label pulse-chase assay was used to measure the extent of protein degradation in a 12 h window (*Figure 5.22D*). The individual KD of **target list two** did not alter cellular viability as measured by any of the assays. Autophagic flux was decreased following the KD of mTOR (67% control) and P62 (61% control), but no change was seen following the KD of other proteins in **target list two**, including LC3B.

5.2.7 Effect of knockdown target list two on MPP$^+$ vulnerability

The same series of assays was repeated in the presence of MPP$^+$ (*Figure 5.23*). No consistent changes in MPP$^+$ vulnerability were observed following any of the KD of **target list two**. However, high levels of inter-experiment variability in the MTT assay may have hindered the

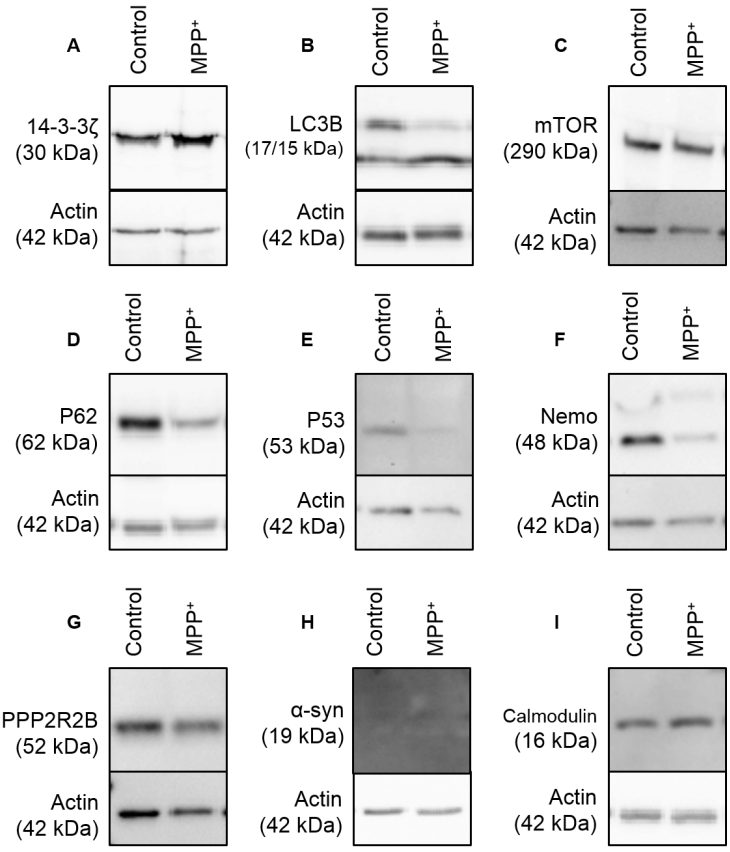

Figure 5.17: **All members of target list two are expressed at protein level in M17 cells.** Cells were treated with MPP^+ (100 μM) for 48 h and protein levels measured by WB.

detection of small effects. Interestingly, and in contrast to the previous figure, no changes to protein degradation were observed in the presence of MPP^+ following any of the KD. As a control, it was confirmed that MPP^+ treatment decreased autophagic flux in combination with transfection with a non-targeting siRNA.

5.2.8 Effect of pairwise knockdown of target list two

Given the earlier success of multiple interventions from **target list one**, the effect of each possible pairwise KD combination of **target list two** was explored in both the absence and presence of MPP^+. Pairwise experiments were performed in a 96-well format, so that each possible combination could be investigated on a single plate. Again, multiple testing corrections were essential and the number of repeats was maximised given both time and cost constraints, resulting in 12 independent experiments for each assay. Calmodulin KD was not used in the pairwise assays due to the need for three distinct siRNAs to effect KD.

The effect of each pairwise KD in both the absence and presence of MPP^+ (100 μM) was measured using the neutral red (*Figure 5.24*), MTT (*Figure 5.25*) and live-cell protease assays (*Figure 5.26*). In the absence of KD (non-targeting siRNA) the following average viabilities

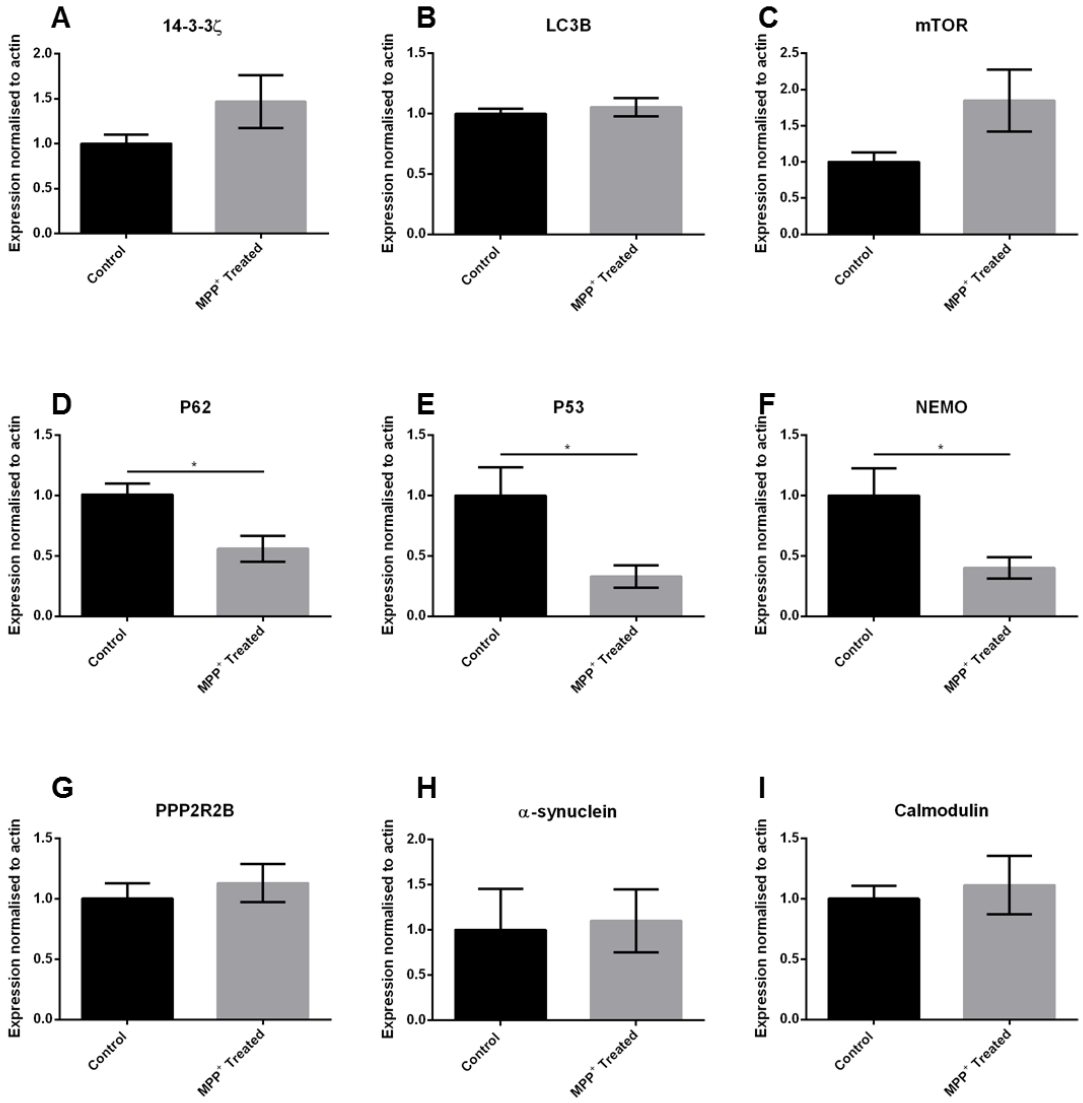

Figure 5.18: **P62, P53 and Nemo protein levels are decreased following 48 h MPP$^+$ treatment, other target list two members are unaltered.** Cells were treated with MPP$^+$ for 48 h and protein levels measured by WB. Band density normalised relative to actin loading controls. Bars represent means ± SEM (n=3). Data were analysed using t tests, * represents P≤0.05.

were seen after MPP$^+$ treatment: neutral red - 40%, MTT - 35%, live-cell protease activity - 74%. Following corrections for multiple testing, no significant effect was seen following any of the pairs of **target list two** KD under either control or MPP$^+$ conditions. Further, when the data from all pairwise KD were grouped there was no difference to average MPP$^+$ vulnerability between KDs and controls (non-targeting siRNA).

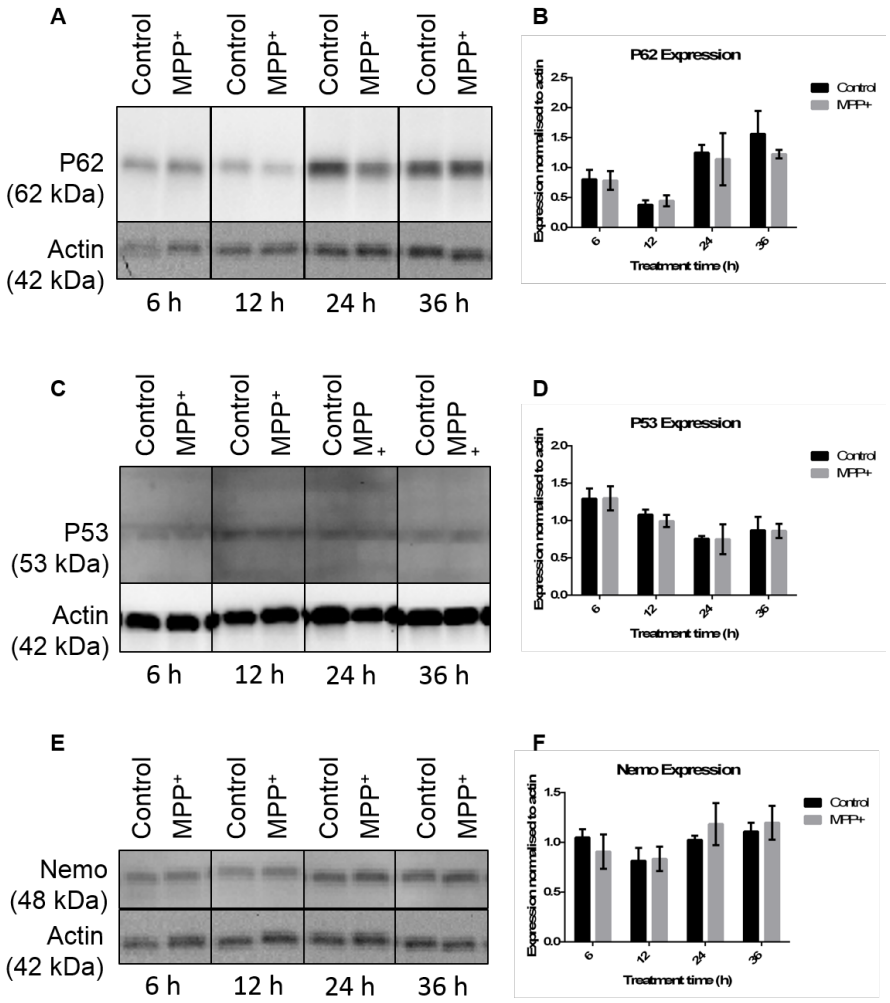

Figure 5.19: **P62, P53 and Nemo expression is unaltered following 6-36 h MPP$^+$ exposure.** Cells were treated with MPP$^+$ (100 μM) for 6-36 h and protein levels measured by WB. Band density normalised relative to actin loading controls. Bars represent means ± SEM (n=3). Data were analysed using a 2-way ANOVA with Sidak multiple comparison test for each time point.

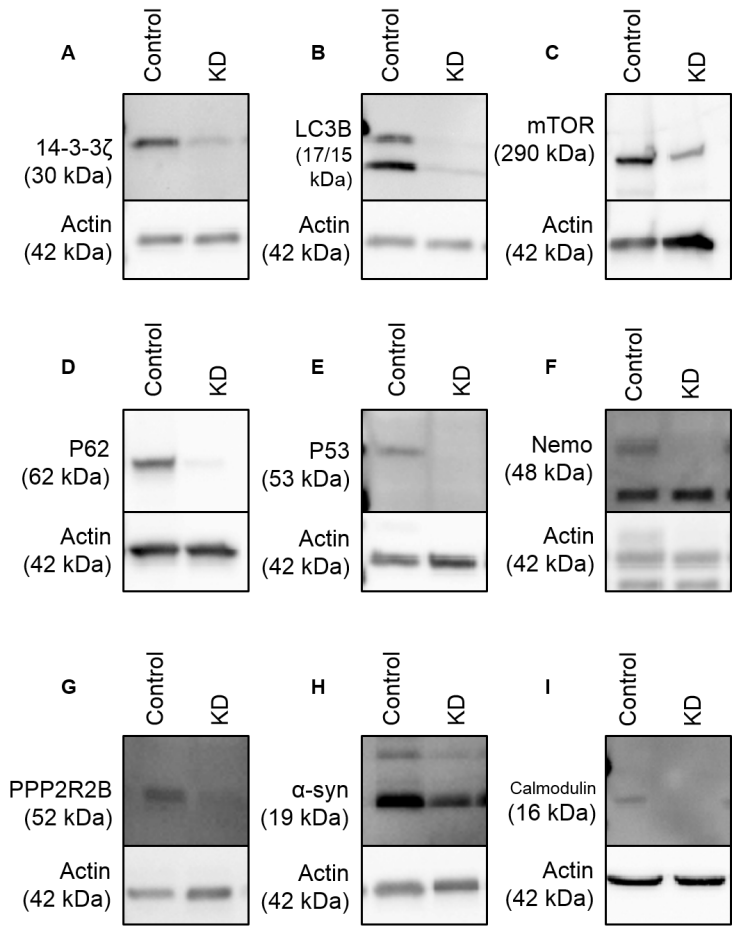

Figure 5.20: **Target list two KD can be achieved using siRNA.** Cells were transfected with appropriate siRNAs (50 or 100 nM) and protein levels assessed by WB 48 h later.

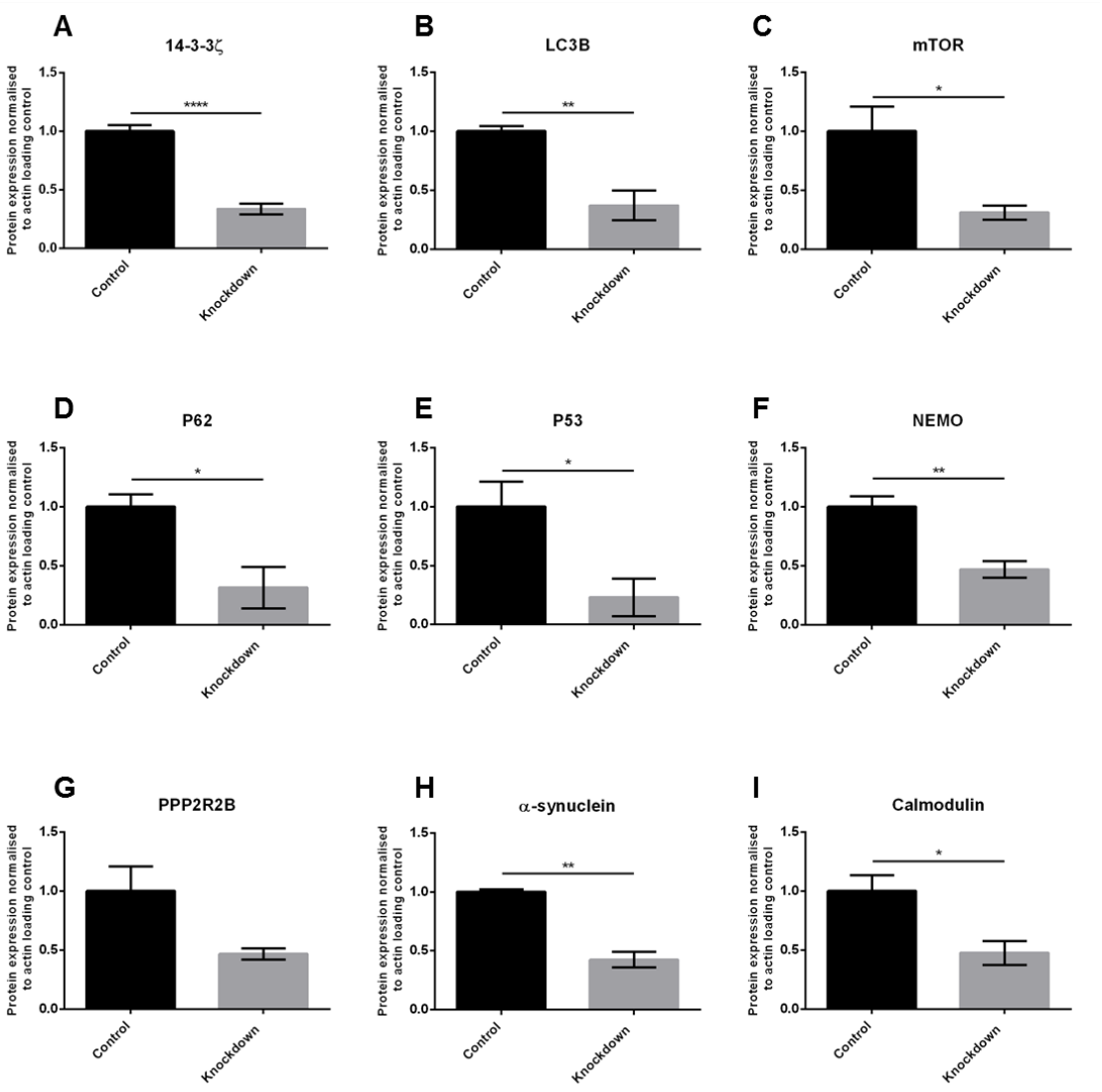

Figure 5.21: **Optimised siRNA conditions achieve 52-77% knockdown of target list two.** Cells were transfected with appropriate siRNAs (50 or 100 nM) and protein levels assessed by WB 48 h later. Band density was normalised relative to actin loading controls. Bars represent means ± SEM (n=3), data were analysed with t tests, * represents P≤0.05, ** represents P≤0.01 and **** represents P≤0.0001.

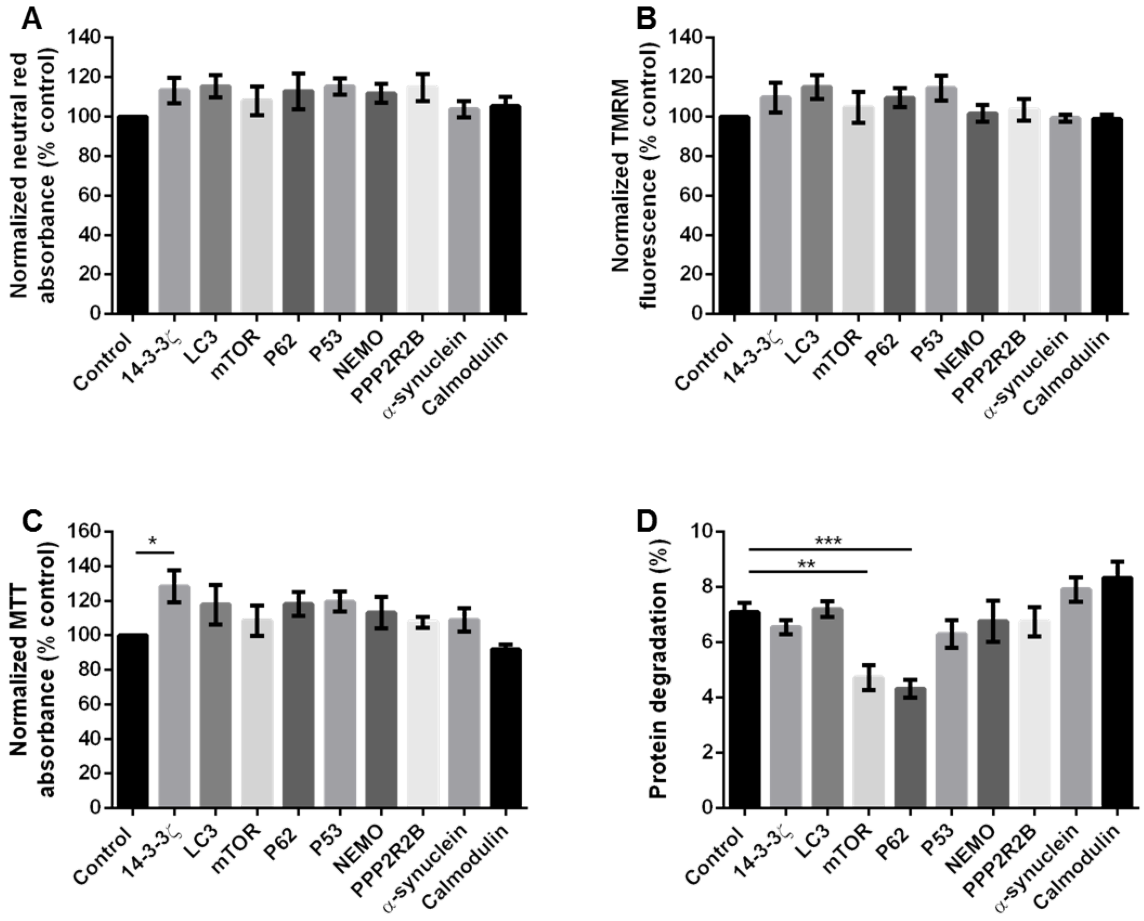

Figure 5.22: **Knockdown of members of target list two does not affect cellular viability.** **A** to **C** Cells were transfected with appropriate siRNAs (50 or 100 nM) (control cells were treated with a non-targeting siRNA) and 48 h later cellular viability was estimated using neutral red absorbance (**A**) (average unnormalised control absorbance was 0.616), TMRM fluorescence (**B**) (average unnormalised control fluorescence was 3863 RFU) and MTT reduction (**C**) (average unnormalised control absorbance was 0.388). **D** Radio-labelled cells were transfected with siRNA (50 or 100 nM), 24 h post transfection the amount of protein breakdown in a 12 h window was calculated using a pulse-chase assay. Bars represent means ± SEM (n=7), data were analysed using a 1-way ANOVA with a Dunnett test for multiple comparisons.

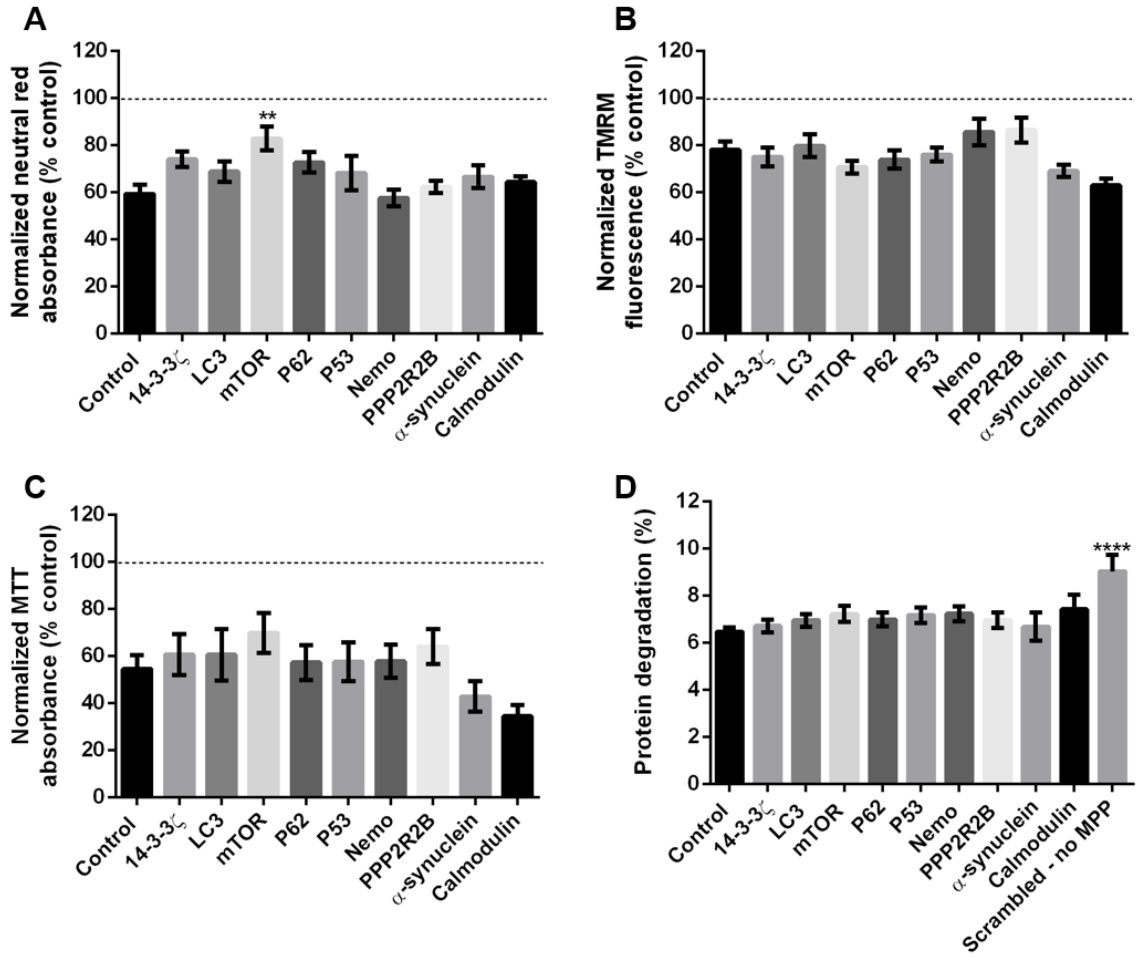

Figure 5.23: **Knockdown of members of target list two does not affect cellular vulnerability to MPP$^+$.** **A** to **C** Cells were transfected with appropriate siRNAs (50 or 100 nM) (control cells were treated with a non-targeting siRNA), 24 h later cells were treated with MPP$^+$ (100 μM) and cellular viability was estimated using neutral red absorbance (36 h post MPP$^+$ exposure) (average unnormalised untreated control absorbance was 0.318) (**A**), TMRM fluorescence (24 h post MPP$^+$ exposure) (average unnormalised untreated control fluorescence was 8569 RFU) (**B**) and MTT reduction (48 h post MPP$^+$ exposure) (average unnormalised untreated control absorbance was 0.318) (**C**). **D** Radio-labelled cells were transfected with siRNA (50 or 100 nM), 24 h post transfection the amount of protein breakdown in a 12 h window was calculated in the presence of MPP$^+$ (100 μM) using a pulse-chase assay. Bars represent means ± SEM (n=7), data were analysed using a 1-way ANOVA with a Dunnett test for multiple comparisons.

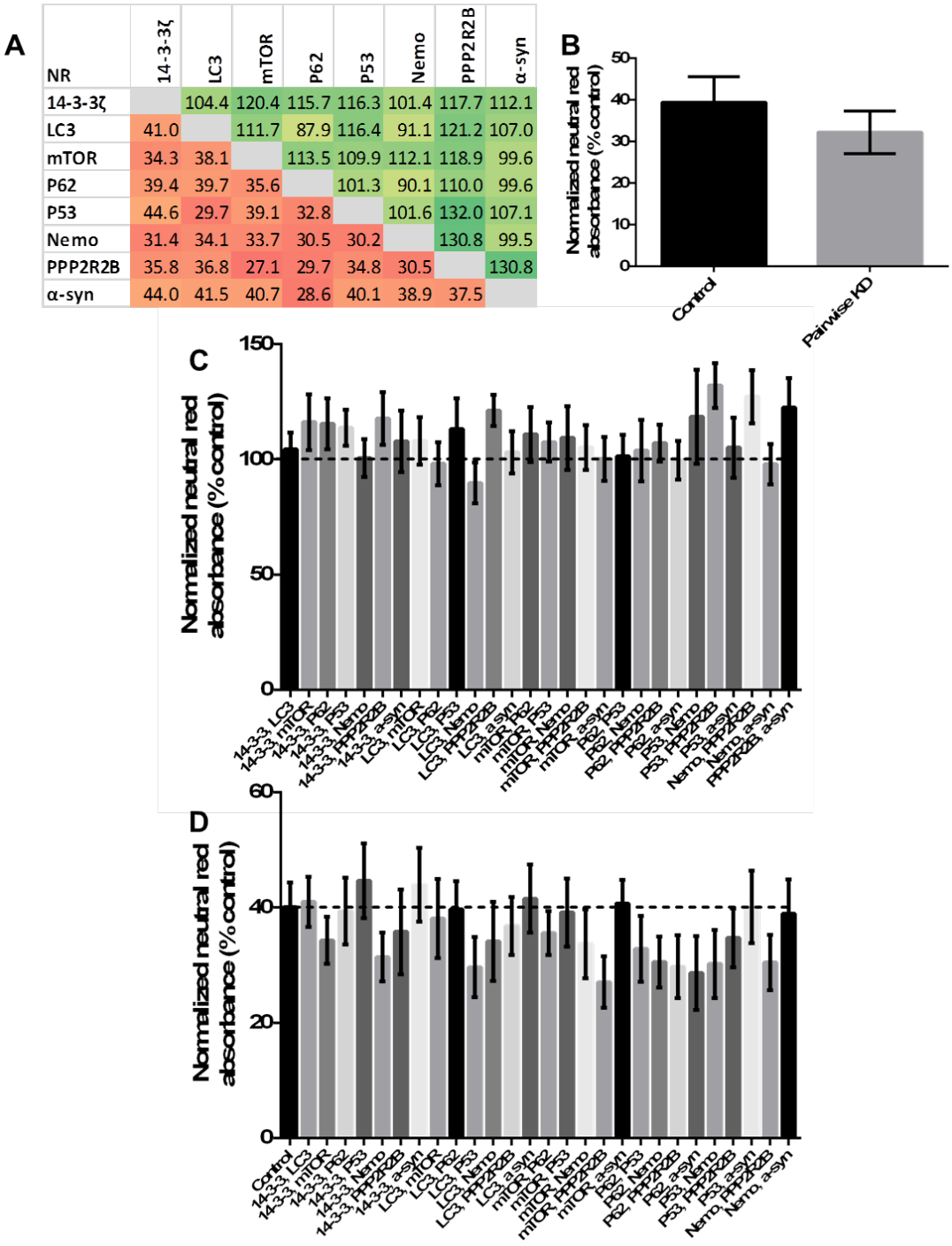

Figure 5.24: **Pairwise knockdown of target list two does not alter neutral red accumulation under control conditions or following MPP$^+$ treatment.** Cells were transfected with pairwise combinations of siRNA (50 or 100 nM) (control cells were treated with a non-targeting siRNA) and cellular viability was estimated using neutral red uptake. **A** Bottom left half of plate was MPP$^+$ treated (100 μM) 24 h after transfection (top right half of plate was not exposed to neurotoxin) and neutral red absorbance measured 36 h later. Average unnormalised control absorbance was 0.917. Viability is shown using a colour scale with green indicating highest viability and red representing lowest viability; the colour scale is consistent across *Figures 5.24*, *5.25* and *5.26*. **B** Overall effect of pairwise KD on cellular vulnerability to MPP$^+$ treatment, bars represent mean ±SEM (n=12) of all wells with and without KD, data were analysed using a t-test. **C** and **D** Neutral red absorbance of each pairwise combination in the absence (**C**) and presence (**D**) of MPP$^+$. Bars represent means ±SEM (n=12), data were analysed using a 1-way ANOVA with a Dunnett test for multiple comparisons.

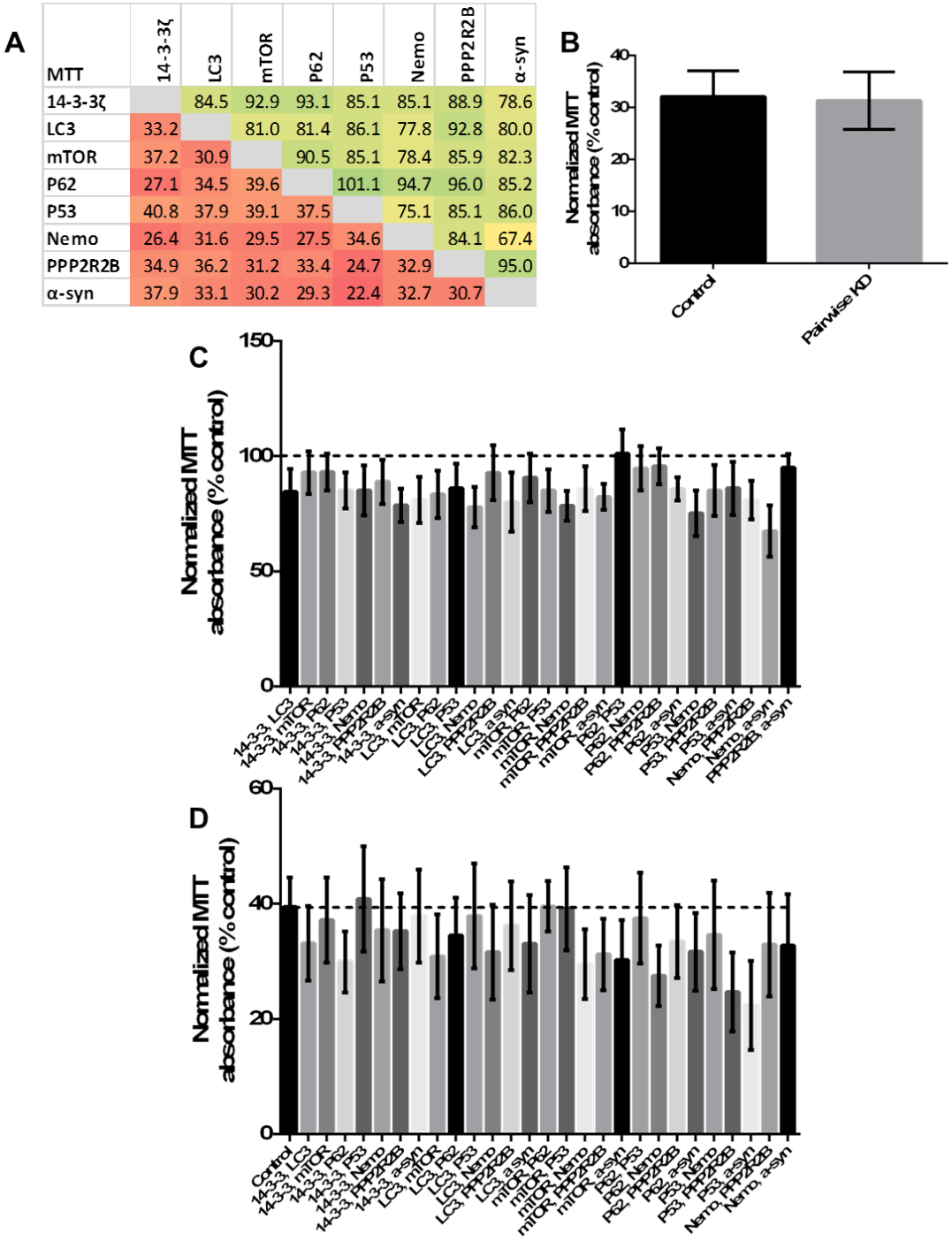

Figure 5.25: **Pairwise knockdown of target list two does not alter MTT reduction under control conditions or following MPP^+ treatment.** Cells were transfected with pairwise combinations of siRNA (50 or 100 nM) (control cells were treated with a non-targeting siRNA) and cellular viability was estimated by MTT reduction. **A** Bottom left half of plate was MPP^+ treated (100 μM) 24 h after transfection (top right half of plate was not exposed to neurotoxin) and MTT reduction was measuerd 48 h later. Average unnormalised control absorbance was 0.698. Viability is shown using a colour scale with green indicating highest viability and red representing lowest viability; the colour scale is consistent across *Figures 5.24*, *5.25* and *5.26*. **B** Overall effect of pairwise KD on cellular vulnerability to MPP^+ treatment, bars represent mean ±SEM (n=12) of all wells with and without KD, data were analysed using a t-test. **C** and **D** MTT absorbance of each pairwise combination in the absence (**C**) and presence (**D**) of MPP^+. Bars represent means ±SEM (n=12), data were analysed using a 1-way ANOVA with a Dunnett test for multiple comparisons.

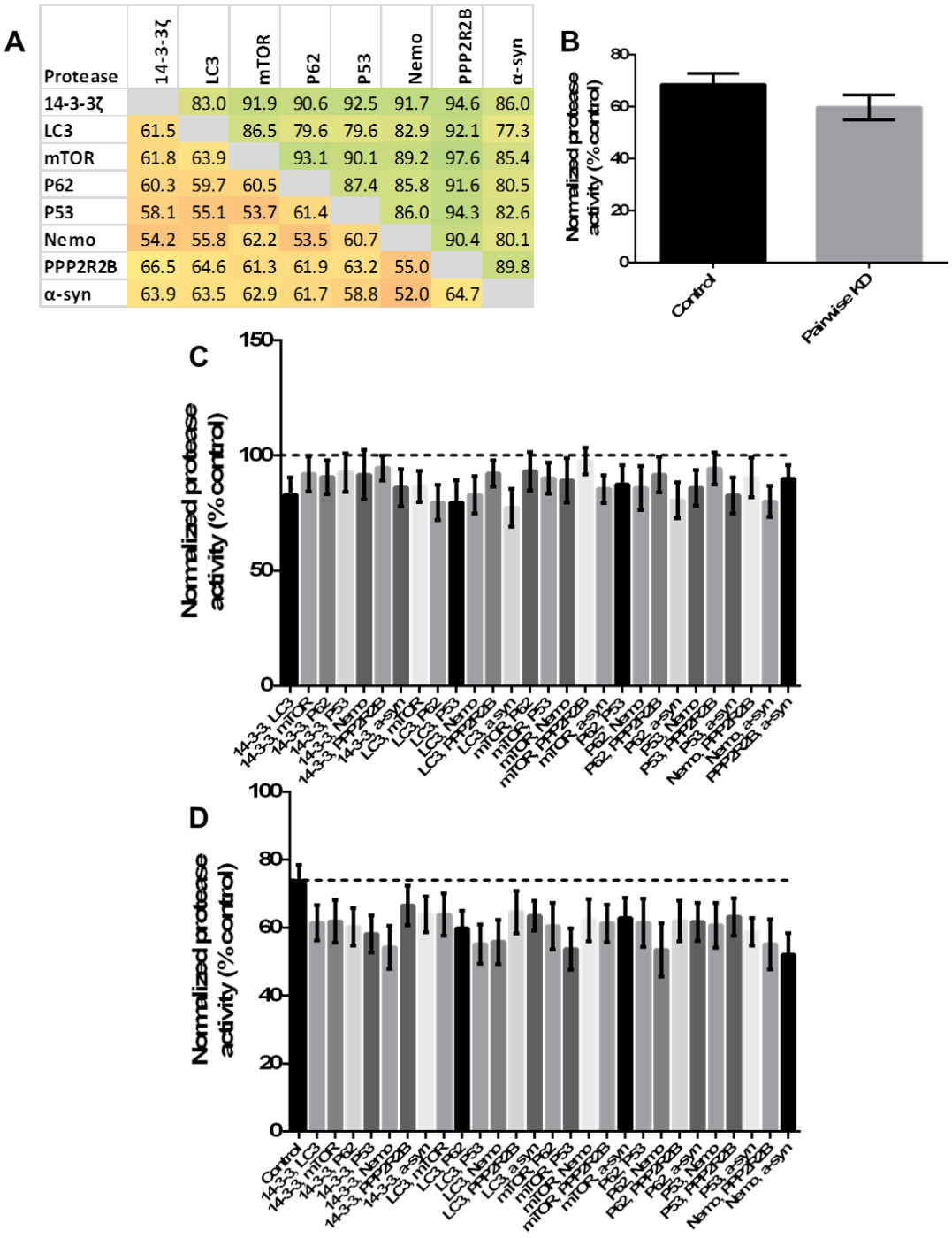

Figure 5.26: **Pairwise knockdown of target list two does not alter live cell protease activity under control conditions or following MPP$^+$ treatment.** Cells were transfected with pairwise combinations of siRNA (50 or 100 nM) (control cells were treated with a non-targeting siRNA) and cellular viability was estimated by live-cell protease activity. **A** Bottom left half of plate was MPP$^+$ treated (100 μM) 24 h after transfection (top right half of plate was not exposed to neurotoxin) and live-cell protease activity was measured 48 h later. Average un-normalised control fluorescence was 555 RFU. Viability is shown using a colour scale with green indicating highest viability and red representing lowest viability; the colour scale is consistent across *Figures 5.24*, *5.25* and *5.26*. **B** Overall effect of pairwise KD on cellular vulnerability to MPP$^+$ treatment, bars represent mean ±SEM (n=12) of all wells with and without KD, data were analysed using a t-test. **C** and **D** Viability of each pairwise combination in the absence (**C**) and presence (**D**) of MPP$^+$. Bars represent means ±SEM (n=12), data were analysed using a 1-way ANOVA with a Dunnett test for multiple comparisons.

5.3 Discussion

The goal of this chapter was to validate two lists of protein targets (**target list one** and **two** *Table 5.1*) identified by network analysis through modulation in an MPP^+ *in vitro* system.

Target list one	Target list two
GBRL2	GBRL2
P62	14-3-3ζ
GBRL1	P53
GABARAP	LC3B
	P62
	α-synuclein
	Nemo
	mTOR
	GBRL1
	Calmodulin
	PPP2R2B

Table 5.1: **Twelve protein targets (across two lists) were predicted to modulate MPP^+ toxicity. Target list one** was generated through subgraph analysis *Subsection 4.2.11* and **target list two** was generated through selective BC analysis *Subsection 4.2.14*.

5.3.1 Modulation target list one

Initial success was achieved with modulation of **target list one**, identified through the subgraph network analysis (*Subsection 4.2.11*). P62 is a molecular adaptor, binding to ubiquitin leading to the aggregation of ubiquitinated proteins [506] and also facilitating their degradation by its interaction with the autophagosome [352]. GABARAP, GBRL1 and GBRL2 are members of the GABARAP subfamily and (along with the LC3 subfamily) are orthologs of the yeast protein ATG8 [370]. The LC3 and GABARAP proteins play a crucial role in autophagosome membrane maturation and also interact with P62 facilitating the selective breakdown of ubiquitinated proteins and organelles [155].

Both transcript and protein levels of all of targets were unaffected by MPP^+ treatment. Although endogenous protein levels of GBRL1 and GBRL2 were low, siRNA mediated KD of P62 and GABARAP was achieved. Despite fairly high levels of GBRL2 transcript, significant protein was not detected by WB (although the antibody detected exogenous GBRL2). However, poor correlation between transcript and protein level may be due to low levels of translation or rapid degradation of the protein and low correlation coefficients have been reported in wide scale studies of bacteria and eukaryotes [517].

Neither of the single KD (modelling node deletions) affected cellular viability or vulnerability

to MPP^+. However, a combined KD of GABARAP and P62 potentiated MPP^+ toxicity as measured by cell counts and neutral red uptake (a marker of cellular ATP). The requirement for multiple interventions supported the theoretical prediction that networks are robust to single interventions and, that to be effective, interventions must be both multiple and targeted [264, 385]. Further, the deleterious effect of KD was only observed in combination with MPP^+ treatment. Biological systems may be robust to deletions under optimal conditions, but not when exposed to additional challenges such as toxins, as has previously been reported in yeast [392]. No change in TMRM fluorescence was observed, suggesting that the effect of the KD lies downstream of mitochondrial insult which is in accordance with the proteins' roles in autophagy.

The goal of this thesis was to effect a rescue of MPP^+ toxicity and OE **target list one** was next optimised. Again, the single modulations did not affect cellular viability or vulnerability to MPP^+. However, a combined OE led to partial protection from MPP^+ cytotoxicity as measured by neutral red and cell counts. In accordance with the KD results, there was no difference in TMRM fluorescence after MPP^+ treatment in control and combined OE cells, supporting the idea that rescue occurred downstream of mitochondrial insult. This is consistent with the MPP^+ rescue achieved by others following α-synuclein KD [79]. Further, Poltl *et al.* demonstrated that caspase inhibitors, and anti-oxidants were capable of rescuing MPP^+ toxicity downstream of initial mitochondrial insult and ATP depletion. The authors suggested that, 'inhibition of complex I by MPP^+ is compatible with cell survival in certain situations' [362]. Live-cell fluorescence microscopy indicated that only 20-30% cells were successfully expressing the GABARAP subfamily-EGFP fusion proteins 48 h after transfection. If a higher transfection efficiency was achieved, a greater protective effect would be expected following the overexpression.

The minimal effective OE set of **target list one** was demonstrated to be made up of P62 and two or more members of the GABARAP subfamily. The redundancy in the GABARAP subfamily was previously demonstrated by Maruyama *et al.* and Weidberg *et al.*, who required a siRNA KD pool to observe a phenotype [353, 519]. The redundancy of proteins is a key tenet of network pharmacology [269] and ensures that biological systems are robust to changes in environmental conditions and gene mutations. There remains the possibility that the need for multiple members of the GABARAP subfamily is a dosage effect. However, it was demonstrated that the number of cells transfected by members of the GABARAP family was the same during individual and combined transfections.

P62 and the GABARAP subfamily have distinct biological roles in the autophagic degradation of proteins. Therefore, it is logical that they are not able to substitute for each other in the

minimal OE set. The proteins' divergent roles are supported by the distinct network topology of P62 and the GABARAP subfamily.

5.3.2 An autophagic mechanism of protection

Given that all members of the OE set had a documented role in autophagy, it was hypothesised that protection occurred via an autophagic mechanism. Others have reported amelioration of MPP^+ toxicity by increasing autophagic flux using sub-lethal hypoxic preconditioning [361], rapamycin [159] and molecules derived from traditional medicines [347, 358, 360]. Earlier in this thesis it was demonstrated that MPP^+ treatment led to decreased autophagic flux (*Subsection 3.2.3*) and it was predicted that increasing autophagy would be neuroprotective.

Levels of LC3B lipidation were not altered following the combined OE either in the absence or presence of MPP^+. However, LC3B lipidation cannot distinguish between rates of autophagosome formation and protein breakdown [350]. Further, the GABARAP subfamily proteins may be able to substitute for LC3s in the autophagosomal membrane making LC3B lipidation a poor marker of autophagosome levels.

Therefore, a radio-label pulse-chase assay was used to measure absolute autophagic flux. MPP^+ was confirmed to decrease autophagic flux within 12 h of treatment. However, neither the combined OE of **target list one** nor the control plasmid altered overall autophagic flux in either the absence or presence of MPP^+.

Given that there was no change in overall protein degradation, it was hypothesised that the combined OE led to the autophagic sequestration of damaged proteins or organelles and thereby offered short-term cellular protection. LB contain large amounts of ubiquitin and it has been proposed that α-synuclein oligomers may be aggregated to protect cells from their toxicity [520]. The work of Tanik *et al.* suggests that although such aggregates colocalise with autophagic proteins, they cannot be effectively degraded [172].

ICC was used to identify LAMP1 and LC3B positive puncta in untransfected cells corresponding to lysosomes and autophagosomes respectively. In contrast to published studies [59], LAMP1 and LC3B colocalisation was not detected under either control or MPP^+ treated conditions. Given that autophagic protein degradation had been confirmed using the pulse-chase analysis it is suggested that the lack of apparent colocalisation is due to the very small puncta size or rapid degradation of autophagosomal markers upon fusion. MPP^+ treatment (36 h, 100 μM) led to retraction of cellular processes and shrinkage of cell bodies, resulting in puncta that were very close together in MPP^+ treated cells and thus their size and number could not be ascertained.

Following the combined OE of **target list one**, puncta were detected which displayed both GFP fluorescence and P62 immunoreactivity. The appropriate antibodies were used to confirm that the GFP fluorescence was due to the GABARAP subfamily fusion proteins. The GFP puncta, therefore, contained all members of the protein OE set. The GFP positive puncta were considerably larger than endogenous puncta; however, macroautophagy has been shown to degrade large cellular aggregates up to 2 μm in size [352]. Colocalisation with LC3B confirmed that the puncta represented functional autophagosomes and not merely protein aggregates. There was no colocalisation between the exogenous autophagosomes and the mitochondrial marker Tom20 suggesting that the **target list one** OE did not increasing mitochondrial turnover. This was consistent with the failure of **target list one** OE to rescue mitochondrial membrane potential following MPP^+ exposure. Further, there was no colocalisation between the autophagosomes and LAMP1 consistent with failed fusion of lysosomes and exogenous autophagosomes which would explain the lack of increased protein turnover. However, LAMP1 and LC3B colocalisation was also not detected under control conditions where protein degradation occured unimpeded.

Earlier results (*Subsection 3.2.3*) suggested that MPP^+ treatment resulted in lysosomal deacidification downstream of ATP depletion. The loss of lysosomal pH may have been responsible for the lack of autophagosome/lysosome fusion and would explain decreased autophagic flux following MPP^+ treatment and the lack of colocalisation in LC3B and LAMP1 staining. Dehay *et al.* have previously reported lysosomal defects in both MPP^+ *in vitro* models and PD brain samples [159] and others have suggested that lysosomal dysfunction lies at the centre of PD pathology [142, 159, 160].

In conclusion, it is suggested that the combined OE leads to increased formation of prominent autophagosomes and sequestration of damaged proteins. Although the autophagosomes cannot be efficiently degraded, sequestration offers short-term protection from MPP^+ neurotoxicity. An alternative possibility, is that **target list one** may decrease cell death through interaction with the apoptotic pathway and GABARAP is known to interact with both the apoptotic protein NIX and the anti-apoptotic protein BCL2 [488, 521].

5.3.3 Modulation of target list two

Following the above success, **target list two** was explored. Again, it was predicted that the targets proteins would be involved in the cross-talk between mitochondrial dysfunction and autophagy in an MPP^+ model of PD. **Target list two** was made up of 11 proteins including three proteins from **target list one** (P62, GBRL1 and GBRL2) in addition to eight new proteins

(14-3-3ζ, PPP2R2B, calmodulin, LC3B, mTOR, Nemo, P53 and α-syn). As outlined in the introduction to this chapter, all of the target proteins have been in some way implicated in PD (*Section 5.1*). This work focussed on siRNA mediated KD because node deletion best tested the BC analyses and KD are more straightforward to achieve in a consistent manner than OE due to availability of prevalidated siRNAs. Endogenous levels of GBRL1 and GBRL2 had already been demonstrated to be very low (*Subsection 5.2.1*), so this thesis focussed on the remaining nine proteins.

There was no change to mRNA levels of any of the members of **target list two** in response to MPP^+ and all targets were detected at protein level. However, in contrast to previous results from within the laboratory [79, 116], levels of α-synuclein were very low and the protein was only detected using a positive control. Other laboratory members have recently had similar difficulties in the identification of this protein in the M17 cell line and it appears that expression levels are low and inconsistent, highlighting a possible concern regarding the use of M17 cells to model PD.

Following MPP^+ treatment there was no change to the expression levels of 14-3-3ζ, LC3B, mTOR, PPP2R2B, α-synuclein or calmodulin. It should be noted that this refers to the total level of LC3B, increased lipidation was observed as previously stated. Some previous studies have demonstrated increased α-synuclein expression following MPP^+ treatment [215, 463], the failure to recapitulate published results may be due to differences between cell lines. Although P62, P53 and Nemo levels were decreased after 48 h MPP^+ treatment, MPP^+ had no significant effect at earlier time points for any of the proteins. It is possible that, although overall P53 levels are constant, the levels of activated protein increases upon MPP^+ treatment [497]. P53 and P62 showed a time dependent accumulation in both control and MPP^+ cells consistent with increased apoptosis/autophagy as culture media is depleted of nutrients.

Next, siRNA mediated KD of each member of **target list two** was optimised such that KD of between 69 and 53% was achieved for each protein. The KD of calmodulin required a pool of three siRNAs because the protein has three corresponding genes and there was no region of consistent sequence across the three transcripts. Optimisation of KD facilitated an investigation into the effects of protein KD on autophagy, cellular viability and vulnerability to MPP^+. Assays suitable for medium-throughput screening in 24- and 96-well plates were selected so that all pairwise combinations could be considered and biological repeats maximised.

P62 KD decreased basal autophagy, but did not affect the process following MPP^+ treatment. P62 plays a crucial role in targeting proteins and organelles for degradation so decreased levels

would be expected to decrease protein turnover [180], some evidence also suggests that P62 regulates autophagy [151]. Following MPP^+ treatment, autophagic flux was not affected by P62 KD, suggesting that autophagy was limited by the number of functional lysosomes (rather than autophagosomes). This hypothesis is consistent with the earlier observation of lysosome deacidification following MPP^+ treatment (*Subsection 3.2.3*) and the extensive study of Dehay *et al.* [159]. Interestingly, despite its use as an autophagic marker, KD of LC3B did not affect the rate of autophagic flux. However, there is considerable redundancy within the human orthologs of ATG8 and others have previously shown that KD of a single member (including LC3B) does not affect the overall autophagic process [353, 519]. mTOR KD decreased basal autophagy, this was somewhat unexpected as inhibition (via rapamycin) leads to an upregulation of autophagy in this model (*Subsection 3.2.3*). Although other studies have reported mTOR independent routes of autophagy and no effect upon mTOR KD [522], there are no published reports of decreased autophagic flux following mTOR KD. It remains possible that decreased levels of the protein may alter the ratio of the mTORC1 and mTORC2 complexes.

Single KD of members of **target list two** did not alter cellular viability or MPP^+ vulnerability. This is in contrast to the protective effect previously reported following α-synuclein KD [79, 114, 115], the divergent results may be due to the very low and inconsistent levels of α-synuclein in the M17 cell line. It was also surprising to see no protective effect following P53 KD as KO mice are protected from MPTP toxicity [480]. However, it is suggested that this is due to remaining P53 following an incomplete KD as residual P53 could still initiate apoptosis. Similarly, Garcia-Garcia *et al.* reported that the use of a dominant-negative form of ATG5 and siRNA mediated KD had opposing effects on MPP^+ vulnerability and suggested that this was due to low levels of ATG5 remaining after KD [188].

Due to the requirement for three distinct siRNAs calmodulin was not included in the pairwise experiments. However, all other possible KD pairings of **target list two** were tested in the absence and presence of MPP^+ via three assays (MTT, neutral read and protease activity). Following multiple testing corrections no significant differences were found following any of the pairwise KD in any of the assays or when considering MPP^+ vulnerability in the KD group as a whole. It is possible that the KD had effects too small to be detected without additional repeats. However, it is suggested that the failure to identify significant alterations to cellular viability or MPP^+ vulnerability following pairwise KD of members of **target list two** stems from the use of the 96-well format. Although siRNA screening approaches have been previously used to identify proteins capable of modulating cellular phenotypes or toxin vulnerability [404, 428] siRNA mediated KD may be less effective under 96-well conditions and it was not

possible to validate KD by WB due to low amounts of protein. Less effective KD would lead to increased residual protein (particularly important for signalling molecules or transcription factors) explaining the divergence from KO models. An alternative, although time consuming approach is the generation of stable KD/KO cell lines using shRNA constructs [523] or ZFN/-TALEN technology [524]. Further, media aspiration steps in 96-well plates had an increased risk of dislodging cells (despite poly-*L*-lysine coating) which may explain the increased variability in the 96-well results. These theories could be tested by repeating pairwise **target list two** KD experiments in 24-well format as was previously successful for **target list one**; however, this would incur significant additional financial costs. The possibility also remains that the network analysis used to generate **target list two** was less effective. However, it was surprising that previously published results for α-synuclein and P53 could not be replicated.

5.3.4 Summary

Protein levels of network targets were successfully modulated in the *in vitro* MPP^+ model and cellular viability, autophagy and MPP^+ vulnerability measured across a number of assays. Four proteins identified through network analysis (**target list one**) were shown to modulate MPP^+ toxicity *in vitro*. A combined KD potentiated MPP^+ neurotoxity and a combined OE resulted in a partial rescue. No effect was seen following single modulations highlighting the need for multiple interventions, a key tenet of network pharmacology [269]. The protective effect observed following combined OE of **target list one** is proposed to occur via an autophagic mechanism with damaged proteins sequestered in prominent autophagosomes similar to the mechanism thought to lead to the formation of LB in the brains of PD patients.

Modulation of individual members or pairwise combinations of **target list two** did not alter MPP^+ vulnerability. The failure to validate *in silico* predictions may be due to the different network analyses employed. The selective BC approach has not been used for the identification of biologically important nodes and may be inappropriate. However, selective BC analysis identified two proteins whose deletion has previously been demonstrated to ameliorate MPP^+ toxicity (α-synuclein and P53). An alternative explanation is that the difference between these two sets of experimental results is the transition to 96-well plates for analysis of KD combinations. Despite these limitations, for the first time PPIN have been used to successfully predict targets that modulate cell death in an *in vitro* MPP^+ model.

Chapter 6

Discussion

This thesis is the first example of the use of a PPIN to identify targets capable of modulating an experimental model of PD. Further, there are few examples of PPIN being successfully experimentally validated in other disease contexts [265]. Through network analyses four proteins (GABARAP, GBRL1, GBRL2 and P62) were identified (*Subsection 4.2.11*) whose combined OE resulted in a rescue of MPP^+ toxicity in an *in vitro* model (*Figure 5.8*). However, no single OE elicited a protective response demonstrating the need for multiple interventions, a key tenet of network pharmacology [264, 269] and a result of the robust nature of biological systems [269, 371]. Rescue occurred via an autophagic mechanism with prominent autophagosomes formed (*Subsection 5.2.4*), these could potentially sequester damaged proteins in a manner reminiscent of LB in the brains of PD patients [172].

6.1 The role of autophagy in PD models

Autophagy is the process of cellular self-degradation and is essential in long-lived cells [157, 158]. Alterations in autophagy have been demonstrated in numerous PD models [7, 145], including MPP^+ [152, 159, 186, 357]. However, there are divergent opinions as to whether autophagic flux is increased or decreased. Through the development of a radio-label pulse-chase assay (*Chapter 3*), it was conclusively demonstrated that MPP^+ treatment resulted in decreased autophagic flux in M17 cells at time points preceding cell death (*Figure 3.17*). Although autophagosome accumulation was observed (as detected by increased LC3B lipidation (*Figure 3.14*) following MPP^+ treatment, accumulation was as a result of defective degradation and not increased autophagosome formation. Dehay *et al.* reported decreased lysosomal levels following MPP^+ treatment [159], but these findings were not replicated in this thesis (*Figure 3.5*). Instead it

is suggested that blocked autophagic flux in the MPP^+ model occurs as a result of lysosome deacidification (demonstrated by decreased neutral red accumulation - *Figure 3.4*) downstream of cellular ATP depletion (*Figure 3.6*). Further, although P62 KD decreased basal autophagy (*Figure 5.22*) the KD had no affect following MPP^+ treatment (*Figure 5.23*) suggesting that functional lysosomal levels were the limiting factor on autophagy following MPP^+ treatment.

Although MPP^+ is just one model of PD, this thesis support the theory that lysosomal dysfunction lies at the centre of PD pathogenesis [142, 159, 160]. Beyond the targets identified in this thesis, there is considerable value in investigating small molecules capable of increasing autophagic flux as potential PD therapeutics. One such possibility is the TFEB activator trehalose which results in increased lysosome biogenesis and autophagic clearance [159].

6.2 Optimisation of cellular viability assays

Beyond the development of the pulse-chase assay, several assays were developed to sensitively measure cell viability following MPP^+ treatment. Neutral red had been shown to accurately measure cellular viability [286, 345], but had not been widely deployed in the context of MPP^+ induced cell death. In this thesis the neutral red protocol was optimised for use in M17 cells following MPP^+ treatment (*Figure 3.4*) and control experiments were conducted to demonstrate that the dye is lysosomally accumulated in a manner dependent on lysosome pH (*Figures 3.6* and *3.7*). Mitochondrial membrane depolarisation is a key marker of MPP^+ induced cell death [209, 327]. Although rhodamine based dyes have been used in conjunction with microscopy and flow cytometry to measure depolarisation [348], this thesis was the first example of TMRM being used in a plate reader based format in conjunction with MPP^+ toxicity (*Figure 3.8*).

Most *in vitro* MPP^+ protocols utilise a continuous MPP^+ exposure. In this thesis, it was demonstrated that as little as 2 h MPP^+ treatment was sufficient to induce a cascade of cellular processes resulting in loss of cellular viability some hours after the neurotoxin removal (*Figure 3.10*). Such protocols offer a less severe MPP^+ treatment regime that could be used to identify therapeutic interventions.

Finally, there has been some debate over the mechanism of MPP^+ induced cell death, with reports of apoptosis, necrosis and caspase independent cell death [190, 330, 525]. In this thesis, annexin-V/7-AAD staining in conjunction with flow cytometry (*Figure 3.11*) and cleaved caspase-3 staining in conjunction with flow cytometry and ICC (*Figures 3.12* and *3.13*) demonstrated that MPP^+ induced apoptotic cell death.

6.3 The use of immortalised cell lines to model PD

In *Chapters 3* and *4* the DA human cell line BE(2)-M17 was used as an *in vitro* model of PD. This cell line has the key advantages of being human-derived and producing DA (*Figure 3.22*). Despite initial hypotheses, DA depletion did not alter MPP^+ sensitivity in the M17 cell line (*Figure 3.23*) and therefore the importance of a DA cell line may lie in the relative levels of VMAT and DAT expressed, known to be a determinant of PD vulnerability [231, 325]. A key disadvantage of the M17 line was the low and inconsistent levels of the protein α-synuclein (*Figure 5.17*).

It would be essential to replicate the findings of this thesis in other cell lines, initially the human SH-SY5Y cell line could be used in both its mitotic and differentiated states, although this cell line does not produce DA. Further, during the course of this thesis, protocols for the generation of DA neurones from iPSC have been significantly improved [51]. It would therefore, now be more feasible to repeat KD and OE in neurones derived from PD patients, although such protocols remain time consuming and expensive. Excitingly, it was recently demonstrated that systemic *in vivo* treatment with brain-targeting exosomes allowed the delivery of α-synuclein siRNA to the brain and efficient protein KD [526]; such an approach could be utilised to extend the KD results of this thesis to *in vivo* models.

6.4 Construction of PPIN

In *Chapter 4* several PPIN were constructed to model MPP^+ toxicity. iRefIndex was used as a consolidated PPI database due to the large quantity of data, mapping of protein isoforms to single canonical identifiers and the minimisation of spoke expansion of complexes [288, 426]. The last two factors have both been shown to introduce error into PPI databases and resultant PPIN [405, 420].

Sampling relies on the principle of 'guilt by association' whereby proteins are more likely to interact with other proteins involved in similar cellular processes [95, 376] and has previously been used to generate disease relevant networks [309, 310, 314, 527]. Although microarray analysis to identify differentially expressed genes was unsuccessful (*Subsection 3.2.5*), a seedlist of MPP^+ related proteins (*Tables 4.2*, *4.3*, *4.4*, *4.5*, *4.6* and *4.7*) was constructed to facilitate sampling. During the course of this project proteomic approaches have become increasingly accessible, such that changes in protein levels following a stimuli can be measured in a high-throughput and hypothesis free manner [402, 528]. Won Choi *et al.* recently reported the use of

proteomic analysis to identify 39 proteins differentially expressed in SH-SY5Y following MPP^+ treatment [529]. Such techniques could be used to generate cell line specific seeds and would offer significant advantages over using differentially expressed genes as gene and protein expression levels have been shown to be poorly correlated [517].

The resulting networks were validated through the identification of high BC nodes (*Subsection 4.2.5*) and the detection of communities corresponding to biological processes implicated in PD/MPP^+ pathology (*Subsection 4.2.6*). The shortest-path and 1-hop network exhibited considerable overlap in terms of the systems-level processes identified through community detection and the nodes with highest BC. Further, many of the same potential therapeutic targets were identified following analysis of the two networks.

It is acknowledged that, beyond the quality of the PPI data, such networks are limited as only physical interactions between protein species are included and they represent a single timepoint in a dynamic system [265]. However, it is suggested that such simplifications allow the emergent properties of biological systems to be explored without over-complications that would limit the utility of network models.

6.5 Identification of targets through the analysis of PPIN

Numerous methods have been reported for identifying potentially important nodes from PPIN [426, 441, 443], but there has been little experimental validation of *in silico* predictions. As well as using previously published metrics (bridging centrality - *Subsection 4.2.8* and Steiner tree analysis - *Subsection 4.2.10*) this thesis developed two analyses based on BC (*Subsections 4.2.11* and *4.2.14*). Network analysis yielded a considerable number of biological plausible results and one target list was successfully validated through *in vitro* experiments (*Subsection 5.2.3*). The techniques for PPIN network analysis developed in this thesis could be applied to other disease models or networks.

When the results of this thesis were compared to Konn's 2012 α-synuclein PPIN [302], several common results were identified. Konn highlights GABARAP as an α-synuclein interactor and potential therapeutic target, this thesis experimentally validates the role of GABARAP in PD *in vitro* models. Further, three more of the targets experimentally tested in this thesis (P62, 14-3-3ζ and calmodulin) were identified by Konn as α-synuclein interactors indicating that the results of this thesis could be replicated in a PPIN based on an alternative (α-synuclein OE) PD model. Additionally, α-synuclein, P62 and 14-3-3ζ were identified as topologically significant

nodes in Rakshit *et al.*'s study of a network of proteins corresponding to genes differentially expressed in PD [446]. However, Rakshit *et al.* did not select these proteins as high priority biomarkers.

Such PPIN analysis complements techniques such as GWAS and microarray studies which have also been used to identify PD genes. There was no overlap between significant risk loci identified through GWAS [31] and targets identified in this thesis. Whereas GWAS identify causal variants, the PPIN analysis aimed to identify potential therapeutic targets, whether or not they were altered in PD. This is in line with most currently approved drugs which do not target proteins whose mutation causes the disease [273]. However, there was some overlap between the PPIN targets investigated in this thesis and genes shown to be differentially expressed in the brains of PD patients. Simunovic *et al.* reported significantly altered expression of α-synuclein, GBRL1 and GBRL2 [340] and Elstner *et al.* demonstrated that the mTOR pathway as a whole was differentially expressed [308]. Although this overlap is interesting it should be noted that mRNA and protein levels show poor correlation [517] and that a protein's levels do not need to be altered to make it a therapeutic target.

This thesis was limited by the underlying PPI data as many human PPI have yet to be explored [407] and high-throughput techniques for PPI identification are error prone [422]. Further there are inconsistencies and inaccuracies in the collation of data in PPI databases [405] which introduce an additional source of error. It would be interesting to repeat analyses using metrics to measure the confidence of PPI and in an extension of this thesis analyses could be extended to weighted networks, where edge weight represents confidence that an interaction genuinely occur [423]. One limitation of the PPIN analysis presented in this thesis is that targets recovered are predominantly proteins that have previously been extensively investigated in the context of PD. The identification of heavily investigated proteins is likely to be a result of the incomplete nature of human PPI data - proteins which have not been investigated have few reported interactions. However, despite the limitations of PPI data, successful predictions were made based on network analysis. Therefore, it is suggested that the utility of network analysis will only increase as the quality of the underlying data is improved.

6.6 Alternative network models

Many proteins involved in core functions are conserved between species [530] and disease related cellular processes are also widely conserved [531] allowing simple organisms, such as *S.cerevisiae* and *Schizosaccharomyces pombe*, to be used to model more complex systems. Further, yeasts are

genetically tractable and amenable to high-throughput assays with large libraries of yeast KO strains [389]. Lindquist and colleagues had previously demonstrated the utility of α-synuclein OE in *S.cerevisiae* [89–94] (*Subsection 1.3.3*). During the preparation of this thesis, an elegant study using *S.pombe* to model spinal muscular atrophy (SMA) was published [532]. The authors expressed WT and mutant forms of UBA1 (ubiquitin-like modifier activating enzyme 1) (mutated in SMA) and identified *S.Pombe* KO strains which had selectively altered (compared to control) growth rates in the presence of both the mutant and WT UBA1. Of the 173 genetic modifiers identified, 145 had orthologous human genes. These genes were converted to proteins and two PPIN formed, one containing only the genetic modifiers connected by human PPI data and the other formed from 1-hop sampling using *S.pombe* PPI data. Clusters within two networks were identified, E3 ubiquitin ligases were identified as potential targets and validated (using a pharmacological inhibitor) in a *Danio rerio* model of spinal muscular atrophy [532]. Such an approach could be utilised for the MPP^+ PD model. Either, a PPIN could be constructed using the seedlist generated in this thesis, but a yeast PPI database (having converted seeds to yeast orthologs). Alternatively, yeast strains could be screened in a hypothesis free manner for modifiers capable of altering cell growth following treatment with inhibitors of the yeast equivalent of complex I.

6.7 Validation of network targets

The four protein targets in **target list one** (GABARAP, GBRL1, GBRL2 and P62), identified in *Subsection 4.2.11* were both KD (*Figure 5.4*) and OE (*Figure 5.6*) in the *in vitro* system. Combined KD potentiated MPP^+ toxicity (*Figure 5.7*) and combined OE resulted in a rescue (*Figure 5.8*). Single interventions were ineffective, confirming the need for multiple interventions. Further, there was redundancy in the minimal OE set (*Figure 5.9*) illustrating the robust nature of biological systems. OE of **target list one** resulted in the formation of prominent autophagosomes (*Figure 5.13*) which were suggested to be protective following MPP^+ mediated lysosome deacidification and consequent decreased autophagic flux.

The members of **target list two**, identified in *Subsection 4.2.14* were successfully KD in the M17 model (*Figure 5.21*). However, neither single (*Figure 5.23*) nor multiple deletions (*Figure 5.24*, *5.25* and *5.26*) modulated MPP^+ induced cytotoxicity using any of the cell viability assays tested. The reasons for the failure to validate *in silico* predictions were not entirely clear, but it is suggested that the switch to a 96-well based format may have been a key factor.

Although not investigated in this thesis, miRNA regulation of mRNA is a key determinant

of protein expression [533]. It would be interesting to investigate whether miRNA regulate expression of **target list one** and whether modulation of miRNA [534] could be utilised to increase protein levels.

6.8 Potential further work

Were the network targets successfully validated in other *in vitro* and *in vivo* models of PD, phenotypic screens for small drug like models capable of increasing protein levels could be instigated. Within the pharmaceutical industry, there has been a trend away from target based screens and back towards phenotypic screening [535], a method which has been suggested to have higher success rates than target based screening [536]. Phenotypic screens can identify successful pharmaceuticals that have multiple targets or whose effects are only apparent in the context of an entire cell and have been used in disease areas including HIV [537], Malaria [538] and cancer [539]. Beyond the proteins highlighted in this thesis, such phenotypic screens could also be used to identify small drug-like molecules capable of rescuing MPP^+ toxicity in a hypothesis free manner.

The techniques for network analysis developed here could be applied more widely, to other disease areas. There is a huge unmet need for antibiotics [540] and a considerable amount of PPI data is available for a number of bacterial species [279, 541]. The identification of combinations of critical nodes within bacterial PPIN would facilitate the development of multi-target antibiotics. Multi-target antibiotics have already gained traction an approach to tackle the problems of antibiotic resistance [542] and it is suggested that analyses of PPIN will make a valuable contribution to this field.

This thesis highlighted the value of PPIN in the development of therapeutics for human diseases. Although such applications are in their infancy, it is suggested that network analysis (and in particular PPIN) will become an increasingly valuable tool for biomedical research.

Appendix A

R code for analysis

A.0.1 Code for removing non-human interactions

```
> irefindex_curr_human = get_irefindex("9606", "current", getwd ())
> human_human_list = data.frame(irefindex_curr_human$taxa, irefindex_curr_human$
    taxb)
> tmp = do.call('paste', c(unname(human_human_list), list(sep=".")))
> irefindex_curr_human = irefindex_curr_human[ tmp == "taxid:9606(Homo_sapiens).
    taxid:9606(Homo_sapiens)"|tmp == "-.taxid:9606(Homo_sapiens)",]
> id_conversion_table_human = create_id_conversion_table(irefindex_curr_human, "
    data", "id_conversion_table_9606_a")
```

A.0.2 Code for sampling

1-Hop sampling

```
> hopSample = function(seedlist, graph){
> temp = 0
> nodes = 0
> unique_nodes = 0
> for (i in 1:length(seedlist)){
> temp =c (which(V(graph)$name==seedlist[i]), neighbors(graph, seedlist[i]))
> nodes=c(temp, nodes)
> }
> unique_nodes=unique(nodes)
> g = induced.subgraph(graph, unique_nodes)
> return(g
> }
```

Shortest-path sampling

```
> pathSample = function(seedlist, graph){
> temp = 0
> nodes = 0
> unique_nodes = 0
> for (i in 1:length(seedlist)){
> temp = get.all.shortest.paths(graph, from=seedlist[i], to=seedlist[1:length(
    seedlist)], mode="all")
> unique_nodes = unique(unlist(temp))
> nodes = c(unique_nodes, nodes)
> nodes = unique(nodes)
> }
> g = induced.subgraph(graph, nodes)
> return(g)
> }
```

A.0.3 Code for community identification

```
> sgc=spinglass.community(all_1hop)
> V(all_1hop)$membership <- sgc$membership
> s0=V(all_1hop)[membership == 0]
> s1=V(all_1hop)[membership == 1]
> s2=V(all_1hop)[membership == 2]
> s3=V(all_1hop)[membership == 3]
> s4=V(all_1hop)[membership == 4]
> s5=V(all_1hop)[membership == 5]
> s6=V(all_1hop)[membership == 6]
> s7=V(all_1hop)[membership == 7]
> s8=V(all_1hop)[membership == 8]
> s9=V(all_1hop)[membership == 9]
> s10=V(all_1hop)[membership == 10]
> s11=V(all_1hop)[membership == 11]
> V(all_1hop)$color=V(all_1hop)$membershi
> names=V(all_1hop)$name
> community=V(all_1hop)$membership
> df=data.frame(names, community)
> getGeneIds<-function(x) {
> temp<-id_conversion_table_human[id_conversion_table_human[,1] == "entrezgene/
    locuslink" & id_conversion_table_human[,4] == x[1],2]
> unique(temp)
> }
> test = apply(df,1,getGeneIds)
> findOddOnesOut<-function(x){
> length(x)
> }
> new = lapply(test,findOddOnesOut)
> name=V(all_1hop)$name
> community=V(all_1hop)$community
> all_communities=(name, community)
> community1=all_communities[which (all_communities$community==1),]
> test = apply(community0,1,getGeneIds)
> getGeneIds<-function(x) {
> temp<-id_conversion_table_human[id_conversion_table_human[,1] == "entrezgene/
    locuslink" & id_conversion_table_human[,4] == x[1],2]
> unique(temp)
> }
> test1= apply(community1,1,getGeneIds)
> community0=as.matrix(test)
#Add names
> V(binary_hop)$ID=sapply((V(binary_hop)$name), getGeneIds)
> b=cut(all_degree, breaks=bins)
> df=data.frame(V(graph_binary)$name, all_degree, b)
> df[sample(nrow(df), 5), ]
> bin1 = subset(df, all_degree < 1.5 & all_degree > 1.0, select=Name)
```

A.0.4 Code for bridging centrality

```
> BridgingCentrality = function(node, graph, hops=1){
> neighborhood = unlist(neighborhood(graph,hops,node))
> invdeg=1/(degree(graph, node))
# Degree returns a 'structured' numeric array - it has a name associated with it.
> between=betweenness(graph, node)
> attributes(between) = NULL
> inversedegree = 0
> bridge=0
#Start from 2 because first element in neighborhood of a node is degree of
    original node
> if (length(neighborhood) > 1) {
> for (i in 2:length(neighborhood)) {
> x = 1/(degree(graph, neighborhood[i]))
> attributes(x) = NULL
> inversedegree = inversedegree + x
> }
> }
```

```
> bridge=invdeg/inversedegree
> bridgecen=bridge*between
> bridgecen=unlist(bridgecen)
> return(bridgecen)
> }
```

A.0.5 Code for selective betweenness centrality

```
#Returns betweenness contributions from only paths between nodes sent as terminals
> selectiveBetweenness = function(graph, terminals){
#Creates blank vector to store running sum of contributions
> b = vector(mode='numeric', length = length(V(graph)))
#Sum over i...
> for (i in 1:length(terminals)){
#Sum over j.... ----> Sums over (i,j) pairs - nodes from terminals list.
> for (j in 1:length(terminals)){
> if (i != j){
#Find shortest paths between i and j -
> shortestPaths = get.all.shortest.paths(graph, to=i, from=j)
#Number of paths between i and j - length of get.all.shortest.paths(realGraph, to=
    i, from=j), for normalisation
> g = length(shortestPaths)
#Number of paths between i and j with k in it, each k is one element in the vector
     x (eventually b)
> x = lapply(1:length(V(graph)), countPaths, shortestPaths)
> n = unlist(x)/g
#Add to running sum of contributions
> b = b+n
> }
> }
> }
> table=data.frame(V(graph)$name)
> table$mito_BC = b
> return(table)
> }
#returns list betweenness for each node in network where each pair comes from
    terminals
#Number of paths with node k (see above) involved
> countPaths = function(node, shortestPaths){
> count=0
#[[1]][[1]] is the first member of the shortest path, as we don't want to count
    starts
> start = shortestPaths[[1]][[1]]
#[[1]][[length(shortestPaths[[1]])]] is the last member of the shortest path, as
    we don't want to count ends
> end = shortestPaths[[1]][[length(shortestPaths[[1]])]]
# && --> AND logical operator. So if (X && Y) means if X=TRUE AND Y=TRUE. || is
    the or symbol.
# != is the inverse operator - makes true = false and false = true.
> for (i in 1:length(shortestPaths)){
> if ( node \%in\% unlist(shortestPaths[i]) && node != end && node != start ){
> count = count+1
> }
> }
```

Appendix B

Results of pairwise betweenness centrality analysis

This work was conducted in collaboration with Andrew Elliott. All code was written and executed by Andrew using the networks I had generated and following a joint discussion of potentially interesting analyses. Initially, the top BC nodes in the experimental binary graphs generated by 1-hop and shortest path sampling with ubiquitin removed were calculated (*Table B.1*). To estimate the combinations that would be predicted to disrupt a maximum

Rank	**Path node**	**BC**	**Hop node**	**BC**
1	14-3-3ζ	0.0445	ABL1	0.1448
2	TRAF6	0.0402	GRB2	0.0510
3	GRB2	0.0396	Fyn	0.0479
4	IKKE	0.0337	Parkin	0.0433
5	SMAD2	0.0267	Src	0.0431
6	ABL1	0.0257	α-synuclein	0.0423
7	Src	0.0233	EGFR	0.0301
8	P53	0.0220	14-3-3ζ	0.0281
9	RB	0.0205	TRAF6	0.0265
10	CTNB1	0.0177	P53	0.0263
11	EGFR	0.0174	Tau	0.0239
12	ANDR	0.0157	SODM	0.0219
13	icrogid:9975260	0.0151	MMP3	0.0213
14	HDAC1	0.0147	VDAC1	0.0197
15	GBRL2	0.0146	GBRL2	0.0190
16	CRCM	0.0138	Caspase-3	0.0183
17	1B42	0.0134	Beclin	0.0178
18	α-synuclein	0.0126	P85A	0.0177
19	Fyn	0.0117	LC3	0.0168
20	icrogid:9983216	0.0117	CTNB1	0.0162

Table B.1: **Top individual node BC.** Top individual node BCs were calculated in networks generated using 1-hop or shortest-path methods.

number of shortest paths the groupwise BC of a set of nodes w was defined as:

$$BC(w) = \sum_{i=1}^{w} \sum_{v \in S_i^{|w|}} (-1)^{i+1} \sum_{a \neq b} \frac{\gamma_{ab}(v)}{\gamma_{ab}} \tag{B.1}$$

Where S_i^w is the set of all subsets of w that are of length i. The pairwise BC of all node pairs in the sampled 1-hop and shortest-path experimental binary networks with ubiquitin removed were calculated. These values were ranked and the top 15 pairs listed, this ranking was compared to the ranking obtained by summing individual BC values (*Table B.2*).

Rank	Path calculated	Path expected	Hop calculated	Hop expected
1	1,2	1,2	1,2	1,2
2	1,3	1,3	1,3	1,3
3	2,3	2,3	1,6	1,4
4	1,4	1,4	1,5	1,5
5	2,4	2,4	1,4	1,6
6	1,5	3,4	1,7	1,7
7	3,4	1,5	1,9	1,8
8	1,6	1,6	1,8	1,9
9	1,7	1,7	1,11	1,10
10	2,5	2,5	1,10	1,11
11	3,5	1,8	1,12	1,12
12	2,6	3,5	1,13	1,13
13	1,8	2,6	1,14	1,14
14	1,9	3,6	1,15	1,15
15	3,6	1,9	1,16	1,16

Table B.2: **Top pairwise BC combinations.** Top pairwise combinations of nodes were predicted in the experimental binary graphs sampled using 1-hop or shortest-path methods. Effect was measured as the number of network shortest paths effected by deletion. Predicted values are from summation of individual BC values. Calculated values were generated using *Equation B.1.*

Bibliography

[1] L M L de Lau and M M B Breteler. Epidemiology of Parkinson disease. *Lancet Neurol.*, 5:525–535, January 2006.

[2] M C de Rijk, M M B Breteler, G A Graveland, A Ott, D E Grobbee, F G A van der Meche, and A Hofman. Prevalence of Parkinson's disease in the elderly: The Rotterdam Study. *Neurology*, 45(12):2143–2146, December 1995.

[3] M J Farrer. Genetics of Parkinson disease: paradigm shifts and future prospects. *Nat. Rev. Genet.*, 7(4):306–18, April 2006.

[4] E R Dorsey, R Constantinescu, J P Thompson, K M Biglan, R G Holloway, K Kieburtz, F J Marshall, B M Ravina, G Schifitto, a Siderowf, and C M Tanner. Projected number of people with Parkinson disease in the most populous nations, 2005 through 2030. *Neurology*, 68(5):384–6, January 2007.

[5] J Jankovic. Parkinson's disease: clinical features and diagnosis. *JNNP*, 79(4):368–76, May 2008.

[6] J A Obeso, M Cruz Rodríguez-Oroz, B Benitez-Temino, F J Blesa, J Guridi, C Marin, and M Rodriguez. Functional organization of the basal ganglia: therapeutic implications for Parkinson's disease. *Movement Disord.*, 23 Suppl 3:S548–59, January 2008.

[7] P Anglade, S Vyas, M T Herrero, P P Michel, J Marquez, M Ruberg, E C Hirsch, and Y Agid. Apoptosis and autophagy in nigral neurons of patients with Parkinson's disease. *Histol. Histopathol.*, 1:25–31, 1997.

[8] H Braak, K Del Tredici, U Rüb, R A I de Vos, E N H Jansen Steur, and E Braak. Staging of brain pathology related to sporadic Parkinson's disease. *Neurobiol. Aging*, 24(2):197–211, March 2003.

[9] M Grazia Spillantini, M L Schmidt, V M Y Lee, J Q Trojanowski, R Jakes, and M Goedert. α-Synuclein in Lewy bodies. *Nature*, 388:839–840, 1997.

[10] J M Fearnley and A J Lees. Ageing and Parkinson's disease: substantia nigra regional selectivity. *Brain*, 114(5):2283–2301, 1991.

[11] T Gonzalez-Hernandez, D Afonso-Oramas, and I Cruz-Muros. Phenotype, compartmental organization and differential vulnerability of nigral dopaminergic neurons. *J. Neural Transm.*, 73:21–37, 2009.

[12] H Braak, E Ghebremedhin, U Rüb, H Bratzke, and K Del Tredici. Stages in the development of Parkinson's disease-related pathology. *Cell Tissue Res.*, 318(1):121–34, October 2004.

[13] J M Milber, J V Noorigian, J F Morley, H Petrovitch, L White, G W Ross, and J E Duda. Lewy pathology is not the first sign of degeneration in vulnerable neurons in Parkinson disease. *Neurology*, 79(24):2307–14, December 2012.

[14] N P Visanji, P L Brooks, L Hazrati, and A E Lang. The prion hypothesis in Parkinson's disease: Braak to the future. *Acta Neuropathol.*, 1(1):2, January 2013.

[15] S Lesage and A Brice. Parkinson's disease: from monogenic forms to genetic susceptibility factors. *Hum. Mol. Genet.*, 18(R1):R48–59, April 2009.

[16] J Trinh and M Farrer. Advances in the genetics of Parkinson disease. *Nat. Rev. Neurol.*, 9(8):445–54, August 2013.

[17] McKusick-Nathans Institute of Genetic Medicine. Online Mendelian Inheritance in Man, 2013.

[18] D Crosiers, J Theuns, P Cras, and C Van Broeckhoven. Parkinson disease: insights in clinical, genetic and pathological features of monogenic disease subtypes. *J. Chem. Neuroanat.*, 42(2):131–41, October 2011.

[19] M H Polymeropoulos. Mutation in the α-synuclein gene identified in families with Parkinson's disease. *Science*, 276(5321):2045–2047, June 1997.

[20] A B Singleton, M Farrer, J Johnson, A Singleton, S Hague, J Kachergus, M Hulihan, T Peuralinna, A Dutra, R Nussbaum, S Lincoln, A Crawley, M Hanson, D Maraganore, C Adler, M R Cookson, M Muenter, M Baptista, D Miller, J Blancato, and J Hardy. α-Synuclein locus triplication causes Parkinson's disease. *Science*, 302:841, 2003.

[21] M C Chartier-Harlin, J Kachergus, C Roumier, V Mouroux, X Douay, S Lincoln, C Levecque, L Larvour, J Andrieux, M Hulihan, and W Nawal. α-Synuclein locus duplication as a cause of familial Parkinson's disease. *Lancet*, 364:1167–1169, 2004.

[22] C Paisan-Ruiz, S Jain, E W Evans, W P Gilks, J Simon, M van der Brug, A Lopez de Munain, S Aparicio, A Martinez Gil, N Khan, J Johnson, J Ruiz Martinez, D Nicholl, I Marti Carrera, A Saenz Pena, R de Silva, A Lees, J F Marti-Masso, J Perez-Tur, N W Wood, and A B Singleton. Cloning of the gene containing mutations that cause PARK8-linked Parkinso's disease. *Neuron*, 44:595–600, 2004.

[23] A Zimprich, S Biskup, P Leitner, P Lichtner, M Farrer, S Lincoln, J Kachergus, M Hulihan, R J Uitti, D B Calne, A J Stoessl, R F Pfeiffer, N Patenge, I C Carbajal, P Vieregge, F Asmus, B Müller-Myhsok, D W Dickson, T Meitinger, T M Strom, Z K Wszolek, and T Gasser. Mutations in LRRK2 cause autosomal-dominant Parkinsonism with pleomorphic pathology. *Neuron*, 44(4):601–7, November 2004.

[24] D G Healy, M Falchi, S S O'Sullivan, V Bonifati, A Durr, S Bressman, A Brice, J Aasly, C P Zabetian, S Goldwurm, J J Ferreira, E Tolosa, D M Kay, C Klein, D R Williams, C Marras, A E Lang, Z K Wszolek, J Berciano, A H V Schapira, T Lynch, K P Bhatia, T Gasser, A J Lees, and N W Wood. Phenotype, genotype, and worldwide genetic penetrance of LRRK2-associated Parkinson's disease: a case-control study. *Lancet Neurol.*, 7(7):583–90, July 2008.

[25] E M Valente, P M Abou-Sleiman, V Caputo, M M K Muqit, K Harvey, S Gispert, Z Ali, D Del Turco, A Bentivoglio, D G Healy, A Albanese, R Nussbaum, R González-Maldonado, T Deller, S Salvi, P Cortelli, W P Gilks, D S Latchman, R J Harvey, B Dallapiccola, G Auburger, and N W Wood. Hereditary early-onset Parkinson's disease caused by mutations in PINK1. *Science*, 304(5674):1158–60, May 2004.

[26] T Kitada, S Asakawa, N Hattori, H Matsumine, Y Yamamura, S Minoshima, M Yokochi, Y Mizuno, and N Shimizu. Mutations in the parkin gene cause autosomal recessive juvenile Parkinsonism. *Nature*, 169(1993):166–169, 1998.

[27] V Bonifati, P Rizzu, M J van Baren, O Schaap, G J Breedveld, E Krieger, M C J Dekker, F Squitieri, P Ibanez, M Joosse, J W van Dongen, N Vanacore, J C van Swieten, A Brice, G Meco, C M van Duijn, B A Oostra, and P Heutink. Mutations in the DJ-1 gene associated with autosomal recessive early-onset Parkinsonism. *Science*, 299(5604):256–9, January 2003.

[28] E Leroy, R Boyer, G Auberger, B Leube, G Ulm, E Mezey, G Harta, M J Brownstein, S Jonnalagada, T Chernova, A Dehejia, C Lavedan, T Gasser, P J Steinbach, K D Wilkinson, and M H Polymeropoulos. The ubiquitin pathway in Parkinson's disease. *Nature*, 395:451–452, 1998.

[29] A Ramirez, A Heimbach, J Gründemann, B Stiller, D Hampshire, L P Cid, I Goebel, A F Mubaidin, A L Wriekat, J Roeper, A Al-Din, A M Hillmer, M Karsak, B Liss, C G Woods, M I Behrens, and C Kubisch. Hereditary Parkinsonism with dementia is caused by mutations in ATP13A2, encoding a lysosomal type 5 P-type ATPase. *Nat. Genet.*, 38(10):1184–91, October 2006.

[30] C M Lill, J T Roehr, M B McQueen, F K Kavvoura, S Bagade, B M Schjeide, L M Schjeide, E Meissner, U Zauft, N C Allen, T Liu, M Schilling, K J Anderson, G Beecham, D Berg, J M Biernacka, A Brice, A L DeStefano, C B Do, N Eriksson, S A Factor, M J Farrer, T Foroud, T Gasser, T Hamza, J A Hardy, P Heutink, E M Hill-Burns, C Klein, J C Latourelle, D M Maraganore, E R Martin, M Martinez, R H Myers, M A Nalls, N Pankratz, H Payami, W Satake, W K Scott, M Sharma, A B Singleton, K Stefansson, T Toda, J Y Tung, J Vance, N W Wood, C P Zabetian, P Young, R E Tanzi, M J Khoury, F Zipp, H Lehrach, J P A Ioannidis, and L Bertram. Comprehensive research synopsis and systematic meta-analyses in Parkinson's disease genetics: The PDGene database. *PLoS Genet.*, 8(3):e1002548, January 2012.

[31] M A Nalls, N Pankratz, C M Lill, C B Do, D G Hernandez, M Saad, A L DeStefano, E Kara, J Bras, M Sharma, C Schulte, M F Keller, S Arepalli, C Letson, C Edsall, H Stefansson, X Liu, H Pliner, J H Lee, R Cheng, M A Ikram, J P A Ioannidis, G M Hadjigeorgiou, J C Bis, M Martinez, J S Perlmutter, A Goate, K Marder, B Fiske, M Sutherland, G Xiromerisiou, R H Myers, L N Clark, K Stefansson, J A Hardy, P Heutink, H Chen, N W Wood, H Houlden, H Payami, A Brice, W K Scott, T Gasser, L Bertram, N Eriksson, T Foroud, and A B Singleton. Large-scale meta-analysis of genome-wide association data identifies six new risk loci for Parkinson's disease. *Nat. Genet.*, 056:1–7, July 2014.

[32] J Simón-Sánchez, C Schulte, J M Bras, M Sharma, J R Gibbs, D Berg, C Paisan-Ruiz, P Lichtner, S W Scholz, D G Hernandez, R Krüger, M Federoff, C Klein, A Goate, J Perlmutter, M Bonin, M A Nalls, T Illig, C Gieger, H Houlden, M Steffens, M S Okun, B A Racette, M R Cookson, K D Foote, H H Fernandez, B J Traynor, S Schreiber, S Arepalli, R Zonozi, K Gwinn, M van der Brug, G Lopez, S J Chanock, A Schatzkin, Y Park, A Hollenbeck, J Gao, X Huang, N W Wood, D Lorenz, G Deuschl, H Chen, O Riess, J A Hardy, A B Singleton, and T Gasser. Genome-wide association study reveals genetic risk underlying Parkinson's disease. *Nat. Genet.*, 41(12):1308–12, December 2009.

[33] W Satake, Y Nakabayashi, I Mizuta, Y Hirota, C Ito, M Kubo, T Kawaguchi, T Tsunoda, M Watanabe, A Takeda, H Tomiyama, K Nakashima, K Hasegawa, F Obata, T Yoshikawa, H Kawakami, S Sakoda, M Yamamoto, N Hattori, M Murata, Y Nakamura, and T Toda. Genome-wide association study identifies common variants at four loci as genetic risk factors for Parkinson's disease. *Nat. Genet.*, 41(12):1303–7, December 2009.

[34] T Peeraully and E K Tan. Genetic variants in sporadic Parkinson's disease: East vs West. *Parkinsonism Rel. Disord.*, 18 Suppl 1:S63–5, January 2012.

[35] C B Do, J Y Tung, E Dorfman, A K Kiefer, E M Drabant, U Francke, J L Mountain, S M Goldman, C M Tanner, J W Langston, A Wojcicki, and N Eriksson. Web-based genome-wide association study identifies two novel loci and a substantial genetic component for Parkinson's disease. *PLoS Genet.*, 7(6):e1002141, June 2011.

[36] P Holmans, V Moskvina, L Jones, M Sharma, A Vedernikov, F Buchel, M Saad, J M Bras, F Bettella, N Nicolaou, J Simón-Sánchez, F Mittag, J R Gibbs, C Schulte, A Durr, R Guerreiro, D Hernandez, A Brice, H Stefánsson, K Majamaa, T Gasser, P Heutink, N W Wood, M Martinez, A B Singleton, M A Nalls, J Hardy, H R Morris, and N M Williams. A pathway-based analysis provides additional support for an immune-related genetic susceptibility to Parkinson's disease. *Hum. Mol. Genet.*, 22(5):1039–49, March 2013.

[37] E M Hill-Burns, W T Wissemann, T H Hamza, S A Factor, C P Zabetian, and H Payami. Identification of a novel Parkinson's disease locus via stratified genome-wide association study. *BMC genomics*, 15(1):118, January 2014.

[38] A McNeill, J Magalhaes, C Shen, K Y Chau, D Hughes, A Mehta, T Foltynie, J M Cooper, A Y Abramov, M Gegg, and A H V Schapira. Ambroxol improves lysosomal biochemistry in glucocerebrosidase mutation-linked Parkinson disease cells. *Brain*, 137(Pt 5):1481–95, May 2014.

[39] W C Nichols, N Pankratz, D K Marek, M W Pauciulo, V E Elsaesser, C A Halter, A Rudolph, J Wojcieszek, R F Pfeiffer, and T Foroud. Mutations in GBA are associated with familial Parkinson disease susceptibility and age at onset. *Neurology*, 72(4):310–6, January 2009.

[40] K Kieburtz and K B Wunderle. Parkinson's disease: evidence for environmental risk factors. *Movement Disord.*, 28(1):8–13, January 2013.

[41] G F Wooten. Are men at greater risk for Parkinson's disease than women? *J. Neurol. Neurosurg. Psychiatry*, 75(4):637–639, April 2004.

[42] M A Hernán, B Takkouche, F Caamaño Isorna, and J J Gestal-Otero. A meta-analysis of coffee drinking, cigarette smoking, and the risk of Parkinson's disease. *Ann. Neurol.*, 52(3):276–84, September 2002.

[43] K M Powers, D M Kay, S A Factor, C P Zabetian, D S Higgins, A Samii, J G Nutt, A Griffith, B Leis, J W Roberts, E D Martinez, J S Montimurro, H Checkoway, and H Payami. Combined effects of smoking, coffee, and NSAIDs on Parkinson's disease risk. *Movement Disord.*, 23(1):88–95, January 2008.

[44] P R Smith, J M Cooper, G G Govan, and A E Harding. Smoking and mitochondrial function: a model for environmental toxins. *QJM*, 86:657–660, 1993.

[45] C M Tanner, F Kamel, G W Ross, J A Hoppin, S M Goldman, M Korell, C Marras, G S Bhudhikanok, M Kasten, A R Chade, K Comyns, M Barber Richards, C Meng, B Priestley, H H Fernandez, F Cambi, D M Umbach, A Blair, D P Sandler, and J W Langston. Rotenone, paraquat, and Parkinson's disease. *Environ. Health Persp.*, 119(6):866–72, June 2011.

[46] S M Goldman, F Kamel, G W Ross, S A Jewell, G S Bhudhikanok, D Umbach, C Marras, R A Hauser, J Jankovic, S A Factor, S Bressman, K E Lyons, C Meng, M Korell, D F Roucoux, J A Hoppin, D P Sandler, J W Langston, and C M Tanner. Head injury, α-synuclein Rep1, and Parkinson's disease. *Ann. Neurol.*, 71(1):40–8, January 2012.

[47] J H Bower, D M Maraganore, B J Peterson, S K McDonnell, J E Ahlskog, and W A Rocca. Head trauma preceding PD: A case-control study. *Neurology*, 60(10):1610–1615, May 2003.

[48] K Takahashi and S Yamanaka. Induction of pluripotent stem cells from mouse embryonic and adult fibroblast cultures by defined factors. *Cell*, 126(4):663–76, August 2006.

[49] K Takahashi, K Tanabe, M Ohnuki, M Narita, T Ichisaka, K Tomoda, and S Yamanaka. Induction of pluripotent stem cells from adult human fibroblasts by defined factors. *Cell*, 131(5):861–72, November 2007.

[50] I H Park, N Arora, H Huo, N Maherali, T Ahfeldt, A Shimamura, M W Lensch, C Cowan, K Hochedlinger, and G Q Daley. Disease-specific induced pluripotent stem cells. *Cell*, 134(5):877–86, September 2008.

[51] S Kriks, J W Shim, J Piao, Y M Ganat, D R Wakeman, Z Xie, L Carrillo-Reid, G Auyeung, C Antonacci, A Buch, L Yang, M Flint Beal, D J Surmeier, J H Kordower, V Tabar, and L Studer. Dopamine neurons derived from human ES cells efficiently engraft in animal models of Parkinson's disease. *Nature*, 480(7378):547–51, December 2011.

[52] V A Morais, D Haddard, K Craesserts, P J De Bock, J Swerts, S Vilain, L Aerts, L Overbergh, A Grunewald, P Seibler, C Klein, K Gevaert, P Verstreken, and B De Strooper. PINK1 loss of function mutations affect mitochondrial complex I activity via NdufA10 ubiquinone uncoupling. *Science*, 322:203–207, 2014.

[53] H N Nguyen, B Byers, B Cord, A Shcheglovitov, J Byrne, P Gujar, K Kee, B Schüle, R E Dolmetsch, W Langston, T D Palmer, and R R Pera. LRRK2 mutant iPSC-derived DA neurons demonstrate increased susceptibility to oxidative stress. *Cell Stem Cell*, 8(3):267–80, March 2011.

[54] H Jiang, Y Ren, E Y Yuen, P Zhong, M Ghaedi, Z Hu, G Azabdaftari, K Nakaso, Z Yan, and J Feng. Parkin controls dopamine utilization in human midbrain dopaminergic neurons derived from induced pluripotent stem cells. *Nat. Comm.*, 3:668, January 2012.

[55] O Cooper, H Seo, S Andrabi, C Guardia-Laguarta, J Graziotto, M Sundberg, J R McLean, L Carrillo-Reid, Z Xie, T Osborn, G Hargus, M Deleidi, T Lawson, H Bogetofte, E Perez-Torres, L Clark, C Moskowitz, J Mazzulli, L Chen, L Volpicelli-Daley, N Romero, H Jiang, R J Uitti, Z Huang, G Opala, L A Scarffe, V L Dawson, C Klein, J Feng, O A Ross, J Q Trojanowski, V M Y Lee, K Marder, D J Surmeier, Z K Wszolek, S Przedborski, D Krainc, T. M. Dawson, and O. Isacson. Pharmacological rescue of mitochondrial deficits in iPSC-derived neural cells from patients with familial Parkinson's disease. *Sci. Transl. Med.*, 4(141):141ra90–141ra90, July 2012.

[56] S J Orenstein, S H Kuo, I Tasset, E Arias, H Koga, I Fernandez-Carasa, E Cortes, L S Honig, W Dauer, A Consiglio, A Raya, D Sulzer, and A M Cuervo. Interplay of LRRK2 with chaperone-mediated autophagy. *Nat. Neurosci.*, 16(4):394–406, March 2013.

[57] D C Schöndorf, M Aureli, F E McAllister, C J Hindley, F Mayer, B Schmid, S P Sardi, M Valsecchi, S Hoffmann, L K Schwarz, U Hedrich, D Berg, L S Shihabuddin, J Hu, J Pruszak, S P Gygi, S Sonnino, T Gasser, and M Deleidi. iPSC-derived neurons from GBA1-associated Parkinson's disease patients show autophagic defects and impaired calcium homeostasis. *Nat. Comm.*, 5:4028, January 2014.

[58] F Soldner, J Laganière, A W Cheng, D Hockemeyer, Q Gao, R Alagappan, V Khurana, L I Golbe, R H Myers, S Lindquist, L Zhang, D Guschin, L K Fong, B J Vu, X Meng, F D Urnov, E J Rebar, P D Gregory, H S Zhang, and R Jaenisch. Generation of isogenic pluripotent stem cells differing exclusively at two early onset Parkinson point mutations. *Cell*, 146(2):318–31, July 2011.

[59] A Sánchez-Danés, Y Richaud-Patin, I Carballo-Carbajal, S Jiménez-Delgado, C Caig, S Mora, C Di Guglielmo, M Ezquerra, B Patel, A Giralt, J M Canals, M Memo, J Alberch, J López-Barneo, M Vila, A M Cuervo, E Tolosa, A Consiglio, and A Raya. Disease-specific phenotypes in dopamine neurons from human iPS-based models of genetic and sporadic Parkinson's disease. *EMBO Mol. Med.*, pages 1–16, March 2012.

[60] F Soldner, D Hockemeyer, C Beard, Q Gao, G W Bell, E G Cook, G Hargus, A Blak, O Cooper, M Mitalipova, O Isacson, and R Jaenisch. Parkinson's disease patient-derived induced pluripotent stem cells free of viral reprogramming factors. *Cell*, 136(5):964–77, March 2009.

[61] J L Badger, O Cordero-Llana, E M Hartfield, and R Wade-Martins. Parkinson's disease in a dish - Using stem cells as a molecular tool. *Neuropharmacology*, 76 Pt A:88–96, January 2014.

[62] B M Jacobs. Stemming the hype: what can we learn from iPSC models of Parkinson's disease and how can we learn it? *J. Parkinsons Dis.*, 4(1):15–27, January 2014.

[63] G Liang and Y Zhang. Genetic and epigenetic variations in iPSCs: potential causes and implications for application. *Cell stem cell*, 13(2):149–59, August 2013.

[64] K Kim, A Doi, B Wen, K Ng, R Zhao, P Cahan, J Kim, M J Aryee, H Ji, L I R Ehrlich, A Yabuuchi, A Takeuchi, K C Cunniff, H Hongguang, S McKinney-Freeman, O Naveiras, T J Yoon, R A Irizarry, N Jung, J Seita, J Hanna, P Murakami, R Jaenisch, R Weissleder, S H Orkin, I L Weissman, A P Feinberg, and G Q Daley. Epigenetic memory in induced pluripotent stem cells. *Nature*, 467(7313):285–90, September 2010.

[65] B Y Hu, J P Weick, J Yu, L X Ma, X Q Zhang, J A Thomson, and S C Zhang. Neural differentiation of human induced pluripotent stem cells follows developmental principles but with variable potency. *PNAS*, 107(9):4335–40, March 2010.

[66] J Bové and C Perier. Neurotoxin-based models of Parkinson's disease. *Neuroscience*, 211:51–76, November 2012.

[67] G C Davis, A C Williams, S P Markey, M H Ebert, E D Caine, C M Reichert, and I J Kopin. Chronic Parkinsonism secondary to intravenous injection of meperidine analogues. *Psychiat. Res.*, 1(3):249–54, December 1979.

[68] R S Burns, P A LeWitt, M H Ebert, H Pakkenberg, and I J Kopin. The clinical syndrome of striatal dopamine deficiency Parkinsonism induced by 1-methyl-4-phenyl-1,2,3,6-tetrahydopyridine (MPTP). *N. Engl. J. Med.*, 312:1418–1421, 1985.

[69] S P Markey, J N Johannessen, C C Chiueh, R S Burns, and M A Herkenham. Intraneuronal generation of a pyridinium metabolite may cause drug-induced parkinsonism. *Nature*, 311(4):464–467, 1984.

[70] J A Javitch, R J D Amato, S M Strittmatter, and S H Snyder. Parkinsonism-inducing neurotoxin, N-methyl-4-phenyl-1,2,3,6-tetrahydropyridine: Uptake of the metabolite N-methyl-4-phenylpyridine by dopamine neurons explains selective toxicity. *PNAS*, 82(April):2173–2177, 1985.

[71] R R Ramsay, J I Salach, and T P Singer. Uptake of the neurotoxin 1-methyl-4-phenylpyridine (MPP+) by mitochondria and its relation to the inhibition of the mitochondrial oxdiation of NAD+-linked substrates by MPP+. *Biochem. Bioph. Res. Co.*, 134(2):743–748, 1986.

[72] R R Ramsay and T P Singer. Energy-dependent uptake of N-methyl-4-phenylpyridinium, the neurotoxic metabolite of 1-methyl-4-phenyl-1,2,3,6-tetrahydropyridine, by mitochondria. *J. Biol. Chem.*, 261(17):7585–7587, 1986.

[73] T P Singer, R R Ramsay, K McKeown, T Trevor, and J R Castagnoli. Mechanism of the neurotoxicity of 1-methyl-4-phenylpyridinium (MPP+), the toxic bioactivation product of 1-methyl-4-phenyl-1,2,3,6-tetrahydropyridine (MPTP). *Toxicology*, 49:17–23, 1988.

[74] C H Pifl, G Schingnitz, and O Hornykiewicz. Effect of 1-Methyl-4-Phenyl-1,2,3,6-tetrahydropyridine on the regional distribution of brain monoaimes in the Rhesus monkey. *Nueoroscience*, 44(3):591–605, 1991.

[75] G Halliday, M T Herrero, K Murphy, H McCann, F Ros-Bernal, C Barcia, H Mori, F J Blesa, and J A Obeso. No Lewy pathology in monkeys with over 10 years of severe MPTP Parkinsonism. *Movement Disord.*, 24(10):1519–23, July 2009.

[76] M G Purisai, A L McCormack, W J Langston, L C Johnston, and D A Di Monte. α-Synuclein expression in the substantia nigra of MPTP-lesioned non-human primates. *Neurobiol. Dis.*, 20(3):898–906, December 2005.

[77] M Vila, S Vukosavic, V Jackson-Lewis, M Neystat, M Jakowec, and S Przedborski. α-Synuclein up-regulation in substantia nigra dopaminergic neurons following administration of the parkinsonian toxin MPTP. *J. Neurochem.*, 74(2):721–9, February 2000.

[78] G Porras, Q Li, and E Bezard. Modeling Parkinson's disease in primates: The MPTP model. *Cold Spring Harb. Perspect. Med.*, 2(3):a009308, March 2012.

[79] B J Ryan, L Lourenço-Venda, M J Crabtree, A B Hale, K M Channon, and R Wade-Martins. α-Synuclein and mitochondrial bioenergetics regulate tetrahydrobiopterin levels in a human dopaminergic model of Parkinson disease. *Free Radic. Biol. Med.*, 67:58–68, October 2014.

[80] K M Pettifer, S Jiang, C Bau, P Ballerini, I D'Alimonte, E S Werstiuk, and M P Rathbone. MPP(+)-induced cytotoxicity in neuroblastoma cells: Antagonism and reversal by guanosine. *Purinergic signalling*, 3(4):399–409, September 2007.

[81] J R Cannon, V M Tapias, H M Na, A S Honick, R E Drolet, and J T Greenamyre. A higly reproducible rotenone model of Parkinson's disease. *Neurobiol. Dis.*, 34(2):279–290, 2009.

[82] T B Sherer, J H Kim, R Betarbet, and J T Greenamyre. Subcutaneous rotenone exposure causes highly selective dopaminergic degeneration and α-synuclein aggregation. *Exp. Neurol.*, 179(1):9–16, January 2003.

[83] J Blesa, S Phani, V Jackson-Lewis, and S Przedborski. Classic and new animal models of Parkinson's disease. *J. Biomed. Biotechnol.*, page 845618, January 2012.

[84] R Andrew, D G Watson, S A Best, J M Midgley, H Wenlong, and R K H Petty. The determination of hydroxydopamines and other trace amines in the urine of parkinsonian patients and normal controls. *Neurochem. Res.*, 18(11):1175–1177, 1993.

[85] D Alvarez-Fischer, C Henze, C Strenzke, J Westrich, B Ferger, G U Höglinger, W H Oertel, and A Hartmann. Characterization of the striatal 6-OHDA model of Parkinson's disease in wild type and α-synuclein-deleted mice. *Exp. Neurol.*, 210(1):182–93, March 2008.

[86] R Soto-Otero, M Mendez-Alverez, A Hermida-Ameijeiras, A M Munoz-Patino, and J L Labandeira-Garcia. Autoxidation and neurotoxicity of 6-hydroxydopamine in the presence of some antioxidants: potential implication in relation to the pathogenesis of Parkinson's disease. *J. Neurochem.*, 74:1605–1612, 2000.

[87] M Asanuma, H Hirata, and J L Cadet. Attenuation of 6-hydroxydopamine-induced dopaminergic nigrostriatal lesions in superoxide dismutase transgenic mice. *Neuroscience*, 85(3):907–17, August 1998.

[88] S Giordano, J Lee, Vi M Darley-Usmar, and J Zhang. Distinct Effects of Rotenone, 1-methyl-4-phenylpyridinium and 6-hydroxydopamine on cellular bioenergetics and cell death. *PloS One*, 7(9):e44610, January 2012.

[89] T F Outeiro and S Lindquist. Yeast cells provide insight into α-synuclein biology and pathobiology. *Science*, 302(5651):1772–5, December 2003.

[90] A A Cooper, A D Gitler, A Cashikar, C M Haynes, K J Hill, B Bhullar, K Liu, K Xu, K E Strathearn, F Liu, S Cao, K A Caldwell, G A Caldwell, G Marsischky, R D Kolodner, J Labaer, J C Rochet, N M Bonini, and S Lindquist. α-Synuclein blocks ER-Golgi traffic and Rab1 rescues neuron loss in Parkinson's models. *Science*, 313(5785):324–8, July 2006.

[91] A D Gitler, A Chesi, M L Geddie, K E Strathearn, S Hamamichi, K J Hill, K A Caldwell, G A Caldwell, A A Cooper, J C Rochet, and S Lindquist. α-Synuclein is part of a diverse and highly conserved interaction network that includes PARK9 and manganese toxicity. *Nat. Genet.*, 41(3):308–15, March 2009.

[92] L J Su, P K Auluck, T F Outeiro, E Yeger-Lotem, J A Kritzer, D F Tardiff, K E Strathearn, F Liu, S Cao, S Hamamichi, K J Hill, K A Caldwell, G W Bell, E Fraenkel, A A Cooper, G A Caldwell, J M McCaffery, J C Rochet, and S Lindquist. Compounds from an unbiased chemical screen reverse both ER-to-Golgi trafficking defects and mitochondrial dysfunction in Parkinson's disease models. *Dis. Model Mech.*, 3(3-4):194–208, 2010.

[93] D F Tardiff, N T Jui, V Khurana, M A Tambe, M L Thompson, C Y Chung, H B Kamadurai, H T Kim, A K Lancaster, K A Caldwell, G A Caldwell, J C Rochet, S L Buchwald, and S Lindquist. Yeast reveal a 'druggable' Rsp5/Nedd4 network that ameliorates α-synuclein toxicity in neurons. *Science*, 342(6161):979–83, November 2013.

[94] C Y Chung, V Khurana, P K Auluck, D F Tardiff, J R Mazzulli, F Soldner, V Baru, Y Lou, Y Freyzon, S Cho, A E Mungenast, J Muffat, M Mitalipova, M D Pluth, N T Jui, B Schüle, S J Lippard, L H Tsai, D Krainc, S L Buchwald, R Jaenisch, and S Lindquist. Identification and rescue of α-synuclein toxicity in Parkinson patient-derived neurons. *Science*, 342(6161):983–7, November 2013.

[95] A L Barabási and Z N Oltvai. Network biology: understanding the cell's functional organization. *Nat. Rev. Genet.*, 5(2):101–13, February 2004.

[96] A L Barabási, N Gulbahce, and J Loscalzo. Network medicine: a network-based approach to human disease. *Nat. Rev. Genet.*, 12(1):56–68, January 2011.

[97] W Dauer, N Kholodilov, M Vila, A C Trillat, R Goodchild, K E Larsen, R Staal, K Tieu, Y Schmitz, C A Yuan, M Rocha, V Jackson-Lewis, S Hersch, D Sulzer, S Przedborski, R Burke, and R Hen. Resistance of α-synuclein null mice to the parkinsonian neurotoxin MPTP. *PNAS*, 99(22):14524–9, October 2002.

[98] S V Kalivendi, S Kotamraju, S Cunningham, T Shang, C J Hillard, and B Kalyanaraman. 1-Methyl-4-phenylpyridinium (MPP+)-induced apoptosis and mitochondrial oxidant generation: role of transferrin-receptor-dependent iron and hydrogen peroxide. *Biochem. J.*, 164:151–164, 2003.

[99] Z L Cai, J J Shi, Y P Yang, B Y Cao, F Wang, J Z Huang, F Yang, P Zhang, and C F Liu. MPP+ impairs autophagic clearance of α-synuclein by impairing the activity of dynein. *Neuroreport*, 20(6):569–73, April 2009.

[100] M Su, J J Shi, Y P Yang, J Li, Y L Zhang, J Chen, L F Hu, and C F Liu. HDAC6 regulates aggresome-autophagy degradation pathway of α-synuclein in response to MPP+ induced stress. *J. Neurochem.*, 117:112–120, 2011.

[101] M R Cookson. α-Synuclein and neuronal cell death. *Mol. Neurodegener.*, 4:9, January 2009.

[102] R Rott, R Szargel, J Haskin, R Bandopadhyay, and A J Lees. α-Synuclein fate is determined by USP9X-regulated monoubiquitination. *PNAS*, 108(46):1–6, 2011.

[103] K Y Chau, J M Cooper, and A V Schapira. Pramipexole reduces phosphorylation of α-synuclein at serine-129. *J. Mol. Neurosci.*, 51(2):573–80, October 2013.

[104] D H Choi, Y S Y J Y G Kim, T H Joh, and M Flint Beal. Role of matrix metalloproteinase 3-mediated α-synuclein cleavage in dopaminergic cell death. *J. Biol. Chem.*, 286(16):14168–77, April 2011.

[105] K C Luk, C Song, P O'Brien, A Stieber, J R Branch, K R Brunden, J Q Trojanowski, and V M Y Lee. Exogenous α-synuclein fibrils seed the formation of Lewy body-like intracellular inclusions in cultured cells. *PNAS*, 106(47):20051–6, November 2009.

[106] K A Conway, S J Lee, J C Rochet, T T Ding, R E Williamson, and P T Lansbury. Acceleration of oligomerization, not fibrillization, is a shared property of both α-synuclein mutations linked to early-onset Parkinsons disease: Implications for pathogenesis and therapy. *PNAS*, 97(2):571–576, 2000.

[107] G K Tofaris and M G Spillantini. Physiological and pathological properties of α-synuclein. *Cell Mol. Life Sci.*, 64(17):2194–201, September 2007.

[108] C R Bodner, C M Dobson, and A Bax. Multiple tight phospholipid-binding modes of α-synuclein revealed by solution NMR spectroscopy. *J. Mol. Biol.*, 390(4):775–90, July 2009.

[109] T Bartels, J G Choi, and D J Selkoe. α-Synuclein occurs physiologically as a helically folded tetramer that resists aggregation. *Nature*, 477(7362):107–10, September 2011.

[110] J Burré, S Vivona, J Diao, M Sharma, A T Brunger, and Thomas C Südhof. Properties of native brain α-synuclein. *Nature*, 498(7453):E4–7, June 2013.

[111] L Lourenço Venda, S J Cragg, V L Buchman, and R Wade-Martins. α-Synuclein and dopamine at the crossroads of Parkinson's disease. *Trends Neurosci.*, 33(12):559–68, December 2010.

[112] J Burré, M Sharma, T Tsetsenis, V Buchman, M R Etherton, and T C Südhof. α-Synuclein promotes SNARE-complex assembly in vivo and in vitro. *Science*, 329(5999):1663–7, September 2010.

[113] T C Südhof and J Rizo. Synaptic vesicle exocytosis. *Cold Spring Harb. Perspect. Biol.*, 3(12), December 2011.

[114] T M Fountaine and R Wade-Martins. RNA interference-mediated knockdown of a-synuclein protects human dopaminergic neuroblastoma cells from MPP+ toxicity and reduces dopamine transport. *J. Neurosci. Res.*, 85:351–363, 2007.

[115] T M Fountaine, L Lourenco Venda, N Warrick, H C Christian, P Brundin, K M Channon, and R Wade-Martins. The effect of α-synuclein knockdown on MPP+ toxicity in models of human neurons. *Eur. J. Neurosci.*, 28(12):2459–73, December 2008.

[116] L P M Lourenco Venda. *Elucidating the role of α-synuclein on dopamine homeostasis using improved human dopaminergic cell models.* PhD thesis, University of Oxford, 2010.

[117] Y Chu and J H Kordower. Age-associated increases of α-synuclein in monkeys and humans are associated with nigrostriatal dopamine depletion: Is this the target for Parkinson's disease? *Neurobiol. Dis.*, 25(1):134–49, January 2007.

[118] C Kim and S J Lee. Controlling the mass action of α-synuclein in Parkinson's disease. *J. Biol. Chem.*, 107(2):303–16, October 2008.

[119] J Xu, S Y Kao, F J S Lee, W Song, L W Jin, and B A Yankner. Dopamine-dependent neurotoxicity of α-synuclein: a mechanism for selective neurodegeneration in Parkinson disease. *Nat. Med.*, 8(6):600–6, June 2002.

[120] M Yamada, T Iwatsubo, Y Mizuno, and H Mochizuki. Overexpression of α-synuclein in rat substantia nigra results in loss of dopaminergic neurons, phosphorylation of α-synuclein and activation of caspase-9: resemblance to pathogenetic changes in Parkinson's disease. *J. Neurochem.*, 91(2):451–61, October 2004.

[121] S Janezic, S Threlfell, P D Dodson, M J Dowie, T N Taylor, D Potgieter, L Parkkinen, S L Senior, S Anwar, B Ryan, T Deltheil, P Kosillo, M Cioroch, K Wagner, O Ansorge, D M Bannerman, J P Bolam, P J Magill, S J Cragg, and R Wade-Martins. Deficits in dopaminergic transmission precede neuron loss and dysfunction in a new Parkinson model. *PNAS*, 110(42):E4016–25, October 2013.

[122] E Rockenstein, M Mallory, M Hashimoto, D Song, C W Shults, I Lang, and E Masliah. Differential neuropathological alterations in transgenic mice expressing alpha-synuclein from the platelet-derived growth factor and Thy-1 promoters. *Journal of neuroscience research*, 68(5):568–78, June 2002.

[123] C Rieker, K K Dev, K Lehnhoff, S Barbieri, I Ksiazek, S Kauffmann, S Danner, H Schell, C Boden, M A Ruegg, P J Kahle, H van der Putten, and D R Shimshek. Neuropathology in mice expressing mouse alpha-synuclein. *PloS One*, 6(9):e24834, January 2011.

[124] M Wakamatsu, A Ishii, Y Ukai, J Sakagami, S Iwata, M Ono, K Matsumoto, A Nakamura, N Tada, K Kobayashi, T Iwatsubo, and M Yoshimoto. Accumulation of phosphorylated α-synuclein in dopaminergic neurons of transgenic mice that express human a-synuclein. *J. Neurosci. Res.*, 1825(April):1819–1825, 2007.

[125] Y Matsuoka, M Vila, S Lincoln, A McCormack, M Picciano, J LaFrancois, X Yu, D Dickson, W J Langston, E McGowan, M Farrer, J Hardy, K Duff, S Przedborski, and D a Di Monte. Lack of nigral pathology in transgenic mice expressing human α-synuclein driven by the tyrosine hydroxylase promoter. *Neurobiol. Dis.*, 8(3):535–9, June 2001.

[126] M Chesselet. In vivo α-synuclein overexpression in rodents: a useful model of Parkinson's disease? *Exp. Neurol.*, 209(1):22–7, January 2008.

[127] C W Olanow, D P Perl, G N Demartino, and K St P Mcnaught. Lewy bodies and aggresomes Lewy-body formation is an aggresome-related process: a hypothesis. *Lancet Neurol.*, 3(August):496–503, 2004.

[128] K M Danzer, D Haasen, A R Karow, S Moussaud, M Habeck, A Giese, H Kretzschmar, B Hengerer, and M Kostka. Different species of alpha-synuclein oligomers induce calcium influx and seeding. *J. Neurosci.*, 27(34):9220–32, August 2007.

[129] L Ko, H C Ko, W L Lin, J G Kulathingal, and S H C Yen. Aggregates assembled from overexpression of wild type α-synuclein are not toxic to human nueronal cells. *J. Neuropathol. Exp. Neurol.*, 67(11):1084–1096, 2008.

[130] H Y Qureshi and H K Paudel. Parkinsonian neurotoxin 1-methyl-4-phenyl-1,2,3,6-tetrahydropyridine (MPTP) and α-synuclein mutations promote tau protein phosphorylation at Ser262 and destabilize microtubule cytoskeleton in vitro. *J. Biol. Chem.*, 286(7):5055–68, February 2011.

[131] T Duka, V Duka, J N Joyce, and A Sidhu. α-Synuclein contributes to GSK-3beta-catalyzed tau phosphorylation in Parkinson's disease models. *FASEB J.*, 23(9):2820–30, September 2009.

[132] E Colla, P H Jensen, O Pletnikova, J C Troncoso, C Glabe, and M K Lee. Accumulation of toxic α-synuclein oligomer within endoplasmic reticulum occurs in α-synucleinopathy in vivo. *J. Neurosci.*, 32(10):3301–5, March 2012.

[133] F Kamp, N Exner, A K Lutz, N Wender, J Hegermann, B Brunner, B Nuscher, T Bartels, A Giese, K Beyer, S Eimer, K F Winklhofer, and C Haass. Inhibition of mitochondrial fusion by α-synuclein is rescued by PINK1, Parkin and DJ-1. *EMBO J.*, 29(20):3571–89, October 2010.

[134] L Devi, V Raghavendran, B M Prabhu, N G Avadhani, and H K Anandatheerthavarada. Mitochondrial import and accumulation of α-synuclein impair complex I in human dopaminergic neuronal cultures and Parkinson disease brain. *J. Biol. Chem.*, 283(14):9089–100, April 2008.

[135] C Hansen, E Angot, A L Bergström, J A Steiner, L Pieri, G Paul, T F Outeiro, R Melki, P Kallunki, and K Fog. α-Synuclein propagates from mouse brain to grafted dopaminergic neurons and seeds aggregation in cultured human cells. *J. Clin. Investig.*, 121(2):715–725, 2011.

[136] K C Luk, V Kehm, J Carroll, B Zhang, P O'Brien, J Q Trojanowski, and V M Y Lee. Pathological α-synuclein transmission initiates Parkinson-like neurodegeneration in nontransgenic mice. *Science*, 338(6109):949–53, November 2012.

[137] E C Freundt, N Maynard, E K Clancy, S Roy, L Bousset, Y Sourigues, M Covert, R Melki, K Kirkegaard, and M Brahic. Neuron-to-neuron transmission of α-synuclein fibrils through axonal transport. *Ann. Neurol.*, 72(4):517–24, October 2012.

[138] A N Sacino, M Brooks, M A Thomas, A B McKinney, S Lee, R W Regenhardt, N H McGarvey, J I Ayers, L Notterpek, D R Borchelt, T E Golde, and B I Giasson. Intramuscular injection of α-synuclein induces CNS α-synuclein pathology and a rapid-onset motor phenotype in transgenic mice. *PNAS*, 111(29), July 2014.

[139] L Alvarez-Erviti, Y Seow, A H Schapira, C Gardiner, I L Sargent, M J A Wood, and J M Cooper. Lysosomal dysfunction increases exosome-mediated α-synuclein release and transmission. *Neurobiol. Dis.*, 42(3):360–7, June 2011.

[140] M Shi, C Liu, T J Cook, K M Bullock, Y Zhao, C Ginghina, Y Li, P Aro, R Dator, C He, M J Hipp, C P Zabetian, E R Peskind, S C Hu, J F Quinn, D R Galasko, W A Banks, and J Zhang. Plasma exosomal α-synuclein is likely CNS-derived and increased in Parkinson's disease. *Acta Neuropathol.*, July 2014.

[141] Jia-Yi Li, Elisabet Englund, Janice L Holton, Denis Soulet, Peter Hagell, Andrew J Lees, Tammaryn Lashley, Niall P Quinn, Stig Rehncrona, Anders Björklund, Hakan Widner, Tamas Revesz, Olle Lindvall, and Patrik Brundin. Lewy bodies in grafted neurons in subjects with Parkinson's disease suggest host-to-graft disease propagation. *Nat. Med.*, 14(5):501–3, May 2008.

[142] R A Nixon. The role of autophagy in neurodegenerative disease. *Nat. Med.*, 19(8):983–997, August 2013.

[143] D Li, J J Shi, C J Mao, S Liu, J D Wang, J Chen, F Wang, Y P Yang, W D Hu, L F Hu, and C F Liu. Alteration of dynein function affects α-synuclein degradation via the autophagosome-lysosome pathway. *Int. J. Mol. Sci.*, 14(12):24242–54, January 2013.

[144] B Ravikumar, A Acevedo-Arozena, S Imarisio, Z Berger, C Vacher, C J O'Kane, S D M Brown, and D C Rubinsztein. Dynein mutations impair autophagic clearance of aggregate-prone proteins. *Nat. Genet.*, 37(7):771–6, July 2005.

[145] R Banerjee, M Flint Beal, and B Thomas. Autophagy in neurodegenerative disorders: pathogenic roles and therapeutic implications. *Trends Neurosci.*, 33(12):541–9, December 2010.

[146] H L Chiang and J F Dice. Peptide sequences that target proteins for enhanced degradation during serum withdrawal. *J. Biol. Chem.*, 263(14):6797–805, May 1988.

[147] C Settembre, C Di Malta, V A Polito, M G Arencibia, F Vetrini, S Erdin, S U Erdin, T Huynh, D Medina, P Colella, M Sardiello, D C Rubinsztein, and A Ballabio. TFEB links autophagy to lysosomal biogenesis. *Science*, 332:1429–1433, May 2011.

[148] E F C Blommaart, J J F P Luiken, P J E Blommaart, G M van Woerkom, and A J Meijer. Phosphorylation of ribosomal protein S6 is inhibitory for autophagy in isolated rat hepatocytes. *J. Biol. Chem.*, 270(5):2320–2326, 1995.

[149] H Harris and D C Rubinsztein. Control of autophagy as a therapy for neurodegenerative disease. *Nat. Rev. Neurol.*, 8(2):108–117, December 2011.

[150] R Kang, H J Zeh, M T Lotze, and D Tang. The Beclin 1 network regulates autophagy and apoptosis. *Cell Death Differ.*, 18(4):571–80, April 2011.

[151] C Chen, M Deng, Q Sun, P Loughran, T R Billiar, and M J Scott. Lipopolysaccharide stimulates p62-dependent autophagy-like aggregate clearance in hepatocytes. *Biomed Res. Int.*, 2014:267350, January 2014.

[152] J H Zhu, C Horbinski, F Guo, S Watkins, Y Uchiyama, and C T Chu. Regulation of autophagy by extracellular signal-regulated protein kinases during 1-methyl-4-phenylpyridinium-induced cell death. *Am. J. Pathol.*, 170(1):75–86, January 2007.

[153] R K Dagda, J Zhu, S M Kulich, and C T Chu. Mitochondrially localized ERK2 regulates mitophagy and autophagic cell stress: implications for Parkinson's disease. *Autophagy*, 4(6):770–782, 2009.

[154] C T Chu, J Zhu, and R Dagda. Beclin 1-independent pathway of damage-induced mitophagy and autophagic stress. *Autophagy*, 3(6):663–666, 2007.

[155] E A Alemu, T Lamark, K M Torgersen, A B Birgisdottir, K Bowitz Larsen, A Jain, H Olsvik, A Overvatn, V Kirkin, and T Johansen. ATG8 family proteins act as scaffolds for assembly of the ULK complex: sequence requirements for LC3-interacting region (LIR) motifs. *J. Biol. Chem.*, October 2012.

[156] Yuya Nishida, Satoko Arakawa, Kenji Fujitani, Hirofumi Yamaguchi, Takeshi Mizuta, Toku Kanaseki, Masaaki Komatsu, Kinya Otsu, Yoshihide Tsujimoto, and Shigeomi Shimizu. Discovery of Atg5/Atg7-independent alternative macroautophagy. *Nature*, 461(7264):654–8, October 2009.

[157] T Hara, K Nakamura, M Matsui, A Yamamoto, Y Nakahara, R Suzuki-Migishima, M Yokoyama, K Mishima, I Saito, H Okano, and N Mizushima. Suppression of basal autophagy in neural cells causes neurodegenerative disease in mice. *Nature*, 441(7095):885–9, June 2006.

[158] M Komatsu, S Waguri, T Chiba, S Murata, J I Iwata, I Tanida, T Ueno, M Koike, Y Uchiyama, E Kominami, and K Tanaka. Loss of autophagy in the central nervous system causes neurodegeneration in mice. *Nature*, 441(7095):880–4, June 2006.

[159] B Dehay, J Bové, N Rodríguez-Muela, C Perier, A Recasens, P Boya, and M Vila. Pathogenic lysosomal depletion in Parkinson's disease. *J. Neurosci.*, 30(37):12535–44, September 2010.

[160] G K Tofaris. Lysosome-dependent pathways as a unifying theme in Parkinson's disease. *Movement Disord.*, 27(11):1364–9, September 2012.

[161] B Kong, T Yang, J W Gu, Y Q Kuang, L Cheng, W T Yang, X K Yang, X Xia, J M Cheng, J H Zhang, and S X Yu. The association between lysosomal protein glucocerebrosidase and Parkinson's disease. *Eur. Rev. Med. Pharmacol. Sci.*, 17:143–151, 2013.

[162] M W J Cleeter, K Y Chau, C Gluck, A Mehta, D A Hughes, M Duchen, N W Wood, J Hardy, J M Cooper, and A H V Schapira. Glucocerebrosidase inhibition causes mitochondrial dysfunction and free radical damage. *Neurochem. Int.*, 62(1):1–7, January 2013.

[163] M E Gegg, D Burke, S J R Heales, J M Cooper, J Hardy, N W Wood, and A H V Schapira. Glucocerebrosidase deficiency in substantia nigra of parkinson disease brains. *Ann. Neurol.*, 72(3):455–63, September 2012.

[164] B Dehay, A Ramirez, M Martinez-Vicente, C Perier, M H Canron, E Doudnikoff, A Vital, M Vila, C Klein, and E Bezard. Loss of P-type ATPase ATP13A2/PARK9 function induces general lysosomal deficiency and leads to Parkinson disease neurodegeneration. *PNAS*, 109(24):9611–6, June 2012.

[165] A M Cuervo, L Stefanis, R Fredenburg, P T Lansbury, and D Sulzer. Impaired degradation of mutant α-synuclein by chaperone-mediated autophagy. *Science*, 305(5688):1292–5, August 2004.

[166] J L Webb, B Ravikumar, J Atkins, J N Skepper, and D C Rubinsztein. α-Synuclein is degraded by both autophagy and the proteasome. *J. Biol. Chem.*, 278(27):25009–13, July 2003.

[167] M Martinez-Vicente, Z Talloczy, S Kaushik, A C Massey, J Mazzulli, E V Mosharov, R Hodara, R Fredenburg, D C Wu, A Follenzi, W Dauer, S Przedborski, H Ischiropoulos, P T Lansbury, D Sulzer, and A M Cuervo. Dopamine-modified α-synuclein blocks chaperone-mediated autophagy. *J. Clin. Investig.*, 118(2):777–788, 2008.

[168] L Alvarez-Erviti, M C Rodriguez-Oroz, J M Cooper, C Caballero, I Ferrer, J A Obeso, and A H V Schapira. Chaperone-mediated autophagy markers in Parkinson disease brains. *Arch. Neurol.*, 67(12):1464–72, December 2010.

[169] L Alvarez-Erviti, Y Seow, A H V Schapira, M C Rodriguez-Oroz, J A Obeso, and J M Cooper. Influence of microRNA deregulation on chaperone-mediated autophagy and α-synuclein pathology in Parkinson's disease. *Cell Death Dis.*, 4(3):e545, January 2013.

[170] K A Malkus and H Ischiropoulos. Regional deficiencies in chaperone-mediated autophagy underlie α-synuclein aggregation and neurodegeneration. *Neurobiol. Dis.*, 46(3):732–44, June 2012.

[171] M Xilouri, O R Brekk, D Kirik, and L Stefanis. LAMP2A as a therapeutic target in Parkinson disease. *Autophagy*, 9(12):2166–8, December 2013.

[172] S A Tanik, C E Schultheiss, L A Volpicelli-Daley, K R Brunden, and V M Y Lee. Lewy body-like α-synuclein aggregates resist degradation and impair macroautophagy. *J. Biol. Chem.*, 288(21):15194–210, May 2013.

[173] Y Watanabe, H Tatebe, K Taguchi, Y Endo, T Tokuda, T Mizuno, M Nakagawa, and M Tanaka. p62/SQSTM1-dependent autophagy of Lewy body-like α-synuclein inclusions. *PloS One*, 7(12):e52868, January 2012.

[174] Q Yang, H She, M Gearing, E Colla, M Lee, J J Shacka, and Z Mao. Regulation of neuronal survival factor MEF2D by chaperone-mediated autophagy. *Science*, 323:124–127, 2009.

[175] A Winslow and D C Rubinsztein. The Parkinson disease protein α-synuclein inhibits autophagy. *Autophagy*, 7(4):429–431, April 2011.

[176] S Geisler, K M Holmström, A Treis, D Skujat, S S Weber, F C Fiesel, P J Kahle, and W Springer. The PINK1/Parkin-mediated mitophagy is compromised by PD-associated mutations. *Autophagy*, 6(7):871–878, October 2010.

[177] C Vives-Bauza, C Zhou, Y Huang, M Cui, R L A de Vries, J Kim, J May, M A Tocilescu, W Liu, H S Ko, J Magrané, D J Moore, V L Dawson, R Grailhe, T M Dawson, C Li, K Tieu, and S Przedborski. PINK1-dependent recruitment of Parkin to mitochondria in mitophagy. *PNAS*, 107(1):378–83, January 2010.

[178] C T Chu. A pivotal role for PINK1 and autophagy in mitochondrial quality control: implications for Parkinson disease. *Hum. Mol. Genet.*, 19(R1):R28–37, May 2010.

[179] V Choubey, M Cagalinec, J Liiv, D Safiulina, M A Hickey, M Kuum, M Liiv, T Anwar, E L Eskelinen, and A Kaasik. BECN1 is involved in the initiation of mitophagy: it facilitates PARK2 translocation to mitochondria. *Autophagy*, 10(6):1105–19, June 2014.

[180] S Geisler, K M Holmström, D Skujat, F C Fiesel, O C Rothfuss, P J Kahle, and W Springer. PINK1/Parkin-mediated mitophagy is dependent on VDAC1 and P62/SQSTM1. *Nat. Cell Biol.*, 12(2):119–31, February 2010.

[181] M E Gegg, J M Cooper, K Y Chau, M Rojo, A H V Schapira, and J W Taanman. Mitofusin 1 and mitofusin 2 are ubiquitinated in a PINK1/parkin-dependent manner upon induction of mitophagy. *Hum. Mol. Genet.*, 19(24):4861–70, December 2010.

[182] F Koyano, K Okatsu, H Kosako, Y Tamura, E Go, M Kimura, Y Kimura, H Tsuchiya, H Yoshihara, T Hirokawa, T Endo, E A Fon, J F Trempe, Y Saeki, K Tanaka, and N Matsuda. Ubiquitin is phosphorylated by PINK1 to activate parkin. *Nature*, 510(7503):162–6, April 2014.

[183] J Alegre-Abarratguie, H Christian, M M P Lufino, R Mutihac, L Lourenço Venda, O Ansorge, and R Wade-Martins. LRRK2 regulates autophagic activity and localizes to specific membrane microdomains in a novel human genomic reporter cellular model. *Hum. Mol. Genet.*, 18(21):4022–34, November 2009.

[184] E D Plowey, S J Cherra, Y J Liu, and C T Chu. Role of autophagy in G2019S-LRRK2-associated neurite shortening in differentiated SH-SY5Y cells. *J. Neurochem.*, 105(3):1048–56, May 2008.

[185] H Gao, W W Yang, Z F Qi, L L Lu, C L Duan, C L Zhao, and H Yang. DJ-1 protects dopaminergic neurons against rotenone-induced apoptosis by enhancing ERK-dependent mitophagy. *J. Mol. Biol.*, August 2012.

[186] X Z Li, C Y Sui, Q Chen, X P Chen, H Zhang, and X P Zhou. Promotion of autophagy at the maturation step by IL-6 is associated with the sustained mitogen-activated protein kinase/extracellular signal-regulated kinase activity. *Mol. Cell. Biochem.*, 380(1-2):219–27, August 2013.

[187] J Lim, Y Lee, S Jung, M B H Youdim, and Y J Oh. Impaired autophagic flux is critically involved in drug-induced dopaminergic neuronal death. *Parkinsonism Rel. Disord.*, 20 Suppl 1:S162–6, January 2014.

[188] A Garcia-Garcia, A Anandhan, M Burns, H Chen, Y Zhou, and R Franco. Impairment of Atg5-dependent autophagic flux promotes paraquat- and MPP-induced apoptosis but not rotenone or 6-hydroxydopamine toxicity. *Toxicol. Sci.*, 136(1):166–82, November 2013.

[189] E Janda, C Isidoro, C Carresi, and V Mollace. Defective autophagy in Parkinson's disease: role of oxidative stress. *Mol. Neurobiol.*, August 2012.

[190] J S Kim-Han, J A Antenor-Dorsey, and K L O'Malley. The Parkinsonian mimetic, MPP+, specifically impairs mitochondrial transport in dopamine axons. *J. Neurosci.*, 31(19):7212–21, May 2011.

[191] C Perier and M Vila. Mitochondrial biology and Parkinson's disease. *Cold Spring Harb. Perspect. Med.*, 2(2):a009332, February 2012.

[192] A Grünewald, B Arns, P Seibler, A Rakovic, A Münchau, A Ramirez, C M Sue, and C Klein. ATP13A2 mutations impair mitochondrial function in fibroblasts from patients with Kufor-Rakeb syndrome. *Neurobiol. Aging*, 33(8):1843.e1–7, August 2012.

[193] V M Mann, J M Cooper, S E Daniel, K Srai, P Jenner, C D Marsden, and A H Schapira. Complex I, iron, and ferritin in Parkinson's disease substantia nigra. *Ann. Neurol.*, 36(6):876–81, December 1994.

[194] L A Bindoff, M A Birch-Machin, N E F Cartlidge, W D Parker, and D M Turnball. Respiratory chain abnormalities in skeletal muscle from patients with Parkinson's disease. *J. Neurol. Sci.*, 104:203–208, 1991.

[195] W D Parker, S J Boyson, and J K Parks. Abnormalities of the electron transport chain in idiopathic Parkinson's disease. *Ann. Neurol.*, 26(6):719–23, December 1989.

[196] M Gu, J M Cooper, J W Taanman, and A H Schapira. Mitochondrial DNA transmission of the mitochondrial defect in Parkinson's disease. *Ann. Neurol.*, 44(2):177–86, August 1998.

[197] Y Kraytsberg, E Kudryavtseva, A C McKee, C Geula, N W Kowall, and K Khrapko. Mitochondrial DNA deletions are abundant and cause functional impairment in aged human substantia nigra neurons. *Nat. Genet.*, 38(5):518–20, May 2006.

[198] M I Ekstrand, M Terzioglu, D Galter, S Zhu, C Hofstetter, E Lindqvist, S Thams, A Bergstrand, F S Hansson, A Trifunovic, B Hoffer, S Cullheim, A H Mohammed, L Olson, and N G Larsson. Progressive parkinsonism in mice with respiratory-chain-deficient dopamine neurons. *PNAS*, 104(4):1325–30, January 2007.

[199] Y Piao, H G Kim, M S Oh, and Y K Pak. Overexpression of TFAM, NRF-1 and myr-AKT protects the MPP(+)-induced mitochondrial dysfunctions in neuronal cells. *Biochim. Biophys.*, 1820(5):577–85, May 2012.

[200] Y C Su and X Qi. Inhibition of excessive mitochondrial fission reduced aberrant autophagy and neuronal damage caused by LRRK2 G2019S mutation. *Hum. Mol. Genet.*, 22(22):4545–4561, June 2013.

[201] X Wang, T G Petrie, Y Liu, J Liu, H Fujioka, and X Zhu. Parkinson's disease-associated DJ-1 mutations impair mitochondrial dynamics and cause mitochondrial dysfunction. *J. Neurochem.*, 121(5):830–9, June 2012.

[202] A K Lutz, N Exner, M E Fett, J S Schlehe, K Kloos, K Lämmermann, B Brunner, A Kurz-Drexler, F Vogel, A S Reichert, L Bouman, D Vogt-Weisenhorn, W Wurst, J Tatzelt, C Haass, and K F Winklhofer. Loss of parkin or PINK1 function increases Drp1-dependent mitochondrial fragmentation. *J. Biol. Chem.*, 284(34):22938–51, August 2009.

[203] J H Zhu, A M Gusdon, H Cimen, B Van Houten, E Koc, and C T Chu. Impaired mitochondrial biogenesis contributes to depletion of functional mitochondria in chronic MPP(+) toxicity: dual roles for ERK1/2. *Cell Death Dis.*, 3:e312, January 2012.

[204] X Wang, B Su, W Liu, X He, Y Gao, R J Castellani, G Perry, M A Smith, and X Zhu. DLP1-dependent mitochondrial fragmentation mediates 1-methyl-4-phenylpyridinium toxicity in neurons: implications for Parkinson's disease. *Aging cell*, 10(5):807–23, October 2011.

[205] R C S Seet, C Y J Lee, E C H Lim, J J H Tan, A M L Quek, W L Chong, W F Looi, S H Huang, H Wang, Y H Chan, and B Halliwell. Oxidative damage in Parkinson disease: Measurement using accurate biomarkers. *Free Radic. Biol. Med.*, 48(4):560–6, February 2010.

[206] A R Esteves, D M Arduíno, R H Swerdlow, C R Oliveira, and S M Cardoso. Oxidative stress involvement in α-synuclein oligomerization in Parkinson's disease cybrids. *Antioxid. Redox Signal.*, 11(3):439–448, 2009.

[207] D T Dexter, J Sian, S Rose, J G Hindmarsh, V M Mann, J M Cooper, F R Wells, S E Daniel, A J Lees, and A H Schapira. Indices of oxidative stress and mitochondrial function in individuals with incidental Lewy body disease. *Ann. Neurol.*, 35(1):38–44, January 1994.

[208] R M Canet-Aviles, M A Wilson, D W Miller, R Ahmad, C Mclendon, S Bandyopadhyay, M J Baptista, D Ringe, G A Petsko, and M R Cookson. The Parkinson's disease protein DJ-1 is neuroprotective due to cysteine-sulfinic acid-driven mitochondrial localization. *PNAS*, 101(24):9103–9108, 2004.

[209] C P Fall and J P Bennett. Characterization and time course of MPP+ -induced apoptosis in human SH-SY5Y neuroblastoma cells. *J. Neurosci. Res.*, 55(5):620–8, March 1999.

[210] D A Drechsel, L P Liang, and M Patel. 1-Methyl-4-phenylpyridinium-induced alterations of glutathione status in immortalized rat dopaminergic neurons. *Toxicol. Appl. Pharm.*, 220(3):341–348, 2007.

[211] A Ghosh, K Chandran, S V Kalivendi, J Joseph, W E Antholine, C J Hillard, A Kanthasamy, and B Kalyanaraman. Neuroprotection by a mitochondria-targeted drug in a Parkinson's disease model. *Free Radic. Biol. Med.*, 49(11):1674–84, December 2010.

[212] M Barkats, P Horellou, P Colin, N Faucon-Biguet, and J Mallet. 1-Methyl-4-phenylpyridinium neurotoxicity is attenuated by adenoviral gene transfer of human Cu/Zn superoxide dismutase. *J. Neurosci.*, 83:233–242, 2006.

[213] C Perier, K Tieu, C Guégan, C Caspersen, V Jackson-Lewis, V Carelli, A Martinuzzi, M Hirano, S Przedborski, and M Vila. Complex I deficiency primes Bax-dependent neuronal apoptosis through mitochondrial oxidative damage. *PNAS*, 102(52):19126–31, December 2005.

[214] K Jomova, D Vondrakova, M Lawson, and M Valko. Metals, oxidative stress and neurodegenerative disorders. *Mol. Cell. Biochem.*, 345(1-2):91–104, December 2010.

[215] S V Kalivendi, S Cunningham, S Kotamraju, J Joseph, C J Hillard, and B Kalyanaraman. α-Synuclein up-regulation and aggregation during MPP+-induced apoptosis in neuroblastoma cells: intermediacy of transferrin receptor iron and hydrogen peroxide. *J. Biol. Chem.*, 279(15):15240–7, April 2004.

[216] HY Zhang, Z G Wang, X H Lu, X X Kong, F Z Wu, L Lin, X Tan, L B Ye, and J Xiao. Endoplasmic reticulum stress: relevance and therapeutics in central nervous system diseases. *Mol. Neurobiol.*, July 2014.

[217] J J M Hoozemans, E S van Haastert, P Eikelenboom, R A I de Vos, J M Rozemuller, and W Scheper. Activation of the unfolded protein response in Parkinson's disease. *Biochem. Bioph. Res. Co.*, 354(3):707–11, March 2007.

[218] D G Graham, S M Tiffany, W R Bell, and W F Gutknecht. Autoxidation versus covalent binding of quinones as the mechanism of toxicity of dopamine, 6-hydroxydopamine, and related compounds towards C1300 neuroblastoma cells in vitro. *Mol. Pharmacol.*, 14:644–653, 1978.

[219] L Zecca, F A Zucca, A Albertini, E Rizzio, and R G Fariello. A proposed dual role of neuromelanin in the pathogenesis of Parkinsons disease. *Neurology*, 67:S8–S11, 2006.

[220] M Bisaglia, E Greggio, D Maric, D W Miller, M R Cookson, and L Bubacco. α-Synuclein overexpression increases dopamine toxicity in BE2-M17 cells. *BMC Neuroscience*, 11:41, January 2010.

[221] J Lotharius and K L O'Malley. The parkinsonism-inducing drug 1-methyl-4-phenylpyridinium triggers intracellular dopamine oxidation. A novel mechanism of toxicity. *J. Biol. Chem.*, 275(49):38581–8, December 2000.

[222] T G Hastings, D A Lewis, and M J Zigmond. Role of oxidation in the neurotoxic effects of intrastriatal dopamine injections. *PNAS*, 93(5):1956–61, March 1996.

[223] W M Caudle, J R Richardson, M Z Wang, T N Taylor, T S Guillot, A L McCormack, R E Colebrooke, D A Di Monte, P C Emson, and G W Miller. Reduced vesicular storage of dopamine causes progressive nigrostriatal neurodegeneration. *J. Neurosci.*, 27(30):8138–48, July 2007.

[224] K M Lohr, A I Bernstein, K A Stout, A R Dunn, C R Lazo, S P Alter, M Wang, Y Li, X Fan, E J Hess, H Yi, L M Vecchio, D S Goldstein, T S Guillot, A Salahpour, and G W Miller. Increased vesicular monoamine transporter enhances dopamine release and opposes Parkinson disease-related neurodegeneration in vivo. *PNAS*, 111(27):9977–82, July 2014.

[225] C Pifl, A Rajput, H Reither, J Blesa, C Cavada, J A Obeso, A H Rajput, and O Hornykiewicz. Is Parkinson's disease a vesicular dopamine storage disorder? Evidence from a study in isolated synaptic vesicles of human and nonhuman primate striatum. *J. Neurosci.*, 34(24):8210–8, June 2014.

[226] A A Dukes, K M Korwek, and T G Hastings. The effect of endogenous dopamine in rotenone-induced toxicity of PC12 cells. *Antioxid. Redox Signal.*, 7(16):630–638, 2005.

[227] G R Kweon, J D Marks, R Krencik, E H Leung, P T Schumacker, K Hyland, and U J Kang. Distinct mechanisms of neurodegeneration induced by chronic complex I inhibition in dopaminergic and non-dopaminergic cells. *J. Biol. Chem.*, 279(50):51783–92, December 2004.

[228] X Li, J C Patel, J Wang, M V Avshalumov, C Nicholson, J D Buxbaum, G A Elder, M E Rice, and Z Yue. Enhanced striatal dopamine transmission and motor performance with LRRK2 overexpression in mice is eliminated by familial Parkinson's disease mutation G2019S. *J. Neurosci.*, 30(5):1788–97, February 2010.

[229] D J Surmeier and P T Schumacker. Calcium, bioenergetics, and neuronal vulnerability in Parkinson's disease. *J. Biol. Chem.*, 288(15):10736–41, April 2013.

[230] J A Goldberg, J N Guzman, C M Estep, E Ilijic, J Kondapalli, J Sanchez-Padilla, and D J Surmeier. Calcium entry induces mitochondrial oxidant stress in vagal neurons at risk in Parkinson's disease. *Nat. Neurosci.*, 15(10):1414–21, October 2012.

[231] K L Double, S Reyes, E L Werry, and G M Halliday. Selective cell death in neurodegeneration: why are some neurons spared in vulnerable regions? *Prog. Neurobiol.*, 92(3):316–29, November 2010.

[232] M J Hurley, B Brandon, S M Gentleman, and D T Dexter. Parkinson's disease is associated with altered expression of CaV1 channels and calcium-binding proteins. *Brain*, 136:2077–97, July 2013.

[233] S M Berger and D Bartsch. The role of L-type voltage-gated calcium channels Cav1.2 and Ca v1.3 in normal and pathological brain function. *Cell Tissue Res.*, 357(2):463–76, July 2014.

[234] D G Nicholls. Oxidative stress and energy crises in neuronal dysfunction. *Ann. N. Y. Acad. Sci.*, 1147:53–60, December 2008.

[235] J Martinez, I Moeller, H Erdjument-Bromage, P Tempst, and B Lauring. Parkinson's disease-associated α-synuclein is a calmodulin substrate. *J. Biol. Chem.*, 278(19):17379–87, May 2003.

[236] D H Lee, Y S Han, E S Han, H Bang, and C S Lee. Differential involvement of intracellular Ca2+ in 1-methyl-4-phenylpyridinium- or 6-hydroxydopamine-induced cell viability loss in PC12 cells. *Neurochem. Res.*, 31(7):851–60, July 2006.

[237] B H M Hunn, S J Cragg, J P Bolam, M G Spillantini, and R Wade-Martins. Impaired intracellular trafficking defines early Parkinson's disease. *Trends Neurosci.*, 2015.

[238] M C Zody, Z Jiang, H C Fung, F Antonacci, L W Hillier, M F Cardone, T A Graves, J M Kidd, Z Cheng, A Abouelleil, L Chen, J Wallis, J Glasscock, R K Wilson, A D Reily, J Duckworth, M Ventura, J Hardy, W C Warren, and E E Eichler. Evolutionary toggling of the MAPT 17q21.31 inversion region. *Nat. Genet.*, 40(9):1076–83, October 2008.

[239] T M Caffrey, C Joachim, S Paracchini, M M Esiri, and R Wade-Martins. Haplotype-specific expression of exon 10 at the human MAPT locus. *Hum. Mol. Genet.*, 15(24):3529–37, December 2006.

[240] Q Zhong, E E Congdon, H N Nagaraja, and J Kuret. Tau isoform composition influences rate and extent of filament formation. *J. Biol. Chem.*, 287(24):20711–9, June 2012.

[241] K Arima, S Hirai, N Sunohara, K Aoto, Y Izumiyama, K Ueda, K Ikeda, and M Kawai. Cellular co-localization of phosphorylated tau- and NACP α-synuclein-epitopes in Lewy bodies in sporadic Parkinson's disease and in dementia with Lewy bodies. *Brain Res.*, 843:53–61, 1999.

[242] B I Giasson, M S Forman, M Higuchi, L I Golbe, C L Graves, P T Kotzbauer, J Q Trojanowski, and V M Y Lee. Initiation and synergistic fibrillization of tau and α-synuclein. *Science*, 300(5619):636–40, April 2003.

[243] Y Chu, G A Morfini, L B Langhamer, Y He, S T Brady, and J H Kordower. Alterations in axonal transport motor proteins in sporadic and experimental Parkinson's disease. *Brain*, 135(Pt 7):2058–73, July 2012.

[244] R Dixit, J L Ross, Y E Goldman, and E L F Holzbaur. Differential regulation of dynein and kinesin motor proteins by tau. *Science*, 319(5866):1086–9, February 2008.

[245] B Roy and G R Jackson. Interactions between tau and α-synuclein augment neurotoxicity in a Drosophila model of Parkinson's disease. *Hum. Mol. Genet.*, 23(11):3008–23, June 2014.

[246] J P Bolam and E K Pissadaki. Living on the edge with too many mouths to feed: Why dopamine neurons die. *Movement Disord.*, 27(12):1478–83, September 2012.

[247] D Sulzer. Multiple hit hypotheses for dopamine neuron loss in Parkinson's disease. *Trends Neurosci.*, 30(5):244–50, May 2007.

[248] A Antonini. Levodopa in the treatment of Parkinsons disease: an old drug still going strong. *Clin. Inter. Aging*, 5:229–38, August 2010.

[249] A H Rajput. Levodopa prolongs life expectancy and is non-toxic to substantia nigra. *Parkinsonism Rel. Disord.*, 8(2):95–100, October 2001.

[250] L W Elmer. Rasagiline adjunct therapy in patients with Parkinson's disease: post hoc analyses of the PRESTO and LARGO trials. *Parkinsonism Rel. Disord.*, 19(11):930–6, November 2013.

[251] R Talati, K Reinhart, W Baker, C M White, and C I Coleman. Pharmacologic treatment of advanced Parkinson's disease: a meta-analysis of COMT inhibitors and MAO-B inhibitors. *Parkinsonism Rel. Disord.*, 15(7):500–5, August 2009.

[252] R Krishna, M Ali, and A A Moustafa. Effects of combined MAO-B inhibitors and levodopa vs. monotherapy in Parkinson's disease. *FNAGI*, 6(July):180, January 2014.

[253] E S Roach. Initial Parkinson disease therapy: levodopa, dopamine agonists, or both? *Arch. Neurol.*, 61:1972–1973, 2004.

[254] D O Claassen, W P M Van Den Wildenberg, K R Ridderinkhof, C K Jessup, M B Harrison, G F Wooten, and S A Wylie. The risky business of dopamine agonists in Parkinson disease and impulse control disorders. *Behav. Neurosci.*, 125(4):492–500, 2011.

[255] O Weinreb, S Mandel, M B H Youdim, and T Amit. Targeting dysregulation of brain iron homeostasis in Parkinson's disease by iron chelators. *Free Radic. Biol. Med.*, 62:52–64, September 2013.

[256] M B H Youdim, M Fridkin, and H Zheng. Novel bifunctional drugs targeting monoamine oxidase inhibition and iron chelation as an approach to neuroprotection in Parkinson's disease and other neurodegenerative diseases. *J. Neural Transm.*, 111(10-11):1455–71, October 2004.

[257] J F Chen, K Xu, J P Petzer, R Staal, Y H Xu, M Beilstein, P K Sonsalla, K Castagnoli, N Castagnoli, and M A Schwarzschild. Neuroprotection by caffeine and A 2A adenosine receptor inactivation in a model of Parkinsons disease. *J. Neurosci.*, 21:2–7, 2001.

[258] M Cieślak, M Komoszyski, and A Wojtczak. Adenosine A(2A) receptors in Parkinson's disease treatment. *Purinergic Signal.*, 4(4):305–12, December 2008.

[259] Y Tao and G Liang. Efficacy of adenosine A2A receptor antagonist istradefylline as augmentation for Parkinson's disease: a meta-analysis of randomized controlled trials. *Cell Biochem. Biophys.*, August 2014.

[260] M B H Youdim, L Kupershmidt, T Amit, and O Weinreb. Promises of novel multi-target neuroprotective and neurorestorative drugs for Parkinson's disease. *Parkinsonism Rel. Disord.*, 20 Suppl 1:S132–6, January 2014.

[261] J P Petzer, S Steyn, K P Castagnoli, J F Chen, M A Schwarzschild, C J Van der Schyf, and N Castagnoli. Inhibition of monoamine oxidase B by selective adenosine A2A receptor antagonists. *Bioorg. Med. Chem.*, 11(7):1299–1310, April 2003.

[262] N Geva-Zatorsky, E Dekel, A A Cohen, T Danon, L Cohen, and U Alon. Protein dynamics in drug combinations: a linear superposition of individual-drug responses. *Cell*, 140(5):643–51, March 2010.

[263] J W Scannell, A Blanckley, H Boldon, and B Warrington. Diagnosing the decline in pharmaceutical R&D efficiency. *Nat. Rev. Drug Discov.*, 11(3):191–200, March 2012.

[264] A L Hopkins. Network pharmacology: the next paradigm in drug discovery. *Nat. Chem. Biol.*, 4(11):682–90, November 2008.

[265] P Csermely, T Korcsmáros, H J M Kiss, G London, and R Nussinov. Structure and dynamics of molecular networks: a novel paradigm of drug discovery: a comprehensive review. *Pharmacol. Ther.*, 138(3):333–408, June 2013.

[266] M J Hartshorn, C W Murray, A Cleasby, M Frederickson, I J Tickle, and H Jhoti. Fragment-based lead discovery using X-ray crystallography. *J. Med. Chem.*, 48(2):403–13, January 2005.

[267] S M Paul, D S Mytelka, C T Dunwiddie, C C Persinger, B H Munos, S R Lindborg, and A L Schacht. How to improve R&D productivity: the pharmaceutical industry's grand challenge. *Nat. Rev. Drug Discov.*, 9(3):203–14, March 2010.

[268] A Mullard. 2013 FDA drug approvals. *Nat. Rev. Drug Discov.*, 13(2):85–89, January 2014.

[269] M P Young, S Zimmer, and A Whitmore. Drug molecules and biology: network and systems aspects. In J. Richard Morphy and C. John Harris, editors, *Designing Multi-Target Drugs*, pages 32–49. RSC Publishing, 2012.

[270] E K Silverman and J Loscalzo. Developing new drug treatments in the era of network medicine. *Clin. Pharmacol. Ther.*, 93(1):26–8, January 2013.

[271] A L Hopkins and C R Groom. The druggable genome. *Nat. Rev. Drug Discov.*, 1(9):727–30, September 2002.

[272] Y Chen, J Zhu, P Y Lum, X Yang, S Pinto, D J MacNeil, C Zhang, J Lamb, S Edwards, S K Sieberts, A Leonardson, L W Castellini, S Wang, M F Champy, B Zhang, V Emilsson, S Doss, A Ghazalpour, S Horvath, T A Drake, A J Lusis, and E E Schadt. Variations in DNA elucidate molecular networks that cause disease. *Nature*, 452(7186):429–35, March 2008.

[273] M A Yildirim, K I Goh, M E Cusick, A L Barabási, and M Vidal. Drug-target network. *Nat. Biotechnol.*, 25(10):1119–26, October 2007.

[274] S Oliver. Guilt-by-association goes global. *Nature*, 403(6770):601–3, February 2000.

[275] P Y Chen, C M Deane, and G Reinert. A statistical approach using network structure in the prediction of protein characteristics. *Bioinformatics*, 23(17):2314–21, September 2007.

[276] M Dreze, D Monachello, C Lurin, M E Cusick, D E Hill, M Vidal, and P Braun. *High-quality binary interactome mapping.*, volume 470. Elsevier Inc., 2 edition, January 2010.

[277] A A Borisy, P J Elliott, N W Hurst, M S Lee, J Lehar, E R Price, G Serbedzija, G R Zimmermann, M A Foley, B R Stockwell, and C T Keith. Systematic discovery of multicomponent therapeutics. *PNAS*, 100(13):7977–82, June 2003.

[278] S Atwell, J M Adams, J Badger, M D Buchanan, I K Feil, K J Froning, X Gao, J Hendle, K Keegan, B C Leon, H J Müller-Dieckmann, V L Nienaber, B W Noland, K Post, K R Rajashankar, A Ramos, M Russell, S K Burley, and S G Buchanan. A novel mode of Gleevec binding is revealed by the structure of spleen tyrosine kinase. *J. Biol. Chem.*, 279(53):55827–32, December 2004.

[279] Y Wang, T Cui, C Zhang, M Yang, Y Huang, W Li, L Zhang, C Gao, Y He, Y Li, F Huang, J Zeng, C Huang, Q Yang, Y Tian, C Zhao, H Chen, H Zhang, and Z G He. Global protein-protein interaction network in the human pathogen Mycobacterium tuberculosis H37Rv. *J. Proteome Res.*, 9:6665–6677, 2010.

[280] K Raman, R Vashisht, and N Chandra. Strategies for efficient disruption of metabolism in Mycobacterium tuberculosis from network analysis. *Mol. Biosyst.*, 5:1740–51, 2009.

[281] R Zoraghi and N E Reiner. Protein interaction networks as starting points to identify novel antimicrobial drug targets. *Curr. Opin. Microbiol.*, 16(5):566–72, October 2013.

[282] V Srinivasa Rao, K Srinivas, G N Sunand Kumar, and G N Sujini. Protein interaction network for Alzheimer's disease using computational approach. *Bioinformation*, 9(19), 2013.

[283] O Folger, L Jerby, C Frezza, E Gottlieb, E Ruppin, and T Shlomi. Predicting selective drug targets in cancer through metabolic networks. *Mol. Syst. Biol.*, 7(501):501, January 2011.

[284] V Ciccarone, B A Spengler, M B Meyers, J L Biedler, and R A Ross. Phenotypic diversification in human neuroblastoma cells: expression of distinct neural crest lineages. *Cancer Res.*, 49:219–225, 1989.

[285] J L Jainchill, S A Aaronson, and G J Todaro. Murine sarcoma and leukemia viruses: assay using clonal lines of contact-inhibited mouse cells. *J. Virology*, 4(5):549–53, November 1969.

[286] G Repetto, A del Peso, and J L Zurita. Neutral red uptake assay for the estimation of cell viability/cytotoxicity. *Nat. Protoc.*, 3(7):1125–31, January 2008.

[287] R M Gronostajski and A Pardee. Protein degradation in 3T3 cells and tumorigenic transformed 3T3 cells. *J. Cell. Physiol.*, 132:127–132, 1984.

[288] S Razick, G Magklaras, and I M Donaldson. iRefIndex: a consolidated protein interaction database with provenance. *BMC Bioinformatics*, 9:405, January 2008.

[289] A Mora. Protein interaction network analysis using iRefR and igraph.

[290] A Mora. iRefR an R package to manage the iRefIndex consolidated protein interaction database.

[291] E J Rossin, K Lage, S Raychaudhuri, R J Xavier, D Tatar, Y Benita, C Cotsapas, and M J Daly. Proteins encoded in genomic regions associated with immune-mediated disease physically interact and suggest underlying biology. *PLoS Genet.*, 7(1):e1001273, January 2011.

[292] K Lage, E O Karlberg, Z M Stø rling, P I Olason, A G Pedersen, O Rigina, A M Hinsby, Z Tümer, F Pociot, N Tommerup, Y Moreau, and S Brunak. A human phenome-interactome network of protein complexes implicated in genetic disorders. *Nat. Biotechnol.*, 25(3):309–16, March 2007.

[293] H J Noh, C P Ponting, H C Boulding, S Meader, C Betancur, J D Buxbaum, D Pinto, C R Marshall, A C Lionel, S W Scherer, and C Webber. Network topologies and convergent aetiologies arising from deletions and duplications observed in individuals with autism. *PLoS Genet.*, 9(6):e1003523, June 2013.

[294] The UniProt Consortium. Activities at the universal protein resource (UniProt). *Nucleic Acids Res.*, 42:D191–8, January 2014.

[295] M Kanehisa, S Goto, Y Sato, M Furumichi, and M Tanabe. KEGG for integration and interpretation of large-scale molecular data sets. *Nucleic Acids Res.*, 40(Database issue):D109–14, January 2012.

[296] A Hamosh, A F Scott, J S Amberger, C A Bocchini, and V A McKusick. Online Mendelian Inheritance in Man (OMIM), a knowledgebase of human genes and genetic disorders. *Nucleic Acids Res.*, 33(Database issue):D514–7, January 2005.

[297] The Gene Ontology Consortium. Gene Ontology: tool for the unification of biology. *Nat. Genet.*, 25:25–29, 2000.

[298] D W Huang, B T Sherman, and R A Lempicki. Systematic and integrative analysis of large gene lists using DAVID bioinformatics resources. *Nat. Protoc.*, 4(1):44–57, January 2009.

[299] M J Jahid and J Ruan. A Steiner tree-based method for biomarker discovery and classification in breast cancer metastasis. *BMC Genomics*, 13 Suppl 6(Suppl 6):S8, January 2012.

[300] M Ray, J Ruan, and W Zhang. Variations in the transcriptome of Alzheimer's disease reveal molecular networks involved in cardiovascular diseases. *Genome Biol.*, 9(10):R148, January 2008.

[301] D Liang, G Han, X Feng, J Sun, Y Duan, and H Lei. Concerted perturbation observed in a hub network in Alzheimer's disease. *PloS One*, 7(7):e40498, January 2012.

[302] M Könn. *Creating a protein-protein interaction network for alpha-synuclein.* PhD thesis, Freien Universität Berlin, 2012.

[303] R M Miller, L M Callahan, C Casaceli, L Chen, G L Kiser, B Chui, T M Kaysser-Kranich, T J Sendera, C Palaniappan, and H J Federoff. Dysregulation of gene expression in the 1-methyl-4-phenyl-1,2,3,6-tetrahydropyridine-lesioned mouse substantia nigra. *J. Neurosci.*, 24(34):7445–54, August 2004.

[304] K J Conn, M D Ullman, M J Larned, P B Eisenhauer, R E Fine, and J M Wells. cDNA microarray analysis of changes in gene expression associated with MPP+ toxicity in SH-SY5Y cells. *Neurochem. Res.*, 28(12):1873–81, December 2003.

[305] E Mazzio and K F A Soliman. Whole genome expression profile in neuroblastoma cells exposed to 1-methyl-4-phenylpyridine. *Neurotoxicology*, 33(5):1156–69, October 2012.

[306] Z Xu, T A Patterson, J D Wren, T Han, L Shi, H Duhart, S F Ali, and W Slikker. A microarray study of MPP+-treated PC12 Cells: Mechanisms of toxicity (MOT) analysis using bioinformatics tools. *BMC Bioinformatics*, 6 Suppl 2:S8, July 2005.

[307] J Wang, Z Xu, H Fang, H M Duhart, T A Patterson, and S F Ali. Gene expression profiling of MPP+-treated MN9D cells: a mechanism of toxicity study. *Neurotoxicology*, 28(5):979–87, September 2007.

[308] M Elstner, C M Morris, K Heim, A Bender, D Mehta, E Jaros, T Klopstock, T Meitinger, D M Turnbull, and H Prokisch. Expression analysis of dopaminergic neurons in Parkinson's disease and aging links transcriptional dysregulation of energy metabolism to cell death. *Acta Neuropathol.*, 122(1):75–86, July 2011.

[309] A G White and A Ma'ayan. Connecting seed lists of mammalian proteins using Steiner trees. *Nat. Proceed.*, pages 1–5, 2008.

[310] K Faust, P Dupont, J Callut, and J van Helden. Pathway discovery in metabolic networks by subgraph extraction. *Bioinformatics*, 26(9):1211–8, May 2010.

[311] R C Gudivada, Xi A Qu, J Chen, A G Jegga, E K Neumann, and B J Aronow. Identifying disease-causal genes using Semantic Web-based representation of integrated genomic and phenomic knowledge. *J. Biomed. Inform.*, 41(5):717–29, October 2008.

[312] J I Satoh, H Tabunoki, and K Arima. Molecular network analysis suggests aberrant CREB-mediated gene regulation in the Alzheimer disease hippocampus. *Dis. Markers*, 27(5):239–52, January 2009.

[313] P Hallock and M A Thomas. Integrating the Alzheimer's disease proteome and transcriptome: a comprehensive network model of a complex disease. *Omics*, 16(1-2):37–49, 2012.

[314] V Limviphuvadh, S Tanaka, S Goto, K Ueda, and M Kanehisa. The commonality of protein interaction networks determined in neurodegenerative disorders (NDDs). *Bioinformatics*, 23(16):2129–38, August 2007.

[315] L A Goodman. Snowball sampling. *Ann. Math. Stat.*, 32(1):148–170, 1961.

[316] Z Tu, C Argmann, K K Wong, L J Mitnaul, S Edwards, I C Sach, J Zhu, and E E Schadt. Integrating siRNA and protein-protein interaction data to identify an expanded insulin signaling network. *Genome research*, 19(6):1057–67, June 2009.

[317] R Core Team. R: A Language and Environment for Statistical Computing, 2013.

[318] M Bastian, S Heymann, and M Jacomy. Gephi: an open source software for exploring and manipulating networks. In *ICWSM*, 2009.

[319] R L Graham and P Hell. On the history of the minimum spanning tree problem. *IEEE Ann. Hist. Comput.*, 7(1):43–57, 1985.

[320] N Betzler. *Steiner tree problems in the analysis of biological networks*. PhD thesis, University of Tubingen, 2006.

[321] S E Dreyfus and R A Wagner. The Steiner problem in graphs. *Networks*, 1:195–207, 1972.

[322] P Klein and R Ravi. A nearly best-possible approximation algorithm for node-weighted Steiner trees. *J. Algorithms*, 19:104–115, 1995.

[323] M S Scott, T Perkins, S Bunnell, F Pepin, D Y Thomas, and M Hallett. Identifying regulatory subnetworks for a set of genes. *Mol. Cell. Proteomics*, 4(5):683–92, May 2005.

[324] W Hwang, Y R Cho, A Zhang, and M Ramanathan. Bridging centrality: identifying bridging nodes in scale-free networks. 2006.

[325] G W Miller, R R Gainetdinov, A I Levey, and M G Caron. Dopamine transporters and neuronal injury. *Trends Pharmacol. Sci.*, 20(10):424–9, October 1999.

[326] R Banerjee, S Sreetama, K S Saravanan, S N Dey, and K P Mohanakumar. Apoptotic mode of cell death in substantia nigra following intranigral infusion of the parkinsonian neurotoxin, MPP+ in Sprague-Dawley rats: cellular, molecular and ultrastructural evidences. *Neurochem. Res.*, 32(7):1238–47, July 2007.

[327] A Petit-Paitel, F Brau, J Cazareth, and J Chabry. Involvment of cytosolic and mitochondrial GSK-3β in mitochondrial dysfunction and neuronal cell death of MPTP/MPP-treated neurons. *PloS One*, 4(5):e5491, January 2009.

[328] C Perier, J Bové, and M Vila. Mitochondria and programmed cell death in Parkinson's disease: apoptosis and beyond. *Antioxid. Redox Signal.*, 16(9):883–95, July 2011.

[329] J L Y Chee, X L Guan, J Y Lee, B Dong, S M Leong, E H Ong, A K F Liou, and T M Lim. Compensatory caspase activation in MPP+-induced cell death in dopaminergic neurons. *Cell Mol. Life Sci.*, 62(2):227–38, January 2005.

[330] C T Chu, J H Zhu, G Cao, A Signore, S Wang, and J Chen. Apoptosis inducing factor mediates caspase-independent 1-methyl-4-phenylpyridinium toxicity in dopaminergic cells. *J. Neurochem.*, 94(6):1685–95, September 2005.

[331] M Vila, V Jackson-Lewis, S Vukosavic, R Djaldetti, G Liberatore, D Offen, S J Korsmeyer, and S Przedborski. Bax ablation prevents dopaminergic neurodegeneration in the 1-methyl-4-phenyl-1.2.3.6-tetrahydropyridine mouse model of Parkinsons disease. *PNAS*, 98(5):2837–2842, 2001.

[332] D Offen, P M Beart, N S Cheung, C J Pascoe, A Hochman, S Gorodin, E Melamed, R Bernard, and O Bernard. Transgenic mice expressing human Bcl-2 in their neurons are resistant to 6-hydroxydopamine and 1-methyl-4-phenyl-1,2,3,6- tetrahydropyridine neurotoxicity. *PNAS*, 95(10):5789–94, May 1998.

[333] Z G Zhang, L Wu, J L Wang, J D Yang, J Zhang, L H Li, Y Xia, L B Yao, Huai-Zhou Qin, and Guo-Dong Gao. Astragaloside IV prevents MPP-induced SH-SY5Y cell death via the inhibition of Bax-mediated pathways and ROS production. *Mol. Cell. Biochem.*, 364(1-2):209–16, May 2012.

[334] S V Kalivendi, D Yedlapudi, C J Hillard, and B Kalyanaraman. Oxidants induce alternative splicing of α-synuclein: Implications for Parkinson's disease. *Free Radic. Biol. Med.*, 48(3):377–83, February 2010.

[335] T Shang, S Kotamraju, H Zhao, S V Kalivendi, C J Hillard, and B Kalyanaraman. Sepiapterin attenuates 1-methyl-4-phenylpyridinium-induced apoptosis in neuroblastoma cells transfected with neuronal NOS: role of tetrahydrobiopterin, nitric oxide, and proteasome activation. *Free Radic. Biol. Med.*, 39(8):1059–74, October 2005.

[336] T A Yacoubian, S R Slone, A J Harrington, S Hamamichi, J M Schieltz, K A Caldwell, G A Caldwell, and D G Standaert. Differential neuroprotective effects of 14-3-3 proteins in models of Parkinson's disease. *Cell Death Dis.*, 1(1):e2, January 2010.

[337] S R Slone, M Lesort, and T A Yacoubian. 14-3-3theta protects against neurotoxicity in a cellular Parkinson's disease model through inhibition of the apoptotic factor Bax. *PloS One*, 6(7):e21720, January 2011.

[338] G Melino, A Stephanou, M Annicchiarico-Petruzzelli, R a Knight, A Finazzi-Agró, and S L Lightman. Modulation of IGF-2 expression during growth and differentiation of human neuroblastoma cells: retinoic acid may induce IGF-2. *Neurosci. Lett.*, 151(2):187–91, March 1993.

[339] M Kurella, L L Hsiao, T Yoshida, J D Randall, G Chow, S S Sarang, R V Jensen, and S R Gullans. DNA microarray analysis of complex biologic processes. *JASN*, 12(5):1072–8, May 2001.

[340] F Simunovic, M Yi, Y Wang, L Macey, L T Brown, A M Krichevsky, S L Andersen, R M Stephens, F M Benes, and K C Sonntag. Gene expression profiling of substantia nigra dopamine neurons: further insights into Parkinson's disease pathology. *Brain*, 132(Pt 7):1795–809, July 2009.

[341] J K Kim. Brain tumor pathway identification by integrating transcriptome and interactome data. *Gene Expression*, pages 1–5, 2011.

[342] M Mistry, J Gillis, and P Pavlidis. Genome-wide expression profiling of schizophrenia using a large combined cohort. *Mol. Psychiatry*, 18(2):215–25, January 2013.

[343] V N Sumantran. Cellular chemosensitivity assays: an overview. In Ian A. Cree, editor, *Cancer Cell Culture: Methods and Protocols*, volume 731 of *Methods in Molecular Biology*, chapter 19, pages 219–236. Humana Press, Totowa, NJ, 2 edition, 2011.

[344] M V Berridge, A N S Tan, K D Mccoy, and R U I Wang. The biochemical and cellular basis of cell proliferation assays that use tetrazolium salts. *Biochemica*, 4:14–19, 1996.

[345] E Borenfreund and H Babich. Comparisons of two in vitro cytotoxicity assays - the neutral red (NR) and tetrazolium MTT tests. *Toxicol. in Vitro*, 2(1):1–6, 1988.

[346] D Offen, Y Sherki, E Melamed, M Fridkin, D E Brenneman, and I Gozes. Vasoactive intestinal peptide (VIP) prevents neurotoxicity in neuronal cultures: relevance to neuroprotection in Parkinsons disease. *Brain Res.*, 854:257–262, 2000.

[347] B Y Cao, Y P Yang, W F Luo, C J Mao, R Han, X Sun, J Cheng, and C F Liu. Paeoniflorin, a potent natural compound, protects PC12 cells from MPP+ and acidic damage via autophagic pathway. *J. Ethnopharmacol.*, 131(1):122–9, August 2010.

[348] R C Scaduto and L W Grotyohann. Measurement of mitochondrial membrane potential using fluorescent rhodamine derivatives. *Biophys. J.*, 76(1 Pt 1):469–77, January 1999.

[349] A Wong and Cortopassi. High-throughput measurement of mitochondrial membrane potential in a neural cell line using a fluorescence plate reader. *Biochem. Bioph. Res. Co.*, 298(5):750–4, November 2002.

[350] D J Klionsky. Guidelines for the use and interpretation of assays for monitoring autophagy. *Autophagy*, 8(4):445–544, 2012.

[351] S J Cherra, S M Kulich, G Uechi, M Balasubramani, J Mountzouris, B W Day, and C T Chu. Regulation of the autophagy protein LC3 by phosphorylation. *J. Cell Biol.*, 190(4):533–539, 2010.

[352] S Pankiv, T H Clausen, T Lamark, A Brech, J A Bruun, H Outzen, A Ø vervatn, G Bjø rkøy, and T Johansen. P62/SQSTM1 binds directly to Atg8/LC3 to facilitate degradation of ubiquitinated protein aggregates by autophagy. *J. Biol. Chem.*, 282(33):24131–45, August 2007.

[353] H Weidberg, T Shpilka, E Shvets, and Z Elazar. Mammalian Atg8s: one is simply not enough. *Autophagy*, 6(6):808–9, August 2010.

[354] D J Klionsky. Autophagy: from phenomenology to molecular understanding in less than a decade. *Nature*, 8:931–937, 2007.

[355] E A Roberts and V Deretic. Autophagic proteolysis of long-lived proteins in nonliver cells. In *Methods in Molecular Biology, Vol 445*, volume 445, chapter Autophagy, pages 111–117. 2008.

[356] R Verhaar, B Drukarch, J G J M Bol, C A M Jongenelen, and M M M Wilhelmus. Tissue transglutaminase cross-links beclin 1 and regulates autophagy in MPP-treated human SH-SY5Y cells. *Neurochem. Int.*, 62(4):486–91, March 2013.

[357] J Rodríguez-Blanco, V Martín, G García-Santos, F Herrera, S Casado-Zapico, I Antolín, and C Rodriguez. Cooperative action of JNK and AKT/mTOR in 1-methyl-4-phenylpyridinium-induced autophagy of neuronal PC12 cells. *J. Neurosci. Res.*, 90(9):1850–60, September 2012.

[358] K Liu, J Huang, R Chen, T Zhang, L Shen, J Yang, and X Sun. Protection against neurotoxicity by an autophagic mechanism. *Braz. J. Med. Biol. Res.*, 45(5):401–407, May 2012.

[359] L Lim, V Jackson-Lewis, L C Wong, G H Shui, a X H Goh, S Kesavapany, a M Jenner, M Fivaz, S Przedborski, and M R Wenk. Lanosterol induces mitochondrial uncoupling and protects dopaminergic neurons from cell death in a model for Parkinson's disease. *Cell Death Differ.*, 19(3):416–27, March 2012.

[360] N Bae, T Ahn, S Chung, M S Oh, H Ko, H Oh, G Park, and H O Yang. The neuroprotective effect of modified Yeoldahanso-tang via autophagy enhancement in models of Parkinson's disease. *J. Ethnopharmacol.*, 134(2):313–22, March 2011.

[361] Y W Tzeng, L Y Lee, P L Chao, H C Lee, R T Wu, and A M Y Lin. Role of autophagy in protection afforded by hypoxic preconditioning against MPP+-induced neurotoxicity in SH-SY5Y cells. *Free Radic. Biol. Med.*, 49(5):839–46, September 2010.

[362] D Pöltl, S Schildknecht, C Karreman, and M Leist. Uncoupling of ATP-depletion and cell death in human dopaminergic neurons. *Neurotoxicology*, 33(4):769–79, August 2012.

[363] V R Potter and A E Reif. Inhibition of an electron transport component by antimycin A. *J. Biol. Chem.*, 194:287–97, 1952.

[364] T Vogiatzi, M Xilouri, K Vekrellis, and L Stefanis. Wild type α-synuclein is degraded by chaperone-mediated autophagy and macroautophagy in neuronal cells. *J. Biol. Chem.*, 283(35):23542–56, August 2008.

[365] H S Ko, Y Lee, J Shin, S S Karuppagounder, B S Gadad, A J Koleske, O Pletnikova, J C Troncoso, V L Dawson, and T M Dawson. Phosphorylation by the c-Abl protein tyrosine kinase inhibits parkin's ubiquitination and protective function. *PNAS*, 107(38):16691–6, September 2010.

[366] M W Cleeter, J M Cooper, and A H Schapira. Nitric oxide enhances MPP(+) inhibition of complex I. *FEBS Lett.*, 504(1-2):50–2, August 2001.

[367] D J Klionsky, A M Cuervo, and P O Seglen. Methods for monitoring autophagy from yeast to human. *Autophagy*, 3(3):181–206, 2007.

[368] N Mizushima. Methods for monitoring autophagy. *Int. J. Biochem. Cell Biol.*, 36(12):2491–502, December 2004.

[369] D K Slonim and I Yanai. Getting started in gene expression microarray analysis. *PLoS Comp. Bio.*, 5(10):e1000543, October 2009.

[370] T Shpilka, H Weidberg, S Pietrokovski, and Z Elazar. Atg8: an autophagy-related ubiquitin-like protein family. *Genome Biol.*, 12(7):226, January 2011.

[371] A L Barabási. *Network Science*. 2012.

[372] V Spirin and L A Mirny. Protein complexes and functional modules in molecular networks. *PNAS*, 100(21):12123–8, October 2003.

[373] T Rito, C M Deane, and G Reinert. The importance of age and high degree, in protein-protein interaction networks. *J. Comp. Bio.*, 19(6):785–95, June 2012.

[374] M E J Newman. Detecting community structure in networks. *EPJ B*, 38(2):321–330, March 2004.

[375] J Reichardt and S Bornholdt. Detecting fuzzy community structures in complex networks with a Potts model. *Phys. Rev. Lett.*, 93:2–5, 2004.

[376] A C F Lewis, N S Jones, M A Porter, and C M Deane. The function of communities in protein interaction networks at multiple scales. *BMC Syst. Biol.*, 4:100, January 2010.

[377] P Erdos and A Renyi. On the strength of connectedness of a random graph. *Acta Mathematica Academiae Scientiarum Hungarica*, 12:261–7, 1964.

[378] A L Barabasi and R Albert. Emergence of scaling in random networks. *Science*, 286(5439):509–512, October 1999.

[379] M E J Newman. Properties of highly clustered networks. *Phys. Rev. E*, 68:1–7, 2003.

[380] A Clauset, C R Shalizi, and M E J Newman. Power-law distributions in empirical data. *SIAM Rev.*, 51(4):661–703, November 2009.

[381] G Lima-Mendez and J van Helden. The powerful law of the power law and other myths in network biology. *Molecular BioSystems*, 5(12):1482–93, December 2009.

[382] M P H Stumpf and M A Porter. Mathematics. Critical truths about power laws. *Science*, 335(6069):665–6, February 2012.

[383] T Rito, Z Wang, C M Deane, and G Reinert. How threshold behaviour affects the use of subgraphs for network comparison. *Bioinformatics*, 26(18):i611–7, September 2010.

[384] W Ali, C Deane, and G Reinert. Protein interaction networks and their statistical analysis. In M P H Stumpf, D J Balding, and M Girolami, editors, *Handbook of Statistical Systems Biology*. John Wiley & Sons Ltd, 2011.

[385] F A Rodrigues, L da Fontoura Costa, and A L Barbieri. Resilience of protein-protein interaction networks as determined by their large-scale topological features. *Mol. Biosyst.*, 7(4):1263–9, May 2011.

[386] D J Watts and S H Strogatz. Collective dynamics of 'small-world' networks. *Nature*, 393(6684):440–2, June 1998.

[387] U Brandes. On variants of shortest-path betweenness centrality and their generic computation. *Soc. Networks*, 30(2):136–145, 2008.

[388] P L Flom, R Friedm, S Strauss, and A Neaigus. A new measure of linkage between two subnetworks. *Connections*, 26(1):62–70, 2004.

[389] A H Tong, M Evangelista, A B Parsons, H Xu, G D Bader, N Pagé, M Robinson, S Raghibizadeh, C W Hogue, H Bussey, B Andrews, M Tyers, and C Boone. Systematic genetic analysis with ordered arrays of yeast deletion mutants. *Science*, 294(5550):2364–8, December 2001.

[390] A Wagner. Robustness against mutations in genetic networks of yeast. *Nat. Genet.*, 24(4):355–61, April 2000.

[391] Z Gu, L M Steinmetz, X Gu, and C Scharfe. Role of duplicate genes in genetic robustness against null mutations. *Nature*, 421:63–66, 2003.

[392] M E Hillenmeyer, E Fung, J Wildenhain, S E Pierce, S Hoon, W Lee, M Proctor, R P St Onge, M Tyers, D Koller, R B Altman, R W Davis, C Nislow, and G Giaever. The chemical genomic portrait of yeast: uncovering a phenotype for all genes. *Science*, 320(5874):362–5, April 2008.

[393] W G Kaelin. The concept of synthetic lethality in the context of anticancer therapy. *Nat. Rev. Cancer*, 5(9):689–98, October 2005.

[394] H Kitano. Towards a theory of biological robustness. *Mol. Syst. Biol.*, 3(137):137, January 2007.

[395] H Jeong, S P Mason, A L Barabási, and Z N Oltvai. Lethality and centrality in protein networks. *Nature*, 411(6833):41–2, May 2001.

[396] M P Joy, A Brock, D E Ingber, and S Huang. High-betweenness proteins in the yeast protein interaction network. *J. Biomed. Biotechnol.*, 2005(2):96–103, June 2005.

[397] H Yu, P M Kim, E Sprecher, V Trifonov, and M Gerstein. The importance of bottlenecks in protein networks: correlation with gene essentiality and expression dynamics. *PLoS Comp. Bio.*, 3(4):e59, April 2007.

[398] K I Goh, M E Cusick, D Valle, B Childs, and M Vidal. The human disease network. *PNAS*, 104(21):8685–8690, 2007.

[399] E Zotenko, J Mestre, Di P O'Leary, and T M Przytycka. Why do hubs in the yeast protein interaction network tend to be essential: reexamining the connection between the network topology and essentiality. *PLoS Comp. Bio.*, 4(8):e1000140, January 2008.

[400] L A N Amaral. A truer measure of our ignorance. *PNAS*, 105(19):6795–6, May 2008.

[401] T Berggå rd, S Linse, and P James. Methods for the detection and analysis of protein-protein interactions. *Proteomics*, 7(16):2833–42, August 2007.

[402] M E Sardiu and M P Washburn. Building protein-protein interaction networks with proteomics and informatics tools. *J. Biol. Chem.*, 286(27):23645–51, July 2011.

[403] C von Mering, R Krause, B Snel, M Cornell, S G Oliver, S Fields, and P Bork. Comparative assessment of large-scale data sets of protein-protein interactions. *Nature*, 417(6887):399–403, May 2002.

[404] N C Turner, C J Lord, E Iorns, R Brough, S Swift, R Elliott, S Rayter, A N Tutt, and A Ashworth. A synthetic lethal siRNA screen identifying genes mediating sensitivity to a PARP inhibitor. *EMBO J.*, 27(9):1368–77, May 2008.

[405] A L Turinsky, S Razick, B Turner, I M Donaldson, and S J Wodak. Literature curation of protein interactions: measuring agreement across major public databases. *Database*, 2010:baq026, January 2010.

[406] L Hakes, J W Pinney, D L Robertson, and S C Lovell. Protein-protein interaction networks and biology–what's the connection? *Nat. Biotechnol.*, 26(1):69–72, January 2008.

[407] M P H Stumpf, T Thorne, E De Silva, R Stewart, H J An, M Lappe, and C Wiuf. Estimating the size of the human interactome. *PNAS*, 105(19):6959–6964, 2008.

[408] C Alfarano, C E Andrade, K Anthony, N Bahroos, M Bajec, K Bantoft, D Betel, B Bobechko, K Boutilier, E Burgess, K Buzadzija, R Cavero, C D'Abreo, I Donaldson, D Dorairajoo, M J Dumontier, M R Dumontier, V Earles, R Farrall, H Feldman, E Garderman, Y Gong, R Gonzaga, V Grytsan, E Gryz, V Gu, E Haldorsen, A Halupa, R Haw, A Hrvojic, L Hurrell, R Isserlin, F Jack, F Juma, A Khan, T Kon, S Konopinsky, V Le, E Lee, S Ling, M Magidin, J Moniakis, J Montojo, S Moore, B Muskat, I Ng, J P Paraiso, B Parker, G Pintilie, R Pirone, J J Salama, S Sgro, T Shan, Y Shu, J Siew, D Skinner, K Snyder, R Stasiuk, D Strumpf, B Tuekam, S Tao, Z Wang, M White, R Willis, C Wolting, S Wong, A Wrong, C Xin, R Yao, B Yates, S Zhang, K Zheng, T Pawson, B F F Ouellette, and C W V Hogue. The biomolecular interaction network database and related tools 2005 update. *Nucleic Acids Res.*, 33(Database issue):D418–24, January 2005.

[409] C Stark, B J Breitkreutz, T Reguly, L Boucher, A Breitkreutz, and M Tyers. BioGRID: a general repository for interaction datasets. *Nucleic Acids Res.*, 34(Database issue):D535–9, January 2006.

[410] A Ruepp, B Brauner, I Dunger-Kaltenbach, G Frishman, C Montrone, M Stransky, B Waegele, T Schmidt, O N Doudieu, V Stümpflen, and H W Mewes. CORUM: the comprehensive resource of mammalian protein complexes. *Nucleic Acids Res.*, 36(Database issue):D646–50, January 2008.

[411] L Salwinski, C S Miller, A J Smith, F K Pettit, J U Bowie, and D Eisenberg. The database of interacting proteins: 2004 update. *Nucleic Acids Res.*, 32(Database issue):D449–51, January 2004.

[412] G R Mishra, M Suresh, K Kumaran, N Kannabiran, S Suresh, P Bala, K Shivakumar, N Anuradha, R Reddy, T M Raghavan, S Menon, G Hanumanthu, M Gupta, S Upendran, S Gupta, M Mahesh, B Jacob, P Mathew, P Chatterjee, K S Arun, S Sharma, K N Chandrika, N Deshpande, K Palvankar, R Raghavnath, R Krishnakanth, H Karathia, B Rekha, R Nayak, G Vishnupriya, H G M Kumar, M Nagini, G S S Kumar, R Jose, P Deepthi, S S Mohan, T K B Gandhi, H C Harsha, K S Deshpande, M Sarker, T S K Prasad, and A Pandey. Human protein reference database–2006 update. *Nucleic Acids Res.*, 34(Database issue):D411–4, January 2006.

[413] D J Lynn, G L Winsor, C Chan, N Richard, M R Laird, A Barsky, J L Gardy, F M Roche, T H W Chan, N Shah, R Lo, M Naseer, J Que, M Yau, M Acab, D Tulpan, M D Whiteside, A Chikatamarla, B Mah, T Munzner, K Hokamp, R E W Hancock, and F S L Brinkman. InnateDB: facilitating systems-level analyses of the mammalian innate immune response. *Mol. Syst. Biol.*, 4(218):218, January 2008.

[414] S Kerrien, Y Alam-Faruque, B Aranda, I Bancarz, A Bridge, C Derow, E Dimmer, M Feuermann, A Friedrichsen, R Huntley, C Kohler, J Khadake, C Leroy, A Liban, C Lieftink, L Montecchi-Palazzi, S Orchard, J Risse, K Robbe, B Roechert, D Thorneycroft, Y Zhang, R Apweiler, and H Hermjakob. IntAct–open source resource for molecular interaction data. *Nucleic Acids Res.*, 35(Database issue):D561–5, January 2007.

[415] A Ceol, A Chatr Aryamontri, L Licata, D Peluso, L Briganti, L Perfetto, L Castagnoli, and

G Cesareni. MINT, the molecular interaction database: 2009 update. *Nucleic Acids Res.*, 38(Database issue):D532–9, January 2010.

[416] U Güldener, M Münsterkötter, M Oesterheld, P Pagel, A Ruepp, H W Mewes, and V Stümpflen. MPact: the MIPS protein interaction resource on yeast. *Nucleic Acids Res.*, 34(Database issue):D436–41, January 2006.

[417] J Goll, S V Rajagopala, S C Shiau, H Wu, B T Lamb, and P Uetz. MPIDB: the microbial protein interaction database. *Bioinformatics*, 24(15):1743–4, August 2008.

[418] P Pagel, S Kovac, M Oesterheld, B Brauner, I Dunger-Kaltenbach, G Frishman, C Montrone, P Mark, V Stümpflen, H W Mewes, A Ruepp, and D Frishman. The MIPS mammalian protein-protein interaction database. *Bioinformatics*, 21(6):832–4, March 2005.

[419] K R Brown and I Jurisica. Online predicted human interaction database. *Bioinformatics*, 21(9):2076–82, May 2005.

[420] A Stojmirović and Y K Yu. ppiTrim: constructing non-redundant and up-to-date interactomes. *Database*, 2011:bar036, January 2011.

[421] A Sinha and H A Nagarajaram. Nodes occupying central positions in human tissue specific PPI networks are enriched with many splice variants. *Proteomics*, pages 1–19, 2014.

[422] C M Deane. Protein interactions: two methods for assessment of the reliability of high throughput observations. *Mol. Cell. Proteomics*, 1(5):349–356, April 2002.

[423] G D Kritikos, C Moschopoulos, M Vazirgiannis, and S Kossida. Noise reduction in protein-protein interaction graphs by the implementation of a novel weighting scheme. *BMC Bioinformatics*, 12(1):239, January 2011.

[424] S Suthram, T Shlomi, E Ruppin, R Sharan, and T Ideker. A direct comparison of protein interaction confidence assignment schemes. *BMC Bioinformatics*, 7:360, January 2006.

[425] P Y Chen, C M Deane, and G Reinert. Predicting and validating protein interactions using network structure. *PLoS Comp. Bio.*, 4(7):e1000118, January 2008.

[426] A Mora and I M Donaldson. Effects of protein interaction data integration, representation and reliability on the use of network properties for drug target prediction. *BMC Boinformatics*, 13(1):294, January 2012.

[427] P Csermely. Strong links are important, but weak links stabilize them. *Trends Biomed. Sci.*, 29(7):331–4, July 2004.

[428] A W Whitehurst, B O Bodemann, J Cardenas, D Ferguson, L Girard, M Peyton, J D Minna, C Michnoff, W Hao, M G Roth, X J Xie, and M A White. Synthetic lethal screen identification of chemosensitizer loci in cancer cells. *Nature*, 446(7137):815–9, April 2007.

[429] I W Taylor, R Linding, D Warde-Farley, Y Liu, C Pesquita, D Faria, S Bull, T Pawson, Q Morris, and J L Wrana. Dynamic modularity in protein interaction networks predicts breast cancer outcome. *Nat. Biotechnol.*, 27(2):199–204, February 2009.

[430] T P Nguyen, W C Liu, and F Jordán. Inferring pleiotropy by network analysis: linked diseases in the human PPI network. *BMC Syst. Biol.*, 5:179, January 2011.

[431] N T Doncheva, T Kacprowski, and M Albrecht. Recent approaches to the prioritization of candidate disease genes. *Wiley Interdiscip. Rev. Syst. Biol. Med.*, 4(5):429–42, 2012.

[432] M Krauthammer, C A Kaufmann, T C Gilliam, and A Rzhetsky. Molecular triangulation: bridging linkage and molecular-network information for identifying candidate genes in Alzheimer's disease. *PNAS*, 101(42):15148–53, October 2004.

[433] L Franke, H van Bakel, L Fokkens, E D de Jong, M Egmont-Petersen, and C Wijmenga. Reconstruction of a functional human gene network, with an application for prioritizing positional candidate genes. *Am. J. Hum. Gen.*, 78(6):1011–25, June 2006.

[434] S Kohler, S Bauer, D Horn, and P N Robinson. Walking the interactome for prioritization of candidate disease genes. *Am. J. Hum. Gen.*, 82:949–958, 2008.

[435] S Navlakha and C Kingsford. The power of protein interaction networks for associating genes with diseases. *Bioinformatics*, 26(8):1057–1063, February 2010.

[436] L Hou, M Chen, C K Zhang, J Cho, and H Zhao. Guilt by rewiring: gene prioritization through network rewiring in Genome Wide Association Studies. *Hum. Mol. Genet.*, pages 1–11, January 2014.

[437] G V Paolini, R H B Shapland, W P van Hoorn, J S Mason, and A L Hopkins. Global mapping of pharmacological space. *Nat. Biotechnol.*, 24(7):805–15, July 2006.

[438] A Ma'ayan, S L Jenkins, J Goldfarb, and R Iyengar. Network analysis of FDA approved drugs and their targets. *Mt. Sinai J. Med.*, 74(1):27–32, 2007.

[439] M J Keiser, V Setola, J J Irwin, C Laggner, A Abbas, S J Hufeisen, N H Jensen, M B Kuijer, R C Matos, B Thuy, R Whaley, R A Glennon, J Hert, K L H Thomas, D Edwards, B K Shoichet, and B L Roth. Predicting new molecular targets for known drugs. *Nature*, 462(7270):175–181, 2010.

[440] M K Sakharkar, P Li, Z Zhong, and K R Sakharkar. Quantitative analysis on the characteristics of targets with FDA approved drugs. *Int. J. Biol. Sci.*, 4(1):15–22, January 2008.

[441] M Zhang, S Su, R K Bhatnagar, D J Hassett, and L J Lu. Prediction and analysis of the protein interactome in Pseudomonas aeruginosa to enable network-based drug target selection. *PloS One*, 7(7):e41202, January 2012.

[442] I J Farkas, T Korcsmáros, I A Kovács, A Mihalik, R Palotai, G I Simkó, K Z Szalay, M Szalay-Beko, T Vellai, S Wang, and P Csermely. Network-based tools for the identification of novel drug targets. *Sci. Signal.*, 4(173), January 2011.

[443] W C Hwang, A Zhang, and M Ramanathan. Identification of information flow-modulating drug targets: a novel bridging paradigm for drug discovery. *Clin. Pharmacol. Ther.*, 84(5):563–72, November 2008.

[444] J Goñi, F J Esteban, N V de Mendizábal, J Sepulcre, S Ardanza-Trevijano, I Agirrezabal, and P Villoslada. A computational analysis of protein-protein interaction networks in neurodegenerative diseases. *BMC Syst*, 2:52, January 2008.

[445] A Beilina, I N Rudenko, A Kaganovich, L Civiero, H Chau, S K Kalia, L V Kalia, E Lobbestael, R Chia, K Ndukwe, J Ding, M A Nalls, M Olszewski, D N Hauser, R Kumaran, A M Lozano, V Baekelandt, L E Greene, J M Taymans, E Greggio, and M R Cookson. Unbiased screen for interactors of leucine-rich repeat kinase 2 supports a common pathway for sporadic and familial Parkinson disease. *PNAS*, 111(7):2626–31, February 2014.

[446] H Rakshit, N Rathi, and D Roy. Construction and analysis of the protein-protein interaction networks based on gene expression profiles of Parkinson's disease. *PloS One*, 9(8):e103047, January 2014.

[447] C Behrends, M E Sowa, S P Gygi, and J W Harper. Network organization of the human autophagy system. *Nature*, 466(7302):68–76, July 2010.

[448] L Li, K Zhang, J Lee, S Cordes, D P Davis, and Z Tang. Discovering cancer genes by integrating network and functional properties. *BMC Med. Genomics*, 2:61, January 2009.

[449] H Mochizuki, H Hayakawa, M Migita, M Shibata, R Tanaka, A Suzuki, Y Shimo-Nakanishi, T Urabe, M Yamada, K Tamayose, T Shimada, M Miura, and Y Mizuno. An AAV-derived Apaf-1 dominant negative inhibitor prevents MPTP toxicity as antiapoptotic gene therapy for Parkinson's disease. *PNAS*, 98(19):10918–10923, 2001.

[450] A Nicotra and S Parvez. Apoptotic molecules and MPTP-induced cell death. *Neurotoxicol. Teratol.*, 24(5):599–605, 2002.

[451] F Burté, L A De Girolamo, A J Hargreaves, and E E Billett. Alterations in the mitochondrial proteome of neuroblastoma cells in response to complex 1 inhibition. *J. Proteome Res.*, 10(4):1974–86, April 2011.

[452] C Van Humbeeck, T Cornelissen, and W Vandenberghe. Ambra1: A Parkin-binding protein involved in mitophagy. *Autophagy*, 7(12):1555–1556, 2011.

[453] R Setsuie, Y L Wang, H Mochizuki, H Osaka, H Hayakawa, N Ichihara, H Li, A Furuta, Y Sano, Y J Sun, J Kwon, T Kabuta, K Yoshimi, S Aoki, Y Mizuno, M Noda, and K Wada. Dopaminergic neuronal loss in transgenic mice expressing the Parkinson's disease-associated UCH-L1 I93M mutant. *Neurochem. Int.*, 50(1):119–29, January 2007.

[454] R Endo, T Saito, A Asada, H Kawahara, T Ohshima, and S I Hisanaga. Commitment of 1-methyl-4-phenylpyrinidinium ion-induced neuronal cell death by proteasome-mediated degradation of p35 cyclin-dependent kinase 5 activator. *J. Biol. Chem.*, 284(38):26029–39, September 2009.

[455] M Naoi, H Ichinose, T Takahashi, I Nagatsu, and T Nagatsu. Reduction of aromatic L-amino acid decarboxylase activity in clonal pheochromocytoma PC12h cells by culture in the presence of N-methyl-4-phenylpyridinium ion (MPP+). *Neurosci. Lett.*, 95(1-3):229–35, December 1988.

[456] J Ara, S Przedborski, A B Naini, V Jackson-Lewis, R R Trifiletti, J Horwitz, and H Ischiropoulos. Inactivation of tyrosine hydroxylase by nitration following exposure to peroxynitrite and 1-methyl-4-phenyl-1,2,3,6-tetrahydropyridine (MPTP). *PNAS*, 95(13):7659–63, June 1998.

[457] M E Haque, K J Thomas, C D'Souza, S Callaghan, T Kitada, R S Slack, P Fraser, M R Cookson, A Tandon, and D S Park. Cytoplasmic Pink1 activity protects neurons from dopaminergic neurotoxin MPTP. *PNAS*, 105(5):1716–21, February 2008.

[458] W L Chien, T R Lee, S Y Hung, K H Kang, M J Lee, and W M Fu. Impairment of oxidative stress-induced heme oxygenase-1 expression by the defect of Parkinson-related gene of PINK1. *J. Neurochem.*, 117(4):643–53, May 2011.

[459] E J Shin, E M Kim, J A Lee, H Rhim, and O Hwang. Matrix metalloproteinase-3 is activated by HtrA2/Omi in dopaminergic cells: relevance to Parkinson's disease. *Neurochem. Int.*, 60(3):249–56, February 2012.

[460] T Shang, S Kotamraju, S V Kalivendi, C J Hillard, and B Kalyanaraman. 1-Methyl-4-phenylpyridinium-induced apoptosis in cerebellar granule neurons is mediated by transferrin receptor iron-dependent depletion of tetrahydrobiopterin and neuronal nitric-oxide synthase-derived superoxide. *J. Biol. Chem.*, 279(18):19099–112, April 2004.

[461] D S Cassarino, C P Fall, R H Swerdlow, T S Smith, E M Halvorsen, S W Miller, J P Parks, W D Parker, and J P Bennett. Elevated reactive oxygen species and antioxidant enzyme activities in animal and cellular models of Parkinson's disease. *Biochim. Biophys. Acta*, 1362:77–86, 1997.

[462] D H Choi, O Hwang, K H Lee, J Lee, M Flint Beal, and Y S Kim. DJ-1 cleavage by matrix metalloproteinase 3 mediates oxidative stress-induced dopaminergic cell death. *Antioxid. Redox Signal.*, 14(11), 2011.

[463] T Duka and A Sidhu. The neurotoxin, MPP+, induces hyperphosphorylation of Tau, in the presence of α-synuclein, in SH-SY5Y neuroblastoma cells. *Neurotox. Res.*, 10(1):1–10, August 2006.

[464] B Thomas, A S Mandir, N West, Y Liu, S A Andrabi, W Stirling, V L Dawson, T M Dawson, and M K Lee. Resistance to MPTP-neurotoxicity in α-synuclein knockout mice is complemented by human α-synuclein and associated with increased β-synuclein and Akt activation. *PloS One*, 6(1):e16706, January 2011.

[465] D C Robertson, O Schmidt, N Ninkina, P A Jones, J Sharkey, and V L Buchman. Developmental loss and resistance to MPTP toxicity of dopaminergic neurones in substantia nigra pars compacta of gamma-synuclein, alpha-synuclein and double alpha/gamma-synuclein null mutant mice. *J. Neurochem.*, 89(5):1126–36, June 2004.

[466] M Girvan and M E J Newman. Community structure in social and biological networks. *PNAS*, 99(12):7821–6, June 2002.

[467] J J Lebrun, K Takabe, and Y Chen. Roles of pathway-specific and inhibitory smads in activin receptor signaling. *Mol. Endocrinol.*, 13(1):15–23, 1999.

[468] T L Chau, R Gioia, J S Gatot, F Patrascu, I Carpentier, J P Chapelle, L O'Neill, R Beyaert, J Piette, and A Chariot. Are the IKKs and IKK-related kinases TBK1 and IKK-epsilon similarly activated? *Trends Biomed. Sci.*, 33(4):171–80, April 2008.

[469] A A Belov and M Mohammadi. Grb2, a double-edged sword of receptor tyrosine kinase signaling. *Sci. Signal.*, 5(November 2012):1–3, 2013.

[470] J Y Chung, H R Park, S J Lee, S H Lee, J S Kim, Y S Jung, S H Hwang, N C Ha, W G Seol, J Lee, and B J Park. Elevated TRAF2/6 expression in Parkinson's disease is caused by the loss of parkin E3 ligase activity. *Lab. Invest.*, 93(6):663–676, 2013.

[471] K Tanji, F Mori, A Kakita, H Takahashi, and K Wakabayashi. Alteration of autophagosomal proteins (LC3, GABARAP and GATE-16) in Lewy body disease. *Neurobiol. Dis.*, 43(3):690–7, September 2011.

[472] C H Jung, S H Ro, J Cao, N M Otto, and D H Kim. mTOR regulation of autophagy. *FEBS Lett.*, 584(7):1287–95, April 2010.

[473] A Hartmann, P P Michel, J D Troadec, A Mouatt-Prigent, B A Faucheux, M Ruberg, Y Agid, and E C Hirsch. Is Bax a mitochondrial mediator in apoptotic death of dopaminergic neurons in Parkinson's disease? *J. Neurochem.*, 76(6):1785–1793, December 2001.

[474] J Michels, P W M Johnson, and G Packham. Molecules in focus: Mcl-1. *Int. J. Biochem. Cell Biol.*, 37(2):267–71, March 2005.

[475] L Puimège, C Libert, and F Van Hauwermeiren. Regulation and dysregulation of tumor necrosis factor receptor-1. *Cytokine Growth Factor Rev.*, March 2014.

[476] D Berg, C Holzmann, and O Riess. 14-3-3 Proteins in the nervous system. *Nat. Rev. Neurosci.*, 4(9):752–62, September 2003.

[477] R J Nichols, N Dzamko, N A Morrice, D G Campbell, M Deak, A Ordureau, T Macartney, Y Tong, J Shen, A R Prescott, and D R Alessi. 14-3-3 binding to LRRK2 is disrupted by multiple Parkinson's disease-associated mutations and regulates cytoplasmic localization. *Biochem. J.*, 430(3):393–404, September 2010.

[478] T Yamada, T Kawamata, D G Walker, and P L Mcgeer. Vimentin immunoreactivity in normal and pathological human brain tissue. *Acta Neuropathol.*, 84:157–162, 1992.

[479] B L Davidson and P B McCray. Current prospects for RNA interference-based therapies. *Nat. Rev. Genet.*, 12(5):329–40, May 2011.

[480] P A Trimmer, T S Smith, A B Jung, and J P Bennett. Dopamine neurons from transgenic mice with a knockout of the p53 gene resist MPTP neurotoxicity. *Neurodegeneration*, 5(3):233–9, September 1996.

[481] D M Bustos. The role of protein disorder in the 14-3-3 interaction network. *Mol. Biosyst.*, 8(1):178–84, January 2012.

[482] Y Sai, K Peng, F Ye, X Zhao, Y Zhao, Z Zou, J Cao, and Z Dong. 14-3-3 proteins in the regulation of rotenone-induced neurotoxicity might be via its isoform 14-3-3epsilon's involvement in autophagy. *Cell. Mol. Neurobiol.*, 33(8):1109–21, November 2013.

[483] Y Kabeya, N Mizushima, A Yamamoto, S Oshitani-Okamoto, Y Ohsumi, and T Yoshimori. LC3, GABARAP and GATE16 localize to autophagosomal membrane depending on form-II formation. *J. Cell Sci.*, 117(Pt 13):2805–12, June 2004.

[484] T Johansen and T Lamark. Selective autophagy goes exclusive. *Nat. Cell Biol.*, 16(5):395–397, May 2014.

[485] J Sawa-Makarska, C Abert, J Romanov, B Zens, I Ibiricu, and S Martens. Cargo binding to Atg19 unmasks additional Atg8 binding sites to mediate membrane-cargo apposition during selective autophagy. *Nat. Cell Biol.*, 16(5):425–33, May 2014.

[486] S Nath, J Dancourt, V Shteyn, G Puente, W M Fong, S Nag, J Bewersdorf, A Yamamoto, B Antonny, and T J Melia. Lipidation of the LC3/GABARAP family of autophagy proteins relies on a membrane-curvature-sensing domain in Atg3. *Nat. Cell Biol.*, 16(5):415–24, May 2014.

[487] A Kaufmann, V Beier, H G Franquelim, and T Wollert. Molecular mechanism of autophagic membrane-scaffold assembly and disassembly. *Cell*, 156(3):469–81, January 2014.

[488] M Schwarten, J Mohrlüder, P Ma, M Stoldt, Y Thielmann, T Stangler, N Hersch, B Hoffmann, R Merkel, and D Willbold. Nix directly binds to GABARAP: a possible crosstalk between apoptosis and autophagy. *Autophagy*, 5(5):690–8, July 2009.

[489] W Yang, X Wang, C Duan, L Lu, and H Yang. α-Synuclein overexpression increases phosphoprotein phosphatase 2A levels via formation of calmodulin/Src complex. *Neurochem. Int.*, 63(3):180–94, September 2013.

[490] D D Sarbassov, D A Guertin, S M Ali, and D M Sabatini. Phosphorylation and regulation of Akt/PKB by the rictor-mTOR complex. *Science*, 307(5712):1098–101, February 2005.

[491] A Ghosh, A Roy, X Liu, J H Kordower, E J Mufson, D M Hartley, S Ghosh, R L Mosley, H E Gendelman, and K Pahan. Selective inhibition of NF-kappaB activation prevents dopaminergic neuronal loss in a mouse model of Parkinson's disease. *PNAS*, 104(47):18754–9, November 2007.

[492] Q Yang and Z Mao. Dysregulation of autophagy and Parkinson's disease: the MEF2D link. *Apoptosis*, 15(11):1410–4, November 2010.

[493] H J Yang, L Wang, Y Y Xia, P N Chang, and Z W Feng. NF-kappaB mediates MPP+-induced apoptotic cell death in neuroblastoma cells SH-EP1 through JNK and c-Jun/AP-1. *Neurochem. Int.*, 56(1):128–34, January 2010.

[494] S H Park, W S Choi, S Y Yoon, Y S Ahn, and Y J Oh. Activation of NF-kappaB is involved in 6-hydroxydopamine-but not MPP+ -induced dopaminergic neuronal cell death: its potential role as a survival determinant. *Biochem. Bioph. Res. Co.*, 322(3):727–33, September 2004.

[495] A K Müller-Rischart, A Pilsl, P Beaudette, M Patra, K Hadian, M Funke, R Peis, A Deinlein, C Schweimer, P H Kuhn, S F Lichtenthaler, E Motori, S Hrelia, W Wurst, D Trümbach, T Langer, D Krappmann, G Dittmar, J Tatzelt, and K-F Winklhofer. The E3 ligase parkin maintains mitochondrial integrity by increasing linear ubiquitination of NEMO. *Mol. Cell*, 49(5):908–21, March 2013.

[496] F D Miller, C D Pozniak, and G S Walsh. Neuronal life and death: an essential role for the p53 family. *Cell Death Differ.*, 7(10):880–8, October 2000.

[497] S J Lee, D C Kim, B H Choi, H Ha, and K T Kim. Regulation of p53 by activated protein kinase C-delta during nitric oxide-induced dopaminergic cell death. *J. Biol. Chem.*, 281(4):2215–24, January 2006.

[498] W Duan, X Zhu, B Ladenheim, Q S Yu, Z Guo, J Oyler, R G Cutler, J L Cadet, N H Greig, and M P Mattson. P53 inhibitors preserve dopamine neurons and motor function in experimental parkinsonism. *Ann. Neurol.*, 52(5):597–606, November 2002.

[499] J R Chang, M Ghafouri, R Mukerjee, A Bagashev, T Chabrashvili, and B E Sawaya. Role of p53 in neurodegenerative diseases. *Neurodegen. Dis.*, 9(2):68–80, January 2012.

[500] C Alves da Costa, C Sunyach, E Giaime, A West, O Corti, A Brice, S Safe, P M Abou-Sleiman, N W Wood, H Takahashi, M S Goldberg, J Shen, and F Checler. Transcriptional repression of p53 by parkin and impairment by mutations associated with autosomal recessive juvenile Parkinson's disease. *Nat. Cell Biol.*, 11(11):1370–5, November 2009.

[501] J Fan, H Ren, N Jia, E Fei, T Zhou, P Jiang, M Wu, and G Wang. DJ-1 decreases Bax expression through repressing p53 transcriptional activity. *J. Biol. Chem.*, 283(7):4022–30, February 2008.

[502] C Alves Da Costa, E Paitel, B Vincent, and F Checler. α-Synuclein lowers p53-dependent apoptotic response of neuronal cells. Abolishment by 6-hydroxydopamine and implication for Parkinson's disease. *J. Biol. Chem.*, 277(52):50980–4, December 2002.

[503] L J Martin, Y Pan, A C Price, W Sterling, N G Copeland, N A Jenkins, D L Price, and M K Lee. Parkinson's disease α-synuclein transgenic mice develop neuronal mitochondrial degeneration and cell death. *J. Neurosci.*, 26(1):41–50, January 2006.

[504] C Alves da Costa and F Checler. Apoptosis in Parkinson's disease: is p53 the missing link between genetic and sporadic Parkinsonism? *Cell. Signal.*, 23(6):963–8, June 2011.

[505] J Lim, H W Kim, M B H Youdim, I J Rhyu, K M Choe, and Y J Oh. Binding preference of P62 towards LC3-ll during dopaminergic neurotoxin-induced impairment of autophagic flux. *Autophagy*, 7(1):51–60, January 2011.

[506] M Komatsu, S Waguri, M Koike, Y S Sou, T Ueno, T Hara, N Mizushima, J I Iwata, J Ezaki, S Murata, J Hamazaki, Y Nishito, S I Iemura, T Natsume, T Yanagawa, J Uwayama, E Warabi, H Yoshida, T Ishii, A Kobayashi, M Yamamoto, Z Yue, Y Uchiyama, E Kominami, and K Tanaka. Homeostatic levels of p62 control cytoplasmic inclusion body formation in autophagy-deficient mice. *Cell*, 131(6):1149–63, December 2007.

[507] E Kuusisto, L Parkkinen, and I Alafuzoff. Morphogenesis of Lewy bodies: dissimilar incorporation of α-synuclein, ubiquitin, and p62. *J. Neuropathol. Exp. Neurol.*, 62(12):1241–53, December 2003.

[508] V I Korolchuk, A Mansilla, F M Menzies, and D C Rubinsztein. Autophagy inhibition compromises degradation of ubiquitin-proteasome pathway substrates. *Mol. Cell*, 33(4):517–27, March 2009.

[509] J Moscat and M T Diaz-Meco. P62 at the crossroads of autophagy, apoptosis, and cancer. *Cell*, 137(6):1001–4, June 2009.

[510] R Mathew, C M Karp, B Beaudoin, N Vuong, G Chen, H Y Chen, K Bray, A Reddy, G Bhanot, C Gelinas, R S Dipaola, V Karantza-Wadsworth, and E White. Autophagy suppresses tumorigenesis through elimination of p62. *Cell*, 137(6):1062–75, June 2009.

[511] V Janssens and J Goris. Protein phosphatase 2A: a highly regulated family of serine/threonine phosphatases implicated in cell growth and signalling. *Biochem. J.*, 353:417–439, 2001.

[512] R K Dagda, C A Barwacz, J T Cribbs, and S Strack. Unfolding-resistant translocase targeting: a novel mechanism for outer mitochondrial membrane localization exemplified by the Bβ2 regulatory subunit of protein phosphatase 2A. *J. Biol. Chem.*, 280(29):27375–82, July 2005.

[513] Y C Wang, C M Lee, L C Lee, L C Tung, H M Hsieh-Li, G J Lee-Chen, and M T Su. Mitochondrial dysfunction and oxidative stress contribute to the pathogenesis of spinocerebellar ataxia type 12 (SCA12). *J. Biol. Chem.*, 286(24):21742–54, June 2011.

[514] W Qian, J Shi, X Yin, K Iqbal, I Grundke-Iqbal, and C X Gong. PP2A regulates tau phosphorylation directly and also indirectly via activating GSK-3β. *J. Alzheimers Dis.*, 19:1221–1229, 2010.

[515] K W Lee, W Chen, E Junn, J Y Im, H Grosso, P K Sonsalla, X Feng, N Ray, J R Fernandez, Y Chao, E Masliah, M Voronkov, S P Braithwaite, J B Stock, and M M Mouradian. Enhanced phosphatase activity attenuates α-synucleinopathy in a mouse model. *J. Neurosci.*, 31(19):6963–71, May 2011.

[516] W T Cheng, Z X Guo, C A Lin, M Y Lin, L C Tung, and K Fang. Oxidative stress promotes autophagic cell death in human neuroblastoma cells with ectopic transfer of mitochondrial PPP2R2B (Bbeta2). *BMC Cell Biol.*, 10(C):91, January 2009.

[517] C Vogel and E M Marcotte. Insights into the regulation of protein abundance from proteomic and transcriptomic analyses. *Nat. Rev. Genet.*, 13(4):227–32, April 2012.

[518] J N Le Grand, F Z Chakrama, S Seguin-Py, A Fraichard, R Delage-Mourroux, M Jouvenot, P Y Risold, and M Boyer-Guittaut. GABARAPL1 (GEC1) antibodies. Target one protein, get one free! *Autophagy*, 7(11):1302–1307, 2011.

[519] Y Maruyama, Y S Sou, S Kageyama, T Takahashi, T Ueno, K Tanaka, M Komatsu, and Y Ichimura. LC3B is indispensable for selective autophagy of p62 but not basal autophagy. *Biochem. Bioph. Res. Co.*, 446(1):309–15, March 2014.

[520] M L Kramer and W J Schulz-Schaeffer. Presynaptic α-synuclein aggregates, not Lewy bodies, cause neurodegeneration in dementia with Lewy bodies. *J. Neurosci.*, 27(6):1405–10, February 2007.

[521] P Ma, M Schwarten, L Schneider, A Boeske, N Henke, D Lisak, S Weber, J Mohrlüder, M Stoldt, B Strodel, A Methner, S Hoffmann, O H Weiergräber, and D Willbold. Interaction of Bcl-2 with the autophagy-related GABAA receptor-associated protein (GABARAP): biophysical characterization and functional implications. *J. Biol. Chem.*, 288(52):37204–15, December 2013.

[522] C Mammucari, G Milan, V Romanello, E Masiero, R Rudolf, P Del Piccolo, S J Burden, R Di Lisi, C Sandri, J Zhao, A L Goldberg, S Schiaffino, and M Sandri. FoxO3 controls autophagy in skeletal muscle in vivo. *Cell metabolism*, 6(6):458–71, December 2007.

[523] C Fellmann and S W Lowe. Stable RNA interference rules for silencing. *J. Biol. Chem.*, 16(1):10–8, January 2014.

[524] T Gaj, C A Gersbach, and C F Barbas. ZFN, TALEN, and CRISPR/Cas-based methods for genome engineering. *Trends Biotech.*, 31(7):397–405, July 2013.

[525] A Nicotra and S H Parvez. Cell death induced by MPTP, a substrate for monoamine oxidase B. *Toxicology*, 153(1-3):157–66, November 2000.

[526] J M Cooper, P B O Wiklander, J Z Nordin, R Al-Shawi, M J Wood, M Vithlani, A H V Schapira, J P Simons, S El-Andaloussi, and L Alvarez-Erviti. Systemic exosomal siRNA delivery reduced alpha-synuclein aggregates in brains of transgenic mice. *Movement Disord.*, 29(12):1476–85, August 2014.

[527] M Pósfai, A Fekete, and G Vattay. Shortest-path sampling of dense homogeneous networks. *Europhys. Lett.*, 89(1):18007, January 2010.

[528] M Vaudel, A Sickmann, and L Martens. Introduction to opportunities and pitfalls in functional mass spectrometry based proteomics. *Biochim. Biophys. Acta*, 1844(1 Pt A):12–20, January 2014.

[529] J W Choi, M Y Song, and K S Park. Quantitative proteomic analysis reveals mitochondrial protein changes in MPP(+)-induced neuronal cells. *Mol. Biosyst.*, 10(7):1940–7, July 2014.

[530] N Shubin, C Tabin, and S Carroll. Deep homology and the origins of evolutionary novelty. *Nature*, 457(7231):818–23, February 2009.

[531] M Costanzo, A Baryshnikova, J Bellay, Y Kim, E D Spear, C S Sevier, H Ding, J L Y Koh, K Toufighi, S Mostafavi, J Prinz, R P St Onge, B VanderSluis, T Makhnevych, F J Vizeacoumar, S Alizadeh, S Bahr, R L Brost, Y Chen, M Cokol, R Deshpande, Z Li, Z Y Lin, W Liang, M Marback, J Paw, B J San Luis, E Shuteriqi, A H Y Tong, N van Dyk, I M Wallace, J A Whitney, M T Weirauch, G Zhong, H Zhu, W A Houry, M Brudno, S Ragibizadeh, B Papp, C Pál, F P Roth, G Giaever, C Nislow, O G Troyanskaya, H Bussey, G D Bader, A C Gingras, Q D Morris, P M Kim, C A Kaiser, C L Myers, B J Andrews, and C Boone. The genetic landscape of a cell. *Science*, 327(5964):425–31, January 2010.

[532] D J Wiley, I Juan, H Le, X Cai, L Baumbach, C Beattie, and G D'Urso. Yeast Augmented Network Analysis (YANA): a new systems approach to identify therapeutic targets for human genetic diseases. *F1000Research*, 3:121, January 2014.

[533] B P Lewis, C B Burge, and D P Bartel. Conserved seed pairing, often flanked by adenosines, indicates that thousands of human genes are microRNA targets. *Cell*, 120(1):15–20, January 2005.

[534] B Gentner, G Schira, A Giustacchini, M Amendola, B D Brown, M Ponzoni, and L Naldini. Stable knockdown of microRNA in vivo by lentiviral vectors. *Nat. Med.*, 6(1):63–66, 2009.

[535] J A Lee, M T Uhlik, C M Moxham, D Tomandl, and D J Sall. Modern phenotypic drug discovery is a viable, neoclassic pharma strategy. *J. Med*, 55(10):4527–38, May 2012.

[536] D C Swinney and J Anthony. How were new medicines discovered? *Nat. Rev. Drug Discov.*, 10(7):507–19, July 2011.

[537] M Van Loock, G Meersseman, K Van Acker, C Van Den Eynde, D Jochmans, B Van Schoubroeck, G Dams, L Heyndrickx, and R F Clayton. A novel high-throughput cellular screening assay for the discovery of HIV-1 integrase inhibitors. *J. Virological Meth,*, 179(2):396–401, February 2012.

[538] F J Gamo, L M Sanz, J Vidal, C de Cozar, E Alvarez, J L Lavandera, D E Vanderwall, D V S Green, V Kumar, S Hasan, J R Brown, C E Peishoff, L R Cardon, and J F Garcia-Bustos. Thousands of chemical starting points for antimalarial lead identification. *Nature*, 465(7296):305–10, May 2010.

[539] J G Moffat, J Rudolph, and D Bailey. Phenotypic screening in cancer drug discovery - past, present and future. *Nat. Rev. Drug Discov.*, 13(8):588–602, July 2014.

[540] K Bush, P Courvalin, G Dantas, J Davies, B Eisenstein, P Huovinen, G A Jacoby, R Kishony, B N Kreiswirth, E Kutter, S A Lerner, S Levy, K Lewis, O Lomovskaya, J H Miller, S Mobashery, L J V Piddock, S Projan, C M Thomas, A Tomasz, P M Tulkens, T R Walsh, J D Watson, J Witkowski, W Witte, G Wright, P Yeh, and H I Zgurskaya. Tackling antibiotic resistance. *Nat. Rev. Microbiol.*, 9(12):894–6, December 2011.

[541] G Butland, J M Peregrin-Alvarez, J Li, W Yang, X Yang, V Canadien, A Starostine, D Richards, B Beattie, N Krogan, M Varvey, J Parkinson, J Greenblatt, and A Emili. Interaction network containing conserved and essential protein complexes in Escherichia coli. *Nature*, 433(February):531–537, 2005.

[542] K Li, L A Schurig-Briccio, X Feng, A Upadhyay, V Pujari, B Lechartier, F L Fontes, H Yang, G Rao, W Zhu, A Gulati, J H No, G Cintra, S Bogue, Y L Liu, K Molohon, P Orlean, D A Mitchell, L Freitas-Junior, F Ren, H Sun, T Jiang, Y Li, R T Guo, S T Cole, R B Gennis, D C Crick, and E Oldfield. Multitarget drug discovery for tuberculosis and other infectious diseases. *J. Med. Chem.*, 57(7):3126–39, April 2014.